Bioluminescence-Mediated Photodynamic Therapy:

A Novel Treatment for Grade 4 Astrocytoma

Jane Ng ***BSc MBBS MRCP MRCS***

University College London

PhD Submission

I, Jane Ng, confirm that the work presented in this thesis is my own. Where information has been derived from other sources, I confirm that this has been indicated in the thesis.

Supervisors

Dr N Henriquez, UCL Institute of Neurology

Mr N Kitchen, The National Hospital for Neurology and Neurosurgery

Professor S Bown, UCL National Medical Laser Centre

Grants

Work generously supported by:

The National Hospital Development Foundation Fellowship

The Royal College of Surgeons Rosetrees Fellowship

The B Braun Research Fellowship

Abstract

Background and Aims

Despite advances in surgery, radiation and chemotherapy, grade 4 astrocytoma, the commonest primary brain tumour, remains incurable with a dire prognosis related to its diffusely infiltrative nature. With photodynamic therapy, pre-treatment with a photosensitising drug and subsequent exposure to light of a specific wavelength can mediate selective tumour destruction. However, it is limited by light penetration. Bioluminescence results from conversion of chemical energy into light. This thesis explores whether bioluminescence generated inside astrocytoma cells *in vitro* and *in in vivo* can mediate PDT: light generation by target cells requires no knowledge of the exact location of every cell, thereby potentially overcoming the diffuse, infiltrative nature of astrocytomas.

Methods

in vitro: genetically modified U87 glioma cells expressing firefly luciferase (U87-*luc*) were generated, pre-treated with the photosensitisers hypericin or *m*THPC, then incubated with d-luciferin to induce bioluminescence. Cell viability was assessed by MTT assay, haemocytometry, and a growth assay. Inhibition by lycopene, an antioxidant that suppresses PDT, was assessed. Control studies used untransfected U87 cells.

in vivo: U87-*luc* cells were xenografted subcutaneously and intracranially into CD1 nu/nu mice. Mice were pre-treated with intraperitoneal *m*THPC then given a 7 day infusion of d-luciferin (subcutaneously implanted pump). Tumour response was followed by bioluminescence imaging, volume measurements, and survival. Tumours were harvested for pathological examination and BrdU immunohistochemistry.

Results

in vitro: bioluminescence-mediated PDT produced significant cell death with both photosensitisers in U87-*luc* cells, which was suppressed by lycopene. There was no effect in untransfected cells that could not generate bioluminescence.

in vivo: in 3 out of 4 trials, including one in an intracranial model, a treatment effect was demonstrated by a significant reduction of proliferation, as assessed by the proportion of BrdU positive cells in the 'treatment' group compared to controls.

Conclusion

Bioluminescence-mediated PDT kills tumour cells *in vitro*. Preliminary evidence of an effect *in vivo* supports the concept being explored further.

Contents

List of Tables

List of Figures

Abbreviations

5-ALA	5-aminolevulinic acid
ANOVA	Analysis of variance
BBB	Blood-brain-barrier
bp	Base pair
bPDT	Bioluminescence-mediated photodynamic therapy
BSA	Bovine serum albumin
$CaCl_2$	Calcium chloride
cm	Centimetre
CI	Confidence interval
CO_2	Carbon dioxide
Da	Dalton
dd	Double-distilled
DMEM	Dulbecco's Modified Eagle Medium
DMSO	Dimethyl sulfoxide
DTT	Dithiothreitol
EDTA	Ethylenedia-inetetraacetic acid
FBS	Fetal bovine serum
HCl	Hydrochloric acid
H_2O	Water
Hr(s)	Hour(s)
Kb	Kilo-base pair
LB	Luria broth base
mM	Millimolar
M	Molar
$MgCl_2$	Magnesium chloride
MGMT	O^6-methylguanine-DNA methyltransferase
Min(s)	Minute(s)
ml(s)	Millilitre(s)
mm	Millimetre
MOPS	3-(N-Morpholino)propanesulfonic acid
MRI	Magnetic resonance imaging
*m*THPC	m-tetrahydrophenylchlorin

MTT	Methylthiazolyldiphenyl-tetrazolium bromide
NaCl	Sodium chloride
NaOH	Sodium hydroxide
nm	Nanometre
N_2	Nitrogen
O_2	Oxygen
OD	Optical density
PDT	Photodynamic therapy
PEG	Polyethelene glycol
PBS	Phosphate buffered saline
rpm	Revolutions per minute
SDS	Sodium dodecyl sulphate
sec(s)	Second(s)
SEM	Standard error of the mean
TAE	Tris-acetate and EDTA
V	Volts
v/v	Volume per volume
w/v	Weight per volume
µl	Microlitre
^0C	Degree celsius

Part 1 Background and Aims

This section will provide a background on the most common primary brain tumour, grade 4 astrocytoma, and will discuss reasons for its resistance to treatment, even to this day. Photodynamic therapy (PDT) will be introduced as an attractive adjunct to conventional treatments, yet it will be seen that the limitations specific to overcoming grade 4 astrocytoma remain. Bioluminescence, as a novel, endogenous, intrinsic light source to mediate photodynamic therapy will be explored: bioluminescence-mediated photodynamic therapy (bPDT). Its ability to overcome the treatment resistant characteristics of grade 4 astrocytoma will be proposed, and the rationale behind the study conducted will be outlined.

Chapter 1 Grade 4 Astrocytoma

High-grade astrocytoma, specifically grade 4 astrocytoma, is an aggressive and highly debilitating primary brain tumour with an exceptionally poor prognosis. Despite advances in medicine over the last century, there has been little improvement in survival. In this chapter, astrocytomas will be defined and classified. Focusing on grade 4 astrocytoma, the most common and deadly of primary brain tumours, its epidemiology will be discussed, illustrating the need for ongoing research into its treatment. The basis underlying the current standard of care of grade 4 astrocytoma will be reviewed, and the failings of this standard highlighted. The fundamental reason for treatment failure will be discussed, and the limitations of each aspect of standard care will be considered. Finally, the need of a novel approach will be appreciated.

1.1 Classification and Epidemiology of Astrocytomas

Gliomas are a type of primary tumour of the brain and spinal cord that are considered to arise from cells of glial origin. Such cells include astrocytes, oligodendrocytes, and ependymal cells. One third of all primary tumours of the brain and spinal cord are malignant, and gliomas account for 80% of these[1]. The most common of the gliomas are astrocytomas, which comprise of 75% of all gliomas[1]. In short, astrocytomas underlie the majority of malignant primary brain and spinal cord tumours.

Based on their pathological appearance, and in order of increasing malignancy, the World Health Organisation has classified astrocytomas from grades 1-4[2], with grades 3 and 4 being considered malignant (see Table 1). Specifically, grade 4 astrocytoma (see Figure 1), also termed glioblastoma multiforme, accounts for almost half (45.6%) of all malignant primary brain and spinal cord tumours, making it the most common malignant tumour of the brain and spinal cord[1].

Grade	Anaplastic Features
1	No anaplastic features
2	Nuclear atypia
3	Nuclear atypia and mitosis
4	Nuclear atypia, mitosis, vascular endothelial proliferation, and necrosis

Table 1 WHO Classification of Astrocytomas[2]

The incidence of grade 4 astrocytoma is 3.19 per 100 000, and the median age of diagnosis is 65 yrs[1]. Importantly, as the Western population ages and the number of adults aged 65 and older is expected to double by 2030, the incidence of cancer is projected to increase significantly: demographic trends for grade 4 astrocytoma project that its incidence rate will increase 66% between 2010 and 2050. Although this does not seem particularly impressive compared to more common cancers such as breast[3], with an incidence of 124.8 per 100 000[3], and lung, with an incidence of 58.7 per 100 000[4], malignant astrocytomas, and particularly grade 4 astrocytoma, have much more devastating prognoses. The 5-year survival for grade 4 astrocytoma is only 5.5%[1] compared to 89.4%[3] and 17.4%[4] for breast and lung cancer, respectively.

1.2 Early Understanding and Treatment

Early data provided an insight into the natural history of grade 4 astrocytoma. A retrospective study of 219 cases of grade 4 astrocytoma presenting to one institution from 1924-1952 found the survival rate of this disease to be 50% at 7 months, 33% at 1 year, and near 0 % at 5 years[5]. Median survival was approximately 9 months. 84% had undergone some degree of tumour resection and 21% had undergone whole brain radiation. Separating those who had treatment from those who had not, the 1 year survival was 35% and 20%, respectively, yet the 2 year survival for both groups was approximately 5%. This indicated that those surviving beyond a year were more a reflection of the intrinsic biology of the tumour than representing the effectiveness of treatment.

A prospective trial conducted by the Brain Tumour Study Group between 1969-1972 reported the median survival of grade 4 astrocytoma to be only 14 weeks with surgical resection alone[6] with the addition of adjuvant radiation doubling survival. The survival benefit of adjuvant radiation was subsequently confirmed in randomised controlled trials[7,8], and the standard of care of those with grade 4 astrocytoma became cytoreductive surgery followed by whole brain radiation for the next several decades.

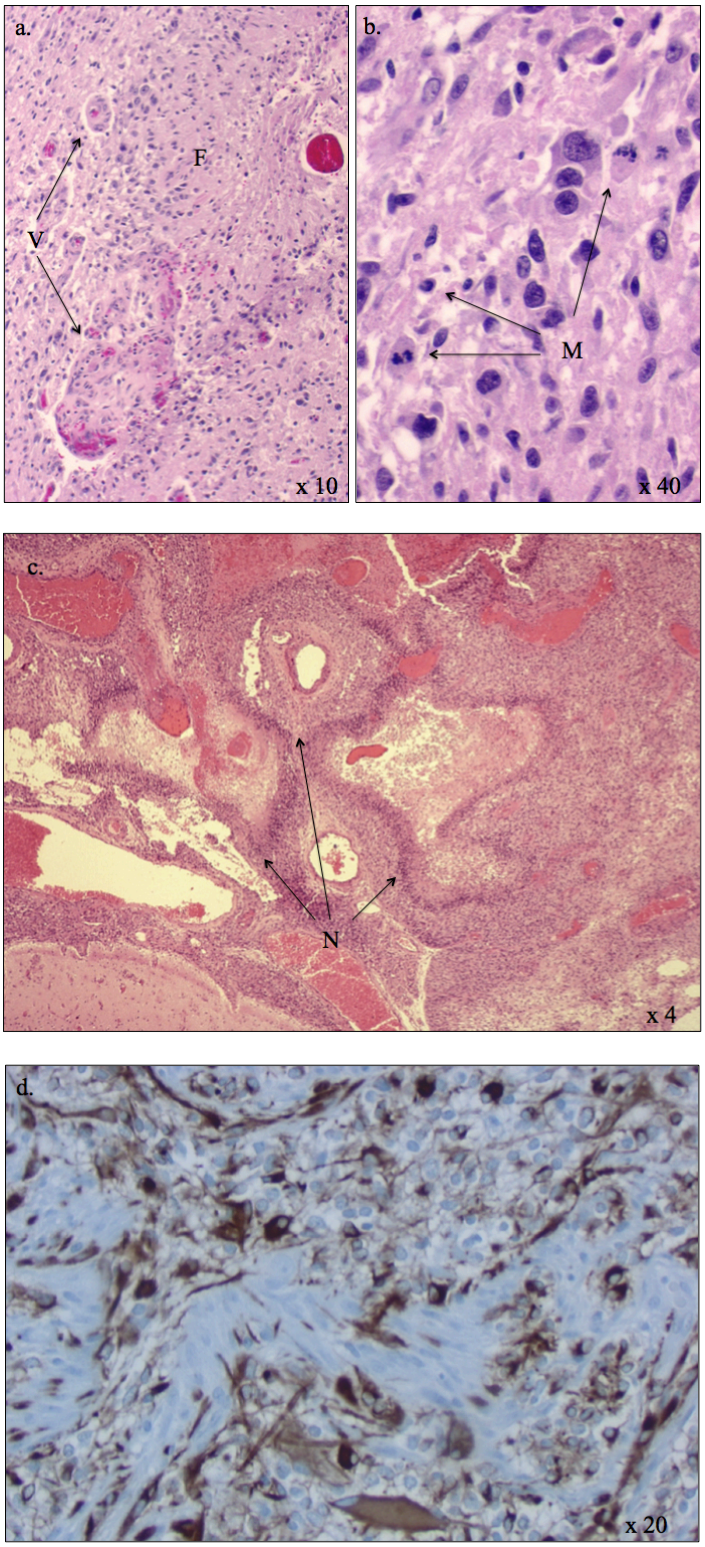

Figure 1 Slides Depicting the Characteristic Pathological Features of Grade 4 Astrocytoma

***Slides are courtesy of Dr S Salamat, University of Wisconsin Neuropathology*. Slides a, b, and c are haematoxylin and eosin stained slides. The hypercellularity on a fibrillary (F) background, which is highlighted by immunohistochemical staining of glial fibrillary acidic protein (slide d), is characteristic of astrocytoma. There is also nuclear atypia, mitoses (M), vascular endothelial proliferation (V) and widespread necrosis (N) with nuclear palisading, all associated specifically with grade 4 astrocytoma.**

1.3 Advances in Chemotherapy

In an effort to improve the poor prognosis of grade 4 astrocytoma, extensive research into various chemotherapeutics was conducted. A meta-analysis of 12 randomised trials investigating the effect of chemotherapy on malignant astrocytoma was published in the *Lancet* in 2002[9]. Data from a total of 3004 patients was analysed: the majority were diagnosed with grade 4 astrocytoma (63%). All patients had undergone some degree of surgical resection followed by radiation, either to the whole brain or the tumour and its margins. Chemotherapeutic agents included carmustine, lomustine, dacarbazine, and mitolactol. Overall, the results favoured the addition of chemotherapy to the standard of care, increasing median survival by 2 months, and increasing 1 year survival by 6% and 2 year survival by 5%. However, findings of this meta-analysis could not be corroborated in subsequent trials. The Medical Research Council Brain Tumour Working Party initiated the largest randomised trial of adjuvant chemotherapy for high-grade astrocytoma in an attempt to provide a definitive answer[10]. Between 1988 and 1997, 674 patients were randomised to receive radiotherapy alone or radiotherapy and procarbazine, lomustine, and vincristine (PCV) chemotherapy. There was no significant difference in the median survival between the groups (9.5 months and 10 months, respectively).

It was not until 2005 did a true advance in the management and understanding of high-grade astrocytoma come to light. Stupp *et al*., conducted a randomised controlled trial investigating the effect of temozolomide, an oral alkylating agent[11]. 573 patients with grade 4 astrocytoma, the majority of whom had undergone debulking surgery, were randomly assigned to receive radiotherapy alone or radiotherapy and temozolamide. At the median follow up of 28 months, the median survival with radiotherapy alone was 12.1 months, whereas that with radiotherapy and temozolomide was 14.6 months; a significant increase. 2 year survival with radiotherapy alone was 10.4%, whereas that with radiotherapy and temozolomide was 26.5%; again, another significant increase. Furthermore, progression free survival with radiotherapy alone was 5.0 months, compared to 6.9 months with radiotherapy and temozolomide, $p < 0.001$. This survival advantage was associated with a low rate of side effects: radiation and temozolomide in combination led to grade 3 and 4 haemotological toxic effects in only 7%. Based upon these results, the inclusion of temozolomide into the treatment protocol for those with grade 4 astrocytoma became standard of care.

Recognising that patients with grade 4 astrocytoma inevitably face disease progression despite maximum therapy including cytoreductive surgery, radiation, and temozolomide, rescue treatments have been investigated. Grade 4 astrocytoma is a highly vascularised tumour[12] and is associated with over-expression of vascular endothelial growth factor (VEGF), a key regular of tumour-associated angiogenesis[13-15]. A recombinant, humanized, monoclonal IgG_1 antibody has been raised against VEGF, bevacizumab (Avastin®). Its action is to inhibit angiogenesis and tumour growth. In 2009, the FDA approved its use for recurrent grade 4 astrocytoma based upon only two, prospective, phase 2 trials, AVF3708g[16] and NCI 06-C-0064E[17]. These studies included adult patients (aged ≥ 18) with histologically confirmed grade 4 astrocytoma that had recurred after prior standard radiotherapy and temozolomide, and both studies had an average follow up of only 4 months. The AVF3708g trial also included a treatment arm comprising of bevacizumab in combination with irinotecan. However, the study was not designed to compare outcomes between the two treatment groups. All efficacy evaluations were based on comparisons with historical control data. The 6 month progression free survival in AVF3708g was 42.6%, and in NCI 06-C-0064E was 29%, both significantly better than historical controls. Subsequently, a phase 3, randomised, double-blind, placebo-controlled trial, was undertaken to evaluate the addition of bevacizumab to the standard protocol of radiation and temozolomide in those with newly diagnosed grade 4 astrocytoma[18]. Adults with confirmed grade 4 astrocytoma were treated with radiotherapy (60Gy) and daily temozolomide. Treatment with bevacizumab or placebo began during week 4 of radiotherapy and was continued for up to 12 cycles of maintenance temozolomide. At the time of disease progression, the assigned treatment was revealed, and bevacizumab therapy could be initiated or continued. A total of 637 patients were studied. There was no significant difference in the duration of overall survival between the bevacizumab and placebo groups (15.7 and 16.1 months, respectively, $p = 0.21$). Progression-free survival was significantly longer in the becavizumab group compared to placebo (10.7 months vs 7.3 months, respectively, $p = 0.007$). Over time, an increased symptom burden, a worse quality of life, and a decline in neurocognitive function were more frequent in the bevacizumab group. Bevacizumab has not become part of standard treatment for newly diagnosed grade 4 astrocytoma, but remains an option for recurrent disease.

The data supporting the use of bevacizumab is not strong. Furthermore, it is important to acknowledge an important confounding factor. VEGF inhibitors have been shown to

cause a rapid and impressive reduction in vascular permeability, resulting in restoration of the blood-brain-barrier (BBB), and decrease in cerebral oedema. Patients consequently feel much better quickly. Moreover, reflecting this dramatic effect, the area of contrast enhancing tumour on T1 weighted MRI is seen to significantly decrease, even within 24 hours[19]: as the BBB is restored, contrast extravasation reduces, so labelled a pseudoresponse. This makes tumour progression difficult to follow: patients on bevacizumab may be seen to clinically decline, but their imaging as judged by contrast enhancing tumour on T1 weighted MRI is seen to be stable. In such cases, the fluid-attenuated inversion recovery (FLAIR) sequence on MRI, which removes the effects of fluid, is better used to follow tumour progression[20], and better correlates with the patients' clinical state. However, tumour progression has been typically judged by the appearance of the contrast enhancing tumour on T1 weighted MRI, and for this reason, it may be that progression free survival has been inaccurately interpreted to be longer than it actually is. Consistent with this is the observation that once a patient has been recognised to have progressed on bevacizumab, their prognosis is extremely poor, with a median survival of only 3.8 ± 1 months[21]. Without using a reliable indicator of progression, the effect of bevacizumab cannot be accurately known. The most robust data is that for newly diagnosed disease, where no overall survival benefit has been associated with adding bevacizumab to the standard treatment protocol[18].

1.4 Advances in Understanding Pathogensis

Interrogating their results further, *Stupp et al*., analysed the relationship between O^6-methylguanine-DNA methyltransferase (MGMT) silencing and survival. MGMT is a DNA repair enzyme that removes alkyl groups from the O^6 position of guanine, acting as an acceptor itself[22]. It is silenced by epigenetic methylation of the CpG dinucleotides in the promoter region of the MGMT gene (*MGMT*)[23]. Consequent loss of MGMT expression results in an inability to remove alkyl groups from methylated guanine and compromises the capacity for DNA repair.

As an alkylating agent, temozolomide alkylates/methylates DNA, most commonly at the O^6 and N^7 positions of guanine residues. This damages the DNA, triggering tumour cell death. Taking into account the *MGMT* promoter methylation status of the patients, only those with tumours containing a methylated *MGMT* promoter i.e. those in whom DNA repair capacity was compromised, benefited from temozolomide: among patients

whose tumour contained a methylated *MGMT* promoter their median survival with radiotherapy alone was 15.3 months compared to 21.7 months with radiotherapy and temozolomide, a significant difference[24]. However, in those with tumours that did not have a methylated *MGMT* promoter, the difference in survival between the two treatment protocols was small and insignificant (11.8 months with radiation alone vs 12.7 months with radiation and temozolomide). Interestingly, irrespective of treatment group, the presence of *MGMT* promoter methylation in the tumour was also an independent favourable prognostic factor.

This study not only added temozolomide to the standard of care for those with grade 4 astrocytoma, but heralded a whole research movement into the molecular classification of brain tumours (see Chapter 10).

1.5 The Challenges of Grade 4 Astrocytoma

Now, a decade on from Stupp *et al*.'s publication[11], the standard of care for those with newly diagnosed grade 4 astrocytoma remains some degree of surgical resection or biopsy followed by radiation and temozolomide. The combination of radiation and temozolomide is that as described by Stupp *et al*. and comprises concurrent radiotherapy and temozolomide followed by adjuvant temozolomide. In those with a good Karnofsky performance score, the median survival is quoted as being between 12 and 18 months. Although this is almost double that in the beginning of the 20th century, the gain in survival remains only in the order of months, and is modest (see Table 2).

	Median Survival, months		
	Surgery Alone	Surgery +Radiation	Surgery+Radiation+Chemotherapy
1958[5]		9	
1978[6]	3.5	7	
2005[11]		12.1	14.6

Table 2 Summary of Median Survival Over Time For Grade 4 Astrocytoma

Information is derived from the studies described in sections 1.2 and 1.3. The data from 1978 has been adjusted from 'weeks' to 'months.' Over half a century the improvement in survival for grade 4 astrocytoma has only been in the order of months, and is modest.

Fundamental to the evasiveness of grade 4 astrocytoma is its infiltrative nature, and this was recognised very early on. Historically, patients were subjected to extensive resections that included lobectomies and even hemispherectomies in the hope that complete excision of the gross tumour and adjacent microscopically invaded tissue would result in cure. Such operations were almost always failures. Disregarding the immediate surgical mortality of such extensive surgeries, in a high percentage of patients, the disease had extended to involve the opposite hemisphere via the corpus callosum, and it was this disease that continued to grow leading to death of the patient: pathological study of 28 consecutive autopsy cases of grade 4 astrocytoma demonstrated that in 21 cases there was gross interhemispheric extension of the disease through the corpus callosum[25].

Developed in 1971, magnetic resonance imaging (MRI) became a standard part of the work up of a patient with a brain tumour by the late 1980s. Typically, high-grade astrocytomas were found to demonstrate prominent heterogeneity in signal intensity: on T2 weighted images, high-grade astrocytomas typically displayed a hyperintense core, a less hyperintense or normal intensity rim, and a surrounding area of high intensity[26] (see Figure 2b). Marked and irregular contrast enhancement was also characteristic (see Figure 2a and c). Traditionally, removal of the enhancing portion of the tumour would be considered a gross total resection. However, histological examination has shown that tumour cells extend at least 2 cm from the radiographical contrast enhancing mass. Specifically, tumour cells have been demonstrated to extend into the outer surrounding area of T2 hyperintensity, and in some cases, even beyond this. In one histologic study[27], at the time of surgical resection or biopsy, biopsy specimens were also taken from areas of the brain considered to be normal on T1 and T2 weighted images. Numbers were limited for ethical reasons. 16 of the 23 and 4 of the 10 biopsies taken from areas considered normal on T1 and T2 weighted images, respectively, demonstrated tumour cells.

It is this diffuse, microscopic infiltration that is fundamental to the recurrence of high-grade astrocytoma following initial treatment. The most common site of recurrence is that of the original tumour location, with more than 90% of patients with high-grade astrocytoma recurring here[28]. Consistent with the diffuse nature of the disease, although less common, grade 4 astrocytoma will also recur through the development of new parenchymal lesions (see Figure 2f) or intraventricular spread remote to the site of the

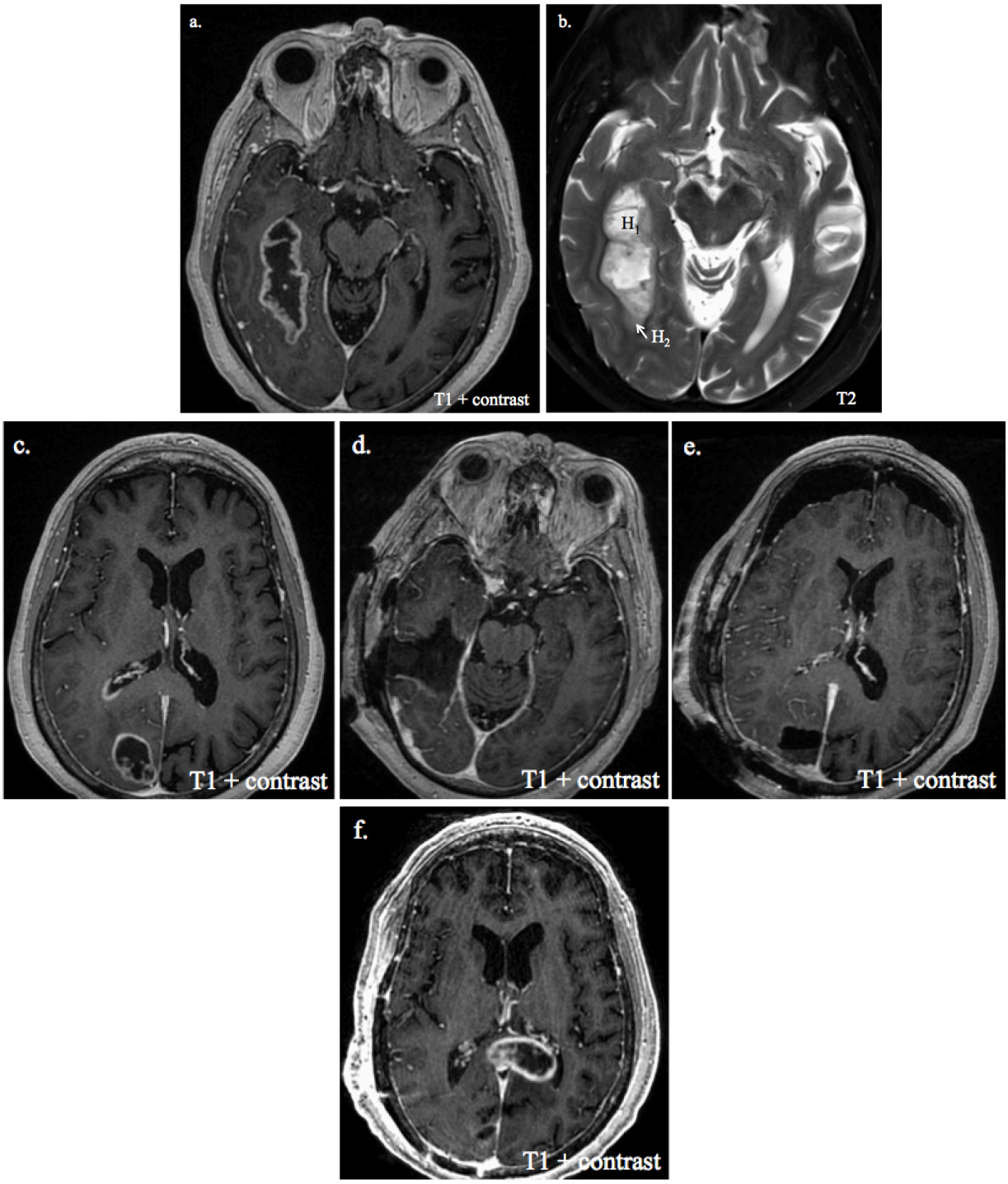

Figure 2 A patient with grade 4 astrocytoma

Images are courtesy of Dr M Baskaya, University of Wisconsin Neurosurgery. **These are axial MR images from a 67 year old female diagnosed with grade 4 astroctyoma. The patient has two main, enhancing foci of disease seen on the T1 acquisitions with contrast: one in the right temporal lobe (a), and one in the right occipital lobe (c). The T2 acquisition (b) illustrates some typical characteristics of grade 4 astrocytoma; the hyperintense core (H_1), a rim of normal intensity surrounded by an area of hyperintensity (H_2). The patient underwent gross total resection of the enhancing disease (d and e). However, despite this and adjuvant radiotherapy and temozolomide, within 3 months, she had progression of disease in the corpus callosum crossing to the left side (f). This was a more aggressive course than expected as the MGMT promoter was methylated.**

original tumour. It may be argued whether grade 4 astrocytoma is ever cured, and whether 'recurrence' is in fact progression of disease. Nevertheless, the mean time to tumour recurrence/progression varies between 4.9 months to 12 months. Of the conventional treatment modalities currently available, each have limitations to tackling the invasive nature of grade 4 astrocytoma.

1.5.1 Limitations of Surgical Resection

Understanding the invasive nature of grade 4 astrocytoma, which eludes the most sensitive of imaging techniques and the most powerful of operating microscopes, it can be seen that a complete resection of the tumour is unattainable. Some surgeons would advocate not only resecting the contrast enhancing part of the tumour, but also the rim of T2 hyperintensity surrounding it, eloquence of the brain permitting. However, tumour cells still extend beyond this. Certainly some degree of resection rather than biopsy alone has been shown to be beneficial[29]. However, whether the extent of surgical resection confers a survival advantage has been contentious. Several authors have attempted to draw conclusions from a number of small retrospective series[30,31]. However, analyses were limited by several factors: extent of resection was often subjective and dependent upon surgeon report as opposed to objective review of post operative imaging; patients were not stratified according to age and performance status, both strong prognostic indicators in themselves. Subsequently, one group from a large US cancer centre published more objective findings of their experience[32]. They analysed 416 consecutive patients with histologically proven grade 4 astrocytoma, who underwent tumour resection between 1993 and 1999. Although the analysis was retrospective, patient demographics, volumetric data and other tumour characteristics identified on MRI were collected prospectively. Five independent predictors of survival were found, one of them being the extent of resection. Defining tumour volume by the area of increased signal intensity on contrast-enhancing T1 weighted MR images, a significant survival advantage was associated with resection of 98% or more of the tumour volume: this resulted in a median survival of 13 months compared to 8.8 months when a lesser resection was achieved. A more recent, similarly designed study, not only corroborated this findings, but suggested that even resections as low as 78% of the total conferred a survival advantage[33].

The closest examination of this issue in a randomised controlled manner was with the use of fluorescence to guide resection. 5-aminolevulinic acid (5-ALA) is a non-fluorescent prodrug that, when given to patients orally, leads to the selective

intracellular accumulation of fluorescent porphyrins in malignant astrocytomas. At the time of surgical resection, using a modified operating microscope, the tumour can be viewed using conventional white light as well as using a violet-blue light, which causes the tumour cells that now contain the porphyrins to fluoresce. With the aid of this fluorescence, the surgeon can resect islands of infiltrative cells that may have escaped notice under conventional white light. In one European centre, 322 patients were randomised to undergo either standard microsurgical resection or fluorescence-guided resection[34], followed by standard protocols for radiation and chemotherapy. Complete resection of the enhancing tumour was achieved in a significantly higher proportion of patients undergoing fluorescence-guided resection (65%) compared to those undergoing standard surgery (36%). Moreover, a higher proportion of those who had undergone fluorescence-guided resection reached 6 month progression free survival (41%) compared to those who had undergone standard surgery (21.1%). However, there was no difference in overall survival between the two groups. These results reflect the diffusely infiltrative nature of the disease: with optimum resection of local disease, the best that was achieved was prolonged time to disease progression, and thus improved symptom-free survival and quality of life. However, as distant malignant cells remained present, overall survival remained unchanged. Fluorescence guided resection will be discussed in more detail in Chapter 2.

Another important limitation of surgery is that in many cases the tumour is intimately associated with an area of eloquence such as the motor cortex or thalamus. In attempting a gross total resection, there is significant risk of leaving the patient with a profound and permanent neurological deficit. Not only is this undesirable, but many oncologists will not commence adjuvant therapy in those with a Karnofsky performance score of less than 60 (a score of 60 is where a person requires occasional assistance but is able to care for most of their personal needs)[35] or if the patient has significant disability: therefore a heroic attempt at a gross total resection leaving a patient with significant deficit would not effectively change the natural history of the disease. In such cases, obtaining a biopsy for a tissue diagnosis then proceeding with adjuvant therapy is more prudent.

1.5.2 Limitations of Radiotherapy

Radiation has been clearly shown to improve survival in high-grade astrocytoma: a meta-analysis of 6 randomised controlled trials demonstrated a significant survival benefit from post-operative radiotherapy[36]. Typically, radiation is given such that the

high-dose volume should incorporate the enhancing tumour plus a limited margin, e.g. 2 cm. The total dose delivered is in the range of 50-60 Gy in fraction sizes of 1.8-2.0 Gy.

However, the response of the disease to radiotherapy clearly reinforces the pathogenicity of the distant islands of tumour cells that extend beyond the main tumour mass. 571 patients with high-grade glioma were randomised to three different chemotherapy regimes[37]. Those accrued in 1980 and 1981 received whole brain radiation, whereas those accrued in 1982 and 1983 were randomly assigned to receive whole brain radiation or whole brain radiation plus a boost to the enhancing tumour plus a 2 cm margin. There was no significant difference in survival between the three chemotherapy arms, and no differences in survival among the three different cohorts of radiation protocols: delivering additional radiation to the main tumour mass provided no survival benefit. More recently, radiosurgery has been used to deliver a high- and well-circumscribed dose of ionising radiation to a target, using a very steep gradient index and stereotactic targeting to minimise the adverse effect of radiation to surrounding structures. In a randomised trial, 200 patients with grade 4 astrocytoma were assigned to receive stereotaxic radiosurgery to the main tumour mass followed by conventional radiation and bis-chloroethylnitrosourea or treatment with conventional radiation and bis-chloroethylnitrosourea alone[38]. The addition of stereotaxic radiosurgery did not confer a survival advantage. Overall, focusing radiation on the main tumour mass is not enough to improve upon survival: it seems that it is the continuing survival of the distant islands of infiltrative cells that subsequently influence prognosis.

The dose of radiation that can be delivered is limited by the risk of a delayed, but well documented, decline in cognitive function[39]. Furthermore, the efficacy of radiation is limited by the development of radiation resistant populations of cells. To overcome these problems, dose intensification strategies have been studied. Hyperfractionation involves the use of a larger number of smaller sized fractions to achieve a total dose of radiation that is higher than conventionally administered radiation in the same overall treatment time. Accelerated fractionation delivers 2 or 3 usual sized fractions each day with the goal of reducing overall treatment time, thereby decreasing the possibility of tumour repopulation during treatment. Hypofractionation uses fewer, but larger,

radiation fractions, again in an effort to reduce the overall treatment time. None of these strategies have been associated with a survival benefit[36].

Use of radiation sensitisers, chemicals that increase the lethal effects of radiation, have also been used to overcome the limitations of radiation. Two classes of radiation sensitisers have been studied in high-grade astrocytoma: hypoxic cell sensitisers and halogenated pyrimidines. Intraoperative *in vivo* measurements and PET studies have demonstrated the presence of hypoxic regions in high-grade astrocytoma, and *in vitro* studies have established that hypoxic cells are 2.5 to 3 times more resistant to radiation than well-oxygenated cells. Hypoxic cell sensitiers, typically nitroimidazoles, work to increase the effect of radiation on hypoxic tumour cells without increasing the radiation effect on the already well-oxygenated normal tissue. There have been 13 randomised studies comparing sensitised radiotherapy with nitroimidazoles to radiotherapy alone, with only one, the earliest and smallest of the studies, showing any benefit[36]. The second class of radiation sensitisers, the halogenated pyrimidines 5-bromodeoxyuridine and 5-iododeoxyuridine, are similar to the normal DNA precursor thymidine, except for having a halogen substituted in place of a methyl group. These compounds are competitively incorporated into DNA in place of thymidine, leading to increased radiation sensitivity: mitotically active tumour cells are more likely to incorporate these compounds than the more slowly replicating surrounding non-tumour cells, thereby making tumour cells more sensitive to the lethal effects of radiation. Compared to historical controls, patients with grade 3 astrocytoma treated with 5-bromodeoxyuridine during radiotherapy followed by adjuvant chemotherapy seemed to have a survival advantage[40], although patients with grade 4 astrocytoma did not[41]. However, the subsequent RTOG randomised controlled trial comparing the effect of radiation with or without 5-bromodeoxyuridine followed by adjuvant chemotherapy on patients with grade 3 astrocytoma did not demonstrate a survival advantage[42].

Although radiotherapy confers a clear survival advantage over surgical resection alone in the management of grade 4 astrocytoma, its effect on the diffuse nature of the disease remains limited. Several strategies to overcome its limitations have been attempted without success.

1.5.3 Limitations of Chemotherapy

Chemotherapy faces many challenges in the treatment of intrinsic tumours of the brain. Among these include overcoming the BBB, unique to treating intrinsic brain tumours;

and overcoming the development of drug resistance, a challenge common to treating all cancers.

1.5.3.1 The Blood Brain Barrier

The endothelium of the cerebral capillary circulation, the anatomic basis of the BBB, is composed of tightly fused junctions, in contrast to the open endothelium of the peripheral circulation. This results in a continuous lipid layer that effectively restricts the movement of molecules into and out of the brain. Only small, electrically neutral, lipid-soluble molecules, with molecular weights up to 500 Da, can penetrate the BBB by passive diffusion. Temozolomide, the only chemotherapeutic agent currently used as standard of care of high-grade astrocytoma[11], is able to cross the BBB due its small size of 194 Da and its lipophilic nature[43]. However, most chemotherapeutic agents do not have these traits.

The limitations of the BBB may not seem so relevant to astrocytomas, as the areas of contrast enhancement that are so characteristic of high grade disease, reflect regions where the BBB has broken down, allowing intravenous contrast to extravasate into the surrounding tissues. However, those distant islands of invasive tumour cells, which do not contrast enhance and are radiographically invisible, can still evade chemotherapy agents because of the BBB.

One strategy to overcome the BBB is to bypass it by directly infusing drug into the brain. In the search for chemotherapeutic agents, research at the National Cancer Institute led to the development of nitrosurea compounds over 40 years ago[44]. Subsequent, generation of more active analogues led to the discovery of one of the first agents effective against malignant glioma: 1,3-bis(2-chloroethyl)-1-nitrosurea (BCNU, carmustine) was shown to be highly effective in the treatment of intracerebral L1210, a murine leukaemia cell line, and in ensuing clinical trials, BCNU was found to confer some survival advantage over radiotherapy alone in patients with malignant glioma[45-47]. However, the systemic toxicities of BCNU, which include haematologic toxicity[48], pulmonary fibrosis[49,50], and secondary acute leukaemia[51,52], proved limiting. Although the activity of systemically administered BCNU on intracranial tumours implied an ability to cross the BBB[53], its toxicity limited its use. In an attempt to reduce these systemic toxicities but to continue benefiting from its efficacy led to research on local delivery methods.

Direct administration of BCNU through a catheter inserted in the surgical cavity was attempted in 1975 with no clear success, most likely due to the short half-life of BCNU in solution and to the limited delivery to the tumour tissue[54]. In the late 1980s, biodegradable polymer wafers that could be loaded with BCNU (Gliadel®, MGI Pharma, Inc.) were developed[55]. Following surgical resection, the wafers could be implanted in the surgical bed, and in the aqueous environment of the brain, hydrolysis of anhydride bonds of the polymer allows release of the BCNU, which diffuses into the surrounding brain tissue. This delivery system was proven superior to systemic administration in animal models and demonstrated limited systemic toxicity[56]. The wafers have been shown to release BCNU *in vivo* over a period of 21 days, the majority of the drug release taking place in the first 5-7 days[57,58] and to degrade completely over a period of 6-8 weeks, with the polymer degradation products being eliminated through the urine[57,59,60].

Efficacy of BCNU-loaded wafers in high-grade glioma has been tested in three randomised, phase III trials. The first was performed in 222 patients with recurrent, malignant brain tumours requiring reoperation, the majority (approximately 62 % of each treatment group) being diagnosed with grade 4 astrocytoma[61]. Patients were randomly assigned to receive biodegradable polymer discs that were either loaded with 3.85% BCNU or not. The median survival of those receiving carmustine-loaded polymer was significantly better than in those receiving the placebo polymer alone (31 weeks vs 23 weeks respectively, $p = 0.006$). Analysing only those with grade 4 astrocytoma, mortality at 6 months was significantly reduced in those receiving BCNU-loaded polymer compared to those receiving the placebo polymer alone (44% vs 64% respectively, $p = 0.02$). Based upon this the Food and Drug Administration of the US approved the use of this treatment in those with recurrent grade 4 astrocytoma, although closer analysis revealed that the survival benefit at 6 months with treatment is lost at 1 year, when no difference in survival between the groups was seen.

Two trials then examined the effect of the drug-loaded wafers on newly diagnosed high-grade gliomas. The first trial was a randomised, double-blind study in only 32 patients[62]. Again, patients were randomised to receive BCNU-loaded polymer discs at the time of surgery or placebo discs. Those in the treatment group had a significantly longer median survival compared to the placebo group (58.1 weeks vs 39.9 weeks respectively, $p = 0.012$). A larger randomised, placebo-controlled trial of 240 patients

followed[63]. The patients again underwent gross total resection and were randomised to receive BCNU-loaded polymer wafers or placebo. Again, the majority of patients had grade 4 astrocytoma. The median survival of those in the treatment group was again significantly greater than those in the placebo group (13.9 months vs 11.6 months respectively, $p = 0.03$). However, the progression free survival in each group was not significantly different and found to be 5.9 months. And, when those with grade 4 astrocytoma were analysed as group, the difference in median survival in the treatment and placebo groups were not significantly different (13.5 months vs 11.4 months respectively, $p = 0.10$).

Overall, there is no robust data supporting a survival benefit to delivering BCNU locally via degradable polymer wafers following resection in grade 4 astrocytoma. However, this is not surprising. The wafers allow delivery of BCNU at high concentrations of up to only 12 mm from the site of the polymer, as demonstrated in animal models[57], while distant regions of the brain are exposed only to very low concentrations[64]. Again, the distant islands of infiltrative cells would be left relatively untouched.

Furthermore, these studies with BCNU-loaded wafers revealed complications of local delivery. During the phase III clinical trials, the complication rate of the treatment group was similar to that of the placebo group[62,63]. However, in clinical practice more treatment-related complications were identified. The rate of post-craniotomy surgical infection after BCNU wafer placement was reported to be as high as 28%[65]. Extensive cerebral oedema that led to severe neurologic complication and death was also associated with BCNU wafer placement[66]. A case report also described obstructive hydrocephalus, severe toxicity and death following BCNU wafer placement when resection had led to a large opening in the ventricle[67].

Drug delivery via polymer wafers relies upon diffusion to distribute the drug through the brain. In an attempt to increase that distance a method of utilising convection to supplement diffusion has been developed, and is known as convection-enhanced delivery (CED)[68]. Convection results from a simple pressure gradient generated by a pump that pushes solute through a catheter targeted within the brain. Resulting bulk flow of interstitial fluid mediates the distribution of the solute, enhancing interstitial drug distribution. To perform CED, one or more catheters are stereotactically

implanted into the desired location via a burr hole or craniotomy. Many phase I and II clinical trials have established the safety of a variety of agents delivered by CED in those with malignant glioma, and include conventional chemotherapeutics[69], cytotoxin-ligand conjugates targeting cell surface receptors[66], monoclonal antibodies with[70] or without[71] radioactive isotope conjugates, antisense oligonucleotides[72], and liposomal vectors engineered to deliver gene therapies[73]. As CED is supposedly more efficient than diffusion-only-mediated delivery, CED infused doses do not need to be as high, thereby limiting local toxicity.

There has only been one completed phase III trial using CED[74]. 296 patients presenting with first recurrence of grade 4 astrocytoma were randomised to receive either carmustine-impregnated polymer wafers or cintredekin besudotox delivered by CED following tumour resection. Cintredekin besudotox is a recombinant chimeric cytotoxin composed of human interleukin-13 (IL13) fused to a truncated, mutated form of *Pseudomonas aeruginosa* exotoxin A. This agent targets and kills tumour cells that express the IL13 receptor, which has been found to have a higher expression in malignant glioma than in low-grade disease of non-neoplastic glia[75]. No significant survival difference was found between the two treatment arms. In spite of several design flaws, including a statistical design that required a greater than 50% survival benefit over the active control arm; no other agents, even those FDA approved, having come close to this mark for recurrent grade 4 astrocytoma, CED overall has been limited by many technological factors. The first is that of catheter design. Early catheters were complicated by significant backflow around the catheter and along the insertion tract: real-time MRI has documented that reflux can be seen along the insertion tract in up to 20% of catheter placements[76]. Furthermore, considerable variability exists between neurosurgeons in surgical technique and placement accuracy: only 68% of catheter placements were performed per protocol specifications in the above phase III trial. Not only is research being conducted in improving catheter design, but also in producing software algorithms that define optimal trajectories that can be incorporated into the intraoperative navigation system typically used by neurosurgeons.

Overall, there has been lack of study into the actual volume of distribution of these drugs in those with disease. The volume of drug distribution achievable has been reported as approximately 570 mm^3 in normal brains of non-human primates[77].

Although the distribution of drug via CED in normal brain is altered by the presence of tumour[76], it has been shown that a drug delivered by CED can penetrate the infiltrative cells at the margin of grade 4 astrocytoma[78]. However, whether CED can deliver drug to distant sites of infiltrative cells to an extent that can impact upon survival significantly has yet to be determined.

1.5.3.2 Drug Resistance

It has been clearly demonstrated that those in whom the *MGMT* promoter is unmethylated i.e. those in whom DNA repair should be intact, temozolomide does not confer a survival benefit[24]. Furthermore, even those in whom the *MGMT* promoter is methylated will eventually succumb to their disease[79], indicating that there must be mechanisms that underlie chemotherapy resistance.

Several of these mechanisms involve DNA repair pathways. For example, the base excision repair pathway. Interestingly, temozolomide causes alkylation of guanine at the O^6 position only 7% of the time. More commonly, alkylation occurs at the N-7 position of guanine and the N-3 position of adenine, and can also occur at abasic sites. The base excision repair pathway mediates repair at these sites and several enzymes are implicated. Activity of poly (ADP-ribose) polymerase (PARP), another family of proteins involved in DNA repair, has been shown to be directly related to temozolomide resistance[80-82], where inhibition of PARP increases susceptibility to temozolomide[81]. Based upon this, a phase I/II trial of temozolomide and the PARP inhibitor ABT-888 was conduced in patients with recurrent, temozolomide-resistant, grade 4 astrocytoma[83] to establish drug dosing, scheduling, and a safety profile. A phase III trial to analyse efficacy awaits. Additionally, *in vitro* and *in vivo* evidence has demonstrated that alkyladenine-DNA glycosylase, the sole enzyme that excises the methyl group from the N-3 position of adenine, and Ape1, the major human abasic site endonuclease, mediate temozolomide resistance[84].

Another DNA repair pathway implicated in drug resistance is the mismatch repair (MMR) pathway. This pathway addresses insertion/deletion loops, and base-base mismatches. The system degrades the error-containing section of the newly synthesized DNA strand and thereby provides DNA polymerase with another chance to generate an error free copy of the template sequence[85]. Aberrant expression of the MMR pathway[86] and upregulation of certain components have been associated with temozolomide resistance[85].

Recently, a novel pathway involving microRNA has been implicated in temozolomide resistance. cMyc is a transcription factor involved in cell cycle progression and apoptosis that is often constitutively expressed in cancer cells. *in vitro* and *in vivo* studies have shown it to be an important positive upstream regulator of the newly described microRNA miR-29c/REV3L axis: cMyc upregulation drives the downregulation of miR-29c, releasing its inhibition on REV3L, a DNA repair polymerase, resulting in increased REV3L expression, and consequent enhanced DNA repair capacity[87]. And hence, another mechanism of temozolomide resistance may be REV3L over expression and consequent sustained DNA repair.

Several other modes of resistance have also been elucidated. One is that of intratumoural heterogeneity. When multiple, spatially distinct biopsies were taken from several grade 4 astrocytomas, significant intratumoural heterogeneity at the transcriptional, methylation, and mutational level was demonstrated[86]. For example, 14% of the cases demonstrated intratumoural heterogeneity in *MGMT* promoter methylation levels with the percentage of methylation varying up to 4-fold within each case. Such intratumoural heterogeneity likely underlies not only resistance to treatment, but explains partial and variable responses to treatment. Interestingly, temozolomide itself has been implicated in promoting drug resistance. Recently, it has been suggested that in *MGMT* promoter methylated patients, treatment with temozolomide induces a hypermutated phenotype, resulting in DNA repair deficiency and enhanced chemo-resistance.

Overall, drug resistance is multi-modal and a significant limitation to chemotherapy.

1.6 Summary

Grade 4 astrocytoma is the commonest primary brain tumour. Despite advances in surgical technique, radiation, and chemotherapy, its prognosis remains poor. Overcoming its diffuse and infiltrative character is a challenge. Surgery and radiation focus on the main enhancing bulk of the disease. Chemotherapeutics are limited by the BBB and resistance mechanisms. It is clear a new approach to treating grade 4 astrocytoma is needed.

Chapter 2 Photodynamic Therapy

PDT is a method of achieving tumour cell kill where a photosensitising agent that localises relatively specifically in the tumour is administered and then activated by light of a specific wavelength. This leads to a sequence of photochemical and photobiologic processes that cause irreversible photodamage to tumour tissue[88].

2.1 Background

Light has been used as therapy for more than 3000 years[89,90]. Ancient Egyptian, Indian and Chinese civilisations used light to treat various diseases including rickets, psoriasis, vitiligo, and skin cancer[91]. At the beginning of the 20th century in Denmark, Niels Finsen discovered the use of red light to treat small pox and UV light from the sun to treat cutaneous tuberculosis, discoveries for which he was subsequently awarded the Nobel Prize[92]. Around the same time, researchers found that certain chemicals in the presence of light would cause cell death. Certain wavelengths of light were found to be lethal to infusoria in the presence of acridine[93]. The development of dermatitis in an epilepsy patient being treated with oral eosin heralded the treatment of skin tumours with topically applied eosin and white light[93]. This interaction between chemical and light was termed 'photodynamic action.'

A decade later, the interaction between porphyrins, which had been identified as being associated with porphyria and skin sensitivity in the mid 1800s, and light was being investigated. Exposure of *Paramecium* and red blood cells to haematoporphyrin and light was found to be lethal. Then in 1975, the combination of haemotoporphyrin derivative (HpD), which was synthesised in the 1960s[94] and could be administered at much smaller doses than crude haematoporphyrin, and red light was found to completely eradicate mammary tumour growth[95] and bladder carcinoma[96] in mice. And thus, the foundations for human trials were laid.

2.2 Mechanism of Action

PDT requires three components, which individually are non-toxic: the first is the photosensitiser, the second is light of a specific wavelength that can activate the photosensitiser, and the third is oxygen. When the photosensitiser is activated by light of a specific wavelength, by absorbing photons, the photosensitiser is transformed from its ground, singlet state into a relatively long-lived, electronically excited, triplet state,

via a short-lived, excited, singlet state (see Figure 3). The photosensitiser in its excited, triplet state, can then undergo two reactions, both of which result in the formation of singlet oxygen, a highly reactive oxygen species[97]. Firstly, it can react directly with a substrate, such as the cell membrane or a molecule and transfer an electron to form free radicals, which can interact with oxygen to produce singlet oxygen: this is termed a type I reaction. Alternatively, as the excited, triplet state photosensitiser returns to its ground, singlet state, it transfers its energy to ground state triplet oxygen, again producing singlet oxygen: this is termed a type II reaction. Both type 1 and type II reactions occur simultaneously, and the ratio between these processes depends on the type of sensitiser used, the concentrations of substrate and oxygen, and the binding affinity of the sensitiser for the substrate[98]. Nevertheless, it is the resulting singlet oxygen that then mediates cell death.

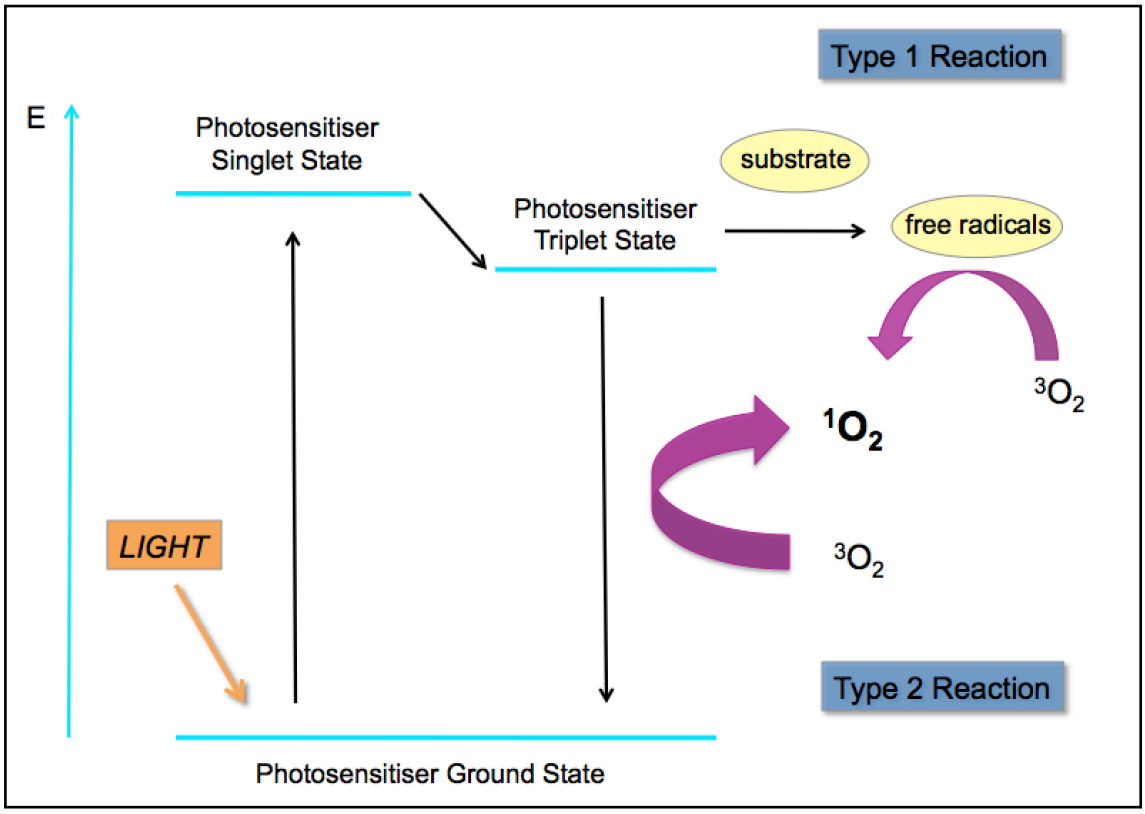

Figure 3 Photodynamic therapy: mechanism of action

When a photosensitiser is activated by light of a specific wavelength it is transformed from its ground, singlet state into a relatively long-lived, electronically excited, triplet state, via a short-lived, excited, singlet state. In its excited, triplet state, it can undergo two reactions. Firstly, it can react directly with a substrate, such as the cell membrane, to form free radicals, which can interact with oxygen to produce singlet oxygen ($^1O_2$): a type I reaction. Alternatively, as the excited, triplet state photosensitiser returns to its ground, singlet state, it transfers its energy to ground state triplet oxygen ($^3O_2$), again producing singlet oxygen: a type II reaction.

Cell death mediated by singlet oxygen can occur via three main mechanisms[88]. Firstly, singlet oxygen can kill cells directly. Secondly, singlet oxygen can damage tumour-associated vasculature, leading to tumour infarction. And finally, this damage that is caused can activate an immune response against the tumour. Although the relative importance of each for the overall tumour response is yet to be defined, it is clear that the combination of all these components is required for long-term tumour control.

The actual extent of photodamage and cytotoxicity that singlet oxygen can impart onto a tumour is determined by several factors. These include the type of photosensitiser, its extracellular and intracellular localisation, and the total dose administered, as well as the total light exposure dose, light fluence rate, oxygen availability, and the time between the administration of the drug and light exposure. Having established a vast library of photosensitisers and an understanding of the wavelengths of light that can activate them and the singlet oxygen that can be produced[99], more recent *in vitro* and *in vivo* studies focus their efforts on studying these variables and finding the optimum conditions that lead to maximum tumour kill.

2.3 Advantages of PDT

By virtue of its mechanism of action, PDT has several unique advantages over conventional therapies. Firstly, PDT is associated with very little toxicity. In the absence of light of a specific wavelength, photosensitisers themselves have very little effect, with only some causing self-limiting changes to liver function if given at high dosages. Its most significant side effect is that of skin and eye photosensitivity, which can last from a few hours to a few months depending on the photosensitiser. The danger comes from prolonged exposure to direct sunlight, and like sun burn, the effect is not immediately noticeable, only becoming apparent a few hours later. Patients must be educated about this and are advised to wear dark glasses and to cover areas of exposed skin when exposed to bright lights until the drug level in the body has fallen to safe levels. If these precautions are adhered to, problems are very rare, and the effects of PDT relatively innocuous.

Secondly, the photodynamic effect is largely localised to tumour tissue, leaving the surrounding normal tissues relatively untouched. The reasons for this are multifactorial. Initially, it was thought that selective uptake of the photosensitiser into the tumour

accounted for the selective effect. To some extent this is true. The peak concentration of the photosensitiser in tumour often occurs later after drug administration than the peak in adjacent normal tissue. In most organs, the ratio of photosensitiser concentration in tumour to normal tissue ranges from 2-3:1. This is enough to allow the identification of precancerous and cancerous lesions, photodynamic diagnosis (see below). However, this is not enough to account for the selectivity of the photodynamic effect. It is now recognised that the selective effect comes from careful targeting of the activating light[100], and also the timing of light delivery to coincide with peak photosensitiser concentration in tumour tissue. Furthermore, as singlet oxygen is highly reactive with a short half-life, only cells close to the area of its production are affected: the half life of singlet oxygen in biological systems is < 0.04 μs and therefore its radius of action is < 0.02 μm. Importantly, PDT is a cold photochemical reaction[101]; there is no tissue heating and connective tissues such as collagen and elastin are largely unaffected. There is therefore much less risk to the integrity of the underlying structures than with thermal laser techniques and surgery, and for this reason, many PDT treated areas also heal with more regeneration and less scarring. This is particularly attractive when treating lesions of the skin, head and neck, and hollow organs, where PDT not only leads to minimal loss of tissue, which can be important cosmetically, but also minimal loss of function.

Thirdly, unlike radiation, which is limited by the amount of ionising radiation that normal tissues can tolerate over time, PDT is not limited by cumulative toxicity. For this reason, PDT has the potential to be given repeatedly, and to be given to tissues that have already been exposed to maximum ionising radiation. Lastly, there is little evidence for the development of resistance to PDT. Overall, for the treatment of cancer, PDT is a safe and complementary adjunct to the conventional therapies of surgery, radiation and chemotherapy.

2.4 Clinical Applications of PDT

In the clinical setting, PDT requires two steps. Firstly, the photosensitiser is administered, either systemically (intravenous or oral), or by topical application. Secondly, after a time interval that varies between minutes and days depending on the photosensitiser, allowing tissue accumulation of the photosensitiser, the light is applied to the site of disease.

2.4.1 Photosensitisers

The first photosensitisers were derived from the naturally occurring, endogenous, porphyrins: the first generation. In overcoming some of the photochemical limitations associated with these, a second wave of completely synthetic compounds that were still based upon the tetrapyrolic structure of the porphyrins was developed: the second generation. More recently, the focus has been on targeting approaches to increase photosensitiser affinity to tumour tissue, and hence the third generation.

2.4.1.1 First Generation Photosensitisers

In 1841, it was discovered that when haemoglobin is subjected to acid hydrolysis, removing the protein and iron, a red-purple substance is left. A few years later in 1844, the chemical composition of this substance was determined, and it was called 'haematin,' later to be renamed 'haematoporphyrin,' after the Greek for purple, 'porphyrus.' Haematoporphyrin was later recognised to confer a powerful photosensitive effect, and in the search of a more soluble photosensitiser, it was treated with sulphuric acid in acetic acid at room temperature for 15 mins, then precipitated out with aqueous sodium acetate, then treated with alkali before neutralisation to a pH of 7.4. This led to a preparation containing a mixture of di- and oligomeric porphyrins that was an extremely powerful photosensitiser, which was called haematoporphyrin derivative (HpD). Commercial development led to various proprietary photosensitisers of which Photofrin® received the first regulatory approval.

PDT was first approved in 1993 in Canada, using Photofrin® for the prophylactic treatment of bladder cancer. As a first generation photosensitiser, it has some limitations. Firstly, the wavelength of light needed for activation, 630 nm, does not have high tissue penetration, and its depth of effect is limited to 0.5 cm. Secondly, its absorption band, measured by the molar absorption coefficient, at this wavelength is weak, 1.170 $M^{-1}cm^{-1}$, therefore its efficiency at transferring energy from light to cytotoxic products is moderate, with a quantum yield of singlet oxygen of 0.01-0.09[99]. Another important consideration is that eye and skin photosensitivity persists for many weeks and patients who have been treated with Photofrin® have to avoid sunlight for 4-6 weeks.

Another endogenous porphyrin in commercial use as a photosensitiser is 5-ALA, sold as Gliolan®. This is a naturally occurring precursor in the haeme biosynthetic pathway. It is a prodrug that is converted endogenously to protoporphyrin IX, which is the

photosensitiser. It is versatile in that it can be administered topically, orally, or intravenously. Although it can be activated by several wavelengths of light, 546, 630 and 646 nm, the quantum yield of singlet oxygen at these wavelengths, 0.54, 0.54 and 0.60, respectively, is modest[99]. Its depth of use is largely constratined to < 0.2 cm. However, one significant benefit is that light sensitivity only lasts 1-2 days. Methyl-ALA and Hex-ALA have also be manufactured as hydrochlorides and sold as Metvix® and Hexvix®, respectively.

2.4.1.2 Second Generation Photosensitisers

To overcome the shortcomings of the endogenous porphyrins, a second generation of photosensitisere were synthetically developed to have longer activation wavelengths and therefore increased depth of effect, higher yields of singlet oxygen, better tumour selectivity, and shorter periods of photosensitivity. Their chemical configuration was based upon the tetrapyrolic structure of the porphyrin.

One of the most thoroughly investigated class of second generation photosensitiser is the chlorins. *meta*-tetrahydroxyphenyl chlorin (*m*THPC), with the generic name Temoporfin®, and the proprietary name Foscan, is a synthetic chlorin and a potent photosensitiser. It is activated by light with a wavelength of 652 nm and its quantum yield of singlet oxygen is 0.3[99]. It has a residual photosensitivity of only 2 weeks.

Other compounds include the benzoporphyrins (Visudyne®) and porphycene (ATMPn). Metallated derivative have also been synthesized (Al, AlPcS4; Si, SiNC; and Sn, SnEt2), although there is no consistent correlation between metallation and increased photodynamic activity[102].

2.4.1.3 Third Generation Photosensitisers

More recently, targeting strategies have been shown to increase the affinity of the photosensitiser for tumour tissue[103]. There have also been reports of selectivity targeting subcellular compartments, including mitochondria[104]. These targeting approaches have led to a third generation of photosensitiser. The potential for these will be discussed further in the Conclusion.

2.4.2 Light sources

Light sources must provide enough light of an appropriate wavelength, in an acceptable treatment time, and with a spatial distribution that matches the target tissue geometry. The three main types of light source in use are filtered high-brightness lamps, light

emitting diode arrays, and continuous wave lasers. In this way, light can be delivered with relative ease to superficial targets, such as the skin and eye, and to hollow organs, such as the oesophagus and bronchus.

Delivery of light to solid organs requires more sophistication. In such cases, light can be delivered directly into the solid tumour by feeding thin diffusing laser fibres through needles placed into the tumour under image guidance: interstitial PDT[101]. This type of treatment requires all light sources to be placed in an equidistant, parallel arrangement to ensure even light distribution. There is a clear parallel with interstitial radiotherapy. The needles can then be partly withdrawn to expose the fibres such that light from each fibre is emitted in a cylindrical distribution. In this way, layers of tumour can be treated, resulting in necrosis throughout even very large tumours. The necrotic tissue is resorbed rather than sloughing off.

2.4.3 Clinical Applications

PDT has mainly been approved for use in treating cancerous and pre-cancerous conditions. However, it has also been approved for use in vascular disease and also in treating infections.

2.4.3.1 Cancerous and pre-cancerous conditions

PDT is a well-established treatment modality in dermatology where it is used to treat superficial non-melanoma skin cancers and precancers such as actinic keratosis, Bowen's disease, and basal cell carcinoma[105]. The photosensitiser commonly used is methyl-ALA, which can be applied topically as a cream. Healing is excellent with minimal scarring, even over bone where the skin has poor vascularity. Although conventional treatments such as surgical excision, cryotherapy, and radiation work well, PDT is of special value for lesions in cosmetically and functionally sensitive areas such as the head and neck region.

Advanced cancers of the lips, tongue, mouth and pharynx carry great morbidity. Heroic surgery is feasible, but is often associated with loss of function (speech, mastication, and swallowing), and is markedly disfiguring. Radiation dries saliva production and destroys bone. PDT with *m*THPC is approved for the treatment of advanced head and neck cancers in those who have failed, or would not tolerate, conventional treatments[101].

PDT has also been approved for use in cancerous and precancerous lesions in hollow organs. By the time lung cancer becomes symptomatic, it is often too advanced for curative treatment. For bulky cancers that are bleeding or causing mechanical obstruction of a major airway, palliative endoscopic re-canalisation using PDT mediated by Photofrin® is an approved treatment. Furthermore, in early lung cancers that have not spread beyond the bronchial wall, PDT is approved for treatment in those who are not fit for surgery or chemoradiation[106]. Barrett's oesophagus, secondary to chronic and excessive reflux, is common and 10-15% of those suffering from it will go on to develop dysplasia, which left untreated will progress to oesophageal cancer. If detected early enough, this can be treated endoscopically with PDT mediated by Photofrin® or radiofrequency ablation. The latter is preferred as it is simpler. However, if the cancer has spread to the deeper layers of the oesophageal wall but no further, PDT is possible, but radiofrequency is not, in patients deemed unfit for surgery and chemoradiation. Hex-ALA has also been approved for the detection of early cancer and precancerous lesions of the bladder (photodynamic diagnosis, see below).

Studies into the use of PDT for the treatment of solid organ cancers are ongoing. The main challenge is light delivery, as discussed above. Organs being investigated include the pancreas, prostate, breast, and bone.

2.4.3.2 Vascular disease

Wet age-related macular degeneration is where macular degeneration is exacerbated by neovascularisation of the macula. PDT mediated by the photosensitiser Visudyne® has been approved in the UK and the US for the treatment of this, and has been shown to prevent disease progression for at least 5 years.

Interestingly, preclinical studies have shown that PDT can reduce the stenosis due to proliferation of arterial smooth muscle cells after balloon angioplasty without reducing the mechanical strength of the artery and without increasing the incidence of thrombosis[100]. Pilot studies of adjuvant PDT after repeat angioplasty for recurrent femoral artery stenosis have shown a low incidence of subsequent restenosis. PDT is an attractive alternative to drug eluting stents at sites of arterial narrowing suitable for balloon angioplasty but unsuitable for stenting[107].

2.4.3.3 Infection

PDT using methylene blue as the photosensitiser is an approved treatment for gum periodonitis that is used widely, particularly in Canada. With an increasing incidence in antibiotic resistant organisms, novel anti-infective therapies are being sought. Studies are underway to investigate the use PDT to treat skin infections, including infected ulcers and acne. Studies are planned for using PDT to sterilize indwelling items such as urinary catheters and the tissue bed if infected joint prostheses have to be removed.

2.5 Clinical Applications in Neurosurgery

Gliomas were one of the first pathologies that the effectiveness of PDT was tested in. In 1972, haematoporphyrin followed by light therapy was proven to be lethal both to glioma cells in culture and in those transplanted subcutaneously in rats[108]. PDT is particularly attractive for use in the brain as its relatively selective action on tumour tissue would leave delicate and potentially eloquent brain tissue untouched. Overall, this should translate into little risk for the development of short- or long-term neurological deficits.

2.5.1 Photosensitiser Localisation

There is evidence that photosensitiers are taken up and retained preferentially by neoplastic tissue. However, this effect is generally not sufficiently pronounced to allow a selective clinical response, except in brain tissue[109], where the absence of the BBB around the tumour aids this selectivity. The ratio of the concentration in tumour to normal brain ranges from 2.5:1 to 4:1 for HpD[110,111], is 4:1 for 5-ALA, and 10:1 for *m*THPC[112].

Despite this preferential uptake, there is some injury to the surrounding normal glia and neurons[113-116], the degree of damage depending on the photosensitiser and its concentration, the time interval of sensitisation to light exposure, and the light density. In animal models, PDT has been shown to initially cause break down of the BBB, swelling of astrocytes and neurones, and after 24 hours, coagulation necrosis in the brain surrounding the tumour. Nevertheless, clinically, this translates very rarely into temporarily increased intracranial pressure that is non-fatal and amenable to standard medical treatment. Overall, therefore, the preferential uptake of photosensitisers into brain tumours is significant enough for a selective clinical response.

2.5.2 Photodynamic Diagnosis and Fluorescence Guided Resection

The type I and II reactions that a photosensitiser undergoes as it returns to its ground state following excitation by a light of a specific wavelength has been discussed, and are what mediate photodynamic-mediated cell death. Additionally, as the photosentiser returns to its ground state, it can also release energy in the form of light, fluorescence. The preferential uptake of photosensitisers into brain tumours and their ability to fluoresce upon excitation by light has been used to delineate the characteristically indistinct borders of high-grade gliomas, termed photodynamic diagnosis (PDD), and to guide resection, fluorescence-guided resection (FGR).

As discussed above, 5-ALA mediated FGR of high-grade glioma has been evaluated in a multi-centre phase III trial[34] where FGR was shown to lead to a significantly higher frequency of complete resections of contrast-enhancing tumours as shown on early postoperative MRI. This translated into a significantly higher 6 month progression-free survival, but did not improve overall survival.

2.5.3 Photodynamic Therapy

Supported by *in vitro*[117,118] and *in vivo* studies[113,118,119], PDT for gliomas was tested in humans. It was applied as an adjunct to surgery, radiotherapy, and chemotherapy in patients with high-grade gliomas, as well as other types of intracranial tumours. PDT was given intraoperatively: patients were typically given the first generation photosensitiser, HpD, prior to surgery, then following either subtotal or gross total resection, the tumour cavity was exposed to light from various types of sources.

The earliest reports of PDT being used to treat high-grade gliomas are from the 1980s[120,121]. No survival advantage was gained. However, PDT was found to be safe and ongoing testing was deemed feasible. Since then, a number of small case series were published. A European group presented 11 patients with grade 4 astrocytoma and 39 patients with recurrent grade 4 astrocytoma treated with PDT[122]. The median survival of those with primary disease was 19 months and the median survival of those with recurrent disease was 7 months. A Canadian group reported on 12 patients with newly diagnosed, and 37 patients with recurrent, grade 4 astrocytoma treated with PDT[123]. For those with newly diagnosed disease, the median survival was 33 weeks with a 1 and 2-year survival of 33 and 0%, respectively. For those with recurrent disease, the median survival was 29 weeks with 1 and 2-year survival of 19 and 3%, respectively.

The largest series examining the effect of PDT on high-grade glioma to date is from Australia and reports on 136 patients[124]. All patients with newly diagnosed tumours had standard postoperative radiotherapy and all those with recurrent tumour had been previously treated with radiotherapy. Chemotherapy was administered to 29% of patients in the study. Focusing on those with grade 4 astrocytoma, which made up over 60% of the subjects, the median survival for patients with newly diagnosed grade 4 astrocytoma (n=31) was 14.3 months, with 25% surviving for more than 36 months and 22% surviving for more than 60 months. Furthermore, for those with recurrent disease (n=55), the median survival was 14.9 months from the time of reoperation, with 41% surviving beyond 24 months and 37% survival beyond 36 months. PDT was only complicated by cerebral oedema in 3 patients, which responded to standard medical therapy. There were no deaths associated with PDT.

The European and Australian data are certainly compelling, indicating that PDT conferred at least a comparable survival advantage to chemotherapy, with considerably less side effects. The difference in findings between the European and Australian groups, and that of the studies in the 1980s and the Canadian group, highlights the importance of light dose. The mean light dose in the early studies ranged between 0.9 and 9 J/cm^2, and in the Canadian study was 58 ± 17 J/cm^2, whereas the mean light dose in the European study was up to 260 J/cm^2 and in the Australian study was 230 J/cm^2. Light dosimetry is certainly important and underdosing the total light dose may be an important contributing factor to many treatment failures.

Whether the degree of photosensitiser uptake into the tumour is associated with the degree of PDT effect is unclear. Work performed by the Australian group demonstrated that the greater the uptake of photosensitiser into the tumour, the better the outcome following PDT in patients with high-grade astrocytoma[125]. This would be consistent with greater singlet oxygen production, and hence greater tumour kill, with greater tumour uptake of photosensitiser. However, this relationship was not demonstrated by the European group[122]. It is possible that a higher tissue concentration of photosensitiser leads to greater light absorption and consequently, less light penetration into the deeper tissues, and hence, a paradoxically lesser PDT effect.

Although encouraging, the case series above are difficult to interpret, as there was no uniformity as to the degree of surgical resection or to the radiotherapy or chemotherapy regimes, predating our current standard of care with temozolomide chemotherapy, as described above. The results from a randomised, phase III trial of PDT for high-grade glioma using HpD were reported at an international meeting by the Canadian group (Muller *et al*., Proceedings of the International Photodynamic Symposium, Brixen, Italy, 2006). The trial did not reveal a survival advantage with PDT. However, results were confounded by the substantial degree of residual tumour left following resection.

2.5.3 Combining Fluorescence Guided Resection and Photodynamic Therapy

As discussed, there is increasing evidence to support that the degree of surgical resection influences survival[32-34]. Respecting this concept, and in light of the findings from the only phase III trial investigating PDT (Muller *et al*., Proceedings of the International Photodynamic Symposium, Brixen, Italy, 2006), the effect of combining FGR and PDT on patients with high-grade glioma has been investigated.

A phase II study involving 22 patients with radiological findings consistent with grade 4 astrocytoma was undertaken to assess the feasibility and effectiveness of combining FGR and intraoperative PDT using the photosensitiser *m*THPC[126]. Patients were given the photosensitiser 4 days prior to surgery to allow it time to reach its maximum concentration within the tumour. At the time of surgery, gross total resection of the tumour was undertaken in the usual fashion. The tumour cavity was then exposed to blue light: *m*THPC has a strong absorption band in the blue-wavelength range, which leads to strong fluorescence in the red part of the visible spectrum, with emission peaks at 652 and 718 nm. The resection was then carried out until no fluorescence was visible. Once FGR was complete, PDT was performed with light at a wavelength of 652 nm. From biopsies taken from fluorescent and non-fluorescent areas, PDD with *m*THPC was found to have a sensitivity and specificity of 87.9% and 95.7%, respectively. A gross total resection, assessed by MRI within 48 hours of surgery, was demonstrated in 75% of patients who underwent FGR/PDT, but only in 52% of the matched pair control group. Furthermore, the median survival for the FGR/PDT group was 9 months, compared to 3.5 months in the matched pair control group. Morbidity included two severe toxic reactions to sunlight, due to inadvertent exposure to direct sunlight, and one patient experienced temporary cerebral oedema, which was responsive to standard medical therapies. This study demonstrated that combining FGR and PDT is feasible and safe, and together, are likely to confer a survival advantage.

A phase III randomised controlled trial was conducted to investigate the effect of 5-ALA and Photofrin® mediated FGR and PDT in patients with grade 4 astrocytoma[127]. 27 patients from a single centre were recruited for this study and 13 were randomised to the study group, and 14 to the control group. Those in the study group received Photofrin® intravenously 48 hrs prior to surgery. Then 3 hrs prior to surgery, they were also given 5-ALA orally. They then underwent gross total resection using standard microsurgical techniques, following which blue light was shone into the tumour cavity, and FGR was used to maximise tumour resection. Once tumour resection was complete, a silicone balloon catheter was inflated to fit the surgical cavity and tunnelled out through the skin. Through this catheter, light at a wavelength of 630 nm could be delivered via a diode laser into the tumour cavity, with a goal dose of 100 J/cm^2. 5 'light' treatments were given: one in the recovery room immediately following surgery, then daily for the next 4 days. The patients also received standard radiotherapy, and were followed every 3 months. Those in the control group underwent gross total resection using standard microsurgical techniques followed by standard radiotherapy. The mean survival of the study group was 52.8 weeks compared to 24.6 weeks in the control group ($p < 0.01$). The study group gained on average 20 points on the Karnofsky performance score ($p < 0.05$). There were no differences in complications or hospital stay between the two groups. The mean time to tumour progression was 8.6 months in the study group compared to 4.8 months in the control group ($p < 0.05$). Although this study was conducted in a small population, the results are certainly encouraging, demonstrating that in combination, FGR and PDT can confer a survival advantage with little morbidity.

The rationale for using two photosensitisers in this phase III trial was that although 5-ALA produces robust fluorescence, its half-life was too short to mediate PDT over 5 days. In contrast, Photofrin®, as a result of being a mixture of molecules that tend to oligomerise, produces variable fluorescence, and also the fluorescence was noted to be very dark red and difficult to see. However, the half-life of Photofrin® allows it to mediate PDT over 5 days. The 'repetitive' PDT technique used here, otherwise termed 'metronomic,' can be likened to the fractionation of radiotherapy. By having a break between 'treatments,' oxygen, an essential component for the photodynamic effect, can be replenished, as can fresh photosensitiser, repleting drug that has been photobleached.

The combination of FGR and PDT certainly seems to have a promising effect in the treatment of grade 4 astroyctoma. Studies with larger numbers of patients all receiving current standard of care with temozolomide chemotherapy are required.

2.5.4 Limitations of PDT

PDT has several advantages over conventional therapies. Being a cold photochemical process with a relatively selective effect on tumour tissue, preserving the surrounding normal brain, leaves little potential for the long term neurocognitive effects that can be associated with radiotherapy. Furthermore, compared to chemotherapeutic agents, side effects are rare, and residual photosensitivity is short-lived and tolerable with the correct precautions. However, PDT remains a focal treatment: light can only penetrate a certain distance, and hence, PDT does not address the diffuse nature of high-grade astrocytoma. Although PDT can induce a host immune response against the tumour, how this contributes to overall tumour control has not been delineated. For PDT to truly improve the outcome of high-grade astrocytoma, a novel way of delivering light to the diffusely infiltrative tumour cells must be found. This study investigates bioluminescence as a novel source.

Chapter 3 Bioluminescence, A Novel Method of Light Delivery

Bioluminescence is the production and emission of light by a living organism. It is a type of chemiluminescence, a chemical reaction during which chemical energy is converted to light energy. Here, a background on bioluminescence will be given, and the possibility of bioluminescence as a light source for PDT will be explored.

3.1 Bioluminescence

The ability to generate bioluminescence exists widely in nature, throughout different ecosystems, and has evolved for several purposes that include defending against predators, hunting prey, and attracting mates. This capacity is most commonly found in species from the ocean, such as dinoflagellates, a type of plankton, and jellyfish, such as those from the *Aequorea* species[128]. Although more rare, terrestrial bioluminescence also exists, such as that from fireflies and click bettles.

In the majority of cases, bioluminescence requires two chemicals; one that produces light, which is generically termed 'luciferin,' and one that catalyses the reaction, which is generically termed 'luciferase.' Simply, luciferase catalyses the oxidation of luciferin, resulting in the generation of light and an inactive molecule, oxyluciferin (see Figure 4).

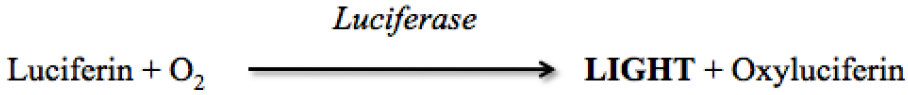

Figure 4 Simplified representation of chemiluminescence

Chemiluminescence results from the oxygenation of 'luciferin,' which is catalysed by 'luciferase.' When this occurs in a living, biological organism, the reaction is termed bioluminescence. O_2 denotes oxygen.

In actuality, the bioluminescence reaction is more complex, and draws parallels with the energy transfers that occur with the photodynamic reaction. For example, in a system that uses beetle luciferase, luciferin binds to the luciferase and then luciferin (LH_2) undergoes adenylation to form luciferyl adenylate (LH_2.AMP)[129]. An enzymatic base then extracts a proton from the 4-C of LH_2 in the LH_2.AMP, forming a carbanion, which reacts rapidly with oxygen. This results in the formation of a high energy, intermediate, dioxetane transition state and the removal of AMP[130]. Subsequent decarboxylation of this intermediate releases energy, which is efficiently transferred

into producing a high yield of singlet, excited state oxyluciferin (LO*). When this decays to ground state oxyluciferin (LO), a photon is emitted.

3.1.1 Wavelengths of Bioluminescence

As a reflection of the diverse habitats in which bioluminescent organisms exist, bioluminescence is produced in a range of colours of the visible electromagnetic spectrum. Most marine bioluminescence is expressed in the blue-green part of the spectrum, as most marine organisms are only sensitive to blue-green colours and are unable to process yellow, red, or violet colours. From land, fireflies emit 'yellow-green' light, while the related click beetle emits light that ranges from orange to green. Furthermore, due to incident light, terrestrial bioluminescence is often brighter: bioluminescent beetles have a quantum yield of light that is much higher than for any other system[131].

Some bioluminescent organisms will synthesize their own luciferin, such as dinoflagellates. However, others not able to synthesize luciferin must acquire it, such as some species of midshipman fish that obtain luciferin from the seed shrimp that they consume. Through evolution, luciferins have varied very little. In contrast, the enzyme, luciferase, is always synthesized by bioluminescent organisms and varies widely in different species. It is this variation in the expression of luciferase, in the setting of the stability of the luciferin, which underlies the range of bioluminescence in the visible electromagnetic spectrum. Interestingly, one organism can generate bioluminescence of different colours: the railroad worm (the larva of a beetle) has a head that will glow red whilst the body glows green. As only one type of luciferin is ingested, this is thought to be due the expression of different luciferases in the different parts of the body, a characteristic believed to have evolved to confuse and frighten predators.

3.1.2 Replicating Bioluminescence

Since the extensive study of bioluminescence in nature, the genes encoding several luciferases from different species have been cloned and are commercially available as reporter vectors, which are ready for cell cloning. Such vectors have been optimised for mammalian expression and fall into two main classes. First are those that encode coelenterazine-utilising luciferases from marine organisms. Coelenterazine is the 'luciferin' that is found in many aquatic organisms. It serves as the substrate for luciferases expressed by marine organisms such as *Renilla reniformis*, the sea pansy, and *Gaussia*, a genus of copepod. Then there are those that encode the benzothiazole

luciferin-utilising beetle luciferases from terrestrial organisms such as the firefly and click beetle.

3.1.3 Utilising Bioluminescence: Bioluminescence Imaging

In the field of tumour research, bioluminescence has gained popularity as a relatively inexpensive, fast, and simple method of imaging tumour progression and response to treatment in animal models. Several tumour cell lines, such as PC-3M-human prostate, A549-human lung, and HT-29-human colon cancer cells have been successfully transfected with the firefly luciferase gene (*luc*): with the addition of d-luciferin, a synthetic luciferase substrate, bioluminescence was demonstrated in all cell lines, and the degree of bioluminescence correlated highly with the number of cells ($r^2 = 0.99$)[132]. C6 rat glioma cells have also been successfully transfected with not only the firefly luciferase gene (*luc*), but also click beetle luciferases (CBGr68*luc* and CBRedl*uc*), and *Renilla reniformis* luciferase (*hRluc*). With the addition of the appropriate luciferin, all cells produced bioluminescence, each luciferase generating a bioluminescence in a different part of of the visible electromagnetic spectrum[133]. All these luciferase transfected cells lines have been transplanted subcutaneously[132], and in the case of the C6 transfected cells, into the liver and lungs of mice[133], where their ability to bioluminesce was maintained when the animals were given intraperitoneal (ip) luciferin. The bioluminescence was detected with the Xenogen IVIS system (Xenogen Corporation, Alameda, CA). When ready for imaging, the animals were anaesthesised with isofluorane, given an ip injection of luciferin, and placed in the imaging chamber, which was able to hold several mice and allowed maintenance of inhalational anaesthesia. The IVIS 100 cooled CCD camera system was used for emitted light acquisition and Living Image software (Xenogen Corp.) was used for data analysis. In all models, bioluminescence imaging (BLI) was found to provide a real-time, non-invasive, quantitative and sensitive analysis of tumour growth, metastasis, and response to therapy.

BLI has been developed most prominently in animal models of prostate cancer. 22Rv1 prostate tumour cells were transfected with *luc*, and once stable luciferase-expressing cells were obtained, they were injected into the left ventricle of a mouse model[134]. Bioluminescence of these transfected tumour cells, after ip injection of luciferin, revealed dissemination of tumour to bone, liver, and the adrenals, replicating tumour behaviour in humans. Subsequent tumour growth was monitored with BLI. Furthermore, BLI has also been used to identify metastases in animal models with

already established prostate cancer: injection of a prostate-specific adenovirus vector that also carries the *luc* gene, which can be expressed from an enhanced prostate-specific antigen promoter (AdPSE-BC-*luc*), demonstrated that the viral vector was not only able to localise to the lung and spinal metastases, but was able to produce sufficient bioluminescence to allow their detection once luciferin was given[135]. This has also been achieved using a lentivirus-based vector[136]. Additionally, a transgenic mouse model where the prostate gland is targeted with a vector carrying the *luc* gene under control of a small, but highly active and specific, supra prostate-specific antigen promoter, has been developed[137]. This model enabled real-time, BLI analysis of the development and responsiveness of the prostate gland to endogenous and exogenously administered androgen. These mice also allowed BLI examination of SV40 T antigen-induced prostate tumourigenesis and the subsequent tumour response to androgen ablation.

Whilst research into the diagnostic potential of bioluminescence is well developed, research into its therapeutic potential remains in infancy.

3.2 Bioluminescence-Mediated Photodynamic Therapy

Despite the many advantages of PDT, as discussed above, one of its biggest challenges lies in the delivery of adequate amounts of light, particularly to deep seated malignancies. Although interstitial PDT has tried to address this, light distribution over the tumour is not homogenous and if metastatic or infiltrative disease is not identified, it goes untreated.

The recognition that bioluminescence might be able to provide a targetable, endogenous light source to activate a photosensitiser, bioluminescence-mediated photodynamic therapy (bPDT) (see Figure 5), was first made in the 1994, in the search for novel ways to treat human immunodeficiency virus (HIV). At that time, although three compounds were approved for treatment, drug-resistant viral variants had already started to emerge, and there was urgency to finding alternative treatments. Hypericin, a naturally occurring photosensitiser, had an innate anti-viral action that was potentiated upon illumination. However, the ability to deliver light to such a diffuse blood-borne organism was challenging. Carpenter *et al*.[138] conducted an experiment to investigate whether a chemiluminescent reaction would be able to provide enough light to activate hypericin resulting in anti-viral action. Equine dermal cells were infected with equine

infectious anaemia virus and incubated with hypericin, luciferin and luciferase. Chemiluminescence was initiated by the addition of ATP. The anti-viral activity of hypericin was successfully induced by this chemiluminescence. Moreover, to ensure proximity of light source to photosensitiser, a tethered molecule of pseudohypericin–luciferin, without compromise to the anti-viral action of pseudohypericin was subsequently synthesised[139].

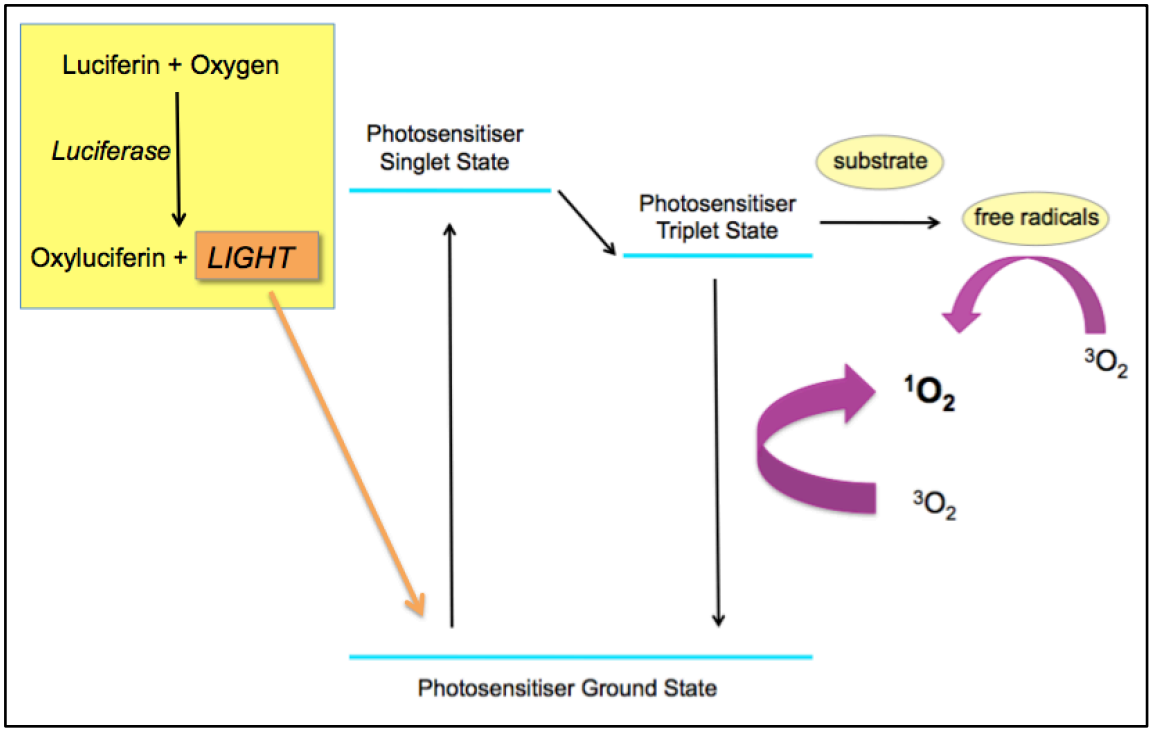

Figure 5 Bioluminescence-mediated photodynamic therapy

Diagramatic representation of bioluminescence-mediated photodynamic therapy: the use of bioluminescence, an endogenous light source, to activate a photosensitiser.

Nearly a decade later, in 2003, bioluminescence, generated by the addition of d-luciferin to luciferase-transfected NIH 3T3 cells, was reported to activate the photosensitser, rose bengal, causing significant phototoxicity and cell death[140]. Attempts at replicating this work by incubating two luciferase-transfected tumour cell lines with the photosensitisers rose bengal and hypericin in turn, then generating bioluminescence with d-luciferin, failed to demonstrate cell kill[141]. However, the doses of d-luciferin used were orders of magnitude less than that used in the first experiment: the maximum dose of d-luciferin used in this experiment was 20 μM compared to the

500 μM in the first study. The most likely reason for failure was that not enough light was generated to activate the photosensitiser.

Overall, the *in vitro* work demonstrates that enough light can be generated from bioluminescence/chemiluminescence to activate a photosensitser and achieve phototoxicity. bPDT is particularly attractive for the treatment of high-grade astrocytomas. Conventional PDT has been demonstrated to cause significant cell death in cell culture and animal models of astrocytoma. However, this has failed to translate into a dramatic survival advantage in human studies. The most likely reason for this is that high-grade astrocytoma is a diffusely infiltrative disease. Not only is there infiltration local to the main tumour bulk, but distant infiltration as well. Although conventional PDT is able to make gains in local control, particularly with second-generation photosensitisers, such as *m*THPC, being activated by light of longer wavelength, and thus achieving deeper tissue penetration, the areas of distant infiltration, that may not even be discernible on imaging, remain elusive. As photosensitisers are taken up preferentially by tumour cells, particularly in the brain, targetable activation by an endogenous light source, for example, the tumour cell itself, may allow these areas of distant infiltration to be overcome.

In the next chapter, the outline of this study into bPDT for high-grade astrocytomas and the rationale behind it is described.

Chapter 4 Bioluminescence-Mediated Photodynamic Therapy for Grade 4 Astrocytoma: Aims and Outline of Study

The overall goal of this study is to provide proof-of-principle that cells from an astrocytoma are amenable to phototoxicity by bPDT. If proof-of-principle is achieved *in vitro*, then attempts at proof-of-principle will be made *in vivo*.

4.1 Photosensitisers and Emitters

In designing this study, the first step was to decide upon which photosensitsers and which bioluminescence systems should be used to test the concept of bPDT. The light dose achieved by bioluminescence is orders of magnitude less than that delivered by an external light source, therefore the ability of bioluminescence to activate a photosensitiser cannot solely result from the radiative absorption of the photons from bioluminescence by the photosensitiser. Another method of activation must also be occurring, and this is likely bioluminescence resonance energy transfer (BRET). BRET involves the non-radiative transfer of energy from a donor enzyme, luciferase, to a suitable acceptor molecule, the photosensitiser, after substrate, luciferin, oxidation[142]. The transfer of excited-state energy is inversely proportional to the sixth power of the distance between donor and acceptor dipoles, providing an effective range of less than 10 nm[143]. For these reasons, the chemical characteristics of the chosen photosensitiser and emitter for bPDT are of key importance.

In order maximise the radiative absorption of photons from bioluminescence by the photosensitiser, the photosensitiser should have an absorption profile that closely matches the emission profile of the bioluminescence. Furthermore, the photosensitiser should absorb photons efficiently i.e. have a high extinction coefficient, and the photosensitiser should have a high quantum yield of singlet oxygen when activated. Lastly, to engage BRET, the photosensitiser, luciferase, luciferin and ATP should all localise to the same cellular compartment.

In literature searching, two photosensitisers became of particular interest, hypericin and *m*THPC, both of which were already associated with research into gliomas.

4.1.1 Hypericin

Hypericin naturally occurs in the *Hypericum* plant species, most commonly represented by *Hypericum perforatum*, or St John's wort. Its recognition as a photosensitiser

originates from the search for the constituents responsible for hypericism, a skin photosensitivity seen in cattle ingesting large amounts of *Hypericum* plants growing on pastures.

Hypericin has been found to be a potent protein kinase inhibitor without light activation. Culture of hypericin with glioma cells led to marked inhibition of growth secondary to apoptosis[144]. Subsequently, photoactivation of hypericin has been shown to cause profound cell kill in several glioma cell lines with relatively low light doses[145,146]. Indeed, the potent effect of hypericin mediated PDT has been demonstrated in many different tumour cell lines[147]. Furthermore, PDT with hypericin in rodents bearing transplanted tumours that include lymphoma, pancreatic cancer, squamous cell carcinoma and bladder cancer have confirmed its potent antitumoural effect[147]. Hypericin's mediation in the anti-viral effect of bPDT has already been discussed[138].

Hypericin has a high extinction coefficient when exited at wavelengths greater than 590 nm, and has the potential for high singlet oxygen quantum yield[99]. Its subcellular localisation is limited to the cytoplasm[148] and it has been observed in all subcellular organelles[146].

4.1.2 mTHPC

*m*THPC is a synthetic, chlorin-based, second generation photosensitiser. Found to cause profound phototoxicity in both *in vitro* studies of non tumour[149,150], tumour[151-155], and specifically, glioma cell lines[156], as well as *in vivo* studies of non-glioma tumour[115,157] and glioma tumour[114,158] bearing animal models, it is now approved for the clinical treatment of head and neck cancers, and has been investigated in a phase II trial of high-grade astrocytoma[126].

*m*THPC has a high extinction coefficient when exited at wavelengths greater than 652 nm, and has the potential for high singlet oxygen quantum yield[99]. The primary sites of *m*THPC localisation are the Golgi apparatus and endoplasmic reticulum[159].

4.1.3 The Emitters

As mentioned above, genes encoding several luciferases for different species are now commercially available. Four luciferases have been chosen for investigation: *hRluc*, CBG68*luc*, *luc*, and CBR*luc*. *hRluc* is the coelenterazine-utilising luciferase from *Renilla reniformis*. *luc* is the benzothiazole luciferin-utilising beetle luciferase from the

firefly, and CBG68*luc* and CBR*luc* are two different types of click beetle luciferase. All vectors were available from the company Promega.

The substrate for *hRluc*, coelenterazine, is extremely unstable in aqueous solutions and has been difficult and inconvenient to use under normal cell culture conditions. Two synthetic substrates for *hRluc* have been developed, EnduRen™[160] and ViviRen™[161] (Promega Corp.), which have different profiles in the amount of bioluminescence they can generate and also how the generation of bioluminescence changes over time. Use of these substrates was planned for this study. However, no data reports on the localisation of these substrates, or of coelenterazine. d-Luciferin is the substrate for *luc*, CBG68*luc* and CBR*luc*, and this has been shown to localise to the cytoplasm[140].

4.1.4 Overlap of Absorption Spectra and Emission Profile

Through literature searching, the absorption spectra of hypericin and *m*THPC, and the emission profiles of the bioluminescence generated by *hRluc*, CBG68*luc*, *luc*, and CBR*luc* were obtained. With the aid of computer simulation, the absorption spectra of hypericin and *m*THPC plotted on the same graph as the emission profiles of the light generated by the above luciferases, and the degree of overlap between absorption and emission spectra assessed (see Figure 6).

Hypericin was reported to have absorption peaks at 470, 545, and 595 nm[162]. These coincided well with the peak emission wavelengths of *hRluc*, CBGr68*luc* and *luc*, which had been shown to be at approximately 480, 540, and 610 nm[133] (see Figure 6a). *m*THPC was reported to have an extremely strong absorption peak in the Soret band spanning approximately 390-430 nm, then less intense peaks at 517, 542, 595, and 650 nm[163]. Although there was not a peak-to-peak match of the absorption of *m*THPC in the Soret band with the peak bioluminescence of *hRluc* at 480 nm, there was reasonable overlap of the curves (see Figure 6b). The absorption peaks of *m*THPC at 542 and 595 nm coincided well with peak emission wavelengths of CBGr68*luc* and *luc* at 540 and 610 nm, respectively. The emission peak of CBR*luc* was found to be subtly longer than that of *luc*. However, the difference was not great enough to afford significant overlap with the 650 nm absorption peak of *m*THPC.

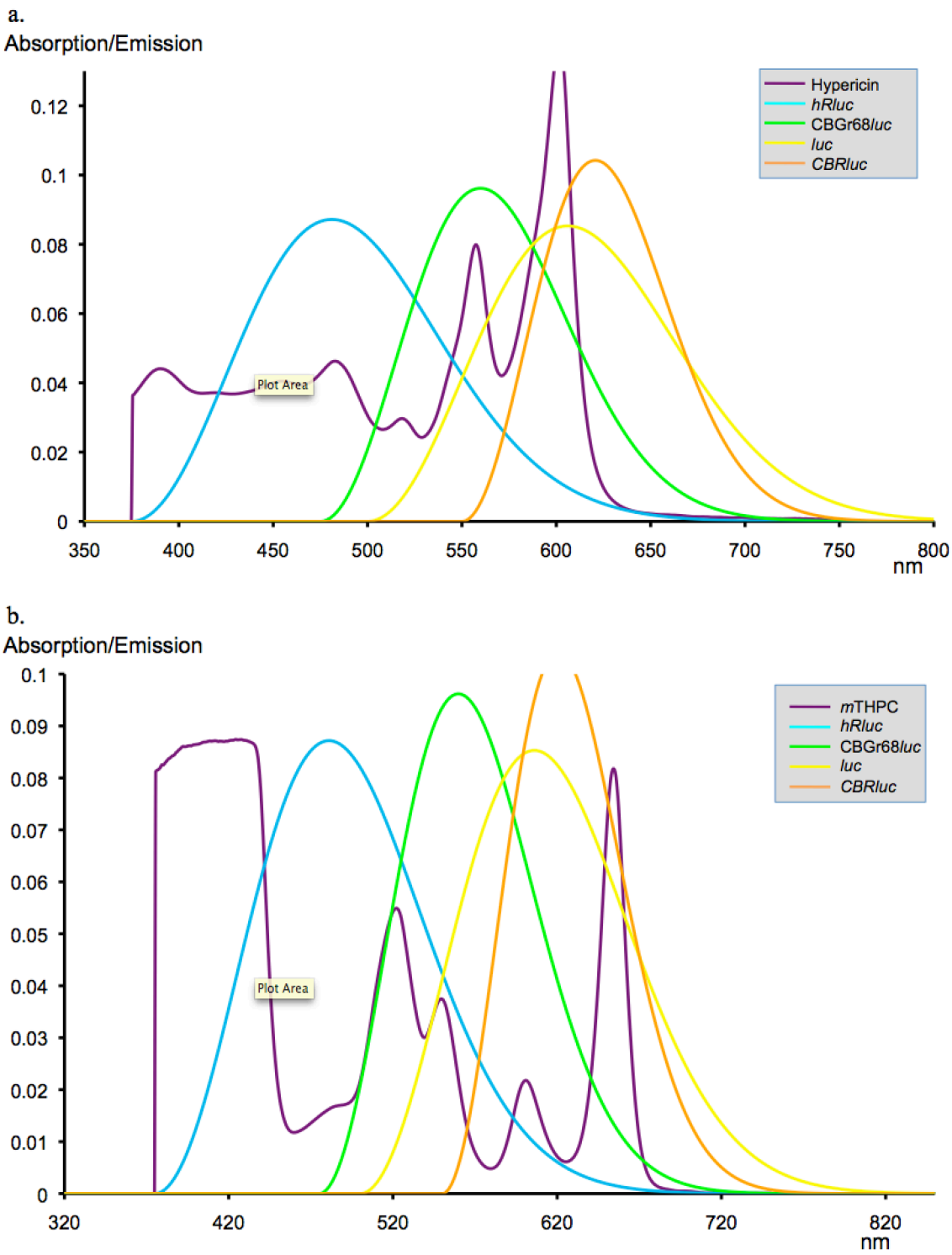

Figure 6 Overlap of the absorption spectra of hypericin (a.) and *m*THPC (b.) with the emission spectra of the bioluminescence generated by *hRluc*, CBGr68*luc*, *luc*, and CBR*luc*

Wavelength of light is represented in nm on the x axis. The y axis represents arbitrary units of absorption and emission. Hypericin has absorption peaks at 470, 545, and 595 nm and these coincided well with the peak emission wavelengths of *hRluc*, CBGr68*luc* and *luc*, which are at 480, 540, and 610 nm, respectively. *m*THPC has a strong absorption peak in the Soret band spanning approximately 390-430 nm, then less intense peaks at 517, 542, 595, and 650 nm. Although there is not a peak-to-peak match of the absorption of *m*THPC in the Soret band with the peak bioluminescence of *hRluc* at 480 nm, there is reasonable overlap of the curves. The absorption peaks of *m*THPC at 542 and 595 nm coincide well with peak emission wavelengths of CBGr68*luc* and *luc* at 540 and 610 nm, respectively.

4.1.5 Decision Made on Photosensitisers and Emitters

Based upon these findings, the decision was made to use the photosensitisers hypericin and *m*THPC for this study. Furthermore, cells would be cloned to express *hRluc*, CBG68*luc*, and *luc*.

Hypericin and *m*THPC both have the potential for a high extinction coefficient: 44 000 $M^{-1}cm^{-1}$ at 527 nm and 22 400 $M^{-1}cm^{-1}$ at 630 nm, respectively, compared to only 1.17 $M^{-1}cm^{-1}$ at 630 nm for Photofrin®. Furthermore, they also have the potential for a relatively high quantum yield of singlet oxygen: depending on the wavelength of excitation and solvent, approximately 0.3 for both hypericin and *m*THPC, compared to only 0.01-0.09 for Photofrin®[99]. Both photosensitisers and d-luciferin seem to co-localise at the very least to the cytoplasm. There is good overlap between the absorption peaks of these photosensitisers and the emission profile of the bioluminescence generated by these luciferases as described. Although there is not a peak-to-peak match between the absorption peak of *m*THPC in the Soret band and the emission profile of the bioluminescence generated by *hRluc*, there is reasonable overlap of the curves, and in view of the extremely high intensity of the absorption and the high quantum yield of singlet oxygen that *m*THPC is capable of, this overlap may be enough to mediate a photodynamic effect.

4.2 Preparing for bPDT

Several stages of experimentation would need to be completed before embarking on bPDT.

4.2.1 Response to Conventional PDT

In this stage, the cell lines used would need to be determined, as would the dose of photosensitiser, the duration of incubation with the photosensitiser, as well as confirmation that these cell lines would be amenable to cell kill by conventional PDT.

It was decided that four cell lines should be tested in this preparatory stage. As the pathology of focus is glioma, specifically, grade 4 astrocytoma, two glioma cell lines originally sourced from two different human grade 4 astrocytomas were chosen for use, U87 and U251. As a comparison neoplastic cell line, MCF-7, derived from a human breast adenocarcinoma was chosen. Lastly, if failing an effect being demonstrated in tumour cell lines, the NIH 3T3 cell line, derived from mouse fibroblasts, was chosen.

The dosages of hypericin and *m*THPC used for *in vitro* experiments are highly variable in the literature, ranging between 0.1 – 250 μM for hypericin[144-146,148,164-167] and 0.1 – 10 μg/ml for *m*THPC[149-156]. As discussed above, it remains controversial whether the greater the tumour concentration of photosensitiser correlates with increased cell kill once activated. However, as the light dose delivered by bioluminescence is orders of magnitude less than that from an external light source, photobleaching is not likely significant. Thus, in order to maximise the amount of singlet oxygen production, the maximum dose of photosensitiser tolerated by each cell line without causing toxicity in itself i.e. the dark toxicity, would need to be determined.

Additionally, reported incubation times vary between 4 – 24 hrs for hypericin and 3 – 24 hrs for *m*THPC. It is suggested that the effectiveness of PDT may be influenced by an interaction between drug dose and incubation time, with higher drug doses[166] and longer incubation times[155] being associated with aggregate formation; aggregates enhance the nonradiative decay of the molecular excited state, thereby reducing the efficacy of PDT. Hence, dark toxic doses of the photosensitisers would need to be determined for both a short incubation and long incubation time.

Having determined the dark toxic doses of photosensitiser for two incubation times, the cell lines would be tested to see if they are amenable to cell kill by conventional PDT. This opportunity was also taken to assess the lowest light dose that could achieve toxicity, termed the threshold of toxicity. If bPDT was subsequently found to be effective, this would give an indication of how much of the bPDT effect was attributable to radiative absorption of the photons from bioluminescence by the photosensitiser compared to BRET.

4.2.2 Generating Luciferase-Expressing Cell Lines and Study of Bioluminescence

Having established whether some or all of the cell lines are amenable to cell kill by conventional PDT, a decision would be made on which cell lines to transfect with the three luciferase genes: *hRluc,* CBG68*luc*, and *luc*. If successful luciferase-expressing cell lines are generated, a study of the character of bioluminescence would be undertaken in order to determine the conditions required to produce maximum bioluminescence. An understanding of how bioluminescence changes over time would also need to be gained.

d-Luciferin would be used as the substrate for *luc* and CBG68*luc*. As discussed above, the substrate for *hRluc*, coelenterazine, is extremely unstable in aqueous solutions, thus two synthetic substrates for *hRluc* will be tested, EnduRen™ and ViviRen™ (Promega).

4.3 Bioluminescence mediated Photodynamic Therapy

4.3.1 *in vitro* studies

By this stage of study, the optimum conditions for bPDT should have been determined. It is envisaged that stable, luciferase-expressing cell lines would be incubated with photosensitiser, then with luciferin, and the degree of cell kill determined. Companion control studies would include repeating the experiments in untransfected cells that would not express luciferase and also repeating experiments in the presence of lycopene, an anti-oxidant, that would prevent the formation of singlet oxygen. The opportunity for co-localisation studies would also be taken.

4.3.2 *in vivo* studies

If results from *in vitro* studies are compelling, then this study would proceed to *in vivo* experiments. Before bPDT could be tested, an animal model with a transplanted, luciferase-expressing tumour would need to be generated. The aim would be to generate a subcutaneous model in the first instance. The simplicity of the model would remove any challenges that the intracerebral microenvironment may pose and would also allow serial physical measurements of tumour size to validate BLI. Depending on progress and time, an attempt at generating an intracranial model would be undertaken. Indeed, luciferase-expressing glioma cells have been successfully transplanted both subcutaneously and intracranially into rodents. If successful models can be generated, the animals can then be treated with photosensitiser, then given systemic luciferin. Outcome measures would include survival, an assessment of tumour size, and histopathological examination of the tumour.

4.4 Statistical Analysis

Data was entered into GraphPad PRISM® Version 6 (GraphPad Software Inc.) and expressed as the mean of observations±standard error (SE). The difference in values between groups was determined by analysis of variance (ANOVA) and Student-*t*-test using PRISM®. Results were considered significant when the value of $p \leq 0.05$.

4.5 Developing Infrastructure

To investigate such an immature concept as bPDT the co-operation of several laboratories was required. The laboratories not only spanned across the University College London campus, but also across the University of London campus, and also involved independent research institutions. I would like to acknowledge and thank the groups and individuals without whom this work could not have been conducted.

University College London National Medical Laser Centre

In addition to Professor S Bown's supervision of this project, his team provided the expertise in photosensitisers and photodynamic therapy and include Mr C Hopper, Dr S Mosse, Dr S Macrobert, Dr J Woodhams, Dr M Austwick, and Ms F Hanaster.

University College London Institute of Neurology, Neuropathology

Dr S Brandner provided the bench space to perform most of the *in vitro* work. His team includes Ms H Naumann, Dr M Shaked-Rabi, Dr P Rodenas Cuadrado, and Dr A Swales.

University College London Institute of Neurology, Prion Centre

Professor P Jat supervised the DNA and cell cloning work. His team includes Ms P Aurora.

University College London Centre for Advanced Biomedical Engineering

Dr M Lythgoe kindly allowed me access to their luminometer and Dr A Jathoul assisted with the generation of the bioluminescence emission spectra.

Queen Mary University of London Institute of Cancer

Professor S Mather and Dr J Foster oversaw the *in vivo* work, and their neuropathology team cut and processed all the pathological specimens.

Cancer Research UK

Dr C DaCosta and Dr N Kanu allowed me weekly access to their luminometer.

University of Wisconsin, Madison, Department of Pathology

Dr S Salamat, whose patient and persistent teaching afforded me the skills to interpret histopathological slides of neurological disease, and Dr M Baskaya, who guided me through the technical and clinical nuances of the surgical management of grade 4 astrocytoma.

Part 2 Original Work

Chapter 5 Materials, General Principles of Cell Culture, and Understanding the Cell Lines

The initial set of experiments focused on becoming familiar with the behaviour of the chosen cell lines and finding a valid method to assess cell survival. Lastly, response of the cell lines to serum starvation was tested, as several drugs and reagents would be constituted in serum free solutions.

5.1 Materials

5.1.1 Cells, cell lines and plasmids

Cells and Cell Line	Supplier
C	
CMV-Fluc	Gift from Professor G Van der Pluijm, Leyden, Netherlands
CMV-hRluc	
J	
JS4 *Escherichia coli* (*E. coli*)	Gift from Professor P Jat, Institute of Neurology, Queen Square
M	
MCF-7	Gift from Professor M Baum, Department of Surgery, University College London
N	
NIH 3T3	Gift from Professor P Jat, Institute of Neurology, Queen Square
P	
pcDNA3.1(+)	Invitrogen
pCBG68-control	Promega
pGL4.70 [hRluc] vector	Promega

U

U251	Gift from Dr T Warr, Institute of Neurology, Queen Square
U87	Gift from Professor S Brandner, Institute of Neurology, Queen, Square

5.1.2 General Reagents

A

Agarose	Sigma-Aldrich
Ampicillin	Sigma-Aldrich

B

Bactotryptone	Sigma-Aldrich
Blue Juice™ Loading Dye	Invitrogen
Bovine Serum Albumin (BSA)	New England Biolabs
Buffer 2	New England Biolabs

C

Calcium chloride ($CaCl_2$)	Sigma-Aldrich

D

Dimethyl sulfoxide (DMSO)	Sigma-Aldrich
Distilled water	Thermo Fischer Scientific
D-luciferin	Caliper Life Sciences
D-luciferin	Promega
D-luciferin	Synchem
D-MEM/F12 (1:1) (IX), liquid with L-Glutamine, without HEPES	GIBCO/Invitrogen
Dulbecco's Modified Eagle Medium(D-MEM) (IX), liquid (High Glucose)	GIBCO/Invitrogen

E

EnduRen™	Promega

F	
Fetal Bovine Serum (FBS)	GIBCO/Invitrogen
Formic Acid	Sigma-Aldrich
FuGENE HD	Roche
F-10 Nutrient Mixture (Ham) (1X), Liquid	GIBCO/Invitrogen
G	
Geneticin (Neomycin, G418)	Invitrogen
Glycerol	
H	
HindIII restriction endonuclease	New England Biolabs
Hypericin	Planta Natural Products
I	
Isopropanol	Sigma-Aldrich
L	
Luciferase assay system	Promega
Luria Broth Base	Invitrogen
M	
Methylthiazolyldiphenyl-tetrazolium bromide (MTT)	Sigma-Aldrich
3-(N-Morpholino)propanesulfonic acid, 4-Morpholinepropanesulfonic acid [MOPS])	Sigma-Aldrich
m-tetrahydroxyphenylchlorin (mTHPC)	Biolitec
O	
Oxoid Agar	Sigma-Aldrich
P	
Phosphate buffered saline (PBS)	Biowhittaker

Q

QIAfilter Plasmid Maxi Kit	Qiagen
QIAfilter Plasmid Mini Kit	Qiagen

R

Renilla Luciferase Assay System	Promega

T

Tris(hydroxymethyl)aminomethane-ethylenedia-inetetraacetic acid, Tris-EDTA (TE) buffer	Sigma-Aldrich
Trypan Blue	Sigma-Aldrich
Trypsin, 0.05% (1x) with ethylenedia-inetetraacetic acid 4Na, liquid (trypsin/EDTA)	GIBCO/Invitrogen
T4 DNA ligase	USB
T4 DNA ligase buffer 10 x	USB

V

ViviRen™	Promega

X

XbaI restriction endonuclease	New England Biolabs

Y

Yeast extract	Sigma-Aldrich

5.2 Mammalian Cell Culture

Cells were maintained in the following manner throughout, with alterations in methodology mentioned in the appropriate sections.

5.2.1 Cell Media

Cell culture media were purchased from Invitrogen and reagents from Biowhittaker and Sigma-Aldrich.

5.2.2 Cell lines

Four cell lines were used: two human-derived glioma lines, U87 and U251; a breast cancer line, MCF-7; and a non-tumour, fibroblast line, NIH 3T3. Each cell line required maintenance in a specific culture media, which was enriched with 10% v/v FBS (see Table 3). Alternatively, for some experiments, media was enriched with 10% v/v heat inactivated FBS. Heat inactivation was achieved by heating FBS to a temperature of 56^0C for 45 minutes.

Cell Line	Culture Medium Required
U87 and NIH 3T3	(D-MEM) (1x), liquid (High Glucose) with L-glutamine, 4500 mg/L D-Glucose, 110 mg/L Sodium Pyruvate
U251	D-MEM/F12 (1:1) (1x), liquid with L-Glutamine, without HEPES
MCF-7	F-10 Nutrient Mixture (Ham) (1x), Liquid with L-glutamine

Table 3 Specific media requirements for each cell line

5.2.3 Cell Culture Conditions

All cell lines were maintained at 5% CO_2, 20% O_2, 95% humidity and 37^0C.

5.2.4 Sub-culturing of Cells (Passaging of Cells)

Cells were grown until a sub-confluent state was reached (approximately 80% confluence). Media was then removed and the cell monolayer washed with 5 ml of PBS. Following aspiration of PBS, cells were detached with 2.5 ml trypsin/EDTA per 80 cm^2 flask at 37^0C for 2 mins. Once cells were adequately detached, the trypsin/EDTA was inactivated with 5 ml of complete media and the contents of the flask transferred to a 15 ml tube for centrifugation at 1000 rpm for 5 mins. Following

centrifugation, the media was aspirated and the remaining pellet resuspended in an appropriate volume of media. Cells were then re-plated at a defined ratio e.g. 1 in 8 of the total cells, or counted using a haemocytometer and plated at the required density. Table 4 shows the typical frequency of cell passaging and ratio of re-plating required for each cell line.

Cell Line	Ratio of Re-plating Required	Frequency of Cell Passaging
U87	1:10 to 1:12	Twice a week
U251	1:3 to 1:5	Once a week
MCF-7	1:10	Twice a week
NIH 3T3	1:12 to 1:14	Twice a week

Table 4 Frequency of cell passaging and ratio of re-plating

5.2.5 Preservations of cells (Freezing down of cells)

Cells from a sub-confluent 80 cm^2 flask were trypsinised, resuspended in complete media and centrifuged at 1000 rpm for 5 minutes to remove any traces of trypsin. Following centrifugation, the supernatant was aspirated and the remaining pellet resuspended in complete media and counted by haemocytometry. Cells were spun down again then resuspended in the appropriate volume of freezing media (40% v/v FBS, 40% v/v complete media, and 20% v/v dimethyl sulfoxide [DMSO]) to attain at least $1x10^6$ cells per ml. The cell solution was transferred into cryovials (1 ml per vial), which were placed in an insulated container containing isopropanol and stored at -80^0C. After 24 hrs, they were transferred to liquid N_2.

5.2.6 Recovery of Frozen Cells (Thawing of cells)

Cells were retrieved from liquid N_2, thawed rapidly at 37^0C, and transferred into a 15 ml falcon tube containing 5 ml of complete media. Cells were then centrifuged for 5 minutes at 1000 rpm to remove DMSO-containing media. Following centrifugation, the supernatant was aspirated and the remaining pellet resuspended in 5 ml of complete media. The cell suspension was then transferred into an 80 cm^2 flask containing 20 ml of complete media. The cells were maintained as above until sub-confluence was reached, then sub-cultured as described above.

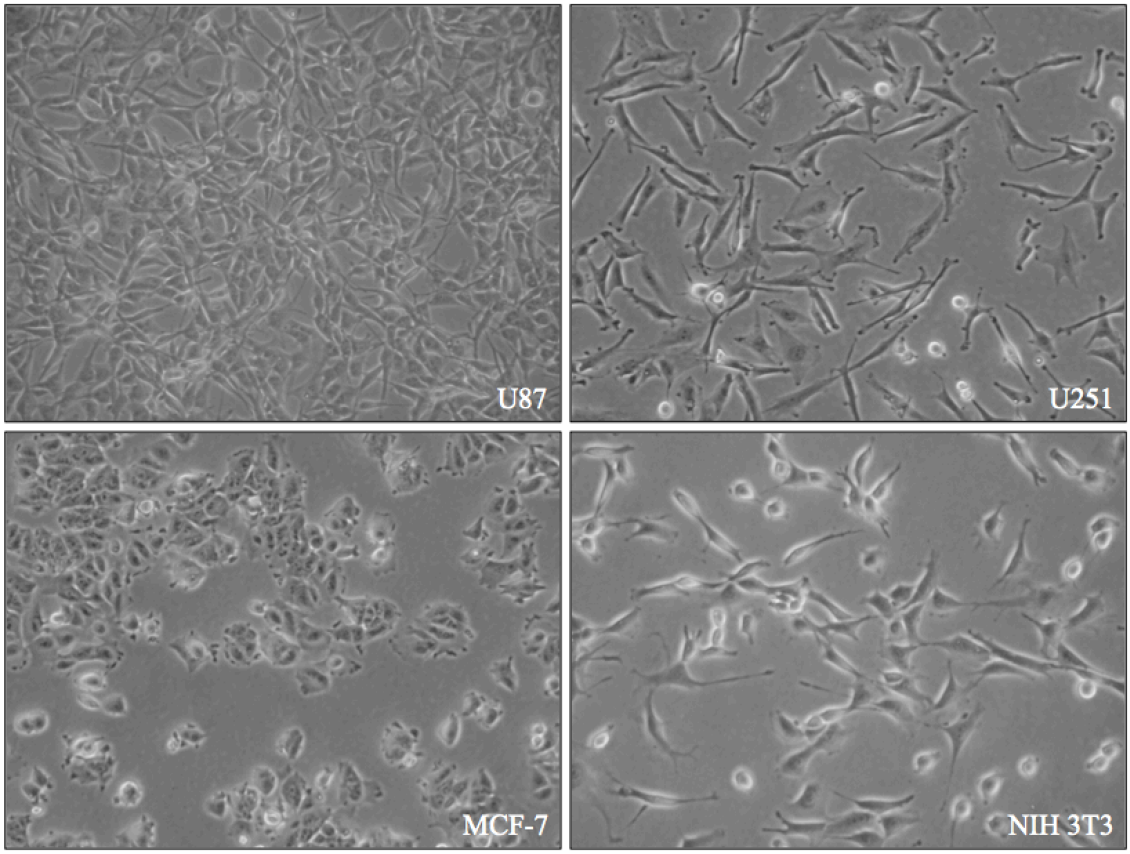

Figure 7 Light microscopy images of cell lines U87, U251, MCF-7 and NIH 3T3, original magnification at x20.

5.3 Cell Viability

5.3.1 Haemocytometry

Viable cells were counted using trypan blue staining and a haemocytometer, viewed under phase-contrast light microscopy at x10 magnification. Following resuspension in an adequate volume, 20 μl of cell solution was added to an equal volume of trypan blue, and 20 μl of the resulting mixture was injected into a haemocytometer. Unstained cells, considered as viable, were counted in the outer four quadrants; each quadrant having an area of 1 mm^2 and the space between the slide and cover slip being 0.1 mm, and hence each quadrant representing a volume of 0.1 mm^3. The number of cells per ml was calculated as follows:

Number of cells per ml = Average number of cells over four quadrants x 2 x 10^4

5.3.2 Cell Viability Assay

The method of transcriptional and translational (MTT) assay is a standard colorimetric assay where a yellow (3-(4,5-Dimethylthiazol-2-yl)-2,5-diphenyltetrazolium bromide) tetrazole dye is reduced to purple formazan in the mitochondria of living cells[168]. After

incubating cells with the dye for a certain amount of time, a solubilisation solution is added to lyse the cells, and release and dissolve the insoluble purple formazan product into a coloured solution. The amount of product can then be quantified by measuring its optical density at a certain wavelength by a standard, multiwell scanning spectrophotometer. The reduction reaction depends upon active reductase enzymes in living mitochondria, and hence, the assay is a precise and rapid method for measuring cell proliferation and survival.

MTT was dissolved in PBS to make a stock solution of 5 mg/ml and stored at -20^{0}C in 1 ml aliquots, thawing the necessary aliquots for each experiment. To establish optimal conditions for the MTT assay, dose-response curves were generated for each cell line. Four doses of cells were plated in triplicate in parallel 96 well plates; cell numbers ranging between 0.125 and 4 x 10^4, depending on the proliferation rate of the cell line. The cells were allowed to incubate for 72 hrs, representing the longest time of future experiments, after which 20 μl of MTT, for U87, MCF7 and NIH 3T3 cells, and 40 μl of MTT for U251 cells, were added to each well of one set of plates, and left to incubate for 3 hrs at 37^{0}C. Media was then aspirated from the wells and 0.1 ml of lysis buffer (95% isopropanol and 5% formic acid) was added to each well. The plate was placed on a gyrator for 10 mins to ensure complete cell lysis. The optical density (OD) of the wells was quantified in a spectrophotometer (TECAN Sunrise™ microplate reader, XFluor4 software) using a test wavelength of 550 nm and reference wavelength of 690 nm. Cells in the second plate were counted by haemocytometry.

Dose-response curves were produced by calculating the mean ± SEM for each triplicate set of results and fitting a best-fit line by linear regression analysis. Where the p value indicated that the chance of generating such a linear relationship was not significantly different from chance, the data was subject to non-linear regression, generating a best-fit curve. This data was used to determine the number of cells that should be plated for future experiments; this number generating an OD and cell count in the linear part of the dose-response curve.

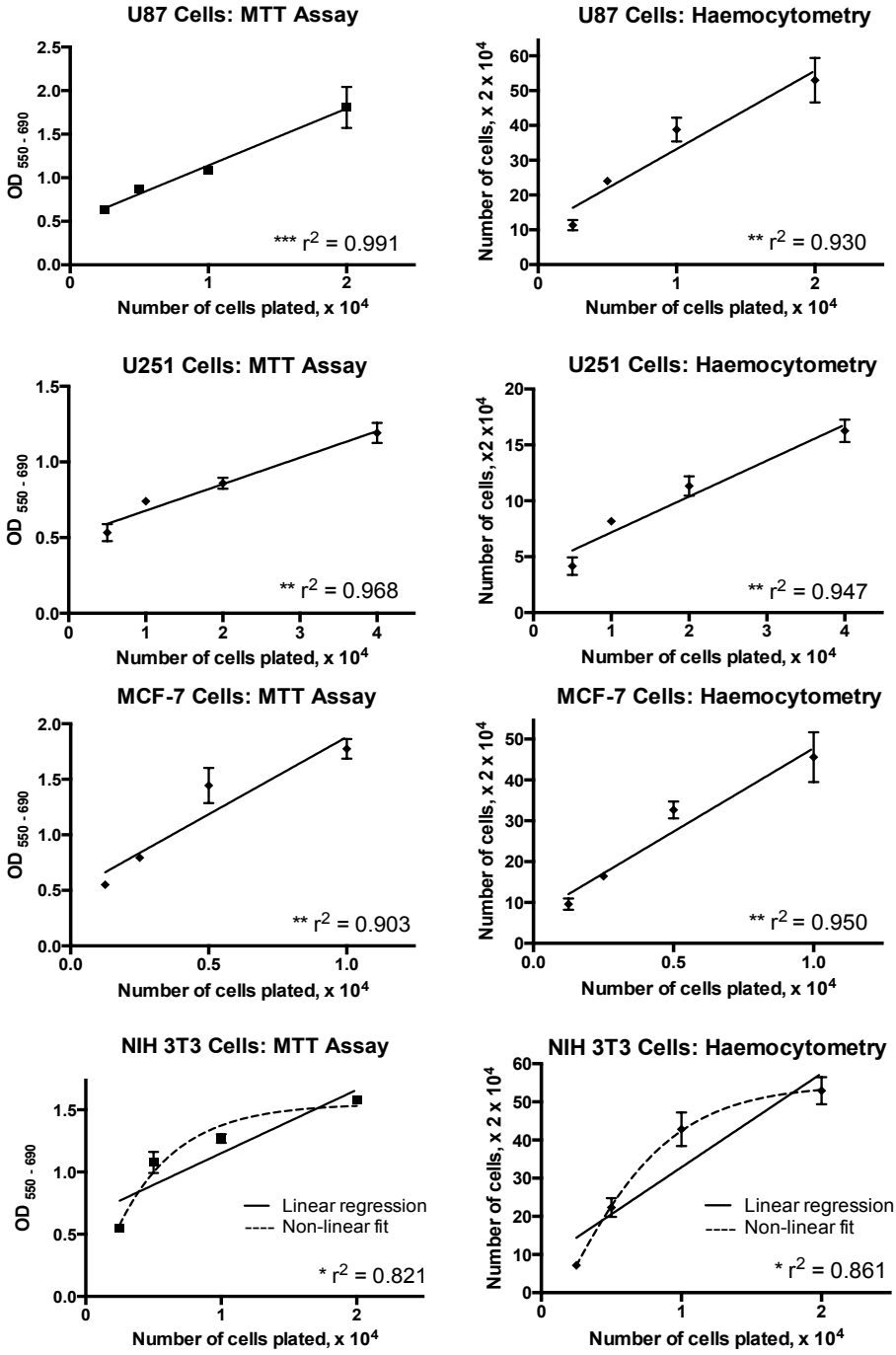

Figure 8 Increasing cell numbers, as demonstrated by haemocytometry, are appropriately reflected by increasing OD, as generated by the MTT assay.

Linear regression of MTT assay and haemocytometry results generated best-fit lines that were significantly different from change for U87, U251 and MCF-7 cells (p = 0.005 and 0.04, p = 0.02 and 0.03, and p = 0.05 and 0.03, respectively), but no significantly different from chance for NIH 3T3 cells (p = 0.09 and 0.07). For NIH 3T3 cells, both the best-fit line from linear regression (—) and the best-fit curve from non-linear regression (----) are shown. r^2 values are quoted in the figure. Asterisks indicate the degree of significance of the r^2 value where * p > 0.05, ** p ≤ 0.05, *** p < 0.01.

Linear regression of results from MTT assays and haemocytometry for U87, U251 and MCF-7 cell lines (see Figure 8) produced best-fit lines that were significantly different from chance ($p = 0.005$ and 0.04, $p = 0.02$ and 0.03, and $p = 0.05$ and 0.03, respectively). However, for NIH 3T3 cells, the best-fit line was not significantly different from chance ($p = 0.09$ and 0.07), hence, non-linear regression analysis was used to generate a best-fit curve. Notably, findings from haemocytometry correlated well with the MTT assay results; increasing cell numbers being reflected by increasing OD (see Figure 8). It was decided that for future experiments 1×10^4 cells for U87 and MCF-7 cells, 2×10^4 cells for U251 cells, and 0.25×10^4 cells for NIH 3T3 cells would be used.

5.4 Effect of Serum Starvation

Sub-confluent cells of each cell line were harvested and plated at a density of 1×10^4 cells for U87 and MCF-7 cells, 2×10^4 cells for U251 cells, and 0.25×10^4 cells for NIH 3T3 cells, per well of a 96 well plate. After 24 hrs incubation, the media was aspirated and cells were washed twice with 0.1 ml of PBS. 0.2 ml of complete media was replaced in the control wells, and 0.2 ml of serum free media was placed in test wells. Cells were plated in triplicate for each condition, and parallel plates were tested. After 48 hrs incubation, an MTT assay was carried out.

All cell lines were sensitive to serum starvation compared to controls (see Figure 9): $p = 0.01$, $p = 0.02$, $p = 0.004$, and $p < 0.0001$ for U87, U251, MCF-7 and NIH 3T3 cells, respectively.

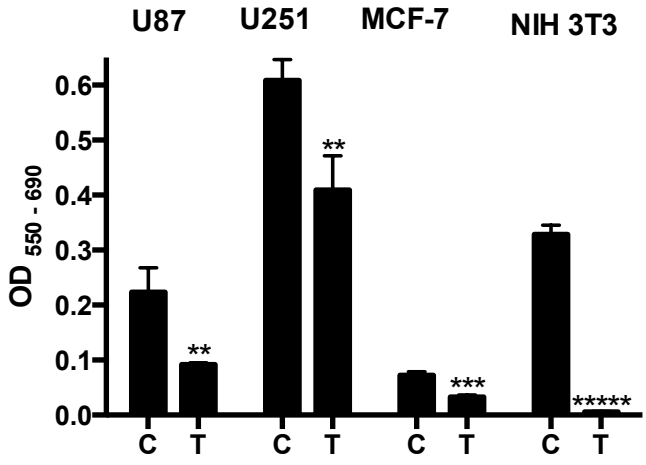

Figure 9 Cell lines are sensitive to serum starvation.

C = control, T = test, serum starved. Asterisks indicate the degree of significance in the difference between the OD of the test wells compared to control wells where * $p > 0.05$, ** $p \leq 0.05$, *** $p < 0.01$, **** $p < 0.001$, ***** $p < 0.0001$.

5.3 Summary and Discussion

Four cell lines; two human-derived glioma lines, U87 and U251; a breast cancer line, MCF-7; and a non-tumour, fibroblast line, NIH 3T3; were successfully cultured, passaged, and stored. The colorimetric MTT assay was found to correlate well with haemocytometry in assessing cell viability, and both methods were employed in ongoing experimentation. Cell viability studies also allowed a determination of the number of cells to be plated for ongoing experimentation: 1×10^4 cells for U87 and MCF-7 cells, 2×10^4 cells for U251 cells, and 0.25×10^4 cells for NIH 3T3 cells, per well of a 96 well plate. Finally, all cell lines were sensitive to serum starvation, thus, further experiments required cells to be incubated in complete media, although drugs and reagents were constituted in serum free solutions.

Chapter 6 Efficacy of Photodynamic Therapy *in vitro*

Before testing whether bioluminescence is able to activate a photosensitiser and cause a photodynamic effect that leads to cell death, experiments were conducted on the cell lines to demonstrate that they were indeed amenable to cell death by conventional PDT. These studies included an assessment of the dark toxicity of the photosensitisers, hypericin and *m*THPC, allowing the maximum sub-lethal doses of the photosensitisers in each cell line to be established: bioluminescence produces much less energy than an external light source, hence use of the maximum sub-lethal dose of photosensitiser allows optimisation of conditions. Furthermore, having incubated the cells with the previously established maximum sub-lethal doses of photosensitiser, not only was an assessment made of whether the cells were amenable to cell kill by conventional PDT, but an assessment of the minimum amount of light required to achieve this cell kill was made in order to gauge the susceptibility of each cell line to PDT. Care was taken to ensure that all lighting was minimised during all steps involving photosensitisers: window blinds were drawn, lights were switched off, and plates were wrapped in aluminium foil when placed in the incubator to avoid inadvertent photoactivation.

6.1 Establishing Dark Toxicity

Dark toxicity refers to the toxicity of the photosensitiser itself, before the application of light.

6.1.1. Preparation of the Photosensitisers

Hypericin was purchased as a powder (10 mg per vial) and stored at -20^{0}C. Before each experiment, the powder was brought to room temperature and a stock solution of 1mM was freshly made by dissolving 0.5 mg of drug (molecular weight 504.45) in 1 ml of DMSO. This was then sterile filtered once. *m*THPC was purchased as a 4 mg/ml solution and stored at 4^{0}C. Before each experiment, the solution was brought to room temperature and a predetermined volume of drug was sterile filtered.

6.1.2 Dark toxicity

To establish the maximum, sub-lethal drug dose, sub-confluent cells of each cell line were harvested and plated at a density of 1 x 10^4 cells for U87 and MCF-7 cells, 2 x 10^4 cells for U251 cells, and 0.25 x 10^4 cells for NIH 3T3 cells, per well of a 96 well plate. Following 24 hrs incubation in standard cell culture conditions, media was aspirated and replaced with 0.1 ml of complete media.

Varying concentrations of hypericin were made up in serum free media from the stock solution and 0.1 ml added to the wells, each concentration in triplicate, to give final concentrations ranging from 0.00160-200 μM. Similarly, varying concentrations of *m*THPC were made up in serum free media and 0.1 ml added to the wells, each concentration in triplicate, to give final concentrations ranging from 0.400-50.0 μg/ml. Cells were incubated with each drug in standard cell culture conditions for two durations: 4 or 24 hrs with hypericin, and 3 or 24 hrs with *m*THPC. They were then washed twice with 0.1 ml of PBS. 0.2 ml of complete media were replaced in the wells and after a further 24 hrs incubation, an MTT assay was conducted. Control cells were similarly treated, but instead of drug, they were incubated with 0.1 ml of serum free media.

A dose that caused a significant reduction in OD compared to control ($p \leq 0.05$) was considered toxic. Several experiments were conducted using different concentrations of drug in order to establish the maximum possible sub-lethal dose. Illustrative results are presented below: in some cases, two experiments on a particular cell line are shown to best demonstrate how the maximum sub-lethal dose was determined. Drug dosages are expressed to 3 significant figures.

6.1.3 Hypericin, Short Incubation

For short incubation (4 hrs) with hypericin (see Figure 10), the maximum, sub-lethal dose was determined to be 12.5 μM ($p > 0.05$) for U87 cells, 0.200 μM ($p > 0.05$) for U251 cells, and 25.0 μM ($p > 0.05$) for MCF-7 and NIH 3T3 cells.

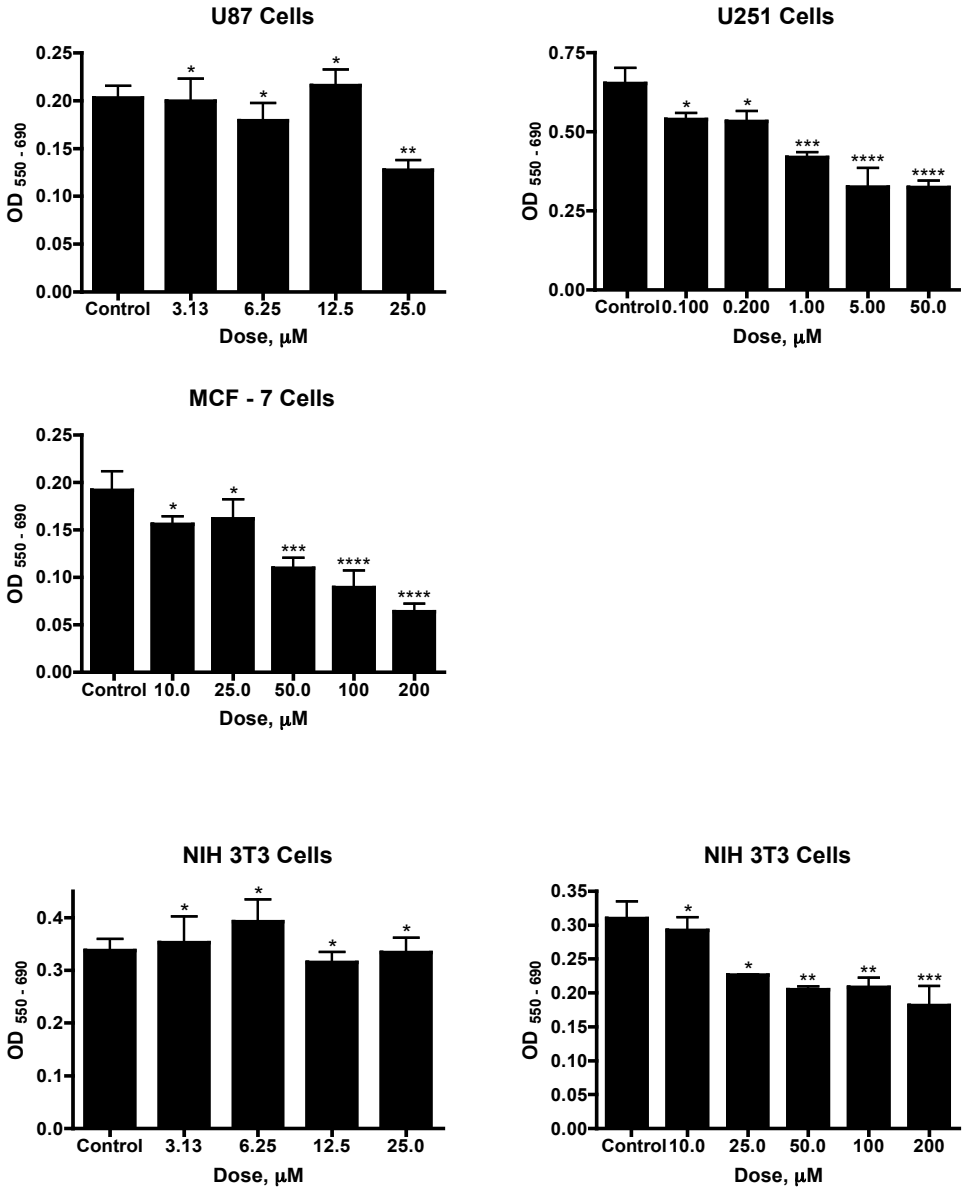

Figure 10 Establishing the maximum, sub-lethal dose of hypericin when incubating with cells for 4 hrs.

Asterisks indicate the degree of significance of the difference in OD between the specified dose and control, where * $p > 0.05$, ** $p \leq 0.05$, *** $p < 0.01$, **** $p < 0.001$. Drug dosages are expressed to 3 significant figures. For short incubation (4 hrs) with hypericin, the maximum, sub-lethal dose was determined to be 12.5 μM ($p > 0.05$) for U87 cells, 0.200 μM ($p > 0.05$) for U251 cells, and 25.0 μM ($p > 0.05$) for MCF-7 and NIH 3T3 cells. Two experiments on NIH 3T3 cells are shown to clearly demonstrate that doses ≤ 25.0 μM are not toxic, but doses > 25.0 μM are.

6.1.4 Hypericin, Long Incubation

For long incubation (24 hrs) with hypericin (see Figure 11), the maximum, sub-lethal dose for U87 and NIH 3T3 cells was determined to be 10.0 μM, which was an arbitrarily chosen dose between the toxic 12.5 μM ($p < 0.01$) and the non-toxic 6.25 μM ($p > 0.05$) doses. 0.00160 μM ($p > 0.05$) was the determined maximum, sub-lethal dose for U251 cells and 12.5 μM ($p > 0.05$) for MCF-7 cells.

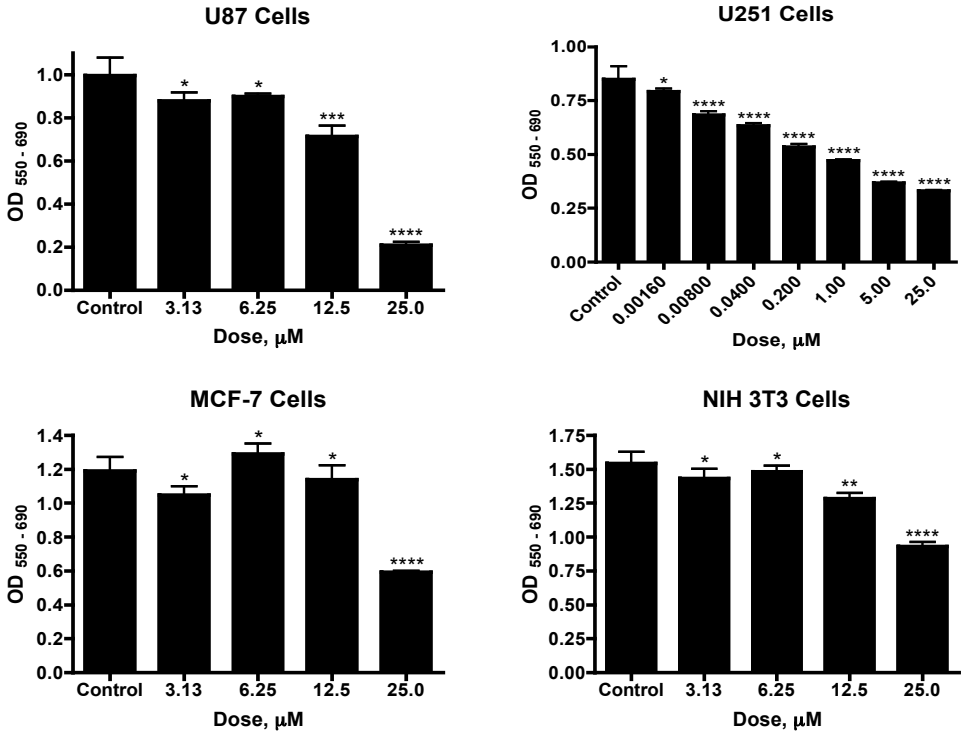

Figure 11 Establishing the maximum, sub-lethal dose of hypericin when incubating with cells for 24 hrs.

Asterisks indicate the degree of significance of the difference in OD between the specified dose and control, where * $p > 0.05$, ** $p \leq 0.05$, *** $p < 0.01$, **** $p < 0.001$. Drug dosages are expressed to 3 significant figures. For long incubation (24 hrs) with hypericin, the maximum, sub-lethal dose was determined to be 10.0 µM for U87 and NIH 3T3 cells, 0.00160 µM ($p > 0.05$) for U251 cells, and 12.5 µM ($p > 0.05$) for MCF-7 cells.

6.1.5 *m*THPC, Short Incubation

For short incubation (3 hrs) with *m*THPC (see Figure 12), the maximum, sub-lethal dose determined for U251 cells was 25.0 µg/ml ($p > 0.05$). Where a certain dose of drug demonstrated inconsistent toxicity, a lower, though consistently sub-lethal dose was determined to be the maximum, sub-lethal dose: 25.0 µg/ml was inconsistently toxic ($p < 0.001$ vs $p > 0.05$) for U87 and MCF-7 cells, hence 12.5 µg/ml ($p > 0.05$) was the determined maximum, sub-lethal dose. For NIH 3T3 cells, a dose of 25.0 µg/ml caused a 32.3% reduction in OD ($p > 0.05$), but as the 95% CI (-0.0833 to 0.398) trended towards significance, this dose was considered toxic, and a dose of 12.5 µg/ml ($p > 0.05$) was set as the maximum, sub-lethal dose.

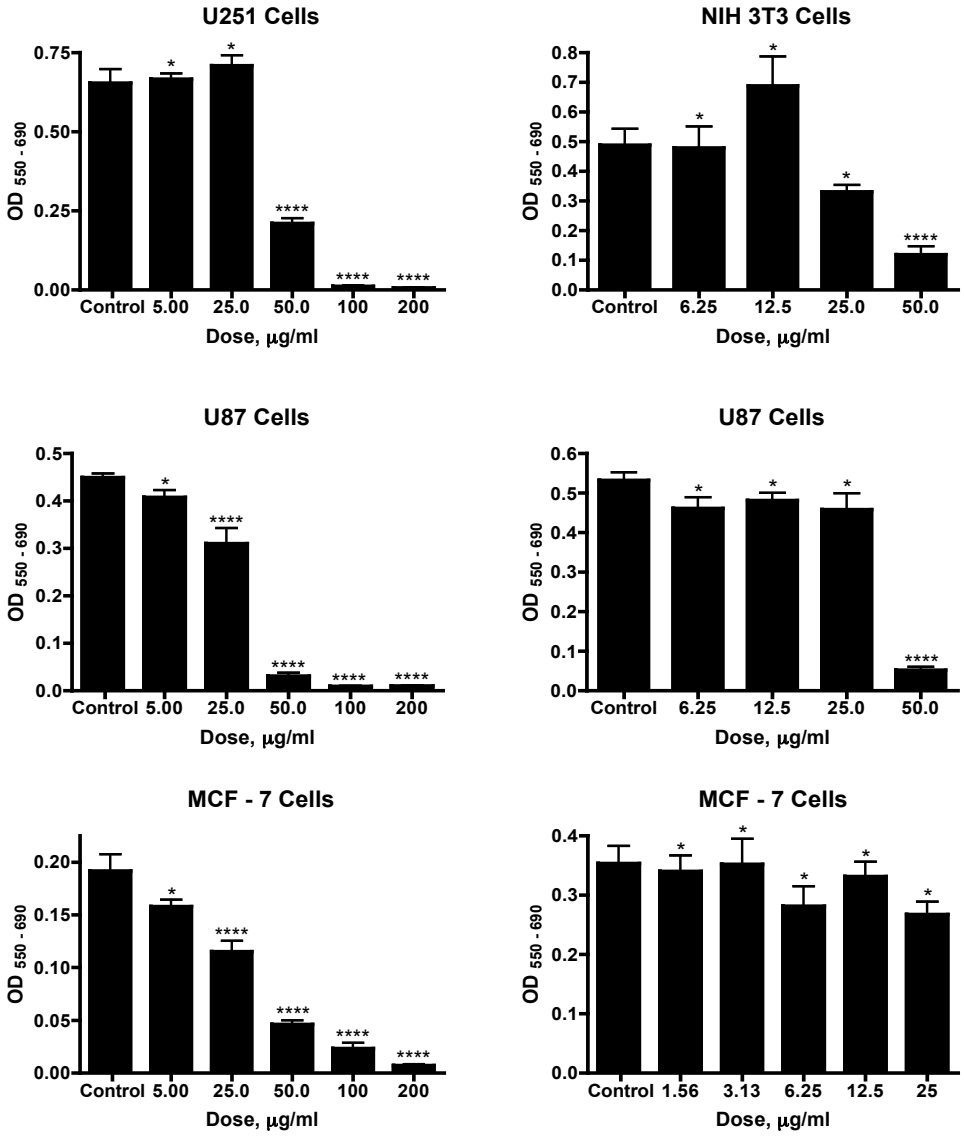

Figure 12 Establishing the maximum, sub-lethal dose of *m*THPC when incubating with cells for 3 hrs.

Asterisks indicate the degree of significance of the difference in OD between the specified dose and control, where * $p > 0.05$, ** $p \leq 0.05$, *** $p < 0.01$, **** $p < 0.001$. Drug dosages are expressed to 3 significant figures. For short incubation (3 hrs) with *m*THPC, the maximum, sub-lethal dose determined to be 25.0 μg/ml ($p > 0.05$) for U251 cells and 12.5 μg/ml ($p > 0.05$) for U87, NIH 3T3, and MCF-7 cells. Two experiments on U87 and NIH 3T3 cells demonstrated the inconsistent toxicity of the 25 μg/ml dose on these two cells lines.

6.1.6 *m*THPC, Long Incubation

For long incubation (24 hrs) with *m*THPC (see Figure 13), the maximum sub-lethal dose was determined to be 2.50 μg/ml ($p > 0.05$) for U87 cells and 5.00 μg/ml p (> 0.05) for U251 cells. 10.0 μg/ml was inconsistently toxic to MCF-7 cells $p < 0.001$ vs $p > 0.05$), hence 5.00 μg/ml ($p > 0.05$) was the determined maximum sub-lethal dose for this cell line. For NIH 3T3 cells, a dose of 5.00 μg/ml caused a 35.8 % reduction in OD ($p > 0.05$), but as the 95% CI (-0.107 to 0.246) trended towards significance, this dose was considered toxic, and a dose of 2.50 μg/ml ($p > 0.05$) became the test dose of choice.

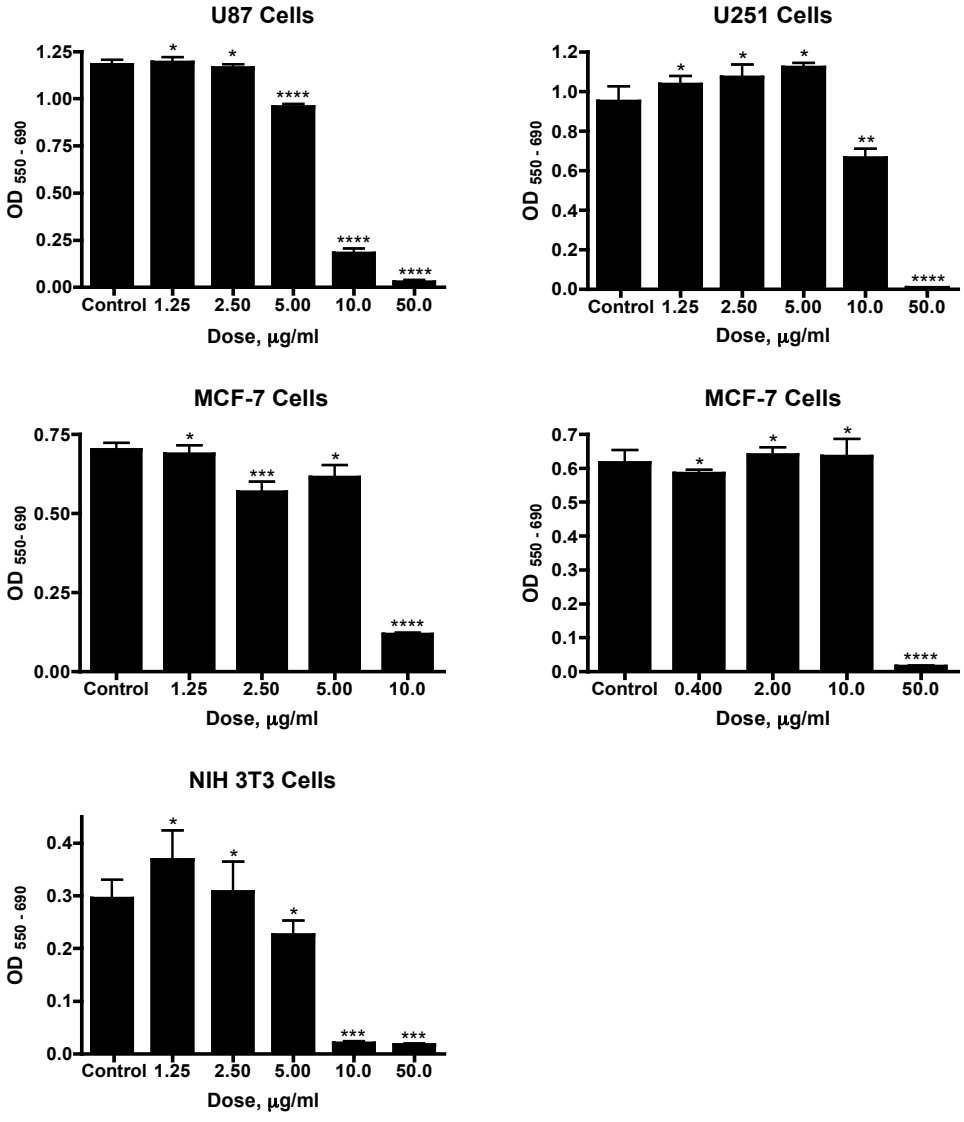

Figure 13 Establishing the maximum, sub-lethal dose of *m*THPC when incubating with cells for 24 hrs.

Asterisks indicate the degree of significance of the difference in OD between the specified dose and control, where * $p > 0.05$, ** $p < 0.05$, *** $p < 0.01$, **** $p < 0.001$. Drug dosages are expressed to 3 significant figures. For long incubation (24 hrs) with *m*THPC, the maximum sub-lethal dose was determined to be 2.50 μg/ml for U87 and NIH 3T3 cells, and 5.00 μg/ml for U251 and MCF-7 cells. Two experiments on MCF-7 cells demonstrated the inconsistent toxicity of a 10.0 μg/ml dose.

The maximum sub-lethal doses determined for hypericin and *m*THPC incubating for short (4 hrs for hypericin, 3 hrs for *m*THPC) and long (24 hrs) durations with each cell line are summarised in Table 5.

	Hypericin Dose μM		*m*THPC Dose μg/ml	
Incubation Time	4 Hrs	24 Hrs	3 Hrs	24 Hrs
U87	12.5	10.0	12.5	2.50
U251	0.200	0.00160	25.0	5.00
MCF7	25.0	12.5	12.5	5.00
NIH 3T3	25.0	10.0	12.5	2.50

Table 5 Maximum sub-lethal doses of photosensitisers for the appropriate incubation times. Drug dosages are expressed to 3 significant figures.

The literature does not report experiments specifically aimed at establishing the maximum sub-lethal dose for the photosensitiers hypericin and *m*THPC in these particular cell lines and under these particular conditions. However, the range of doses established here for both incubation times do lie within the ranges that have been reported for use for photodynamic therapy *in vitro* (as cited in section 4.2.1): 0.1 – 250 μM for hypericin and 0.1 – 10 μg/ml for *m*THPC. Furthermore, as would be expected, the maximum sub-lethal dose at the longer incubation time is less than that for the shorter incubation time for both drugs in all cell lines. It is noted that the maximum sub-lethal dose of hypericin in the U251 cell line is orders of magnitude less than that of the other cell lines. Although this could be a spurious result, it was replicated. The literature does not report hypericin being used with the U251 cell line for verification.

6.2 Conventional Photodynamic Therapy

Before investigating the efficacy of bPDT, the toxicity of conventional PDT was confirmed. The threshold of toxicity, the lowest light dose at which toxicity was achieved in cells that had been incubated with photosensitiser, was also noted.

Sub-confluent cells of each cell line were harvested and plated at a density of 1 x 10^4 cells for U87 and MCF-7 cells, 2 x 10^4 cells for U251 cells, and 0.25 x 10^4 cells for NIH 3T3 cells, per well of a 96 well plate. Following 24 hrs incubation in standard cell culture conditions, media was aspirated and replaced with 0.1 ml of complete media.

Wells were designated as either control or test. Control wells were further divided into pure 'control' wells, which were exposed to neither drug nor light; 'drug only' wells, which were exposed only to drug, but no light; and 'light only' wells, which were exposed only to light, but no drug. 'Test' wells were exposed to both drug and light. Each condition was tested in triplicate.

Photosensitisers were made up in 0.1 ml of serum free media and added to 'drug only' and 'test' wells to give a final concentration equal to the maximum sub-lethal concentrations, as established above (see Table 5). 'Control' and 'light only' wells received 0.1 ml of serum free media. After the appropriate incubation time (4 and 24 hrs for hypericin, 3 and 24 hrs for *m*THPC), all wells were washed twice with 0.1 ml of PBS, following which 0.2 ml of complete media was added to each well. 'Light only' and 'test' wells were then exposed to varying durations of blue light illumination (Lumisource, maximum output at 420 nm 7 $mWcm^{-2}$, Biotech, Oslo, Norway), ranging from 1 sec to 500 secs (120 secs x 7 $mWcm^{-2}$ equivalent to 840 $mJcm^{-2}$). Cells were then replaced in standard cell culture conditions for a further 24 hrs, after which an MTT assay was performed.

Regarding 'light only' wells, the mean OD for each exposure time was compared. In most circumstances, there was no significant difference between these groups, and in no circumstances did light cause a significant fall in OD (see Appendix A1). In a few circumstances, light did cause a significant increase in OD, indicating stimulation of cell growth. For ease of interpretation, the mean OD of the 'light only' wells exposed to the longest duration of light i.e. the greatest fluence of light, was used as the overall 'light only' control for comparison with the other conditions.

The OD for each condition, 'drug only,' 'light only,' and 'test,' was compared to 'control' wells. A significant reduction in OD compared to 'control' ($p \leq 0.05$) was considered toxic.

6.2.1 Hypericin, Short Incubation

For short incubation (4 hrs) with hypericin (see Figure 14), all cells lines were amenable to toxicity from conventional PDT and a clear dose-response was seen with increasing doses of light. The threshold of toxicity was 50 secs light illumination (350 $mJcm^{-2}$) for U87 and NIH 3T3 cells, resulting in the OD falling to 27.6% ($p < 0.0001$) and 3.77% ($p < 0.0001$) of control, respectively. Although light seemed to stimulate

growth in NIH 3T3 cells, these cells demonstrated toxicity from a photodynamic effect. The threshold of toxicity was 180 secs of light illumination (1260 $mJcm^{-2}$) for U251 cells, resulting in the OD falling to 61.8% ($p < 0.0001$) of control. Examining the effect of 5 and 50 secs light illumination on U251 cells, p values would indicate that the reduction in OD to 87.4% ($p < 0.0001$) and 89.0% ($p \leq 0.05$) of control for cells exposed to 'drug only' and 'test' cells exposed to 5 secs light illumination, respectively, was significant. However, as the fall in OD was small, and the trend was strongly towards no significant difference compared to control (95% CI 0.0185 to 0.159 and 0.00365 to 0.151, respectively), these variations were not considered significantly different from control. Although light seemed to stimulate growth in MCF-7 cells, these cells demonstrated toxicity from a photodynamic effect, and the threshold of toxicity was 20 secs light illumination (140 $mJcm^{-2}$), resulting in the OD falling to 35.4% ($p < 0.0001$) of control.

6.2.2 Hypericin, Long Incubation

For long incubation (24 hrs) with hypericin (see Figure 15), all cell lines were amenable to toxicity from conventional PDT, except U251 cells, and in those cell lines amenable to toxicity from PDT, a dose-response was also demonstrated. The threshold of toxicity was 50 secs light illumination (350 $mJcm^{-2}$) for U87 cells, resulting in the OD falling to 23.5% ($p < 0.0001$) of control, and 20 secs light illumination (140 $mJcm^{-2}$) for MCF-7 cells, resulting in the OD falling to 61.6% ($p < 0.0001$) of control. The addition of 'drug only' seemed to lead to slight cell growth in these two cell lines compared to control ($p \leq 0.05$). However, the degree of growth was small and the 95% CI indicated a strong trend towards no significant difference compared to control (138.2%, -0.364 to -0.0672, and 118.5%, -0.128 to -0.00286, respectively), and therefore these differences were treated as being not significantly different to control. Furthermore, U87 cells exposed to 'drug' then 5 secs light illumination seemed to undergo growth stimulation (OD 134% of control, $p < 0.01$). However, as this degree of stimulation was small and the 95% CI strongly trended towards no significant difference compared to control (- 0.0339 to - 0.0423), this was considered not significantly different from control. Regarding NIH 3T3 cells, the threshold of toxicity was 20 secs light illumination (140 $mJcm^{-2}$), which led to a fall in OD to 36.6% of control ($p < 0.0001$). Although 'test' cells exposed to 5 and 10 secs light illumination led to a fall in OD to 62.0% and 53.6% of control ($p < 0.01$ and $p < 0.001$, respectively, when compared to control), when compared to cells that had received 'drug only,' this

fall was not significantly different, and thus, the toxicity seen in these test cells were likely due to dark toxicity.

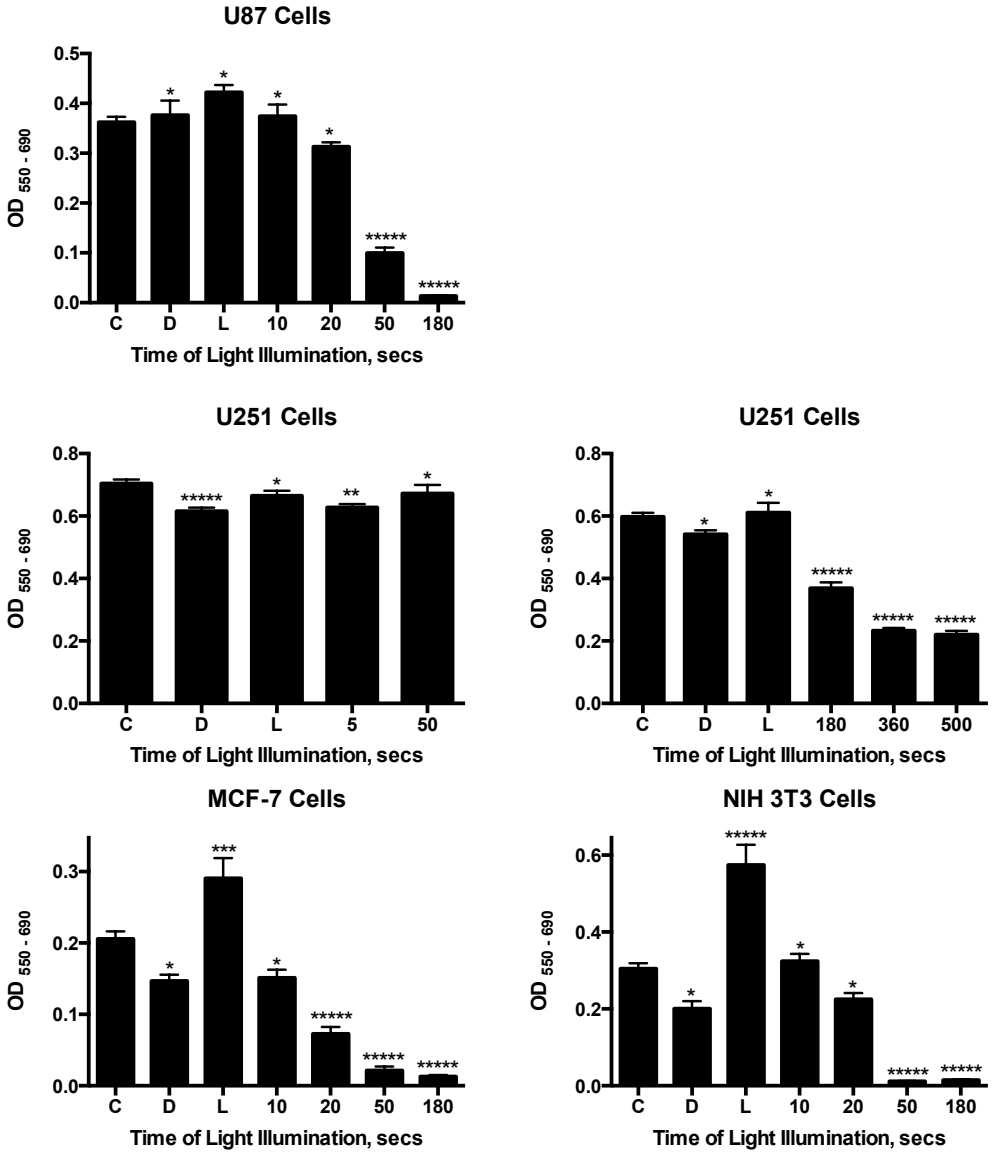

Figure 14 The effect of conventional PDT on cells lines incubated with hypericin for 4 hrs.

C = control, D = drug only, L = light only. Numbers on the x axis refer to the time in secs that cells incubated with drug were exposed to light, and represent the 'test' wells. Asterisks indicate the degree of significance of the difference in OD between each condition and control, where * $p > 0.05$, ** $p \leq 0.05$, *** $p < 0.01$, **** $p < 0.001$, ***** $p < 0.0001$. All cell lines were amenable to toxicity from conventional PDT and demonstrated a clear dose-response. The threshold of toxicity was 50 secs of light illumination (350 $mJcm^{-2}$) for U87 and NIH 3T3 cells; 180 secs of light illumination (1260 $mJcm^{-2}$) for U251 cells; and 20 secs light illumination (140 $mJcm^{-2}$) for MCF-7 cells.

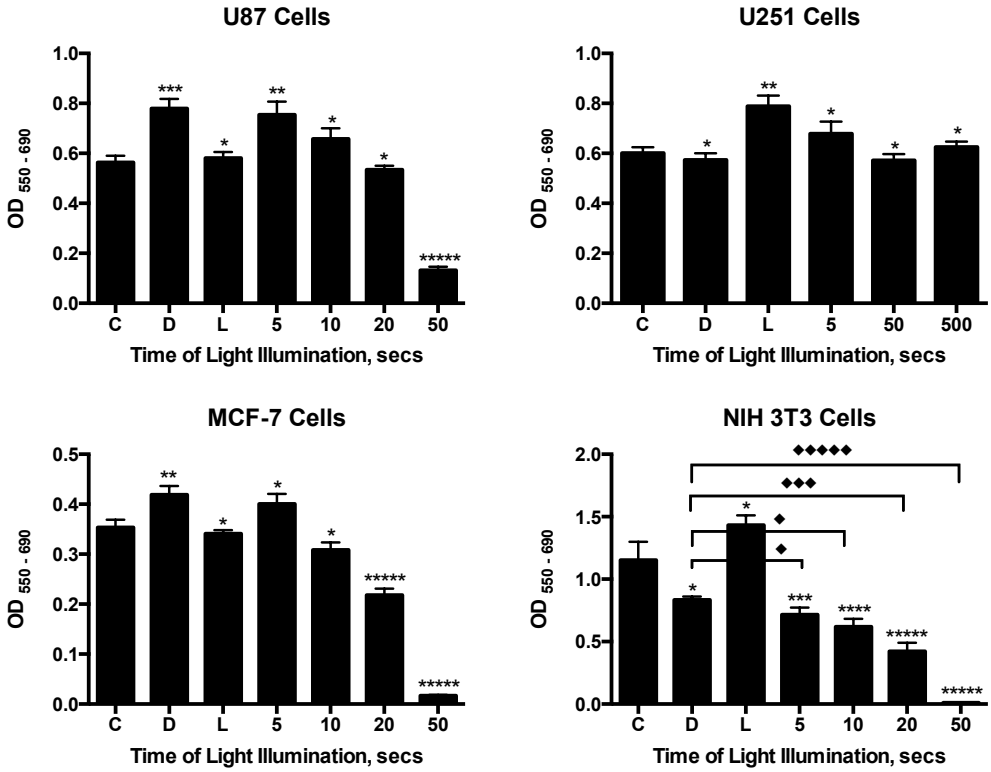

Figure 15 The effect of conventional PDT on cells lines incubated with hypericin for 24 hrs.

C = control, D = drug only, L = light only. Numbers on the x axis refer to the time in secs that cells incubated with drug were exposed to light, and represent the 'test' wells. Asterisks indicate the degree of significance of the difference in OD between each condition and control, where * $p > 0.05$, ** $p \leq 0.05$, *** $p < 0.01$, **** $p < 0.001$, ***** $p < 0.0001$. For NIH 3T3 cells, the diamonds indicate the degree of significance of the difference in OD between each condition and 'drug only' cells, where ◆$p > 0.05$, ◆◆$p \leq 0.05$, ◆◆◆$p < 0.01$, ◆◆◆◆$p < 0.001$, ◆◆◆◆◆$p < 0.0001$. All cell lines were amenable to toxicity from conventional PDT, except for the U251 cell line. Of the cell lines amenable to PDT, a dose-response was demonstrated. The threshold of toxicity was 50 secs of light illumination (350 mJcm^{-2}) for U87 cells, and 20 sec light illumination (140 mJcm^{-2}) for MCF-7 an NIH 3T3 cells.

6.2.3 *m*THPC, Short Incubation

For short incubation (3 hrs) with *m*THPC (see Figure 16), all cells lines were amenable to toxicity from conventional PDT and a clear dose-response was seen with increasing doses. The threshold of toxicity was 3 secs light illumination (21 mJcm^{-2}) for U87 cells, resulting in the OD falling to 70.7% ($p < 0.001$) of control; and 1 sec light illumination (7 mJcm^{-2}) for U251 cells, resulting in the OD falling to 41.7% of control ($p < 0.0001$). The threshold of toxicity was 20 secs light illumination (140 mJcm^{-2}) for MCF-7 cells, resulting in the OD falling to 66.0% ($p < 0.001$) of control: although exposure of these cells to 'drug' then 1 sec of light seemed to cause stimulation of growth (124%, $p \leq 0.05$), the degree of growth was small, and the 95% CI trended towards no significant

difference compared to control (- 0.0965 to - 0.000815), and thus this effect was considered as such. Although exposure of NIH 3T3 cells to 'light only' caused stimulation of cell growth, toxicity to PDT was indeed demonstrated and the threshold of toxicity was 3 secs light illumination (21 mJcm^{-2}), resulting in the OD falling to 38.3% ($p < 0.0001$) of control.

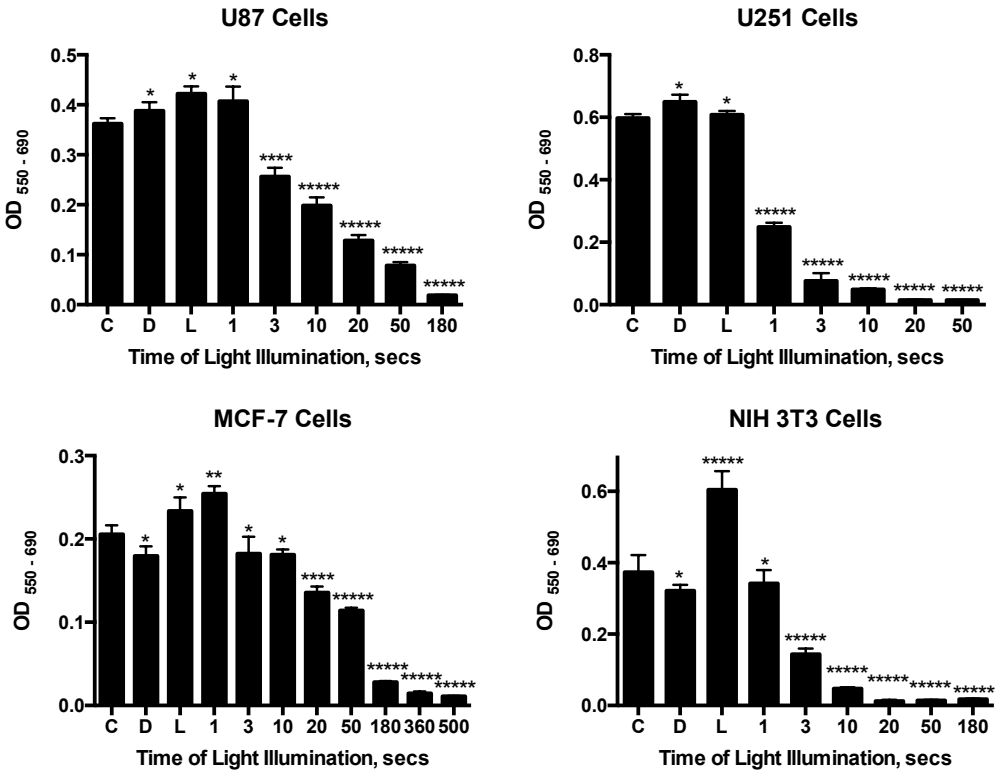

Figure 16 The effect of conventional PDT on cell lines incubated with *m*THPC for 3 hrs.

C = control, D = drug only, L = light only. Numbers on the x axis refer to the time in secs that cells incubated with drug were exposed to light, and represent the 'test' wells. Asterisks indicate the degree of significance of the difference in OD between each condition and control, where * $p > 0.05$, ** $p \leq 0.05$, *** $p < 0.01$, **** $p < 0.001$, ***** $p < 0.0001$. All cell lines were amenable to toxicity from conventional PDT and demonstrated a clear dose-response. The threshold of toxicity was 3 secs of light illumination (21 mJcm^{-2}) for U87 and NIH 3T3 cells; 1 sec of light illumination (7 mJcm^{-2}) for U251 cells; and 20 secs light illumination (140 mJcm^{-2}) for MCF-7 cells.

6.2.4 mTHPC, Long Incubation

For long incubation (24 hrs) with *m*THPC (see Figure 17), all cell lines were amenable to toxicity from conventional PDT and a clear dose-response was seen with increasing doses of light. The threshold of toxicity was 3 secs light illumination (21 mJcm^{-2}) for U87, U251 and NIH 3T3 cells, resulting in the OD falling to 51.5% of control ($p < 0.01$), 10.6% of control ($p < 0.0001$), and 30.3% of control ($p < 0.0001$), respectively. Although exposure of U251 cells to 'light only' seemed to cause toxicity with the OD

91.5% of control ($p \leq 0.05$), this fall in OD was small and the 95% CI trended strongly towards no significant difference to control (0.00341 to 0.116), and hence was treated as such. Similarly, although exposure of MCF-7 cells to 'drug' then 5 secs light seemed to cause toxicity (OD 82.2% of control, $p \leq 0.05$), the fall in OD was small and the 95% CI trended strongly towards no significant difference to control (0.00202 to 0.206), and hence was treated as such. The threshold of toxicity was 20 secs light illumination (140 $mJcm^{-2}$) for MCF-7 cells, resulting in the OD falling to 53.4% of control ($p < 0.0001$).

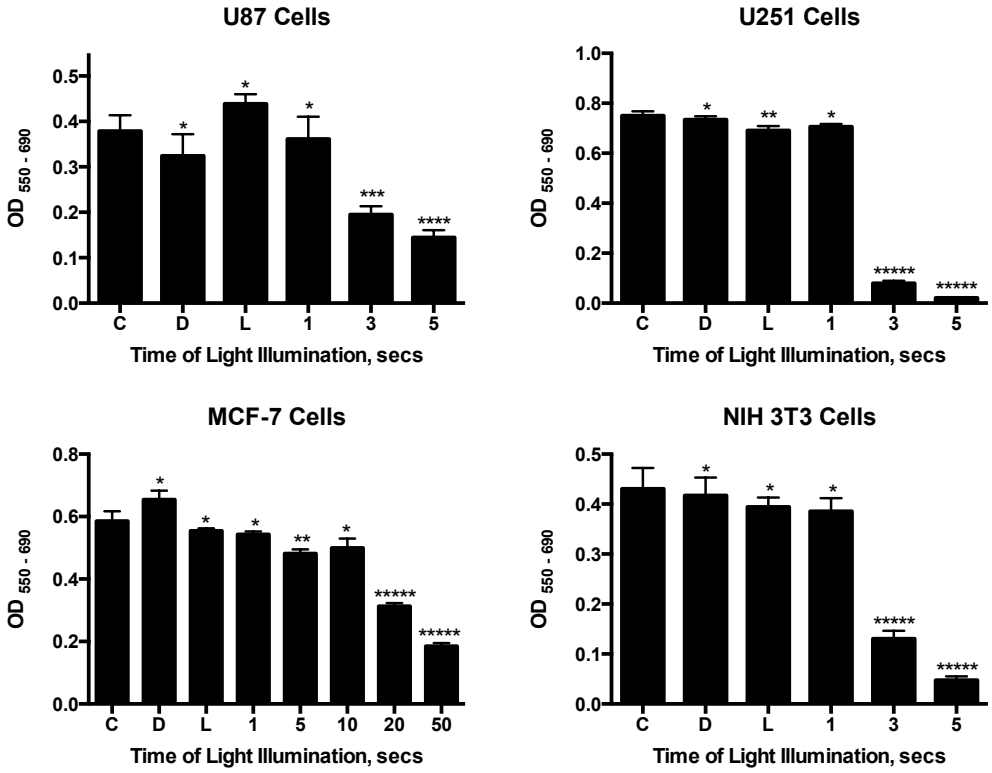

Figure 17 The effect of conventional PDT on cell lines incubated with *m*THPC for 24 hrs.

C = control, D = drug only, L = light only. Numbers on the x axis refer to the time in secs that cells incubated with drug were exposed to light, and represent the 'test' wells. Asterisks indicate the degree of significance of the difference in OD between each condition and control, where * $p > 0.05$, ** $p \leq 0.05$, *** $p < 0.01$, **** $p < 0.001$. ***** $p < 0.0001$. All cell lines were amenable to toxicity from conventional PDT and demonstrated a clear dose-response. The threshold of toxicity was 3 secs light illumination (21 $mJcm^{-2}$) for U87, U251 and NIH 3T3 cells. The threshold of toxicity was 20 secs light illumination (140 $mJcm^{-2}$) for MCF-7 cells.

All cells lines were amenable to cell kill by conventional PDT (see Table 6). Regarding the use of hypericin as the photosensitiser, U251 cells seemed the most resistant to PDT: exposure to light after short incubation with hypericin was associated with the highest threshold of toxicity and after long incubation with hypericin had no effect at

all. However, this is most likely a reflection of the unusually low maximum sub-lethal dose of photosensitiser that could be used rather than an inherent resistance to PDT. There are no reports of U251 cells being used for PDT with hypericin as a photosenstiser. MCF-7 and NIH 3T3 cells had comparable responses to PDT, with similar thresholds of toxicity: although NIH 3T3 cells had a higher threshold of toxicity than MCF-7 after short incubation with hypericin, the resultant cell kill was profound. Apart from U251 cells, U87 cells incubated with hypericin were the most resistant to cell kill by conventional PDT, although the degree of cell kill achieved at the threshold of toxicity was profound. There was no marked difference in the effect to PDT between short or long incubation with hypericin.

Regarding the use of *m*THPC as a photosensitiser, U251 cells were the most susceptible to cell kill by conventional PDT, having the lowest threshold of toxicity after short incubation with the photosensitiser, and having the most profound cell kill after long incubation with photosensitiser at a threshold of toxicity comparable to other cell lines. MCF-7 cells were the least susceptible to cell kill by conventional PDT, having the highest threshold of toxicity. U87 and NIH 3T3 cells had similar thresholds of toxicity. However, a greater degree of cell kill was achieved in NIH 3T3 for both photosensitiser incubation times. Longer incubation with *m*THPC seemed to provide some advantage, with mildly increased cell kill at similar fluences. This would be consistent with the photosensitiser forming aggregates after 24 hr incubation[155], which are associated with less photodynamic efficacy[149,166,169].

PDT with *m*THPC as the photosensitiser was more effective than with hypericin, with lower thresholds of toxicity achieved for all cell lines, except for the MCF-7 cell line, which had a similar threshold of toxicity after incubation with both photosensitiers at short and long incubation times.

	Hypericin, Threshold of Toxicity, $mJcm^{-2}$ (% of control)		*m*THPC, Threshold of Toxicity, $mJcm^{-2}$ (% of control)	
Incubation Time	4 Hrs	24 Hrs	3 Hrs	24 Hrs
U87	350 (27.6)	350 (23.5)	21 (70.7)	21 (51.5)
U251	1260 (61.8)	-	7 (41.7)	21 (10.6)
MCF7	140 (35.4)	140 (61.6)	140 (66.0)	140 (53.4)
NIH 3T3	350 (3.77)	140 (36.6)	21 (38.3)	21 (30.3)

Table 6 Summary of the threshold of toxicity for each cell line

The threshold of toxicity i.e. the lowest light dose at which toxicity was achieved is reported for each photosensitiser and both their incubation times in each cell line. The percentage cell survival is noted in brackets.

6.3 Summary and Discussion

Before testing the concept of bPDT, cell lines were tested to investigate their response to conventional PDT. This provided an opportunity to establish their dark toxicity and to note the lowest light doses at which toxicity can be achieved, the threshold of toxicity, providing an estimation of the relative susceptibility of the cell lines to PDT.

Maximum sub-lethal doses of the photosensitisers at two incubation times were established in all cell lines. All cell lines were amenable to cell kill by PDT. Results from the U251 cell line incubated with hypericin were unreliable. Although MCF-7 cells incubated with hypericin were least resistant to cell kill by PDT, when incubated *m*THPC, were the most resistant to PDT. Based on these results, the decision was made to proceed with the U87 and NIH 3T3 cell lines for ongoing experimentation. Furthermore, for studies involving their incubation with photosensitisers, their maximum sub-lethal dose for the appropriate incubation time would be used.

Chapter 7 Generating Bioluminescent Cell Lines and Characterising Bioluminescence

The aim was to produce cell lines that would generate bioluminescence at three different wavelengths. Plasmids containing firefly (*luc*), click beetle (CBG68*luc*), and Renilla *(hRluc)* luciferase, which would produce bioluminescence with peak emission wavelengths at 560 nm, 537 nm and 480 nm, respectively, were cloned for cell transfection.

A brief overview of the DNA cloning process is illustrated in Figure 18. As a plasmid containing firefly luciferase, CMV-*luc,* had been kindly donated by Professor G Van der Pluijm, only plasmids containing click beetle and Renilla luciferase, CMV-CBG68*luc* and CMV-*hRluc* respectively, had to be generated. In short, click beetle and Renilla luciferase genes were purchased as vectors, along with a backbone vector, and these vectors were multiplied by bacterial transformation. Once multiplied and extracted, the vectors underwent digestion by specific restriction endonucleases. The luciferase genes could then be ligated into the backbone vector, thereby forming the desired plasmids.

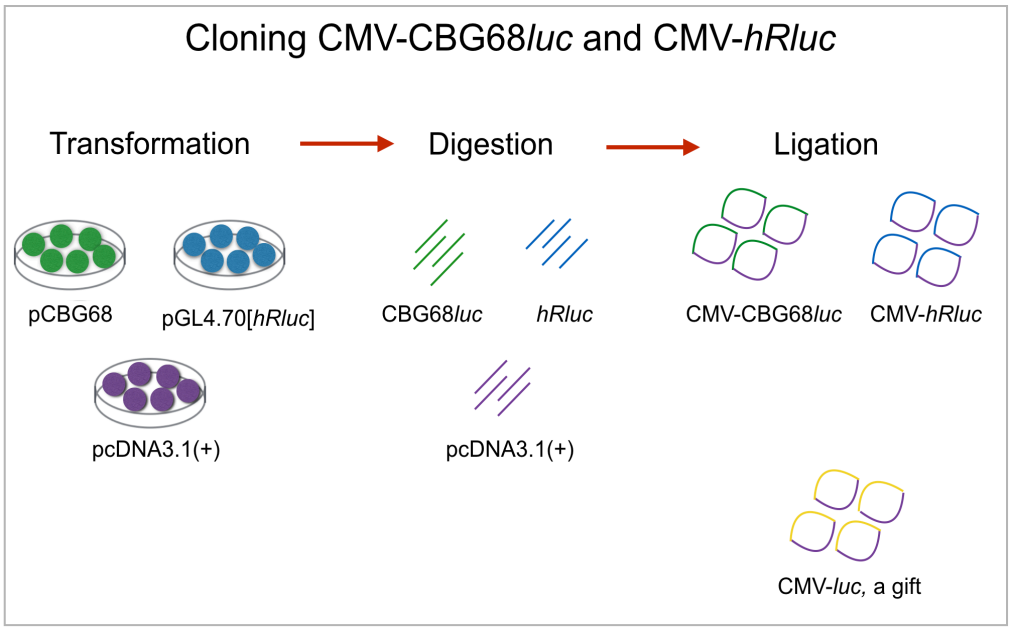

Figure 18 An overview of DNA cloning.

The luciferase genes, CBG68*luc* and *hRluc,* were purchased as vectors, pCBG68 and pGL4.70[*hRluc*], respectively. These vectors, along with the backbone vector pcDNA3.1(+), were multiplied by bacterial transformation. Once extracted, the vectors underwent digestion by specific restriction endonucleases. The resulting luciferase genes could then be ligated into the backbone vector, forming the desired plasmids.

A more detailed description of the DNA cloning process will now be given and results presented, with specific protocols regarding bacterial and DNA manipulation considered in the following sections.

7.1 DNA Cloning

7.1.1 Vectors and plasmids

The luciferase genes of CBG68*luc* and *hRluc* were purchased as vectors, pCBG68 and pGL4.70[*hRluc*] respectively, from Promega (see Appendix 2). A pcDNA3.1(+) backbone vector containing an origin of replication for *E.Coli*, a CMV promoter, and sequences for ampicillin and neomycin resistance, was purchased from Invitrogen (see Appendix 2). CMV-*luc*, a plasmid containing firefly luciferase in a pcDNA3.1(+) backbone, ready for cell transfection, was kindly given by Professor G Van der Pluijm.

7.1.2 Cloning CMV-CBG68*luc* and CMV-*hRluc*

Copies of pCBG68, pGL4.70[*hRluc*], and pcDNA3.1(+) were multiplied by bacterial transformation. For each vector, several bacterial colonies were selected for large-scale preparation and an example of the yields are given below (see Table 7).

Sample	Yield, ηg/μl
pCBG68*luc* 1	1212.30
pCBG68*luc* 2	1518.90
pGL4.0[*hRluc*] 1	3690.54
pGL4.0[*hRluc*] 2	2756.77
pcDNA3.1(+)	3933.25

Table 7 An example of the DNA yields from bacterial transformation and large-scale preparation of vectors pCBG68, pGL4.70[*hRluc*], and pcDNA3.1(+), in preparation for cloning CMV-CBG68*luc* and CMV-*hRluc*

pCBG68 has HindIII and XbaI restriction endonuclease recognition sites on the 5' and 3' ends of the luciferase gene, respectively (see Appendix 2). Similarly, pGL4.70[*hRluc*] has HindIII and BamHI recognition sites. pcDNA3.1(+) also has these recognition sites in a forward orientation in its multiple cloning region. pCBG68 and one sample of pcDNA3.1(+) were digested with the restriction endonucleases HindIII and XbaI, and pGL4.70[*hRluc*] and another sample of pcDNA3.1(+) were digested with Hind III and BamHI. Successful digestion was confirmed with gel electrophoresis (see Figure 19).

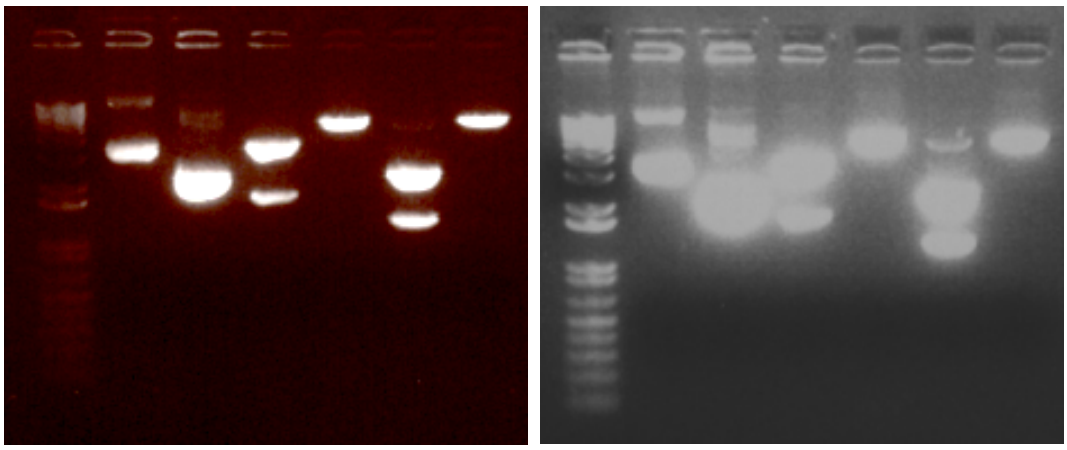

Figure 19 Gel electrophoresis demonstrating successful digestion of pCBG68, pGL4.70[*hRluc*], and pcDNA3.1(+).

Two different exposures of the same gel are shown. Columns from left to right: 1 Kb DNA ladder; undigested pCBG68 (5248 bp); undigested pGL4.70[*hRluc*] (3653 bp); pCBG68 digested with HindIII and XbaI (CBG68*luc* = 1628 bp); pcDNA3.1(+) digested with HindIII and XbaI (5168 bp); pGL4.70[*hRluc*] digested with HindIII and BamHI (*hRluc* = 1058 bp); pcDNA3.1(+) digested with HindIII and BamHI (5230 bp).

Repeat gel electrophoresis was performed and the digested pcDNA3.1(+), CBG68*luc* and *hRluc* fragments were isolated, then extracted from the agarose gel. Another gel was run to confirm successful isolation of pcDNA3.1(+), and the CBG68*luc* and *hRluc* inserts (see Figure 20). CBG68*luc* and *hRluc* were then ligated with the similarly digested pcDNA3.1(+) to produce CMV-CBG68*luc* and CMV-*hRluc*, respectively. Two negative controls were made by ligating HindIII/XbaI-digested pcDNA3.1(+) with itself, and ligating HindIII/BamHI-digested pcDNA3.1(+) also with itself. Competent bacteria were then transformed with each of these plasmids. The positive control was bacteria transformed with CMV-*luc* given by Professor G Van der Pluijm. 16-18 colonies of bacteria transformed with CMV-CBG68l*uc* were seen after 24 hr incubation. No colonies were seen with bacteria transformed with CMV-*hRluc*, or the negative controls. Multiple colonies were seen with the positive control. Results indicated successful cloning of CMV-CBG68*luc*, but failure to clone CMV-*hRluc*.

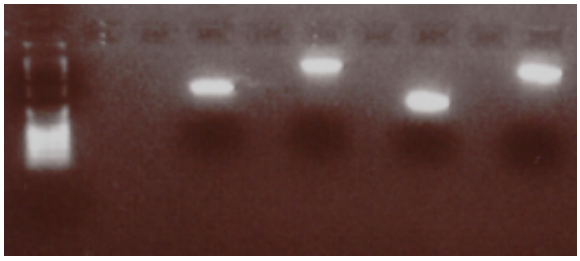

Figure 20 Gel electrophoresis confirming successful isolation of digested pcDNA3.1(+), and CBG68*luc* and *hRluc* inserts.

Columns from left to right: 1 Kb DNA ladder; CBG68*luc* insert (1628 bp); pcDNA3.1(+) digested with HindIII and XbaI (5168 bp); *hRluc* insert (1058 bp); pcDNA3.1(+) digested with HindIII and BamHI (5230 bp).

10 colonies of CMV-CBG68*luc* transformants were harvested for small-scale plasmid preparation. Plasmid obtained from each colony underwent digestion with HindIII, XbaI or both. Gel electrophoresis of these samples showed that all colonies, except for colony 9, contained the CBG68*luc* insert (see Figure 21).

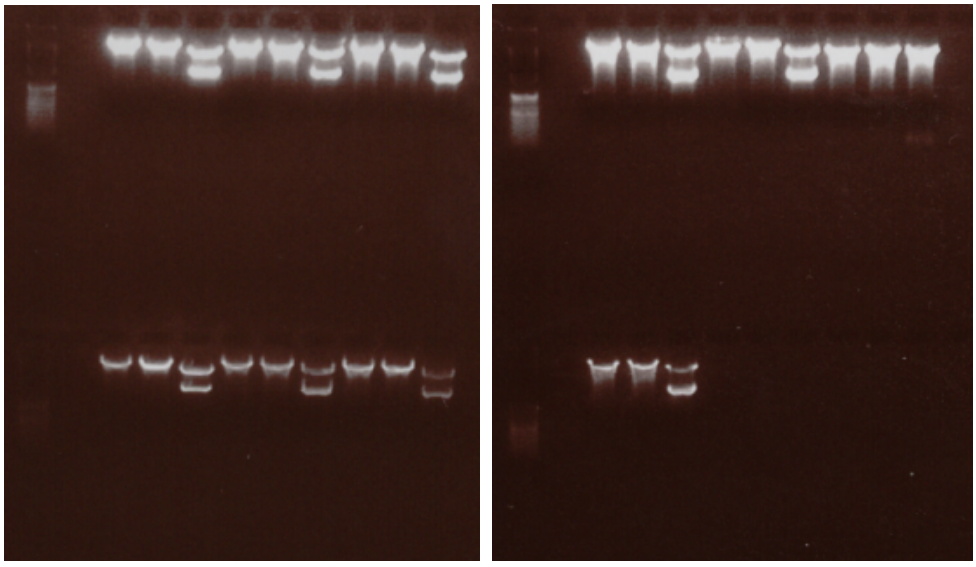

Figure 21 Gel electrophoresis of CMV-CBG68*luc* from 10 transformants.

A 1 kb ladder is seen in the far left column of each gel. For each transformant, three digests are seen; one digested with HindIII only, one digested with XbaI only, and the last digested with both HindIII and XbaI. All transformants, except for colony 9 (third transformant in the top row of the second gel), are seen to contain the CBG68*luc* insert.

A repeat attempt was made to clone CMV-*hRluc*, following the steps described above. Gel electrophoresis confirmed successful digestion of pGL4.70[*hRluc*] and pcDNA3.1(+) with HindIII and BamHI (see Figure 22). However, ligation of *hRluc* into pcDNA3.1(+) and transformation into competent bacteria yielded no transformants. It was suspected that the SV40 late polyA signal just downstream to the *hRluc* gene was interfering with gene expression. Further examination of the pGL4.70[*hRluc*] sequence revealed an XbaI site at the 3' end of the *hRluc* gene, upstream to the SV40 late polyA signal. Steps described above were repeated to clone CMV-*hRluc*, but this time digesting pGL4.70[*hRluc*] with HindIII and XbaI. Gel electrophoresis revealed successful enzyme digestion (see Figure 23). The *hRluc* insert was ligated into pcDNA3.1(+) that had previously been successfully digested with HindIII and XbaI (see Figure 19 and Figure 20), then transformed into competent bacteria. This yielded 4 colonies, indicating successful cloning of CMV-*hRluc*. The negative control was ligating HindIII/XbaI-digested pcDNA3.1(+) with itself, then transforming this into competent bacteria, which yielded no colonies. The positive control was bacteria transformed with CMV-*luc*, which yielded multiple colonies.

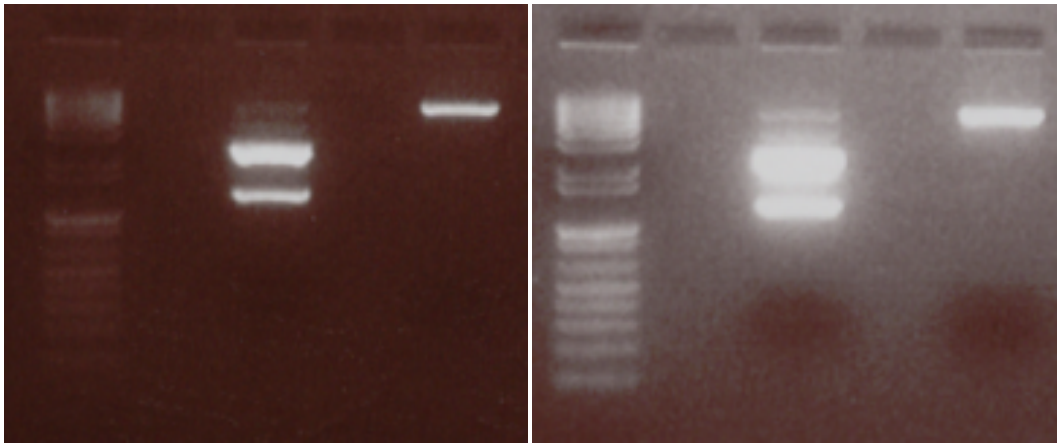

Figure 22 Gel electrophoresis demonstrating successful digestion of pGL4.70[*hRluc*], and pcDNA3.1(+) with HindIII and BamHI

Two different exposures of the same gel are shown. Columns from left to right: 1 Kb DNA ladder; pGL4.70[*hRluc*] digested with HindIII and BamHI (*hRluc* = 1058 bp); pcDNA3.1(+) digested with HindIII and BamHI (5230 bp).

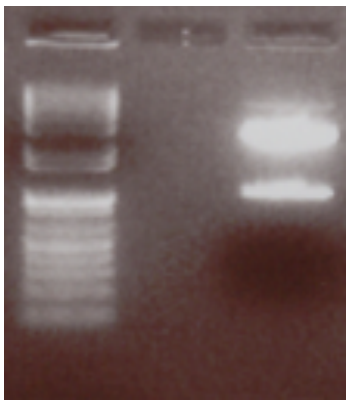

Figure 23 Gel electrophoresis of pGL4.0[*hRluc*] digested with HindIII and XbaI

Columns from left to right: 1 Kb DNA ladder; pGL4.70[*hRluc*] successfully digested with HindIII and XbaI (*hRluc* = 1058 bp).

All 4 colonies were picked for small-scale plasmid preparation. Plasmid obtained from each colony underwent digestion with HindIII, XbaI or both. Gel electrophoresis of these samples showed that all colonies, except for colony 2, contained the *hRluc* insert (see Figure 24).

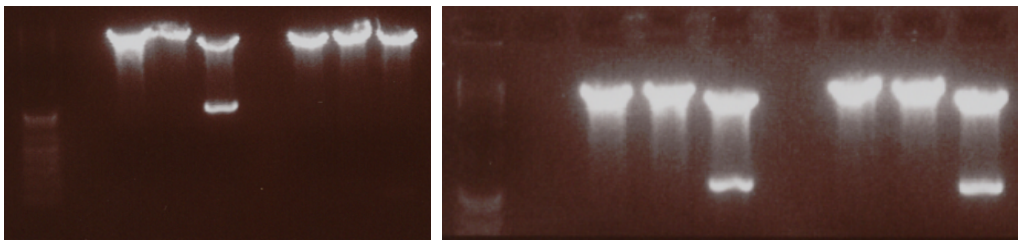

Figure 24 Gel electrophoresis of CMV-*hRluc* from 4 transformants.

A 1 kb ladder is seen in the far left column of each gel. For each transformant, three digests are seen; one digested with HindIII only, one digested with XbaI only, and the last digested with both HindIII and XbaI. All transformants, except for colony 2 (second transformant of the first gel), are seen to contain the *hRluc* insert.

7.1.3 Preparing DNA for Cell Cloning

Bacterial transformants of a colony demonstrating the presence of CBG68*luc* and *hRluc* inserts were used for large-scale plasmid preparation, to produce a stock of CMV-CBG68*luc* and CMV-*hRluc*. Similarly, a stock of CMV-*luc* was also generated. The yields obtained are shown below (see Table 8).

Sample	Yield, ηg/μl
CMV-*luc*	6021.39
CMV-CBG68*luc*	4149.39
CMV-*hRluc*	3479.97

Table 8 An example of the DNA yields from large-scale preparation plasmids CMV-*luc*, CMV-CBG68*luc*, and CMV-*hRluc*.

As a final check, samples of CMV-CBG68*luc* and CMV-*hRluc* obtained were digested with HindIII only, XbaI only, and both endonucleases. Gel electrophoresis showed that CBG68*luc* and *hRluc* inserts were present, respectively (see Figure 25).

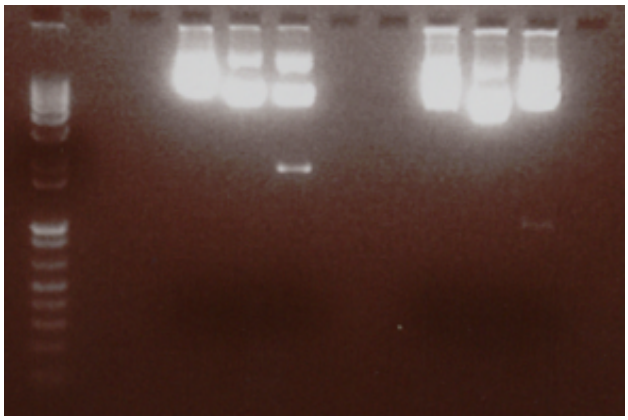

Figure 25 Gel electrophoresis of CMV-CBG68*luc* and CMV-*hRluc* showing the presence of CBG68*luc* and *hRluc* inserts, respectively.

Columns from left to right: 1 Kb DNA ladder; CMV-CBG68*luc* digested with HindIII only, CMV-CBG68*luc* digested with XbaI only; CMV-CBG68*luc* digested with HindIII and XbaI (CBG68*luc* = 1628 bp); CMV-*hRluc* digested with HindIII only, CMV-*hRluc* digested with XbaI only; CMV-*hRluc* digested with HindIII and XbaI (*hRluc* = 1058 bp).

Protocols followed for bacterial and DNA manipulation will now be described.

7.2 Bacterial Manipulations

7.2.1 Bacterial Strains

The JS4 *E. coli* strain was used for plasmid manipulation and preparation. JS4 is a *rec*A1 derivative of MC1061 and has the following genotype: F$^-$*ara*D139, Δ(*ara, leu*)7697, Δ(*lac*)χ74, *gal*U, *gal*K, *hsd*R2 (rk$^-$ mk$^-$), *mcr*A, *mcr*BC, *rps*L(Strr) *thi*, *rec*A.

7.2.2 Media and Bacterial Growth

E. coli cells were grown in LB Broth (25g/L Luria Broth Base) or Super Broth (32 g/L bactotryptone, 20 g/L yeast extract, 10 g/L MOPS). 15 g/L of agar (Oxoid) was added to LB medium when preparing LB agar plates. To make up the media, all the components were dissolved in dd H_2O and autoclaved for 20 min at 121^0C. When required, ampicillin was added to give a final concentration of 100 μg/ml.

7.2.3 Preparation of Competent Bacteria

The JS4 bacteria kindly given had already been made competent using the following method. 5 ml of LB medium was inoculated with a single bacterial colony and incubated overnight with shaking at 37^0C. The subsequent culture was decanted into 500 ml of LB medium and grown at 37^0C with aeration for 2.0-2.5 hr until the optical density (OD) reading at 600 nm (OD_{600}) reached 1.0-1.2 (mid-exponential phase). Bacteria were then harvested by centrifugation at 2500 rpm for 20 min; resuspended in 5 ml of ice-cold, 0.1 molar (M) calcium chloride ($CaCl_2$); and placed on ice for 20 min. Bacteria were centrifuged again and resuspended in 5 ml of ice-cold 85:15 solution 0.1 M $CaCl_2$ and glycerol. 1 ml aliquots were placed in liquid N_2-chilled 1.5 ml microfuge tubes and stored at -80^0C.

7.2.4 Bacterial Transformation

1 ml of frozen, competent, JS4 bacteria was thawed on ice. Once thawed, 0.9 ml of ice-cold 0.1 M $CaCl_2$ was added and 0.1 ml of this mixture was then added to each DNA sample to be transformed. The DNA/bacteria samples were placed on ice for 30 min followed by heat shock at 42^0C for 90 sec. The transformations were returned to ice where 1 ml of LB medium was added to each specimen, which were then incubated at 37^0C for 30 min. Each sample was plated on pre-warmed, 10 cm^2, LB agar plates containing ampicillin, at a final concentration of 100 μg/ml, and incubated overnight at 37^0C. A negative control plated with competent, JS4 bacteria that had not been transformed was also prepared.

7.3 DNA Manipulations

7.3.1.DNA Preparation

All vector and plasmid preparations, both small and large scale, were carried out using QIAGEN kits, following manufacturer instructions.

7.3.1.1 Small Scale Plasmid Preparation

All solutions and buffers used were from the QIAfilter Plasmid Mini Kit, QIAGEN. All centrifugation occurred at a speed of 13 000 rpm.

Liquid cultures of transformed bacteria picked from single colonies and transferred to 5 ml of LB medium containing ampicillin, were grown with vigorous shaking at 37^0C overnight. 1.5 ml samples were then transferred to 2 ml microfuge tubes and centrifuged for 30 sec. The resultant pellet was resuspended in 250 µl of buffer P1 (50 mM Tris/HCl, pH 8.0, 10 mM EDTA and 100 mg/ml RNAse A, stored at 4^0C), following which 250 µl of buffer P2 (200 mM NaOH and 1 % SDS) was added and gently mixed by inversion. 350 µl of solution buffer N3 (3.0 M sodium acetate, pH5.5) was then added and also mixed by inversion. The samples were centrifuged for 10 min and the supernatant transferred to a QIAprep spin column. The column was centrifuged for 1 min and the flow-through discarded. The column was then washed with 0.75 ml of buffer PE and centrifuged again for 1 min. The flow-through was again discarded and the column centrifuged for an additional 2 min to remove any residual buffer. DNA was then eluted with 50 µl of buffer EB. After 1 min, the column was centrifuged for 1 min. The flow-through DNA was collected and stored at -20^0C.

7.3.1.2 Large Scale Plasmid Preparation

All solutions and buffers used were from the QIAfilter Plasmid Maxi Kit, QIAGEN.

200 ml of Super Broth containing 100 µg/ml of ampicillin was inoculated with an overnight culture of transformed bacteria from a single colony. After incubation at 37^0C with vigorous shaking for 24h, bacteria were harvested at 6000 rpm for 15 min at 4^0C using a Sorvall GS3 rotor. The bacterial pellet was resuspended in 10 ml of buffer P1. 10 ml of buffer P2 was then added. After incubation at room temperature for 5 min, 10 ml of chilled, neutralisation buffer P3 was added and the resultant lysate transferred to a QIAfilter cartridge. Following incubation at room temperature for 10 min, the lysate was transferred to a pre-equilibrated QIAGEN-tip 500 column (equilibration buffer QBT: 750 mM NaCl, 50 mM MOPS, pH 7.0, 15 % ethanol v/v, and 0.15 % Triton X-100) and allowed to enter the resin under gravity. The column was then washed twice with 30 ml of Buffer QC (1 M NaCl, 50 mM MOPS, pH 7.0, and 15 % ethanol). DNA was eluted with 15 ml of elution buffer OF (1.25 M NaCl, 50 mM Tris-HCl, pH 8.5, and 15 % ethanol) and precipitated in 10.5 ml of isopropanol at room temperature. Centrifugation was then performed at 4^0C 8000 rpm for 15 min using a

Sorvall SS-34 rotor, the only deviation from the standard protocol. The DNA pellet was washed with 1 ml 70% ethanol, transferred to a 1.5 ml vial, and centrifuged at 11 000 rpm for 5 min. Having decanted away the supernatant, the pellet was allowed to air dry, then redissolved in 0.1-0.2 ml of TE.

7.3.2 DNA Quantification

To determine DNA concentration, the OD of the solution was measured at 260 nm (OD_{260}) using a BioRad spectrophotometer (Bio-Rad Smart Spec™ 3000 Spectrophotometer). The DNA concentration was calculated using the relationship 1 OD unit at 260 nm = 50 μg/ml DNA.

7.3.3 Restriction Digests

Restriction digests of DNA plasmids were performed using restriction endonculeases from New England Biolabs. 5 μg of DNA was used for digestion. For HindIII and XbaI digestions, 3 μl of 10x buffer 2 (10 mM Tris-HCl, 50 mM NaCl, 10 mM $MgCl_2$, 1 mM DTT, pH 7.9 at 25^0C) was added to the DNA. For HindIII and BamHI digestions, 3 μl of 10x buffer 3 (50 mM Tris-HCl, 100 mM NaCl, 10 mM $MgCl_2$, 1 mM DTT, pH 7.9 at 25^0C) was added to the DNA. To the DNA/buffer mix, 0.5 μl of 100x BSA and 1 μl of each enzyme was added, with ddH_20 being used to make a total volume of 30 μl. 3 hr incubation at 37^0C was performed for all digestion reactions, followed by inactivation at 70^0C for 20 min. After resting at 4^0C for a few minutes, the digests were stored at -20^0C.

7.3.4 DNA-Agarose Gel Electrophoresis

DNA fragments were loaded with 1x DNA loading buffer (BlueJuice™, 65% (w/v) sucrose, 10 mM Tris-HCl [pH 7.5], 10 mM EDTA, and 0.3 % (w/v) bromophenol blue) and fractionated by electrophoresis on 1 % (w/v) agarose gels prepared in 1x TAE (40 mM Tris-acetate and 2 mM EDTA) with 0.5 μg/ml ethidium bromide. Electrophoresis in 1x TAE was carried out in electrophoresis tanks and DNA fragments were separated at a constant voltage of 70 V for a minimum of 30 min. Samples were loaded alongside 5 μl 1 Kb DNA ladder. Ethidium bromide stained DNA fragments were then visualised on a UVP (Dual Density UV transilluminator) and an image produced and printed with a Sony video graphic printer.

7.3.5 Extraction of DNA from Agarose Gels

DNA restriction fragments were separated on agarose gels with the electrophoresis running a constant voltage of 50 V for 1 hr. The resulting fragments were viewed with

a long wavelength UV emission transilluminator and the desired band isolated with a scalpel. DNA was then purified using the QIAquickGel Extraction Kit (QIAGEN), following instructions in the QIAquick Spin Handbook (QIAGEN): all centrifugation took place at 13 000 rpm for 1 min. To dissolve the gel, 3 volumes of buffer QG were added to the gel slice, which was then incubated at 50^0C for 10 min. Once dissolved, 1 gel volume of isopropanol was mixed with the sample, which was then transferred to a QIAquick spin column and centrifuged. To remove all traces of agarose, a further 0.5 ml of buffer QG was added to the column, which was centrifuged again. As a wash, 0.75 ml of buffer PE was added to the column and centrifuged. To elute the DNA, 30 µl of buffer EB was added to the column and centrifuged.

7.3.6 Ligation

15 µl ligation reactions were performed using 1 µl T4 DNA Ligase and 1.5-2 µl 10x ligation buffer (500 mM Tris-HCl pH7.5, 100 mM $MgCl_2$, 100 mM DTT, 10 mM ATP, and 250 µg/ml BSA). A ratio of 2:1 for vector DNA:insert DNA was used. Final samples were centrifuged at 13 000 rpm for 1 min, then stored overnight at 16^0C.

7.4 Cell Cloning: Generating Stable Luciferase-Expressing Cell Lines

U87 cells were transfected with CMV-*luc,* CMV-CBG68*luc* and CMV-*hRluc* to generate monoclonal and polyclonal lines. NIH 3T3 cells were transfected with CMV-*luc* to generate monoclonal and polyclonal lines.

A brief overview of the cell cloning process is illustrated in Figure 26. In short, cells were transfected with the desired plasmid using a transfection agent. After 48 hours of incubation, the standard culture media was replaced with a neomycin-containing, selection media. After further incubation, surviving cells, presumably those successfully transfected with plasmid, were either allowed to grow to 80% confluence, thereby generating a polyclonal line, or were harvested, replated such as to allow single cells to form colonies, each colony then being harvested and allowed to grow to 80% confluence, thereby generating monoclonal lines.

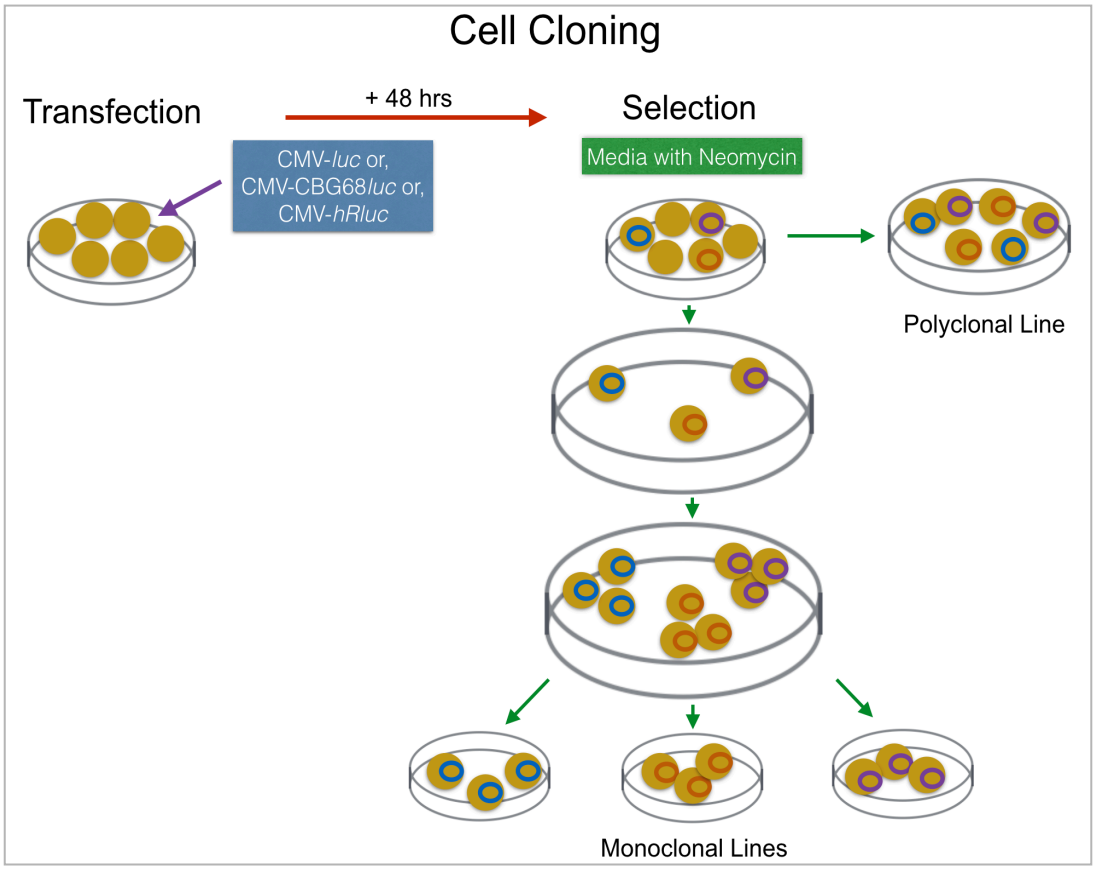

Figure 26 An overview of cell cloning.

Cells were transfected with the desired plasmid using a transfection agent. After 48 hours of incubation, the standard culture media was replaced with a neomycin-containing, selection media. After further incubation, surviving cells, were either allowed to grow to 80% confluence, thereby generating a polyclonal line, or were harvested, replated such as to allow single cells to form colonies, each colony then being harvested and allowed to grow to 80% confluence, thereby generating monoclonal lines.

A more detailed description of the cell cloning process now follows.

7.4.1 DNA Transfection of Cells

Cells were harvested by trypsinisation, plated at a density of $1.5x10^6$ cells per well of a 24 well plate, and incubated overnight. The transfection reagent, FuGENE HD, mediated transfection of cells with luciferase-containing plasmids. A series of 1 ml tubes were filled with 200 ml of serum free media. Pre-determined amounts of plasmid, then FuGENE HD was added to each tube at ratios of 3:1 and 3:2 FuGENE HD:plasmid, and immediately shaken. The mixture was left to incubate for 15 mins at room temperature. The contents were then added to appropriately labelled wells. There were also two controls: cells to which only serum free media was added, and those to which only FuGENE HD in serum free media was added. The cells were then placed in an incubator.

7.4.2 Transient Transfection

After 48 hrs of incubation, media was aspirated from the transfected cells, and the wells were washed with 0.5 ml of PBS. Cells were then prepared for a luciferase assay, as below.

7.4.3 Selection of Stable Transfectants

Following 48 hrs of incubation, media was aspirated from the transfected cells and replaced with complete media containing 1 mg/ml of neomycin. Cells were then incubated for a further 5 days.

7.4.4 Isolation of Monoclonal Luciferase-Expressing Lines

After transfection, selection with 1 mg/ml of neomycin, and 5 days of incubation, surviving cells were trypsinised and transferred from the 24 well plate to a 10 cm^2 plate. Cells were maintained in selection media; fresh media being changed every 3-4 days. Once individual colonies had established, single colonies were picked using sterile cloning discs. Media was aspirated from the dish. Trypsin-soaked cloning discs (0.5 cm^2 diameter) were then placed over the colonies. Following 1-2 mins incubation at 37^0C, discs, now holding the detached colony, were retrieved with a Pasteur pipette on light suction and transferred to individual wells of a 24 well plate containing fresh selection media. Cells were allowed to attach to the wells at 37^0C overnight, following which the discs were removed with a Pasteur pipette on light suction. Each colony was allowed to grow to 80% confluence, then progressively expanded into T80 cm^2 flasks.

7.4.5 Generation of Polyclonal Luciferase-Expressing Lines

Once cells had been transfected and exposed to selective media, they were allowed to grow to 80% confluence in the wells of the 24 well plate. Cells in each well were then progressively expanded into T80 cm^2 flasks.

7.4.6 Cell Culture of Luciferase-Expressing Lines

Monoclonal and polyclonal luciferase-expressing cell lines were sub-cultured and maintained in similar cell culture conditions as described in Chapter 6. The only exception was that luciferase-expressing cell lines were maintained in complete media containing 1 mg/ml neomycin at all times.

7.5 Characterising Bioluminescence

The degree of bioluminescence produced by each luciferase-expressing cell line generated was studied using two methods, the luciferase assay and the live cell assay.

7.5.1 Luciferase Assay

7.5.1.1 Preparation of Reagents

For CMV-*luc* and CMV-CBG68*luc* transfected cell lines, the luciferase assay was carried out using the Luciferase Assay System from Promega. The assay reagent was prepared by adding the vial of luciferase assay substrate with the luciferase assay buffer provided. The reagent was divided into 0.5 ml aliquots and stored at -70^{0}C. Before each experiment, the appropriate volume of reagent was thawed and allowed to equilibrate to room temperature, and 4 volumes of distilled water was added to 1 volume of the 5x luciferase assay lysis buffer provided, to make a 1x lysis buffer.

For CMV-*hRluc* transfected cell lines, the Renilla Luciferase Assay System from Promega was used. The reagent was prepared before each experiment by adding 1 volume of the 100x Renilla luciferase assay substrate to 100 volumes of the Renilla luciferase assay buffer provided. The 5x Renilla luciferase assay lysis buffer provided was prepared as above, to make a 1x lysis buffer.

7.5.1.2 Preparation of Cells

When analysing the effect of transient transfection, 48 hrs after transfection, cells were prepared in the wells that they had been transfected in. For stable transfectants, cells were harvested, following trypsinization, and plated at a density of 1x10^4 cells per well of a 24 well plate and allowed to incubate for 24 hrs. All cell lines tested were at the same passage number.

7.5.1.3 The assay

Media was aspirated from wells and cells washed with PBS. 0.1 ml of 1x lysis buffer was then added to each well and the plate rocked at room temperature for 5 mins, ensuring complete cell lysis. The lysate was stored at -20^{0}C. When ready to run the assay, the lysate was thawed and 5 µl lysate was transferred into the wells of a white, half area, Corning 96 well plate. 25 µl reagent was then added to each well and bioluminescence measured immediately on a luminometer. For transient transfectants, there were three controls, untransfected cells (C), untransfected cells that had been exposed to serum free media (C_M), untransfected cells that had been exposed to serum

free media and FuGENE HD (C_{Fu}). For stable transfectants, the only control was untransfected cells.

The method of cell transfection using the transfection reagent FuGENE HD was successful, as demonstrated by conducting a luciferase assay on U87 and NIH 3T3 cells transiently transfected with CMV-*luc* (see Figure 27). For U87 cells, there was no significant difference in light production between a 3:1 (28 200 ± 11 500 RLU) or 3:2 (27 800 ± 4 370 RLU) FuGENE HD:plasmid ratio ($p > 0.05$). However, for NIH 3T3 cells, a 3:1 FuGENE HD:plasmid ratio produced significantly more light (12 200 ± 1 950 RLU) compared to a 3:2 FuGENE HD:plasmid ratio (4 910 ± 934 RLU), indicating a more efficient transfection ($p < 0.01$) with a 3:1 FuGENE HD:plasmid ratio. Transfection of U87 cells produced more light than transfection of NIH 3T3 cells. There was no significant between the three controls, C, C_M and C_{Fu}, for each cell line.

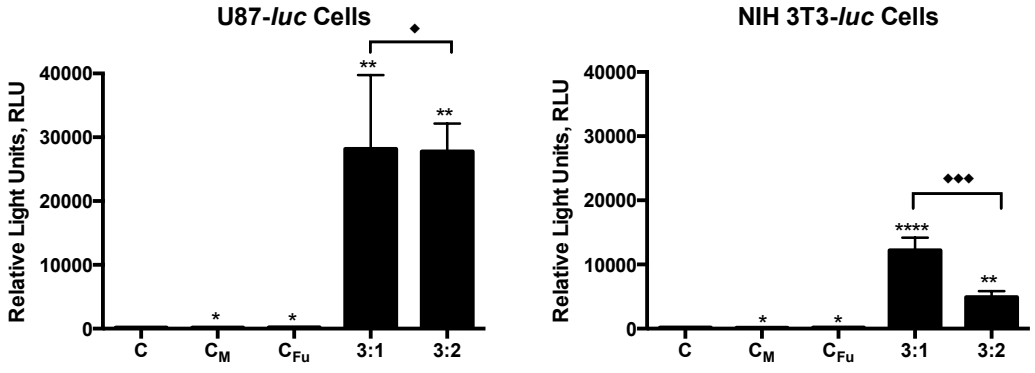

Figure 27 Luciferase Assay of U87 and NIH 3T3 transiently transfected with CMV-*luc*.

C = untransfected cells only; C_M = untransfected cells exposed to serum free media only; C_{Fu} = untransfected cells exposed to serum free media and FuGENE HD; 3:1, ratio of FuGENE HD:plasmid ; 3:2, ratio of FuGENE HD:plasmid. Asterisks indicate the degree of significance compared to C where * $p > 0.05$, ** $p \leq 0.05$, *** $p < 0.01$, **** $p < 0.001$. The diamonds represent the degree of significance between the two test conditions where ◆ $p > 0.05$, ◆◆ $p \leq 0.05$, ◆◆◆ $p < 0.01$, ◆◆◆◆ $p < 0.001$. For U87 cells, there was no significant difference in light production between a 3:1 (28 200 ± 11 500 RLU) or 3:2 (27 800 ± 4 370 RLU) FuGENE HD:plasmid ratio ($p > 0.05$). However, for NIH 3T3 cells, a 3:1 FuGENE HD:plasmid ratio produced significantly more light (12 200 ± 1 950 RLU) compared to a 3:2 FuGENE HD:plasmid ratio (4 910 ± 934 RLU) ($p < 0.01$).

Furthermore, stable, monoclonal U87-*luc* and NIH 3T3-*luc* transfectants were successfully generated (see Figure 28). For U87-*luc*, all cell lines generated significant amounts of light compared to control (A1, 90 100 ± 8 010 RLU; B1, 84 200 ± 3 030 RLU; B2, 73 600 ± 2 380 RLU; D1, 94 300 ± 3 340 RLU; E1, 161 000 ± 9 210 RLU; $p < 0.0001$). There was no significant difference in light production between cell lines A1, B1, B2 and D1. However, E1 produced significantly more light compared to the other cell lines ($p < 0.0001$). For NIH 3T3-*luc* cells, two of three lines, E1 and F1, produced significant amounts of light compared to control (E1, 1 410 ± 270 RLU; F1, 1 680 ± 94.3, $p < 0.001$), with no significant difference between the two cell lines.

Stable polyclonal U87-*luc* and NIH 3T3-*luc* cells were also generated (see Figure 28). For U87-*luc* cells, 1 way ANOVA analysis of the data indicated that one cell line, P6, produced a significant amount of light compared to control (447 000 ± 34 700 RLU, $p < 0.001$). However, cell lines P4 and P5 produced 51 200 ± 3 670 RLU and 15 100 ± 1 590 RLU of light, respectively. Although p values did not reach significance, this was likely due to the orders of magnitude difference in light generated by the P6 cell line. When P6 was excluded from analysis, the light generated by the P4 and P5 cell lines became significant compared to control ($p < 0.001$). For NIH 3T3-*luc* cells, four out of the eight polyclonal lines produced a significant amount of light compared to control (A2, 3 420 ± 303 RLU; γ3, 4 670 ± 387 RLU; D4, 1 150 ± 114 RLU; E4, 2 750 ± 191 RLU; $p < 0.001$).

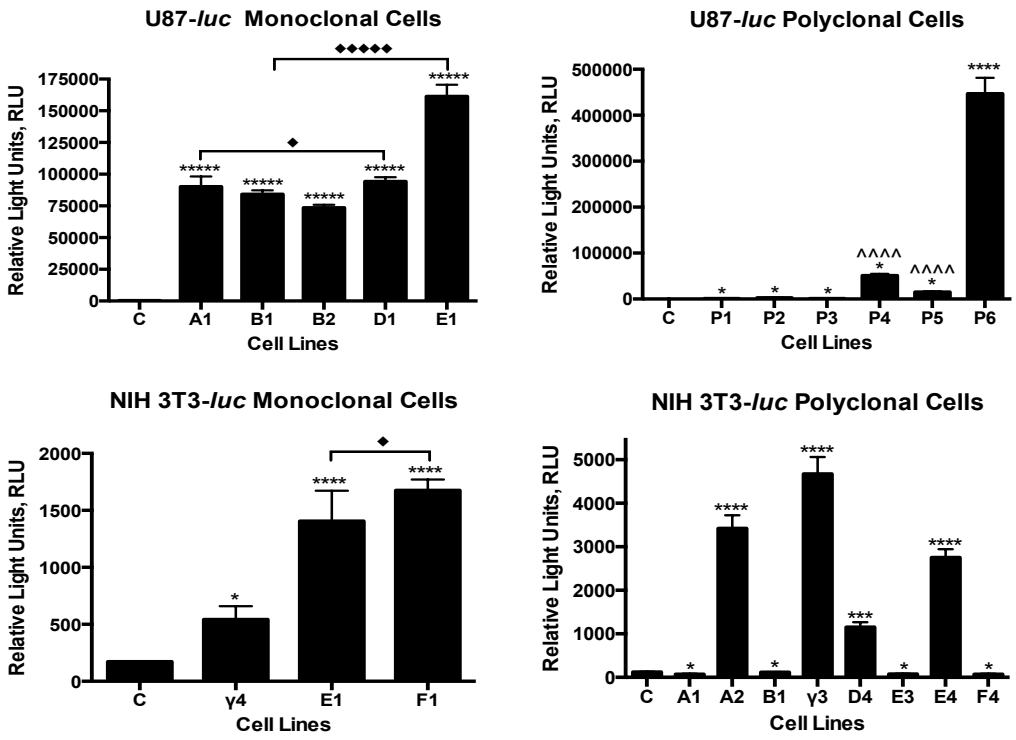

Figure 28 Luciferase assay of monoclonal and polyclonal U87-*luc* cell lines and NIH 3T3-*luc* cell lines

C = untransfected cells. The remaining 'test' conditions represent the various cell lines generated. Asterisks indicate the degree of significance in RLU of the test conditions compared to control, where * $p > 0.05$, ** $p \leq 0.05$, *** $p < 0.01$, **** $p < 0.001$, ***** $p < 0.0001$. Diamonds indicate the degree of significance in RLU between the test conditions, where ◆$p > 0.05$, ◆◆$p \leq 0.05$, ◆◆◆$p < 0.01$, ◆◆◆◆$p < 0.001$, ◆◆◆◆◆$p < 0.0001$. Regarding U87-*luc* polyclonal cells, ^^^^ indicate $p < 0.001$ compared to control having excluded P6 from the analysis. All U87-*luc* monoclonal cell lines generated significantly more light than control, with no significant difference between cell lines A1, B1, B2, D1; but with cell line E1 producing significantly more light than the rest of the cell lines. For NIH 3T3-*luc* monoclonal cells, 2 cell lines, E1 and F1, produced significantly more light than control. 3 U87-*luc* polyclonal lines produced significant amounts of light, with the P6 cell line generating orders of magnitude more light than cell lines P4 and P5. 4 NIH 3T3-*luc* polyclonal lines produced significantly more light than control.

Stable U87-CBG68*luc* monoclonal and polyclonal lines were generated (see Figure 29). Regarding monoclonal cells, the E1 cell line produced significant amounts of light (378 000 ± 39 300 RLU, $p < 0.001$) compared to control. On initial 1 way ANOVA analysis, the light produced by cell line γ2 (9 480 ± 968 RLU) did not reach significance. However, this was likely due to the orders of magnitude difference in light generated by the E1 cell line. When E1 was excluded from analysis, the light generated by the γ2 cell line became significant ($p < 0.001$). All U87-CBG68l*uc* polyclonal cell lines generated significant amounts of light compared to control (P1 78 500 ± 3140 RLU, P2 113 000 ± 7 220, P3 36 900 ± 4 760 RLU, P4 36 400 ± 2 940, P5

43 520 ± 4 160, P6 81 800 ± 4 190 RLU, P7 33 500 ± 3 340, and P8 58 000 ± 3 530 RLU, $p < 0.001$).

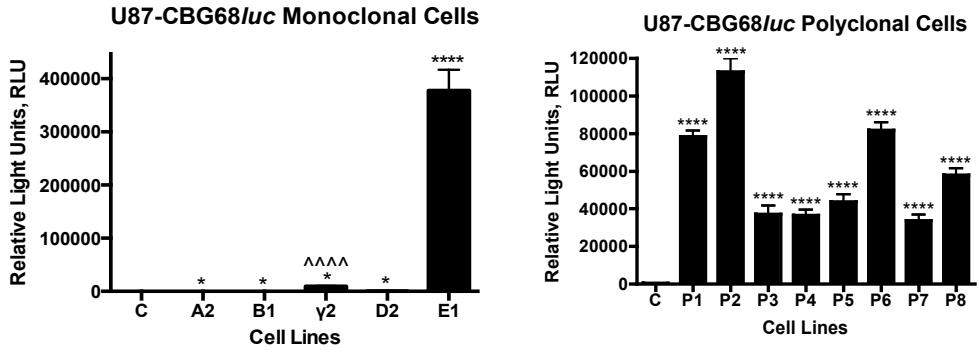

Figure 29 Luciferase assay of U87-CBG68l*uc* monoclonal and polyclonal lines

C = untransfected cells. The remaining 'test' conditions represent the various cell lines generated. Asterisks indicate the degree of significance in RLU compared to C where * $p > 0.05$, ** $p \leq 0.05$, *** $p < 0.01$, **** $p < 0.001$. ^^^^ indicate $p < 0.001$ compared to control having excluded E1 from the analysis. U87-CBG68l*uc* E1 cells generated significant amounts of light compared to control. When E1 cells were removed from analysis the amount of light produced by the γ2 cell line also reached significance. All polyclonal cell lines generated significant amounts of light compared to control.

Stable U87-*hRluc* monoclonal and polyclonal lines were generated (see Figure 30). Regarding monoclonal cells, cell line E produced significant amounts of light (713 000 ± 72 200 RLU, $p < 0.001$) compared to control. On initial 1 way ANOVA analysis, the light produced by cell lines D (46 800 ± 13 400 RLU) and I (89 400 ± 10 600 RLU) did no reach significance. However, this was likely due to the orders of magnitude difference in light generated by cell line E. When E was excluded from the analysis, the light generated by cell lines D and I became significant ($p < 0.001$). U87-*hRluc* polyclonal cell lines also generated significant amounts of light compared to control. Initial analysis revealed that cell lines P2, P4 and P6 generated a light signal significantly different to control (151 400 ± 2 800 RLU, $p < 0.01$; 415 000 ± 61 600 RLU, $p < 0.001$; and 178 000 ± 22 100 RLU, $p < 0.001$, respectively). When these cell lines were removed from analysis, so comparing signal of similar orders of magnitude, signal from cell lines P1, P3, P5 and P7, also reached significance (39 600 ± 3 250 RLU, 34 700 ± 3 850 RLU, 80 300 ± 4 160 RLU, and 40 200 ± 3 810 RLU, respectively, $p < 0.001$).

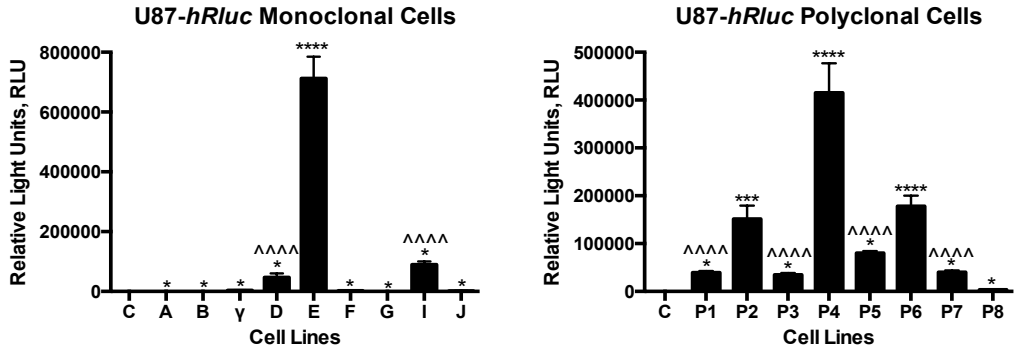

Figure 30 Luciferase assay of U87-*hRluc* monoclonal and polyclonal lines

C = untransfected cells. The remaining 'test' conditions represent the various cell lines generated. Asterisks indicate the degree of significance in RLU compared to C where * p > 0.05, ** p ≤ 0.05, *** p < 0.01, **** p < 0.001. ^^^^ indicate p < 0.001 compared to control having excluded cell lines generating signal of a higher order of magnitude from the analysis. U87-*hRluc* cell line E generated significant amounts of light compared to control. When cell line E was removed from analysis the amount of light produced by cell lines D and I reached significance. Polyclonal cell lines P2, P4 and P6 were found to generate significant amounts of light. After removing these from the analysis, cell lines P1, P3, P5 and P7, were also found to generate significant amounts of light.

Overall, more polyclonal than monoclonal cell lines capable of bioluminescence were generated: as described in detail above, 4 NIH 3T3-*luc* polyclonal cell lines capable of bioluminescence were generated compared to 2 NIH 3T3-*luc* monoclonal lines; and similarly, 8 U87-CBG68*luc* polyclonal cell lines were generated compared to 2 monoclonal lines; and 7 U87-*hRluc* polyclonal cell lines were generated compared to 3 monoclonal lines. The only exception was the U87-*luc* cell line, where 5 U87-*luc* monoclonal cell lines capable of bioluminescence were generated compared to 3 polyclonal lines. Furthermore, regarding U87 luciferase transfected cells (see Figure 31), although more polyclonal cell lines producing bioluminescence in the order of hundreds of thousands of RLU were generated compared to monoclonal lines, at least 1 monoclonal line was generated that was capable of producing an exceptional amount of light (U87-CBG68*luc* E1, 378 000 ± 39 300 RLU, $p < 0.001$; and U87-*hRluc* E, 713 000 ± 72 200 RLU, $p < 0.001$). Again, U87-*luc* was the exception: with U87-*luc* P6, a polyclonal line, producing an exceptional amount of light (447 000 ± 34 700 RLU, $p < 0.001$) compared to the monoclonal lines. Consistent with the transient transfectants, much greater bioluminescence was produced by U87 luciferase-transfected cells compared to NIH-3T3 luciferase-transfected cells, whether monoclonal or polyclonal. For this reason, ongoing characterisation of bioluminescence was carried out in the U87 transfected cells only.

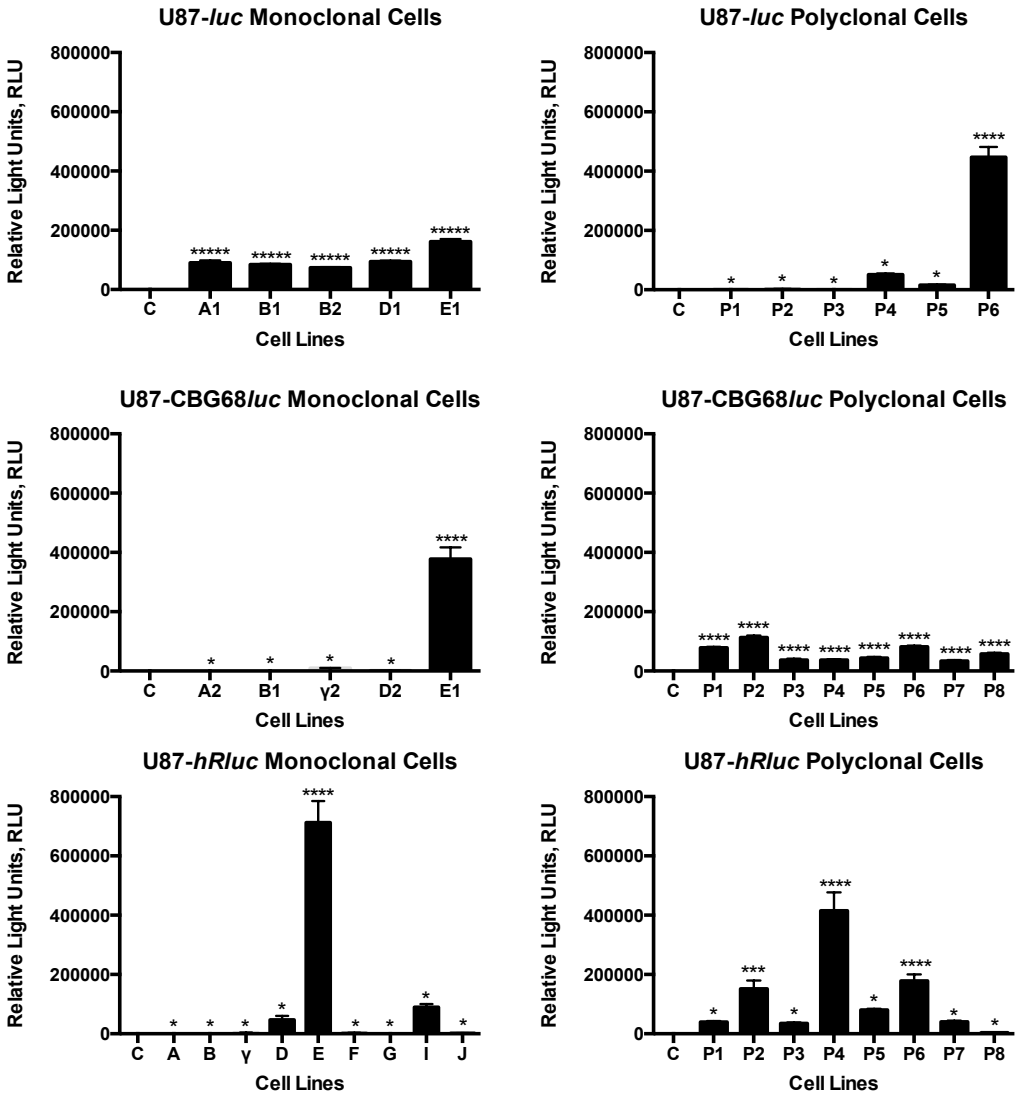

Figure 31 Summary of the Luciferase Assays carried on U87-*luc*, U87-CBG68*luc* and U87-*hRluc* monoclonal and polyclonal lines.

C = untransfected cells. Asterisks indicate the degree of significance in RLU of the test conditions compared to control, where * $p > 0.05$, ** $p \leq 0.05$, *** $p < 0.01$, **** $p < 0.001$, ***** $p < 0.0001$. Although more polyclonal cell lines producing bioluminescence in the order of hundreds of thousands of RLU were generated compared to monoclonal lines, at least 1 monoclonal line was generated that was capable of producing an exceptional amount of light (U87-CBG68*luc* E1 378 000 ± 39 300 RLU, $p < 0.001$;and U87-*hRluc* E, 713 000 ± 72 200 RLU, $p < 0.001$). Again, U87-luc was the exception with U87-*luc* P6, a polyclonal line, producing an exceptional amount of light (447 000 ± 34 700 RLU, $p < 0.001$) compared to the monoclonal lines.

7.5.2 Live Cell Assay

U87-*luc* and U87-*hRluc* cells were chosen to test the live cell assay.

7.5.2.1 Preparation of Reagents

For U87-*luc* cells, d-luciferin was used as the substrate. A 5 mM stock solution of d-luciferin (molecular weight = 318.4) was made by dissolving it in PBS. The solution was stored in 1 ml aliquots at -20^{0}C.

For U87-*hRluc* cells, EnduRen™ was used as the substrate. A 60 mM stock solution was made by dissolving the substances in tissue grade DMSO. The solution was stored in 1 ml aliquots at -20^{0}C.

7.5.2.2 Preparation of Cells

Cells were harvested and plated in white, flat bottom, tissue culture treated, 96 well plates (Sigma), at a density of 1x10^4 cells per well. Cells were replaced into the incubator.

7.5.2.3 The Assay

After 24 hrs incubation, media was aspirated from each well and replaced with 0.1 ml of complete media. 5 mM of d-luciferin was added to U87-*luc* cells and 60 mM of EnduRen™ was added to U87-*hRluc* cells, making final concentrations of 2.5 mM and 30 mM, respectively. Each cell line was tested in triplicate. The bioluminescence from the U87-*luc* cells was measured immediately after the substrate was added, whereas that from U87-*hRluc* cells was measured after 1 hour incubation with the substrate. The control was untransfected cells to which substrate was added.

Bioluminescence generated by U87-*luc* monocloncal cell lines was compared (see Figure 32). The live cell assay demonstrated that all cell lines produced bioluminescence that was significantly different from control. Cell lines A1 and D1 produced the most light (35 000 ± 2 060 RLU and 36 600 ± 2 440 RLU, respectively), with no significant difference between them. Cell lines B1, B2 and E1 produced significantly less light (20 300 ± 1 550 RLU**,** 16 200 ± 1 080 RLU, and 22 700 ± 1 020 RLU, respectively) than cell lines A1 and D1, although there was no significant difference between them. The luciferase assay was not predictive of the results of the live cell assay (see Figure 32): in contrast to the live cell assay, the luciferase assay demonstrated that E1 generated significantly more light than the other cell lines (161 000 ± 9 210 RLU, $p < 0.0001$), as discussed above. Furthermore, the luciferase assay generated 2.5 to 7 fold more light than the live cell assay.

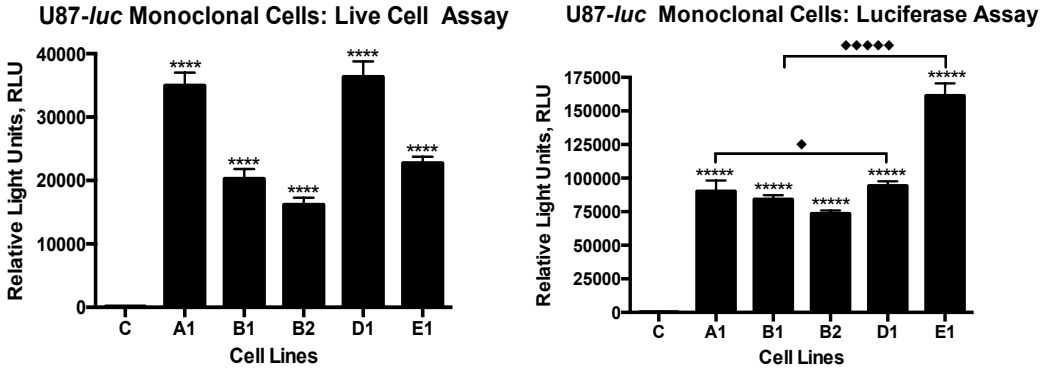

Figure 32 U87-*luc* Monoclonal Cells: Comparing the Live Cell Assay with the Luciferase Assay

C = untransfected cells. Asterisks indicate the degree of significance in RLU of the test conditions compared to control, where * $p > 0.05$, ** $p \leq 0.05$, *** $p < 0.01$, **** $p < 0.001$, ***** $p < 0.0001$. Diamonds indicate the degree of significance in RLU between the test conditions, where ◆$p > 0.05$, ◆◆$p \leq 0.05$, ◆◆◆$p < 0.01$, ◆◆◆◆$p < 0.001$, ◆◆◆◆◆$p < 0.0001$. The live cell assay demonstrated that cell lines A1 and D1 produced the most light with no significant difference between them. Cell lines B1, B2 and E1 produced significantly less light in comparison, although there was no significant difference between them. In contrast, the luciferase assay showed that E1 produced significantly more light than control and the other cell lines. Furthermore, the luciferase assay generated 2.5 to 7 fold more light than the live cell assay.

Bioluminesence generated by U87-*hRluc* monoclonal cell lines was also compared (see Figure 33). Cell line E was seen to produce significantly more light than control (89 300 ± 4 820 RLU, $p < 0.001$. On initial 1 way ANOVA analysis, the light produced by cell lines γ, D and I did not reach significance. However, this was likely due to the orders of magnitude difference in light generated by cell line E. When cell line E was excluded from analysis, the light generated by cell lines γ, D and I (3 880 ± 115 RLU, 1 400 ± 122 RLU, and 4 240 ± 122 RLU, respectively) became significantly greater than control, $p < 0.001$. With U87-*hRluc* monoclonal cells, the luciferase assay was more predictive of the live cell assay (see Figure 33): the luciferase assay also demonstrated that cell line E produced significantly more light than the other cell lines, and that once cell line E was removed from analysis, the light produced by cell lines D and I would become significant, as described above. However, in contrast to the live cell assay, even with cell line E removed from the analysis, the bioluminescence from cell line γ was not significantly different from control in the luciferase assay. Again, the luciferase assay generated a whole order of magnitude more light than the live cell assay.

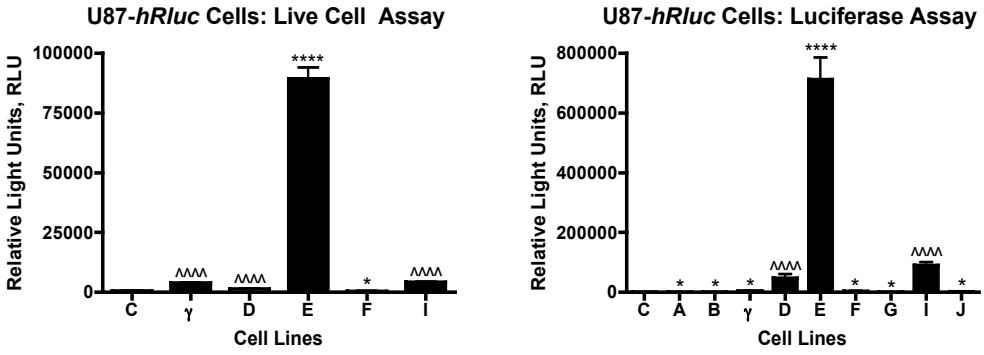

Figure 33 U87-*hRluc* Monoclonal Cells: Comparing the Live cell Assay with the Luciferase Assay

C = untransfected cells. Asterisks indicate the degree of significance in RLU of the test conditions compared to control, where * $p > 0.05$, ** $p \leq 0.05$, *** $p < 0.01$, **** $p < 0.001$, ***** $p < 0.0001$. ^^^^ indicate $p < 0.001$ compared to control having excluded cell lines generating signal of a higher order of magnitude from the analysis. The live cell assay demonstrated that cell line E produced significantly more light than control. On initial 1 way ANOVA analysis, the light produced by cell lines γ, D and I did not reach significance. However, when cell line E was excluded from analysis, the light generated by cell lines γ, D and I became significantly greater than control, $p < 0.001$. The luciferase assay demonstrated similar results, although, even with excluding cell line E from the analysis, cell line γ was not seen to produce significant amounts of light. The luciferase assay was seen to generate a whole order of magnitude more light than the live cell assay.

The luciferase assay generates significantly more bioluminescence than the live cell assay, and this is demonstrated across two different cell lines. In the lysis process, the luciferase-containing plasmids that have been transfected but have not been incorporated into the cellular DNA are now exposed to the nuclear enzymes that mediate transcription and translation, and hence more luciferase can be generated, and stronger bioluminescence achieved with the addition of substrate. Moreover, there may be poor correlation between the luciferase assay and live cell assay as the amount of plasmid that has not been incorporated into the cellular DNA will be unpredictable. Further contributing to the poor correlation between the two assays, some cells from this glioma derived cell line may express a transporter pump[170] that causes efflux of luciferase, reducing the bioluminescence generated, and this would not be reflected by the luciferase assay.

For the purposes of investigating bPDT, the live cell assay is a more accurate measure of the light that would be available to mediate a photodynamic effect in a live, luciferase-producing cell. For this reason, the live cell assay was used for the remainder of the experiments.

7.5.3 Generating Optimal Bioluminescence

Having successfully generated luciferase-transfected U87 cell lines that were capable of bioluminescence, the conditions required to generate optimal bioluminescence were studied. The maximum, non-toxic dose of substrate was established. Then using this dose of substrate, the effect of substrate manufacturer, substrate solvent, and cell culture conditions on bioluminescence were investigated.

7.5.3.1 d-Luciferin Toxicity

U87-*luc* and U87-CBG68*luc* cells were harvested and plated in 96 well plates at a density of $1x10^4$ cells per well. Cells were replaced into the incubator. After 24 hrs incubation, media was aspirated from each well and replaced with 0.1 ml of complete media. d-Luciferin was diluted in varying amounts of PBS and 0.1 ml was added to give final concentrations ranging from 0.313 to 5 mM. Control cells had 0.l ml of PBS added. Cells were incubated overnight, to replicate test conditions, and an MTT assay was subsequently conducted. The toxicity of d-luciferin from three different manufacturers, Promega, Caliper Life Sciences (CLS) and Synchem was compared.

2.5 mM was the maximum dose of d-luciferin, from all manufacturers, that could be tolerated by U87-*luc* cells (see Figure 34). 2.5 mM of d-luciferin only cause mild toxicity in U87-CBG68l*uc* cells (68.1% of control, $p < 0.01$, 95% CI 0.0591 – 0.275).

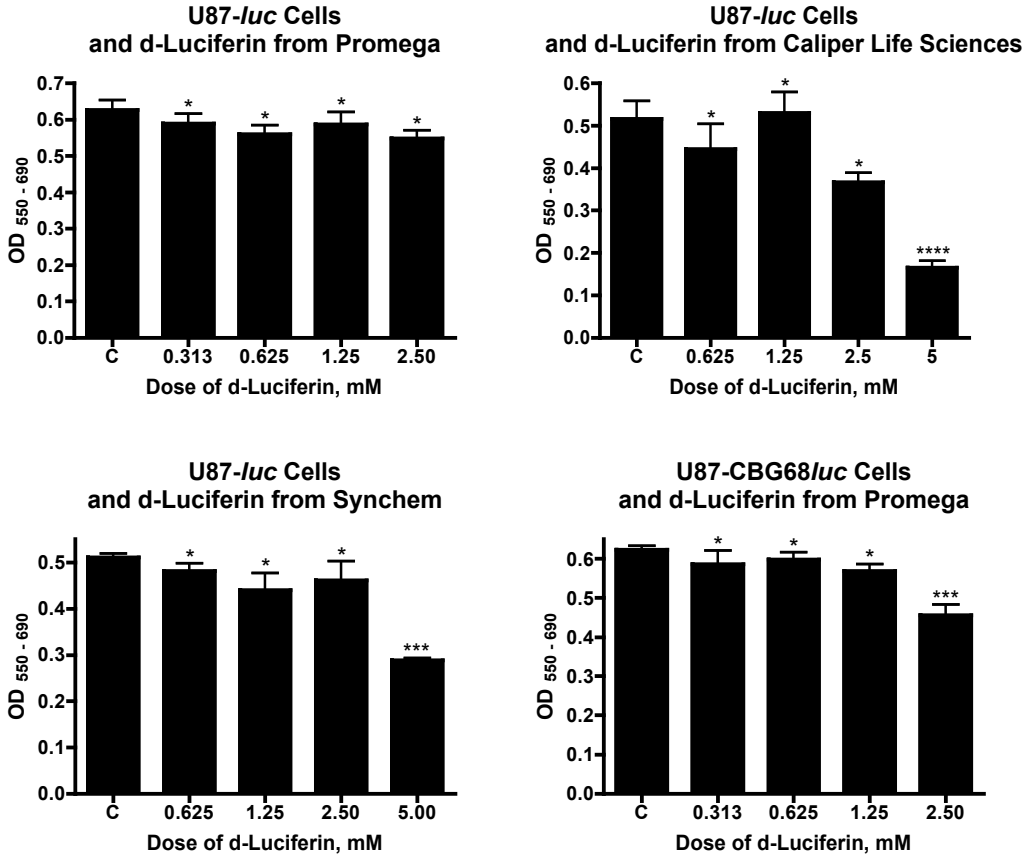

Figure 34 d-Luciferin Toxicity

C = control. Numbers on the x axis refer to the dose of d-luciferin. Asterisks indicate the degree of significance of the difference in OD between each condition and control, where * $p > 0.05$, ** $p \leq 0.05$, *** $p < 0.01$, **** $p < 0.001$, ***** $p < 0.0001$. 2.5mM was the maximum dose of d-luciferin, from all manufacturers, tolerated by U87-*luc* cells. However, this dose did cause toxicity in U87-CBG68*luc* cells, but this was only mild (68.1% of control, $p < 0.01$, 95% CI 0.0591 – 0.275).

7.5.3.2 EnduRen™ Toxicity

U87-*hRluc* cells were harvested and plated in 96 well plates at a density of $1x10^4$ cells per well. Cells were replaced into the incubator. After 24 hrs incubation, media was aspirated from each well and replaced with 0.1 ml of complete media. EnduRen™ was diluted in varying amounts of PBS and 0.1 ml was added to give final concentrations of 37.5, 75, 150, 300 and 600 μM. Control cells had 0.1 ml of PBS added. The plate was incubated overnight and an MTT assay then conducted.

A dose of 75 μM was found to cause minimal toxicity (98.6% of control, $p < 0.05$, 95% CI 0.0269 – 0.26) (see Figure 35).

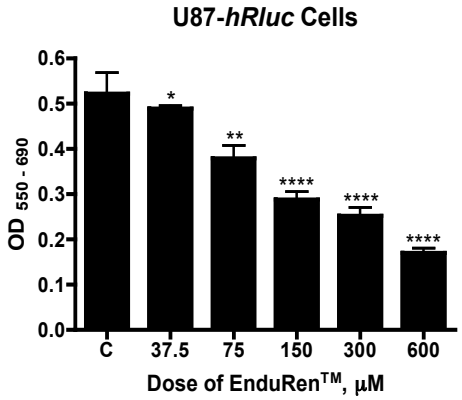

Figure 35 EnduRen™ Toxicity

C = control. Numbers on the x axis refer to the dose of Enduren™. Asterisks indicate the degree of significance of the difference in OD between each condition and control, where * p > 0.05, ** p ≤ 0.05, *** p < 0.01, **** p < 0.001, ***** p < 0.0001. 75 µM was found to only cause minimal toxicity (98.6% of control, p < 0.05, 95% CI 0.0269 – 0.26), and hence, the manufacturer recommended test dose of 60 µM was chosen for future testing.

7.5.3.3 ViviRen™ Toxicity

ViviRen™ is another substrate for Renilla luciferase that produces bioluminescence that has different properties to that produced by EnduRen™. It was therefore investigated as a possible alternative to EnduRen™.

Three conditions using the substrate ViviRen™ were tested. U87-*hRluc* cells were harvested and plated in 96 well plates at a density of $1x10^4$ cells per well. Cells were replaced into the incubator. After 24 hrs incubation, media was aspirated from each well and replaced with 0.1 ml of complete media. Firstly, ViviRen™ was diluted in varying amounts of PBS and 0.1 ml of ViviRen™ was added to give final concentrations of 3.75, 7.5, 15, 30 and 60 µM. Control cells had 0.1 ml of PBS added. The plate was incubated overnight and an MTT assay then conducted. Secondly, the initial experiment was repeated, but instead of incubating the cells overnight with ViviRen™, the incubation period was for only 1 hour, after which an MTT assay was conducted. Thirdly, cells were prepared as for the initial ViviRen™ toxicity experiment with similar doses of drug added. However, the plate was then incubated for 1 hr, following which the cells were washed twice with PBS and 0.1 ml of complete media replaced. 0.1 ml of EnduRen™ was then added to give a final concentration of 30 µM. The plate was incubated for a further 24 hrs, following which an MTT assay was performed. Control cells were treated similar to test cells, but instead of substrate, they received 0.1 ml of PBS.

Following incubation with ViviRen™ for 24 hrs (see Figure 36), 7.5 μM of ViviRen™ was found to be the maximum non-toxic dose (81.3 % of control, $p > 0.05$, 95% CI -0.0451 – 0.269). However, by shortening the incubation time with ViviRen™ to 1 hr, the maximum non-toxic dose increased to 30 μM: although the difference in $OD_{550-690}$ between control and cells incubated with 30 μM ViviRen™ was found to be significantly different, $p < 0.01$, the OD of cells incubated with 30 μM ViviRen™ was only 74.8% of control and the 95% CI 0.0585 – 0.181. In support of this, when incubating with ViviRen™ for 1 hr, followed by incubation with 30 μM EnduRen™, use of 30 μM of ViviRen™ under these conditions caused no significant toxicity (105% of control, $p > 0.05$, 95% CI -0.151 – 0.100).

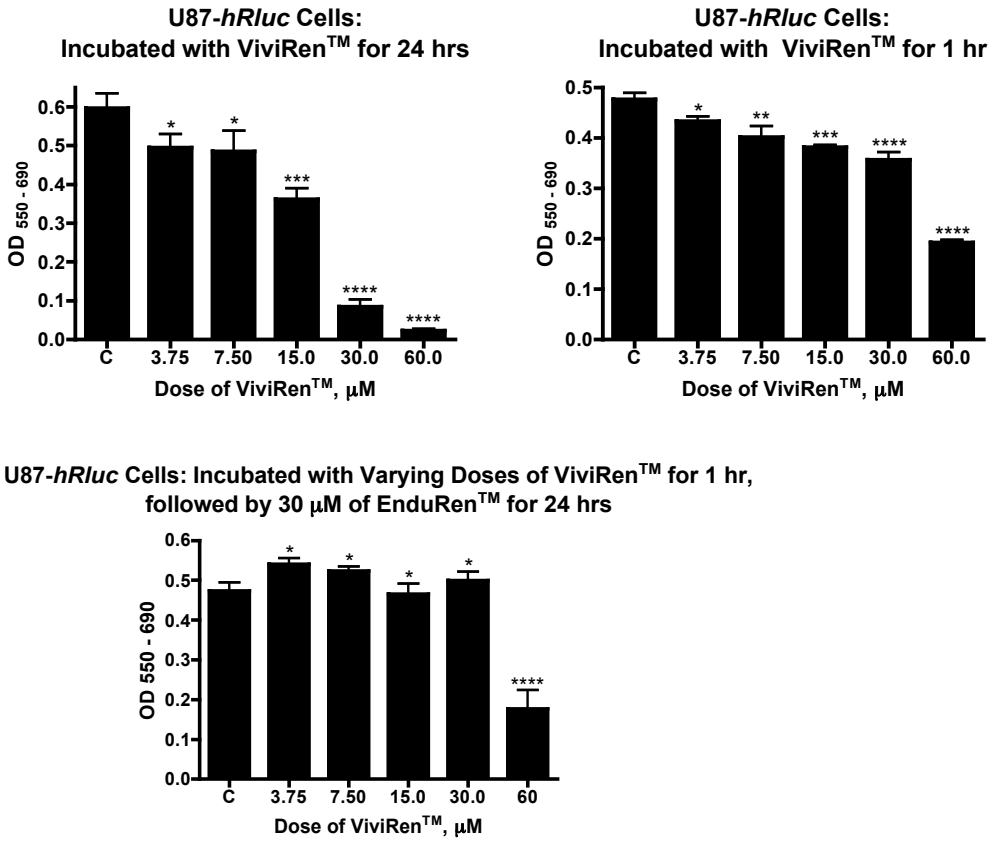

Figure 36 ViviRen™ Toxicity

C = control. Numbers on the x axis refer to the dose of Viviren™. Asterisks indicate the degree of significance of the difference in OD between each condition and control, where * $p > 0.05$, ** $p \leq 0.05$, *** $p < 0.01$, **** $p < 0.001$, ***** $p < 0.0001$. When incubating with Viviren™ for 24 hrs, the maximum non-toxic dose was 7.5 μM (81.3 % of control, $p > 0.05$, 95% CI -0.0451 – 0.269). By shortening the incubation time with Viviren™ to 1 hour, the maximum non-toxic dose was increased to 30 μM (74.8% of control, $p < 0.01$, 95% CI 0.0585 – 0.181). Additionally, when incubating with ViviRen™ for 1 hr, followed by incubation with 30 μM EnduRen™, use of 30 μM of ViviRen™ under these conditions caused no significant toxicity (105% of control, $p > 0.05$, 95% CI -0.151 – 0.100).

7.5.3.5 Effect of Substrate Manufacturer

d-Luciferin is produced by a number of manufacturers, which include Promega, CLS, and Synchem. These experiments were conducted to study if the amount of bioluminescence generated by the d-luciferin produced by these manufacturers differed.

U87-*luc* and U87-CBG68*luc* cells were harvested and plated in white, flat bottom, tissue culture treated, 96 well plates (Sigma), at a density of $1x10^4$ cells per well. Cells were replaced into the incubator. After 24 hrs incubation, media was aspirated from each well and replaced with 0.1 ml of complete media. Live cell assays were then performed using a final concentration of 2.5 mM d-luciferin from each manufacturer and the resulting bioluminescence compared (see Figure 37).

In U87-*luc* cells, the bioluminescence generated by d-luciferin from Promega was slightly greater than that generated by CLS, the latter being 83.8% ($p \leq 0.05$) and 88.3% ($p < 0.001$) of that generated by Promega in B1 and D1 cell lines, respectively. In contrast, the bioluminescence generated by d-luciferin from Synchem was considerably less than that of Promega and CLS (1.31% and 1.90%, $p < 0.0001$, of the bioluminescence generated by Promega, in the B1 and D1 cell lines respectively). In U87-CBG68*luc* cells, there was no significant difference in the bioluminescence generated by d-luciferin from Promega and CLS. d-luciferin from Synchem was not tested in U87CBG68*luc* cells in view of its poor performance in U87-*luc* cells.

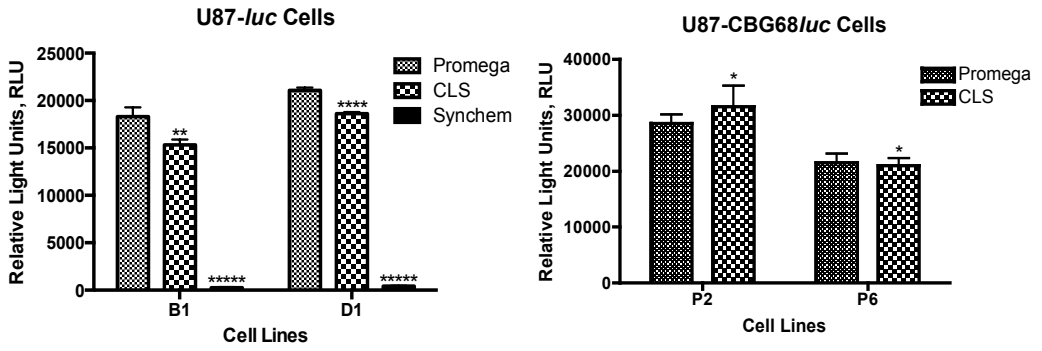

Figure 37 Effect of Substrate Manufacturer on Bioluminescence

Cell lines are identified on the x axis. Asterisks indicate the degree of significance of the difference in RLU generated by d-luciferin from each of the manufacturers CLS and Synchem, compared to the RLU generated by the d-luciferin from Promega, where * $p > 0.05$, ** $p \leq 0.05$, *** $p < 0.01$, **** $p < 0.001$, ***** $p < 0.0001$. In U87-*luc* cells, the bioluminescence generated by d-luciferin from Promega was slightly greater than that generated by CLS, the latter being 83.8% ($p \leq 0.05$) and 88.3% ($p < 0.001$) of that generated by Promega in B1 and D1 cell lines, respectively. In contrast, the bioluminescence generated by d-luciferin from Synchem was considerably less than that of Promega and CLS (1.31% and 1.90%, $p < 0.0001$, of the bioluminescence generated by Promega, in the B1 and D1 cell lines respectively). In U87-CBG68*luc* cells, there was no significant difference in the bioluminescence generated by d-luciferin from Promega and CLS.

7.5.3.6 Effect of Substrate Solvent

In the experiments thus far, the substrates have been diluted in PBS. The effect on bioluminescence generated by diluting the substrates in PBS and serum free media was compared. Furthermore, the effect of phenol red in serum free media on bioluminesence was also investigated.

U87-*luc* and U87-*hRluc* cells were harvested and plated in white, flat bottom, tissue culture treated, 96 well plates (Sigma), at a density of $1x10^4$ cells per well. Cells were replaced into the incubator. After 24 hrs incubation, media was aspirated from each well and replaced with 0.1 ml of complete media. Live cell assays were then performed using final concentrations of 2.5 mM d-luciferin and 60 μM of EnduRen™ for U87-*luc* and U87-*hRluc* cells, respectively. The effect of diluting d-luciferin and EnduRen™ with either PBS or serum free media on bioluminescence to make these final concentrations was compared. Furthermore, in U87-*luc* cells, the effect of diluting d-luciferin in serum free media without phenol red on bioluminescence was also studied (see Figure 38).

For U87-*luc* cells, diluting d-luciferin in serum free media generated significantly less bioluminescence than diluting the substrate in PBS: diluting substrate in serum free

media generated 54.1% of the bioluminescence that was achieved by diluting the substrate in PBS ($p<0.01$). Furthermore, there was no significant difference in the bioluminescence generated by using either serum free media or serum free media without phenol red to dilute the substrate (54.1% vs 58.5% of the bioluminescence achieved by diluting the substrate in PBS, $p > 0.05$). Similarly, for U87-*hRluc* cells, diluting EnduRen™ in serum free media generated significantly less bioluminsence than diluting the subtrate in PBS: diluting substrate in serum free media generated 54.3% of the bioluminescence achieved by diluting the substrate in PBS ($p < 0.001$).

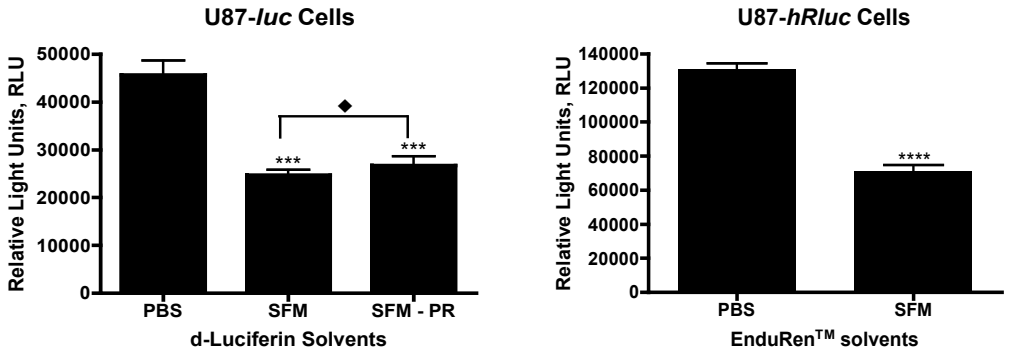

Figure 38 The Effect of Substrate Solvent on Bioluminescence

Solvent is identified on the x axis, where PBS is phosphate buffered saline, SFM is serum free media, and SFM – PR is serum free media without phenol red. Asterisks indicate the degree of significance of the difference in RLU generated by using the different solvents compared to using PBS as the solvent, where * $p > 0.05$, ** $p \leq 0.05$, *** $p < 0.01$, **** $p < 0.001$, ***** $p < 0.0001$. The diamond indicates the degree of significance of the difference in RLU generated by using SFM-PR compared to SFM, where ◆ $p > 0.05$. For U87-*luc* and U87-*hRluc* cells, diluting d-luciferin in serum free media generated significantly less bioluminescence than diluting the substrate in PBS (54.1%, $p < 0.01$, and 54.3%, $p < 0.001$, respectively, of the bioluminescence that was achieved by diluting the substrate in PBS). Furthermore, in U87-*luc* cells there was no significant difference in the bioluminescence generated by using either serum free media or serum free media without phenol red to dilute the substrate (54.1% vs 58.5% of the bioluminescence achieed by diluting the substrate in PBS, $p > 0.05$).

7.5.3.7 Effect of Cell Culture Media

Finally, the effect of cell culture media on bioluminescence generated was investigated. Cells were cultured in complete media or with complete media made with heat-inactivated serum (see section 5.2.2).

U87-*luc* cells were grown under standard cell culture conditions in either standard complete media or complete media made with heat-inactivated serum. For the latter, an aliquot of cells was directly thawed, then passaged in complete media with heat-

inactivated serum. Cells were then harvested and plated in white, flat bottom, tissue culture treated, 96 well plates (Sigma), at a density of $1x10^4$ cells per well, in their appropriate media. Cells were replaced into the incubator. After 24 hrs incubation, media was aspirated from each well and replaced with 0.1 ml of the appropriate complete media. Live cell assays were then performed using final concentrations of 2.5 mM d-luciferin (see Figure 39).

Culturing U87-*luc* cells in heat-inactivated serum led to a significant decline in the bioluminescence generated: cells cultured in heat-inactivated serum generated 60.0% of the bioluminescence that was achieved by cells grown in standard media, $p < 0.01$.

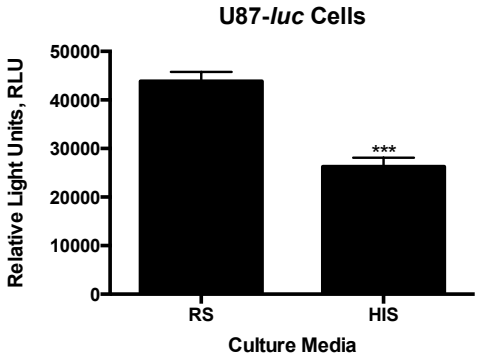

Figure 39 The Effect of Cell Culture Media on Bioluminescence

The cell culture media is identified on the x axis, where RS is regular, standard, complete media and HIS complete media with heat-inactivated serum. Asterisks indicate the degree of significance of the difference in RLU generated by cells cultured in complete media with heat-inactivated serum compared to those cultured in standard complete media, where * $p > 0.05$, ** $p \leq 0.05$, *** $p < 0.01$, **** $p < 0.001$, ***** $p < 0.0001$. Culturing U87-*luc* cells in heat-inactivated serum led to a significant decline in the bioluminescence, generating 60.0% of the bioluminesence that was achieved by cells grown in standard media, $p < 0.01$.

7.5.4 Characterising Bioluminescence

Having established the optimal conditions necessary to achieve maximal bioluminescence, the properties of the bioluminescence itself was studied: dose-response curves were generated for each of the substrates d-luciferin, EnduRen™, and ViviRen™, then a study of how bioluminescence decays over time was conducted. Finally, the emission profiles of the bioluminescence generated by firefly and Renilla luciferase from cells of this model were compared to the absorption spectra of the photosensitisers, hypericin and *m*THPC.

7.5.4.1 Dose-Response

U87-*luc* and U87-*hRluc* cells were harvested and plated in white, flat bottom, tissue culture treated, 96 well plates (Sigma), at a density of $1x10^4$ cells per well. Cells were replaced into the incubator. After 24 hrs incubation, media was aspirated from each well and replaced with 0.1 ml of complete media. Live cell assays were then performed using increasing doses of substrate: for U87-*luc* cells, d-luciferin was added to give final concentrations of 0.313, 0.625, 1.25 and 2.50 mM; for U87-*hRluc* cells, EnduRen™ and ViviRen™ were added to give final concentrations of 1.50, 7.00, 15.0, 30.0 and 60.0 μM. 0.1 ml of PBS was added to control cells.

The dose-response curves (see Figure 40) for d-luciferin and EnduRen™ revealed that the maximum, non-toxic doses established, 2.5 mM and 60 μM respectively, produced maximum bioluminescence, 9 270 ± 427 RLU and 24 700 ± 1092 RLU respectively. Furthermore, there was little advantage to increasing the dose of EnduRen™ beyond 30 μM, the dose used in combination with ViviRen™ in section 8.5.3.3, which produced 25 800 ± 1330 RLU of bioluminescence. The dose-response curve for ViviRen™ demonstrated that a maximum bioluminescence of 151 000 ± 5630 RLU was achieved with 60 μM ViviRen™. In contrast, this was significantly greater than the bioluminescence achieved with the maximum, non-toxic doses of 7.50 μM with 24 hr incubation and 30 μM with 1 hr incubation, which produced 30 200 ± 1 560 RLU and 99 300 ± 18 100 RLU respectively.

Finally, the maximum bioluminescence achieved with EnduRen™ was approximately 3 times more than that of d-luciferin. Moreover, the maximum bioluminescence achieved with ViviRen™ was 6 times more than that of EnduRen™. Although the maximum, non-toxic doses of ViviRen™ generated less bioluminescence than the maximum possible bioluminescence, the bioluminescence generated by these doses was still substantially greater than the maximum bioluminescence achieved by d-luciferin and EnduRen™: 7.50 μM of ViviRen™ generated 3 and 1.2 times more bioluminescence than that possible with d-luciferin and EnduRen™ respectively; and 30 μM generated 11 and 4 times more bioluminescence than that possible with d-luciferin and EnduRen™ respectively.

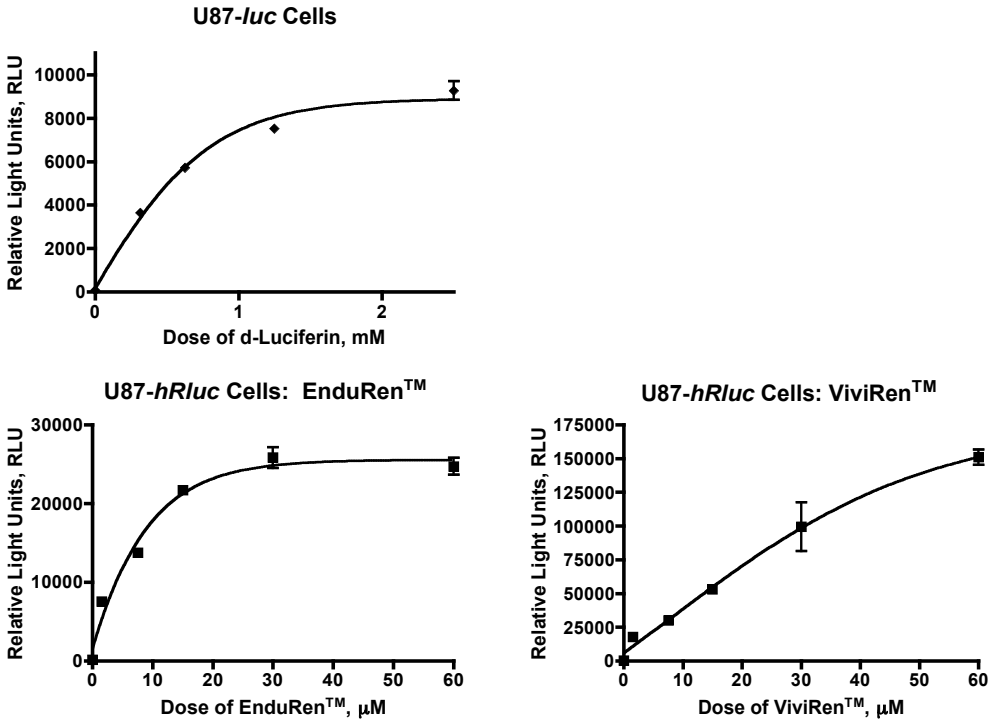

Figure 40 Dose-Response of Substrate

The maximum, non-toxic doses established for d-luciferin and EnduRen™, 2.5 mM and 60 µM respectively, produced the maximum possible bioluminescence. Furthermore, there was little advantage to increasing the dose of EnduRen™ beyond 30 µM. For ViviRen™, although the maximum, non-toxic doses, 7.50 µM with 24 hr incubation and 30 µM with 1 hr incubation, did not generate the maximum possible bioluminescence, which was achieved with 60 µM, the bioluminescence achieved with these doses still exceeded the maximum achieved with d-luciferin and EnduRen™.

7.5.4.2 Change in Bioluminescence Over Time

U87-*luc* and U87-*hRluc* cells were harvested and plated in white, flat bottom, tissue culture treated, 96 well plates (Sigma), at a density of $1x10^4$ cells per well. Cells were replaced into the incubator. After 24 hrs incubation, media was aspirated from each well and replaced with 0.1 ml of complete media. d-Luciferin was added to U87-*luc* cells to give a final concentration of 2.5 mM. The plate was then placed in the luminometer and bioluminescence measured at 2.5, 15, 30, 45 and 60 mins after the addition of substrate. EnduRen™ was added to U87-*hRluc* cells to give a final concentration of 60 µM. The plate was then placed in the luminometer and bioluminescence measured at 90, 150 and 210 mins after the addition of substrate. The plate was kept incubated between readings. ViviRen™ was added to U87-*hRluc* cells to give a final concentration of 60 µM. The plate was then placed in the luminometer and bioluminescence measured at 2 and 60 mins after the addition of substrate. The plate was replaced in the incubator between readings. Results were plotted and a best-fit line

calculated. Experimental design was limited by access to the luminometer. Although, not a comprehensive study of the change in bioluminescence over time, the aim of the experiments was to confirm that the substrates behaved in our model in a similar way to that reported in the literature.

Bioluminescence from d-luciferin is reported to peak at approximately 3 mins, then falls and plateaus to a level that persists for at least 20 mins[140]. Consistent with this, our study (see Figure 41) demonstrated peak bioluminescence (21 100 ± 280 RLU) occurring close to 2.5 mins, before falling off to a plateau that was sustained for at least 1 hr (16 000 ± 420 RLU).

EnduRen™ has been shown to generate a bioluminescence that peaks at approximately 90 mins, which then remains constant for more than 24 hours, and in some cell lines, this can persist for up to 3 days[160]. Consistent with this, our study (see Figure 41) showed a slower time to peak bioluminescence compared to d-luciferin, with high levels of bioluminescence (89 300 ± 4 820 RLU) demonstrated at 90 mins. Although this level of bioluminescence was not sustained, it decayed gradually and still remained at a high level (47 600 ±1 730 RLU) at 210 mins.

Peak bioluminescence generated by ViviRen™ has been shown to occur within 2 mins of the substrate being added to cells[161]. The bioluminescence then gradually decays over time. The peak bioluminescence achieved with ViviRen™ is approximately 10 times greater than that achieved with EnduRen™. Furthermore, if a cell line is exposed to either VivRen™ or EnduRen™, after 45 mins the level of bioluminescence generated with each substrate becomes similar and remains so for at least 60 mins. Our study (see Figure 41) confirmed the rapid peak of bioluminescence, 986 000 ± 96 900 RLU at 2 mins, which was also 10 times that of the peak bioluminescence achieved with EnduRen™ (89 300 ± 4 820 RLU). In contrast to the literature, in our model, the fall in bioluminescence with ViviRen™ was more rapid, reaching 25 700 ± 189 RLU at 60 mins, with little overlap of a plateau phase for EnduRen™.

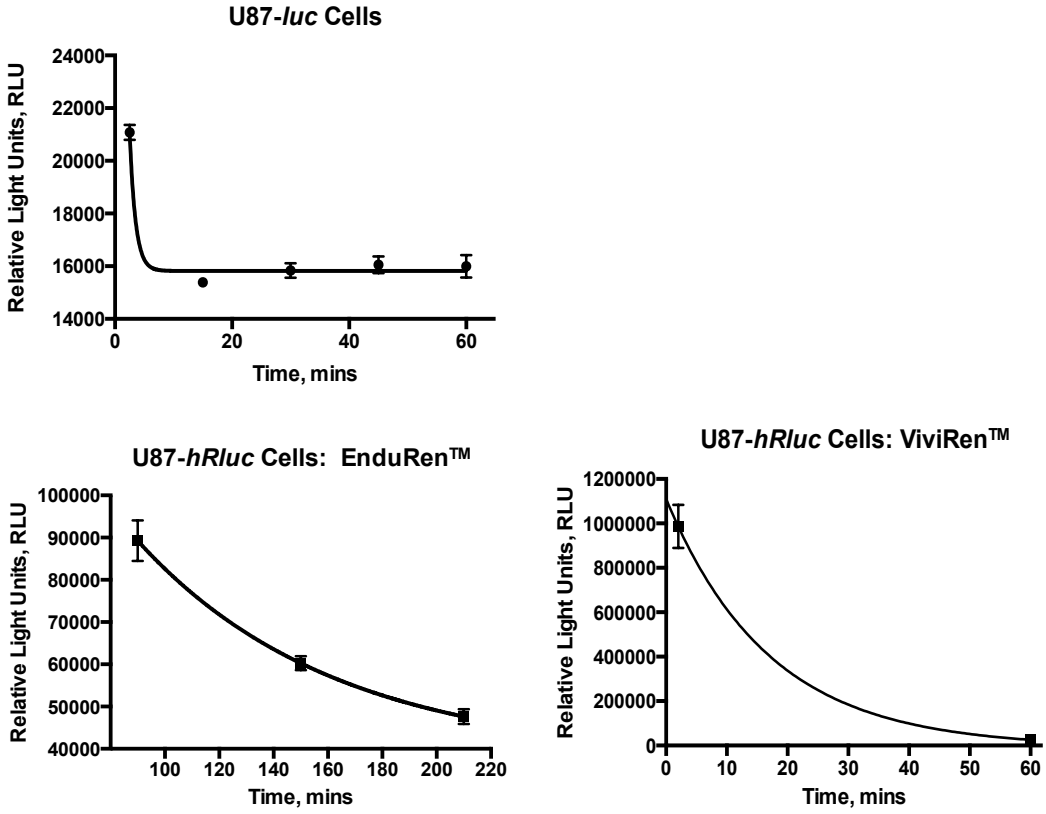

Figure 41 Change in Bioluminescence Over Time

Peak bioluminescence from d-luciferin occurred at approximately 2.5 mins (21 100 ± 280 RLU), then fell to a plateau that persisted for at least 1 hour (16 000 ± 420 RLU). Bioluminescence generated by EnduRen™ peaked later at approximately 90 mins (89 300 ± 4 820 RLU), then gradually decayed, with high levels still at 210 mins (47 600 ±1 730 RLU). Bioluminescence from ViviRen™ peaked quickly, 986 000 ± 96 900 RLU at 2 mins, then fell rapidly, reaching 25 700 ± 189 RLU at 60 mins. Overall, the change in bioluminescence generated by the substrates was similar to that reported in the literature.

7.5.4.3 Comparing the Emission Profile of Bioluminescence with the Absorption Spectra of the Photosensitisers

According to the luciferase assay described above, lysates of U87-*luc* and U87-*hRluc* cells were prepared to obtain emission profiles of firefly luciferase and Renilla luciferase, respectively. U87-*luc* and U87-*hRluc* cells were plated at a density of $1x10^4$ cells and $1x10^5$ cells, respectively, per well of a 24 well plate, and allowed to incubate for 24 hrs. Media was then aspirated from the wells and cells washed with PBS. 0.1 ml of 1x lysis buffer was then added to each well and the plate rocked at room temperature for 5 mins, ensuring complete cell lysis. 20 µl of lysate was transferred into the wells of a white, half area, Corning 96 well plate. 100 µl of d-luciferin and EnduRen™ was then added to each well of U87-*luc* and U87-*hRluc* lysate, respectively. The luminometer plates were then placed in turn into a fluorometer (Thermo Electro Corp). Signal was captured between 400 and 800 nm, and a 3 sec integration time was set to allow the signal to equilibrate.

The absorption spectra of hypericin (0.5 mg/ml in DMSO) and *m*THPC (0.5 mg/ml in PBS) were recorded in a CARY 1E Varian spectrophotometer. The background absorption profile of DMSO and PBS were subtracted to yield the absorption spectrum of hypericin and *m*THPC, respectively.

Results from the emission profiles and the absorption spectra were normalised to the maximum value. Each emission profile was then plotted against the absorption spectra of both photosensitisers (see Figure 42). The peak bioluminescence from the oxidation of d-luciferin by firefly luciferase was found to lie between 546 – 574 nm, with the maximum at approximately 560 nm, as expected from the literature[140]. There was reasonable overlap of this emission profile with the absorption spectra of hypericin and *m*THPC, both consistent with that reported in the literature[155,166], with peak emission coinciding with the absorption peaks of hypericin at 557 nm and that of *m*THPC at 550 nm. The peak bioluminescence from oxidation of EnduRen™ by Renilla luciferase was found to lie between 451 – 505 nm, with the maximum at approximately 487 nm, which corresponds well to the reported 480 nm in the literature[171]. This emission profile overlapped poorly with the absorption spectrum of hypericin. There was some overlap with the absorption spectrum of *m*THPC, although peak emission did not coincide with any peak of absorption.

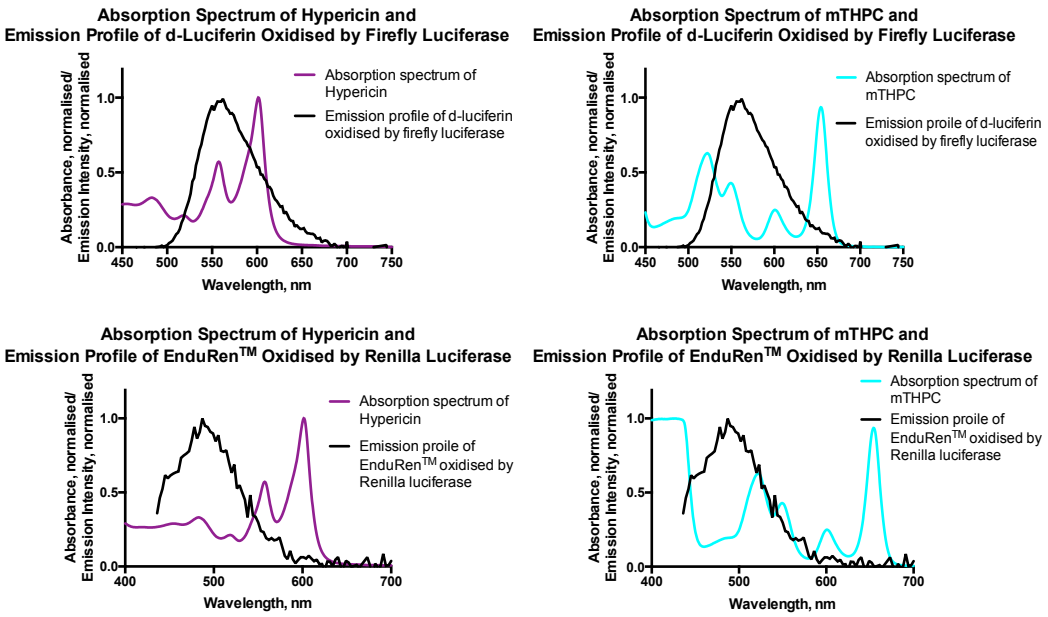

Figure 42 Emission profiles of firefly luciferase and Renilla luciferase compared to the Absorption Spectra of Hypericin and *m*THPC

The peak bioluminescence of firefly luciferase lay between 546 – 574 nm, with the maximum at approximately 560 nm, which overlapped well with the absorption peaks of hypericin at 557 nm and *m*THPC at 550 nm. The peak bioluminescence of Renilla luciferase lay between 451 – 505 nm, with the maximum at approximately 487 nm, which did not overlap well with the absorption peaks of hypericin or *m*THPC.

7.6 Summary and Discussion

U87 cells were successfully transfected to produce stable firefly luciferase, click beetle luciferase, and Renilla luciferase-expressing cell lines, U87-*luc*, U87-CBG68*luc*, and U87-*hRluc*, respectively. The bioluminescence generated was tested with luciferase and live cell assays. The live cell assay was deemed a more accurate measure of the light that would be available to mediate a photodynamic effect in a live cell, and hence, this assay was used in the experiments henceforth to quantify bioluminescence.

For U87-*luc* cells, d-luciferin is the appropriate substrate. The maximum tolerated dose of 2.5 mM was also found to be the dose that produced maximum bioluminescence. Promega was found to produce a substrate that generated higher levels of bioluminescence compared to that obtained from other vendors. Dissolving the substrate in PBS generated higher levels of bioluminescence than using serum free media as a solvent. There was no gain in bioluminescence in culturing cells in heat-inactivated serum. The bioluminescence generated by adding d-luciferin to U87-*luc* cells was seen to peak within minutes, then fall to a plateau that remained stable for at least 1 hr. Based on these findings, in the experiments henceforth, d-luciferin was

purchased from Promega, dissolved in PBS, added to cells maintained in complete media to achieve a final dose of 2.5 mM, and incubated with the cells for 24 hrs. d-Luciferin was also used similarly for U87-CBG68*luc* cells.

Two substrates were tested in U87-*hRluc* cells, EnduRen™ and ViviRen™. Although the maximum tolerated dose of EnduRen™ was 75 μM and the manufacturer recommended dose is 60 μM, its dose response curve showed that there was little to be gained in the level of bioluminescence going beyond 30 μM. Furthermore, dissolving EnduRen™ in PBS produced superior levels of bioluminescence compared to using serum free media as a solvent. The bioluminescence produced by EnduRen™ was seen to gradually peak then gradually fall to a plateau that would likely maintain high levels of bioluminescence over days. Based on these findings, in the experiments henceforth, EnduRen™ was dissolved in PBS, added to cells maintained in complete media to achieve a final dose of 30 μM, and incubated with the cells for 24 hours.

The maximum tolerated dose of ViviRen™ was 7.5 μM for 24 hrs incubation and 30 μM for 1 hr incubation. Although neither dose achieved maximum bioluminescence, the bioluminescence of both doses still exceeded the maximum bioluminescence that could be achieved with EnduRen™. Furthermore, the bioluminescence achieved with ViviRen™ peaked within minutes, and decayed extremely quickly. If a bPDT effect could be demonstrated with EnduRen™ following the conditions above, to optimise the bioluminescence, cells could be incubated with 30 μM of ViviRen™ for 1 hr, followed by 30 μM of EnduRen™ for 24 hrs, which has been shown not to be toxic.

There was good overlap of the emission profile of the bioluminescence generated by the oxidation of d-luciferin by firefly luciferase with the absorption spectra of hypericin and *m*THPC, hence studies started with U87-*luc* cells. If successful, studies would proceed with U87-CBG68*luc* cells: although an emission profile of the bioluminescence generated by the oxidation of d-luciferin by click beetle luciferase was not obtained, the literature indicates reasonable overlap between this and the absorption spectra of the photosensitsers. Finally, experiments would be repeated with U87-*hRluc* cells with the understanding that the overlap of the emission profile of the bioluminescence generated by the oxidation of EnduRen™ by Renilla luciferase with the absorption spectra of the photosensitisers was suboptimal. If this model worked, then optimising it using ViviRen™ would be an option.

Chapter 8 Using Bioluminescence to Mediate Photodynamic Therapy *in vitro*

Having successfully produced luciferase-expressing cell lines and having established the optimal conditions for generating bioluminescence, studies proceeded to investigate whether the bioluminescence generated from these cell lines could activate a photosensitiser to cause a photodynamic effect that would lead to cell death: bioluminescence-mediated photodynamic therapy (bPDT). Encouraged by the overlap of the emission profile of the bioluminescence generated by the oxidation of d-luciferin by firefly luciferase with the absorption spectra of hypericin and *m*THPC, studies started with U87-*luc* cells. If successful, studies would proceed with U87-CBG68*luc* cells. Finally, experiments would be repeated with U87-*hRluc* cells with the understanding that the overlap of the emission profile of the bioluminescence generated by the oxidation of EnduRen™ by Renilla luciferase with the absorption spectra of the photosensitisers was suboptimal.

8.1 Variation in Methodology

In these experiments, there were some variations in the details of the methodology followed thus far, and these are as follows.

8.1.1 Culture Media

All luciferase-expressing cell lines were maintained in complete media containing 1 mg/ml neomycin at all times. This will still be referred to as 'media' for ease of discussion.

8.1.2 Use of the Live Cell Assay

A live cell assay was conducted once a week on the cell lines being tested to ensure that the cells continued to generate stable bioluminescence.

8.1.3 Cell Viability: Use of the Growth Assay

In addition to the MTT assay and haemocytometry, as described above, cell viability was also assessed by a growth assay. Where a growth assay was planned, cells were plated in parallel plates that were treated similarly. When ready for the initial cell viability assessment with an MTT assay and/or haemocytometry, the plate designated for a growth assay was treated as follows. Media was aspirated from the wells, which were then washed twice with 0.1 ml of PBS. 0.04 ml of trypsin was added to the wells, which were allowed to incubate for 1 min until the cells had detached. The cells of each well were then resuspended in 0.1 ml of media then transferred to the wells of a 12 well

plate. Additional complete media was added to each well to achieve a total volume of 1.5 ml. The cells were left to incubate until the control cells had reached subconfluence, typically 5 days, after which the surviving cells were counted by haemocytometry. Media was changed every other day.

8.2 U87-*luc* Cell Line

Subconfluent U87-*luc* cells were harvested following trypsinisation, plated at a density of $1x10^4$ cells per well of a 96 well plate, and allowed to adhere over 24 hrs at 37^0C. Media was then aspirated from the wells and 0.1 ml of fresh complete media replaced. Wells were designated as either control or test.

Control wells were further divided into pure 'control' wells, which were exposed to neither photosensitiser nor d-luciferin; 'drug only' wells, which were exposed only to photosensitiser but not d-luciferin; and 'light only' wells, which were exposed only to d-luciferin but not photosensitiser. For experiments with hypericin, controls also included, 'DMSO only' wells that were only exposed to DMSO but not photosensitiser or d-luciferin, and 'DMSO+light' wells that were exposed to DMSO and d-luciferin but not to photosensitiser, to account for the DMSO that hypericin was reconstituted in. 'Test' wells were exposed to both photosensitiser and d-luciferin.

0.1 ml of photosensitiser was added to the appropriate wells to give final concentrations of either 12.5 μM or 10.0 μM of hypericin for 4 hrs and 24 hrs incubation respectively, or 12.5 μg/ml or 2.5 μg/ml of *m*THPC for 3 hrs and 24 hrs incubation respectively. For experiments with hypericin, DMSO was added to'DMSO only' and 'DMSO+light' controls at this time: the same proportion of DMSO as hypericin stock solution used to give the desired concentration of hypericin was added to serum free media to give a final volume of 0.1 ml to be added to each well. The remaining wells had 0.1 ml of serum free media added. After incubating for the appropriate time, all wells were washed twice with 0.1 ml PBS and 0.1 ml of fresh complete media was replaced. 0.1 ml of d-luciferin was then added to the appropriate wells to give a final concentration of 2.5 mM. Remaining wells had 0.1 ml of PBS added. Cells were allowed to incubate for a further 20-24 hrs, following which cell viability was assessed by haemocytometry, MTT assay, and/or growth assay. Each condition was tested in triplicate. Experiments were repeated a minimum of three times. The most representative results are shown.

Experiments were conducted in the two monoclonal lines that generated the greatest amount of bioluminescence, the monoclonal line that generated the least bioluminescence, and the polyclonal line that generated the most bioluminescence. Furthermore, as another control, experiments were repeated in U87 cells that had not been transfected with CMV-*luc*.

8.2.1 Hypericin, Short Incubation

Incubation with hypericin for 4 hrs, then subsequent incubation with d-luciferin (see Figure 43), led to > 50% cell death in all U87-*luc* (3 monoclonal and 1 polyclonal) cell lines. Specifically, incubation with photosensitiser then d-luciferin led to a fall in the cell population to 48.8 ± 7.42%, 45.2 ± 2.76%, 40.5 ± 1.33%, and 40.5 ± 2.44% of control ($p < 0.0001$) in the U87-*luc* D1, A1, B1 monoclonal cell lines, and the polyclonal cell line, respectively.

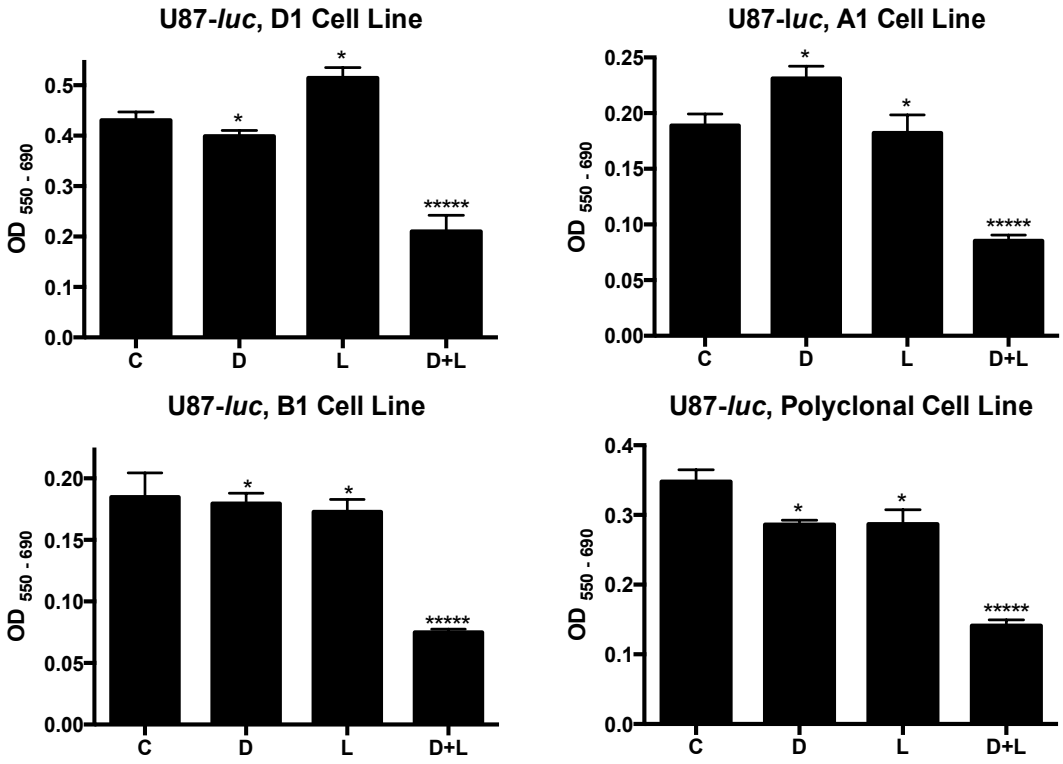

Figure 43 The effect of incubating U87-*luc* cell lines with hypericin for 4 hrs followed by d-luciferin, as demonstrated by the MTT assay

C = control, D = drug only, L = d-luciferin only, D+L = cells exposed to drug and d-luciferin. Asterisks indicate the degree of significance of the difference in OD between each condition and control, where * $p > 0.05$, ** $p \leq 0.05$, *** $p < 0.01$, **** $p < 0.001$, ***** $p < 0.0001$. Incubation with hypericin for 4 hrs, then d-luciferin, led to > 50% cell death in all U87-*luc* (3 monoclonal and 1 polyclonal) cell lines: in this way, there was a fall in the cell population to 48.8 ± 7.42%, 45.2 ± 2.76%, 40.5 ± 1.33%, and 40.5 ± 2.44% of control ($p < 0.0001$) in U87-*luc* D1, A1, B1 monoclonal cell lines, and the polyclonal cell line, respectively.

The effect of the interaction between hypericin and d-luciferin was confirmed by haemocytometry and growth assay in U87-*luc* monoclonal and polyclonal lines (see Figure 44). In the monoclonal cell line, incubation with hypericin for 4 hrs followed by exposure to d-luciferin led to a fall in the cell population to 61.5 ± 4.68% of control ($p < 0.01$). This fall was more pronounced in the growth assay, where these 'test' cells were found to be 55.3 ± 4.16% of control ($p < 0.0001$). Similarly, in the polyclonal cell line, incubation with hypericin for 4 hrs followed by exposure to d-luciferin led to a fall in the cell population to 34.3 ± 2.48% of control ($p < 0.0001$), and this fall was again found to be more profound on the growth assay where test cells were 13.0 ± 2.48% of control ($p < 0.0001$). These experiments were also performed with DMSO controls: there was no significant difference between these and other controls, demonstrating that DMSO was an inactive solvent, supporting the contention that it was an interaction between hypericin and d-luciferin that led to cell death.

The experiment was repeated in U87 cells that had not been transfected with CMV-*luc*: thus, these were cells that would not produce bioluminescence with the addition of d-luciferin. In this experiment, incubation of cells with hypericin for 4 hrs then d-luciferin did not lead to significant cell death (see Figure 45). *This demonstrates that it is not the chemical interaction between hypericin and d-luciferin that leads to cell death, but the interaction between hypericin and the bioluminescence generated by the addition of d-luciferin that is the cause of cell death: bioluminescence-mediated photodynamic therapy (bPDT).*

Furthermore, a dose-response with bPDT was demonstrated: increasing the dose of d-luciferin, which has been shown to increase the degree of bioluminescence (see Figure 40), increased the degree of cell death (see Figure 46): incubating U87-*luc* cells with hypericin for 4 hrs, followed by incubating the cells with 0.625 mM of d-luciferin led to a fall in the cell population to 69.0 ± 4.70% of control ($p > 0.05$), incubating the cells with 1.25 mM of d-luciferin led to a fall to 62.2% ± 3.60% of control ($p \leq 0.05$), and incubating the cells with 2.50 mM led to a fall to 29.3% ± 2.26% of control ($p < 0.0001$).

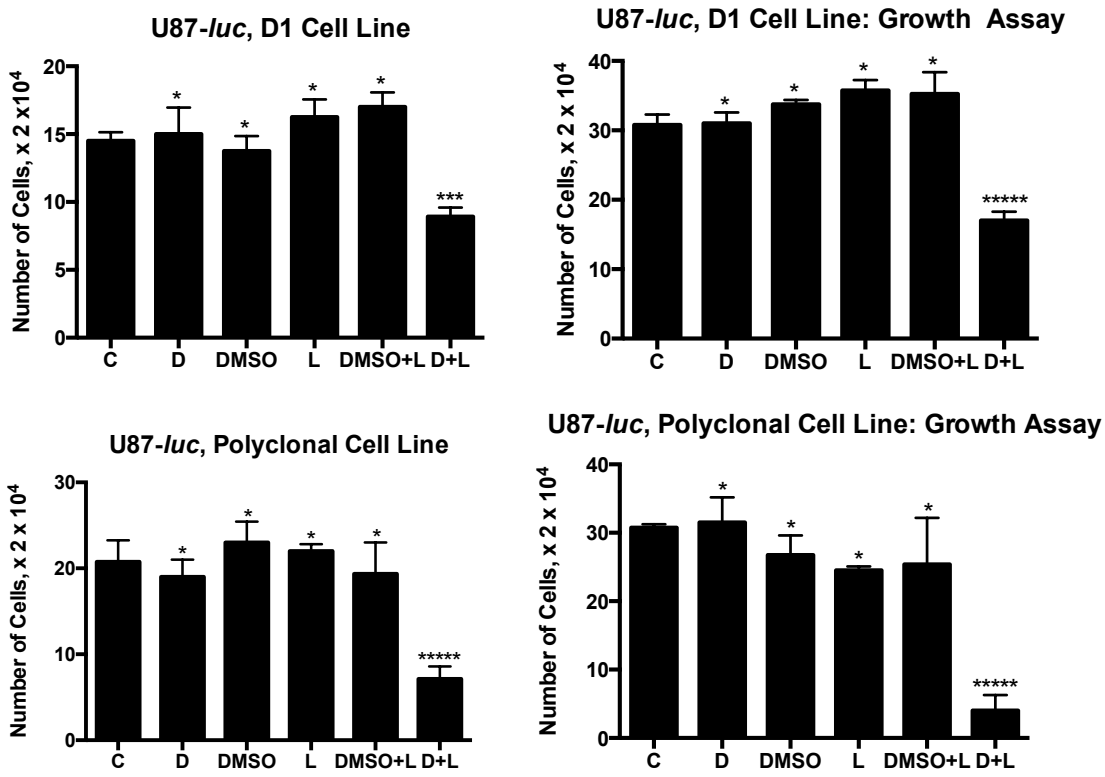

Figure 44 The effect of incubating U87-*luc* cell lines with hypericin for 4 hrs followed by d-luciferin, as demonstrated by haemocytometry and growth assay

C = control, D = drug only, DMSO = DMSO only, L = d-luciferin only, DMSO+L = cells exposed to DMSO and d-luciferin, D+L = cells exposed to drug and d-luciferin. Asterisks indicate the degree of significance of the difference in cell number between each condition and control, where * $p > 0.05$, ** $p \leq 0.05$, *** $p < 0.01$, **** $p < 0.001$, ***** $p < 0.0001$. Following incubation with hypericin for 4 hrs, then exposure to d-luciferin, the cell population fell to 61.5 ± 4.68% ($p < 0.01$) and 34.3 ± 2.48% of control ($p < 0.0001$), in monoclonal and polyclonal cell lines respectively. On growth assay, this fall was more profound, with the test cell population falling to 55.3 ± 4.16% ($p < 0.0001$) and 13.0 ± 2.48% of control ($p < 0.0001$), in monoclonal and polyclonal cell lines respectively. Notably, there was no significant difference between DMSO controls and other controls, demonstrating that DMSO was indeed an inactive solvent.

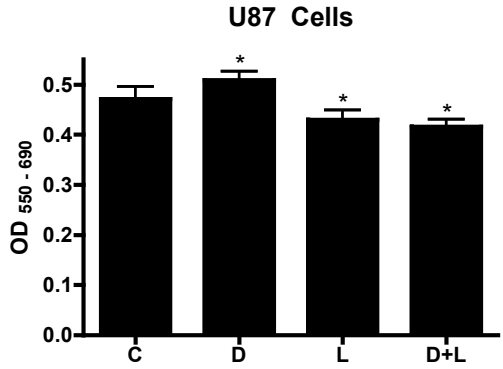

Figure 45 Effect of incubating U87 cells that have not been transfected with CMV-*luc* with hypericin for 4 hrs then d-luciferin

C = control, D = drug only, L = d-luciferin only, D+L = cells exposed to drug and d-luciferin. Asterisks indicate the degree of significance of the difference in OD between each condition and control, where * $p > 0.05$, ** $p \leq 0.05$, *** $p < 0.01$, **** $p < 0.001$, ***** $p < 0.0001$. In cells that do not have the ability to produce bioluminescence with the addition of d-luciferin, no significant cell death occurred when the cells were incubated with hypericin for 4 hrs then d-luciferin.

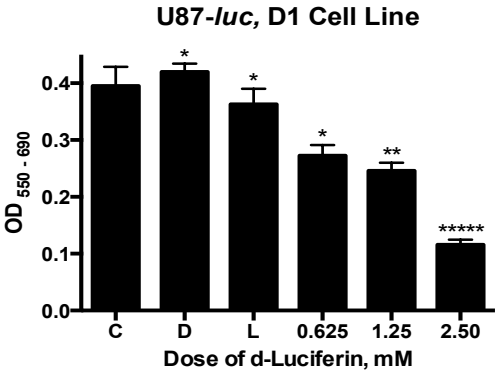

Figure 46 The dose-response of bPDT, demonstrated in a monoclonal U87-*luc* cell line incubated with hypericin for 4 hrs

C = control, D = drug only, L = d-luciferin only. Numbers on the x axis refer to the dose of d-luciferin that cells incubated with drug were exposed to, and represent the 'test' wells. Asterisks indicate the degree of significance of the difference in OD between each condition and control, where * $p > 0.05$, ** $p \leq 0.05$, *** $p < 0.01$, **** $p < 0.001$. ***** $p < 0.0001$. A dose-response with bPDT was demonstrated: increasing the dose of d-luciferin, and hence the amount of bioluminescence, increased the degree of cell death: following 4 hrs incubation with hypericin, incubation with 0.625 mM, 1.25 mM, and 2.50 mM of d-luciferin led to a fall in the cell population to 69.0 ± 4.70% of control ($p > 0.05$), 62.2% ± 3.60% of control ($p \leq 0.05$), and 29.3% ± 2.26% of control ($p < 0.0001$), respectively.

8.2.2 Hypericin, Long Incubation

Incubation with hypericin for 24 hrs, then subsequent incubation with d-luciferin (see Figure 47), led to > 50% cell death in all U87-*luc* (3 monoclonal and 1 polyclonal) cell lines. Specifically, incubation with photosensitiser then d-luciferin led to a fall in the cell population to 26.1 ± 2.29% ($p < 0.0001$), 32.1 ± 5.22% ($p < 0.0001$), 26.1 ± 2.49% ($p < 0.0001$), and 27.3 ± 0.46% ($p < 0.001$) of control, in the U87-*luc* D1, A1, B1 monoclonal cell lines, and the polyclonal cell line, respectively.

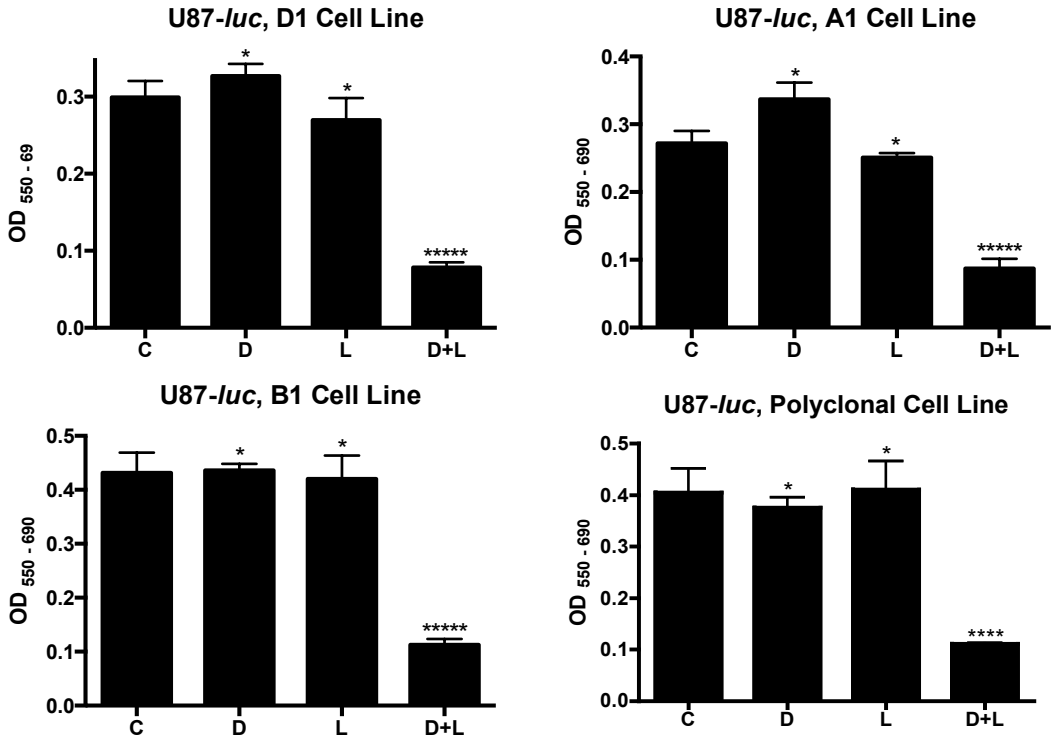

Figure 47 The effect of incubating U87-*luc* cell lines with hypericin for 24 hrs followed by d-luciferin, as demonstrated by the MTT assay

C = control, D = drug only, L = d-luciferin only, D+L = cells exposed to drug and d-luciferin. Asterisks indicate the degree of significance of the difference in OD between each condition and control, where * $p > 0.05$, ** $p \leq 0.05$, *** $p < 0.01$, **** $p < 0.001$, ***** $p < 0.0001$. Incubation with hypericin for 24 hrs, then d-luciferin, led to > 50% cell death in all U87-*luc* (3 monoclonal and 1 polyclonal) cell lines: in this way, there was a fall in the cell population to 26.1 ± 2.29% ($p < 0.0001$), 32.1 ± 5.22% ($p < 0.0001$), 26.1 ± 2.49% ($p < 0.0001$), and 27.3 ± 0.46% ($p < 0.001$) of control in U87-*luc* D1, A1, B1 monoclonal cell lines, and the polyclonal cell line, respectively.

The effect of the interaction between hypericin and d-luciferin was confirmed by haemocytometry and growth assay in U87-*luc* monoclonal and polyclonal lines (see Figure 48). In the monoclonal cell line, incubation with hypericin for 24 hrs followed by exposure to d-luciferin led to a fall in the cell population to 31.4 ± 3.34% of control ($p < 0.0001$). This fall was also reflected in the growth assay, where these 'test' cells

were found to be 34.6 ± 3.74% of control ($p < 0.0001$). Similarly, in the polyclonal cell line, incubation with hypericin for 24 hrs followed by exposure to d-luciferin led to a fall in the cell population to 34.0 ± 3.72% of control ($p < 0.0001$), and this fall was found to be more profound on the growth assay where test cells were 17.8 ± 3.32% of control ($p < 0.0001$). In the growth assay of the polyclonal cell line, there was a mild fall in the 'drug only' cells to 70.0 ± 4.23% of control ($p < 0.01$), which was not thought to contribute significantly to the overall result. These experiments were also performed with DMSO controls: there was no significant difference between these and other controls, demonstrating that DMSO was an inactive solvent, supporting the contention that it was an interaction between hypericin and d-luciferin that led to cell death.

The experiment was repeated in U87 cells that had not been transfected with CMV-*luc*: thus, these were cells that would not produce bioluminescence with the addition of d-luciferin. In this experiment, incubation of cells with hypericin for 24 hrs then d-luciferin did not lead to significant cell death (see Figure 48). *This demonstrates that it is not the chemical interaction between hypericin and d-luciferin that leads to cell death, but the interaction between hypericin and the bioluminescence generated by the addition of d-luciferin that is the cause of cell death: bioluminescence-mediated photodynamic therapy (bPDT).*

Furthermore, a dose-response with bPDT was demonstrated: increasing the dose of d-luciferin, which has been shown to increase the degree of bioluminescence (see Figure 40), increased the degree of cell death (see Figure 50): incubating U87-*luc* cells with hypericin for 24 hrs, followed by incubating the cells with 0.625 mM of d-luciferin led to a fall in the cell population to 50.4 ± 2.55% of control ($p < 0.0001$), incubating the cells with 1.25 mM of d-luciferin led to a fall to 37.0% ± 2.20% of control ($p < 0.0001$), and incubating the cells with 2.50 mM led to a fall to 15.2% ± 0.580% of control ($p < 0.0001$).

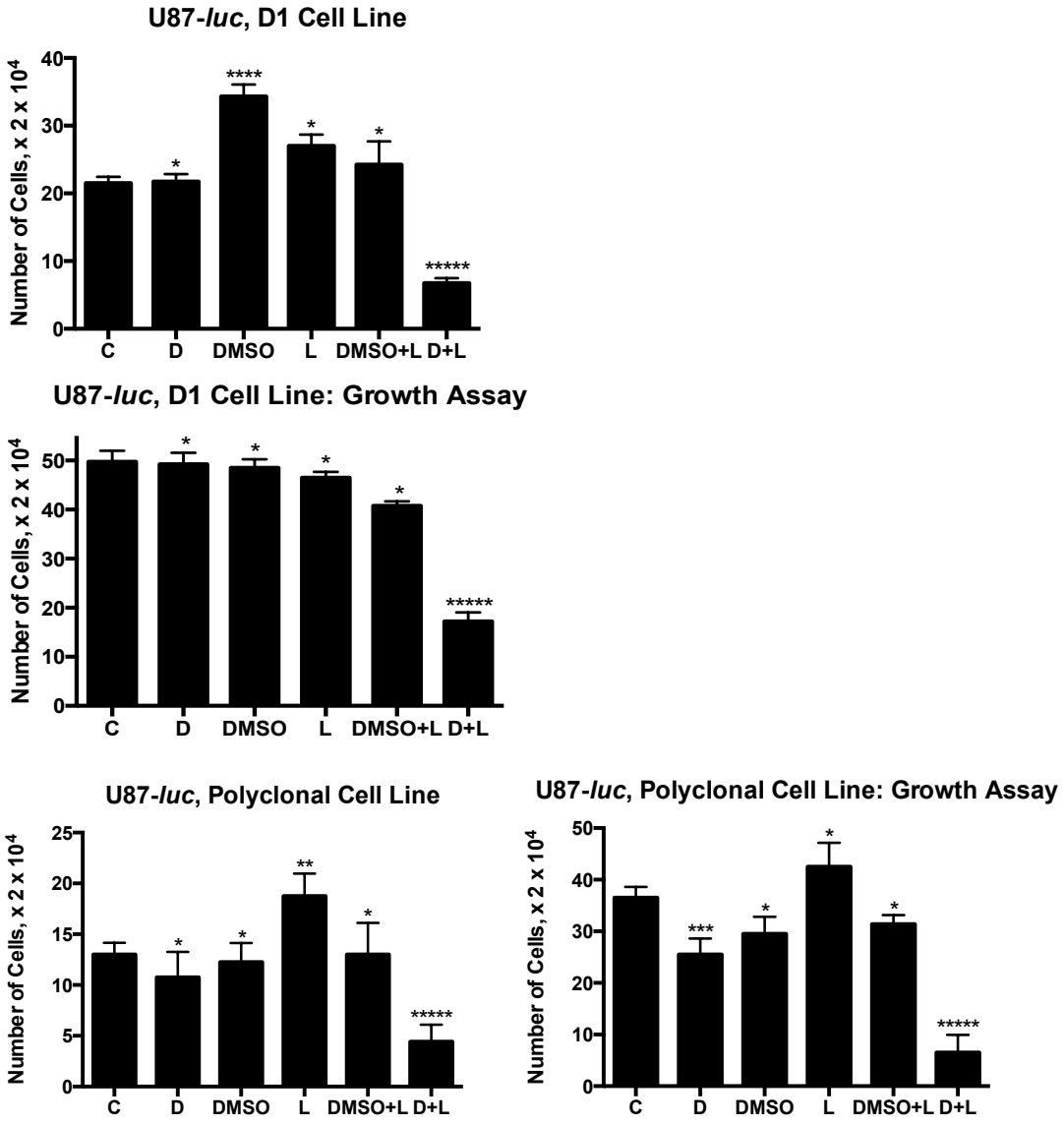

Figure 48 The effect of incubating U87-*luc* cell lines with hypericin for 24 hrs followed by d-luciferin, as demonstrated by haemocytometry and growth assay

C = control, D = drug only, DMSO = DMSO only, L = d-luciferin only, DMSO+L = cells exposed to DMSO and d-luciferin, D+L = cells exposed to drug and d-luciferin. Asterisks indicate the degree of significance of the difference in cell number between each condition and control, where * $p > 0.05$, ** $p \leq 0.05$, *** $p < 0.01$, **** $p < 0.001$, ***** $p < 0.0001$. Following incubation with hypericin for 24 hrs, then exposure to d-luciferin, the cell population fell to 31.4 ± 3.34% ($p < 0.0001$) and 34.0 ± 3.72% of control ($p < 0.0001$), in monoclonal and polyclonal cell lines respectively. On growth assay, this fall persisted, with the test cell population falling to 34.6 ± 3.74% ($p < 0.0001$) and 17.8 ± 3.32% of control ($p < 0.0001$), in monoclonal and polyclonal cell lines respectively. Notably, there was no significant difference between DMSO controls and other controls, demonstrating that DMSO was indeed an inactive solvent. The mild fall in the 'drug only' cells in the growth assay of the polyclonal cell line to 70.0 ± 4.23% of control ($p < 0.01$), was not thought to contribute significantly to the overall result.

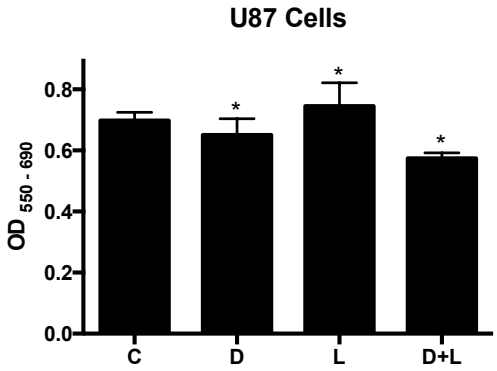

Figure 49 Effect of incubating U87 cells that have not been transfected with CMV-*luc* with hypericin for 24 hrs then d-luciferin

C = control, D = drug only, L = d-luciferin only, D+L = cells exposed to drug and d-luciferin. Asterisks indicate the degree of significance of the difference in OD between each condition and control, where * p > 0.05, ** p ≤ 0.05, *** p < 0.01, **** p < 0.001, ***** p < 0.0001. In cells that do not have the ability to produce bioluminescence with the addition of d-luciferin, no significant cell death occurred when the cells were incubated with hypericin for 24 hrs then d-luciferin.

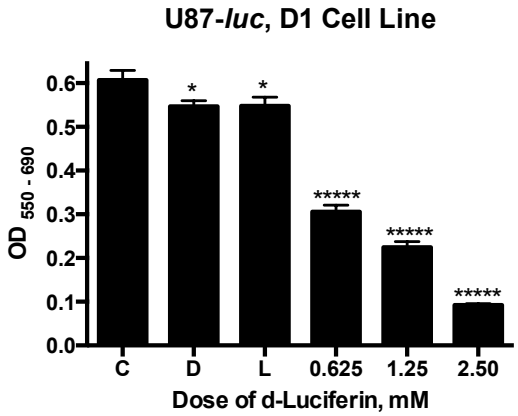

Figure 50 The dose-response of bPDT, demonstrated in a monoclonal U87-*luc* cell line incubated with hypericin for 24 hrs

C = control, D = drug only, L = d-luciferin only. Numbers on the x axis refer to the dose of d-luciferin that cells incubated with drug were exposed to, and represent the 'test' wells. Asterisks indicate the degree of significance of the difference in OD between each condition and control, where * p > 0.05, ** p ≤ 0.05, *** p < 0.01, **** p < 0.001. ***** p < 0.0001. A dose-response with bPDT was demonstrated: increasing the dose of d-luciferin, and hence the amount of bioluminescence, increased the degree of cell death: following 24 hrs incubation with hypericin, incubation with 0.625 mM, 1.25 mM, and 2.50 mM of d-luciferin led to a fall in the cell population to 50.4 ± 2.55%, 37.0 ± 2.20%, and 15.2 ± 0.580% of control (p < 0.0001), respectively.

Experiments thus far show that the bioluminescence generated by the addition of d-luciferin to luciferase-producing cells was able to activate a photosensitiser, hypericin, and mediate a photodynamic effect resulting in significant cell death: bPDT. In some cases, the growth assay revealed a more profound fall in cell survival than appreciated on initial haemocytometry. The longer incubation with hypericin led to a more profound fall in cell survival.

In order to investigate bPDT further, experiments were repeated but with a different photosensitiser, *m*THPC. Having provided proof of principle above, experiments with *m*THPC were performed in two cell lines, a monoclonal and a polyclonal line.

8.2.3 *m*THPC, Short Incubation

Incubation with *m*THPC for 3 hrs, then subsequent incubation with d-luciferin (see Figure 51), did not seem to lead to significant cell death when using the MTT assay as an assessment of cell viability. However, when assessing cell viability using haemocytometry, the test cell population was seen to fall to 22.1 ± 3.32% of control ($p < 0.0001$). Furthermore, the test cell population in the growth assay was seen to be 49.8 ± 3.03% of control ($p < 0.0001$).

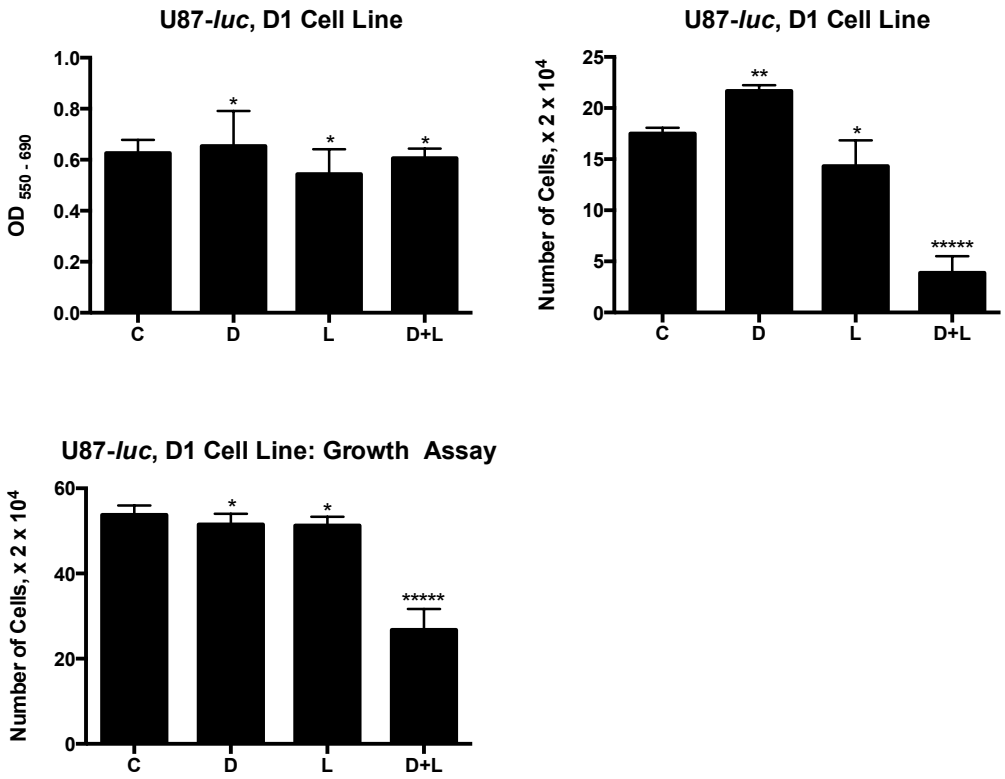

Figure 51 The effect of incubating a U87-*luc* monoclonal cell line with *m*THPC for 3 hrs followed by d-luciferin, as demonstrated by the MTT assay, haemocytometry and growth assay

C = control, D = drug only, L = d-luciferin only, D+L = cells exposed to drug and d-luciferin. Asterisks indicate the degree of significance of the difference in OD or cell number between each condition and control, where * $p > 0.05$, ** $p \leq 0.05$, *** $p < 0.01$, **** $p < 0.001$, ***** $p < 0.0001$. Incubation with *m*THPC for 3 hrs, then subsequent incubation with d-luciferin, did not seem to lead to significant cell death when using the MTT assay as an assessment of cell viability. However, when assessing cell viability using haemocytometry and the growth assay, the test cell population was seen to fall to 22.1 ± 3.32% and 49.8 ± 3.03% of control ($p < 0.0001$) respectively.

The reason for the disparity between results from the MTT assay and the cell counting techniques, haemocytometry and growth assay, was unclear. Experiments were repeated, but this time using U87-*luc* monoclonal cells that had been cultured and passaged 4 times in complete media made with heat inactivated serum (see Figure 52). In this cell population, incubation with *m*THPC for 3 hrs, then exposure to d-luciferin, again did not seem to lead to significant cell death when using the MTT assay as an assessment of cell viability. However, when assessing cell viability using haemocytometry, the test cell population was seen to fall to 47.2 ± 8.17% of control ($p < 0.01$). Furthermore, the test cell population in the growth assay was seen to have fallen more profoundly to 21.8 ± 4.00% of control ($p < 0.0001$).

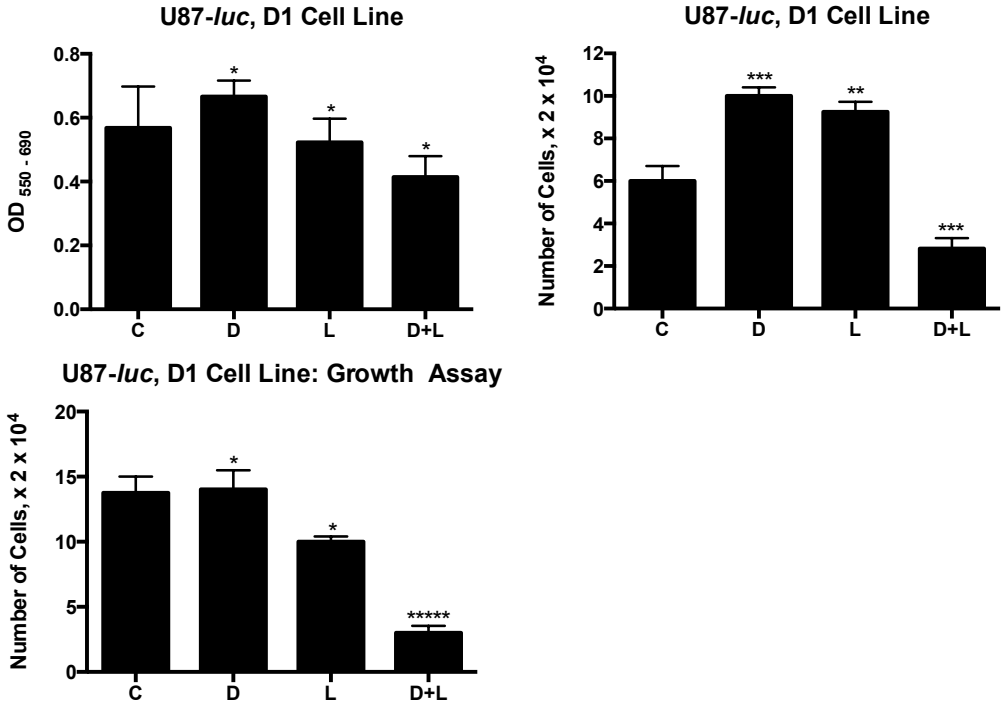

Figure 52 The effect of incubating a U87-*luc* monoclonal cell line, which has been passaged in complete media made with heat inactivated serum, with *m*THPC for 3 hrs followed by d-luciferin, as demonstrated by the MTT assay, haemocytometry and growth assay

C = control, D = drug only, L = d-luciferin only, D+L = cells exposed to drug and d-luciferin. Asterisks indicate the degree of significance of the difference in OD or cell number between each condition and control, where * $p > 0.05$, ** $p \leq 0.05$, *** $p < 0.01$, **** $p < 0.001$, ***** $p < 0.0001$. Incubation with *m*THPC for 3 hrs, then subsequent incubation with d-luciferin, did not seem to lead to significant cell death when using the MTT assay as an assessment of cell viability. However, when assessing cell viability using haemocytometry and the growth assay, the test cell population was seen to fall to 47.2 ± 8.17% ($p < 0.01$) and 21.8 ± 4.00 % ($p < 0.0001$) of control respectively.

The experiment was then repeated in a U87-*luc* polyclonal line. Incubation with *m*THPC for 3 hrs, then subsequent incubation with d-luciferin (see Figure 53), again did not seem to lead to significant cell death when using the MTT assay as an assessment of cell viability. However, when assessing cell viability using haemocytometry, the test cell population was seen to fall to 25.8 ± 4.00% of control ($p < 0.0001$). Furthermore, the test cell population in the growth assay was seen to have fallen more profoundly to 4.26 ± 1.57% of control ($p < 0.0001$).

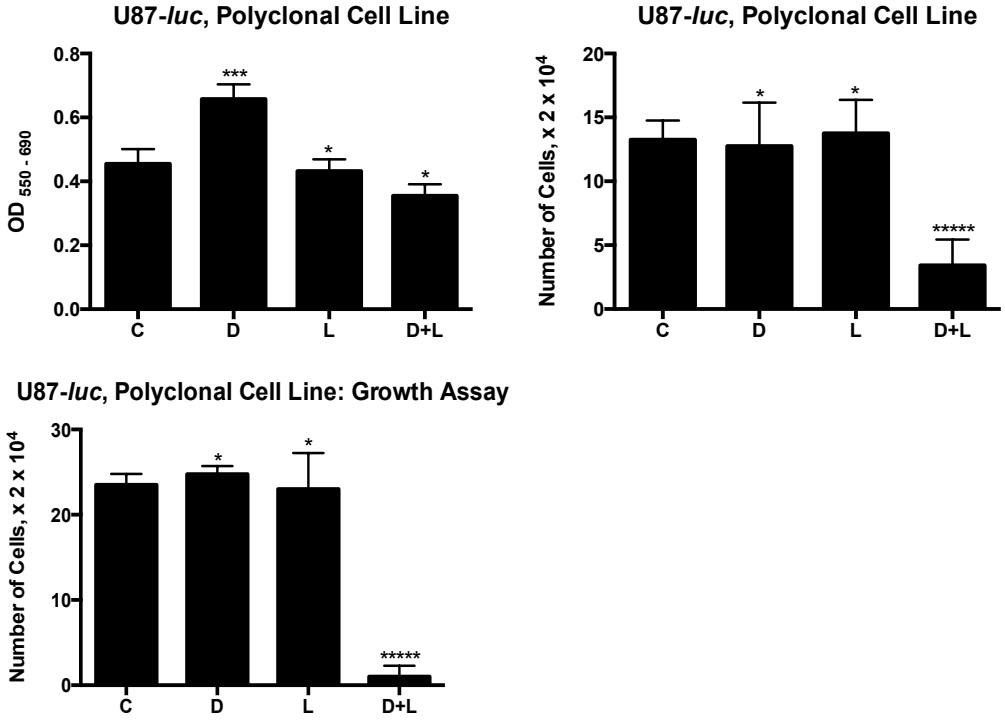

Figure 53 The effect of incubating a U87-*luc* polyclonal cell line with *m*THPC for 3 hrs followed by d-luciferin, as demonstrated by the MTT assay, haemocytometry and growth assay

C = control, D = drug only, L = d-luciferin only, D+L = cells exposed to drug and d-luciferin. Asterisks indicate the degree of significance of the difference in OD or cell number between each condition and control, where * $p > 0.05$, ** $p \leq 0.05$, *** $p < 0.01$, **** $p < 0.001$, ***** $p < 0.0001$. Incubation with *m*THPC for 3 hrs, then subsequent incubation with d-luciferin, did not seem to lead to significant cell death when using the MTT assay as an assessment of cell viability. However, when assessing cell viability using haemocytometry and the growth assay, the test cell population was seen to fall to 25.8 ± 4.40% and 4.26 ± 1.57% of control ($p < 0.0001$) respectively.

The experiment was then repeated, but this time using U87-*luc* polyclonal cells that had been cultured and passaged 4 times in complete media made with heat inactivated serum (see Figure 54). In this cell population, incubation with *m*THPC for 3 hrs, then exposure to d-luciferin, again did not seem to lead to significant cell death when using the MTT assay as an assessment of cell viability. However, when assessing cell viability using haemocytometry, the test cell population was seen to fall to 9.55 ± 2.26% of control ($p < 0.0001$). Furthermore, the test cell population in the growth assay was seen to have fallen more profoundly to 5.59 ± 1.62% of control ($p < 0.0001$). In the growth assay, there was a mild fall in the 'light only' control to 79.7 ± 3.70% of control ($p < 0.01$), which was not considered to have contributed significantly to the overall effect on the test cells.

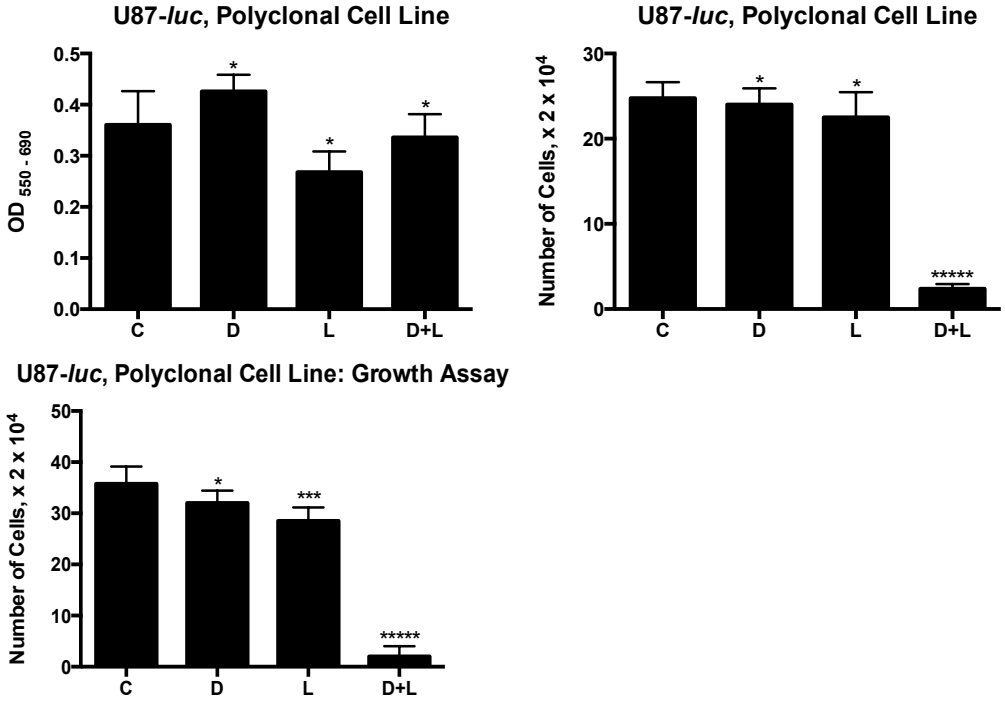

Figure 54 The effect of incubating a U87-*luc* polyclonal cell line, which has been passaged in complete media made with heat inactivated serum, with *m*THPC for 3 hrs followed by d-luciferin, as demonstrated by the MTT assay, haemocytometry and growth assay

C = control, D = drug only, L = d-luciferin only, D+L = cells exposed to drug and d-luciferin. Asterisks indicate the degree of significance of the difference in OD or cell number between each condition and control, where * $p > 0.05$, ** $p \leq 0.05$, *** $p < 0.01$, **** $p < 0.001$, ***** $p < 0.0001$. Incubation with *m*THPC for 3 hrs, then subsequent incubation with d-luciferin, did not seem to lead to significant cell death when using the MTT assay as an assessment of cell viability. However, when assessing cell viability using haemocytometry and the growth assay, the test cell population was seen to fall to 9.55 ± 2.26% and 5.59 ± 1.62 % of control ($p < 0.0001$) respectively. In the growth assay, there was a mild fall in the 'light only' control to 79.7 ± 3.70% of control ($p < 0.01$), which was not considered to contribute significantly to the overall effect on the test cells.

8.2.4 *m*THPC, Long Incubation

Incubation with *m*THPC for 24 hrs, then subsequent incubation with d-luciferin (see Figure 55), did not seem to lead to significant cell death when using the MTT assay as an assessment of cell viability. However, when assessing cell viability using haemocytometry, the test cell population was seen to fall to 43.8 ± 4.41% of control ($p < 0.0001$). Furthermore, the test cell population in the growth assay was seen to be 59.7 ± 7.48% of control ($p < 0.01$).

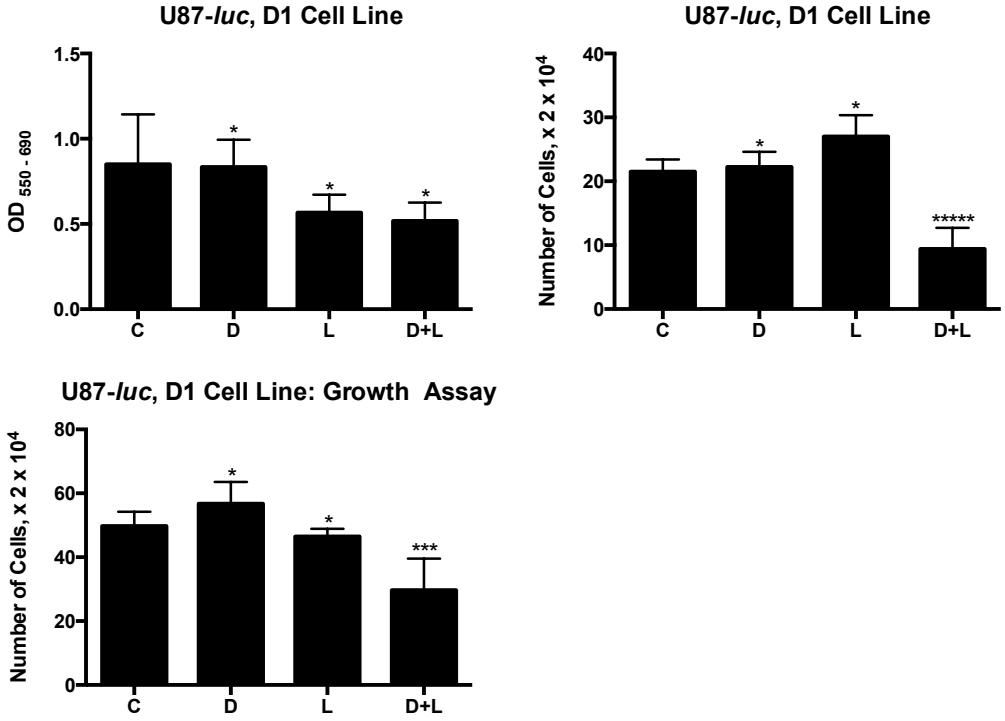

Figure 55 The effect of incubating a U87-*luc* monoclonal cell line with *m*THPC for 24 hrs followed by d-luciferin, as demonstrated by the MTT assay, haemocytometry and growth assay

C = control, D = drug only, L = d-luciferin only, D+L = cells exposed to drug and d-luciferin. Asterisks indicate the degree of significance of the difference in OD or cell number between each condition and control, where * $p > 0.05$, ** $p \leq 0.05$, *** $p < 0.01$, **** $p < 0.001$, ***** $p < 0.0001$. Incubation with *m*THPC for 24 hrs, then subsequent incubation with d-luciferin, did not seem to lead to significant cell death when using the MTT assay as an assessment of cell viability. However, when assessing cell viability using haemocytometry and the growth assay, the test cell population was seen to fall to 43.8 ± 4.41% and 59.7 ± 7.48% of control ($p < 0.0001$) respectively.

Similarly, incubation of a U87-*luc* polyclonal cell line with *m*THPC for 24 hrs, then d-luciferin (see Figure 56), led to a fall in cell population to 31.9 ± 3.65% of control ($p < 0.0001$). Furthermore, this fall was also reflected in the growth assay, where these 'test' cells were found to be 31.1 ± 6.56% of control ($p < 0.0001$).

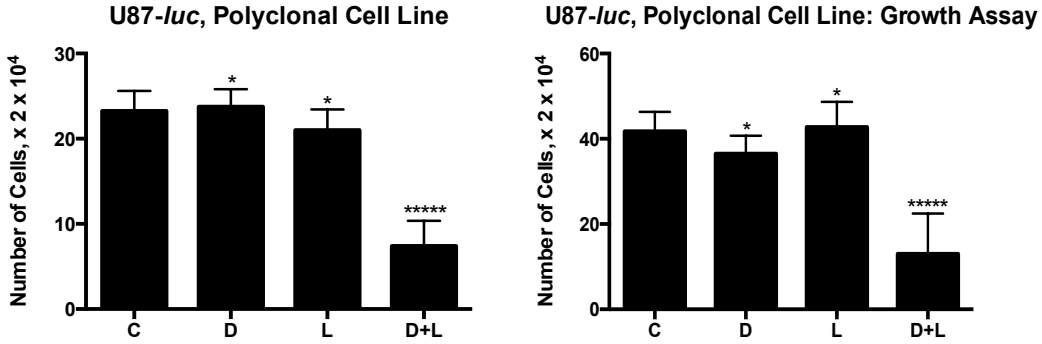

Figure 56 The effect of incubating a U87-*luc* polyclonal cell line with *m*THPC for 24 hrs followed by d-luciferin, as demonstrated by haemocytometry and growth assay

C = control, D = drug only, L = d-luciferin only, D+L = cells exposed to drug and d-luciferin. Asterisks indicate the degree of significance of the difference in cell number between each condition and control, where * $p > 0.05$, ** $p \leq 0.05$, *** $p < 0.01$, **** $p < 0.001$, ***** $p < 0.0001$. Incubation with *m*THPC for 24 hrs, then subsequent incubation with d-luciferin, led to fall in the cell population to 31.9 ± 3.65% and 31.1 ± 6.56% of control ($p < 0.0001$) as demonstrated by haemocytometry and growth assay respectively.

These experiments show that bioluminescence, generated by the addition of d-luciferin to luciferase-producing cells, can activate another photosensitiser, *m*THPC, and mediate a photodynamic effect causing significant cell death; another demonstration of bPDT. In contrast to hypericin, the shorter incubation with *m*THPC led to a more profound fall in cell survival. Similar to experiments with hypericin, in the majority of cases, the growth assay demonstrated a more profound fall in cell survival than that seen on initial haemocytometry, which was what was typically seen when cells were incubated with *m*THPC for 3 hrs.

The reason for the MTT assay not providing an accurate indication of cell viability in this model is not clear. It was a phenomenon seen consistently in monoclonal as well as polyclonal cell lines, so not a characteristic inherent to the monoclonal line. It is not surprising that culturing cells in heat inactivated serum, which inactivates complement, did not improve the efficacy of the assay, as the reaction of the assay does not interact with the complement cascade.

8.3 U87-CBG68*luc*

Having successfully demonstrated the concept of bPDT in U87-*luc* cells, experiments proceeded in a different cell line, U87-CBG68*luc*, but still using the same substrate to generate bioluminescence, d-luciferin.

8.3.1 Hypericin, Short Incubation

Incubation with hypericin for 4 hrs, then subsequent incubation with d-luciferin (see Figure 57), led to a fall in the cell population to 20.0 ± 2.22% of control ($p < 0.001$). Having already shown that DMSO is an inactive solvent, experiments were only performed with a 'DMSO+L' control: there was no significant difference between this and other controls, confirming that DMSO was indeed an inactive solvent, supporting the contention that it was an interaction between hypericin and d-luciferin that led to cell death.

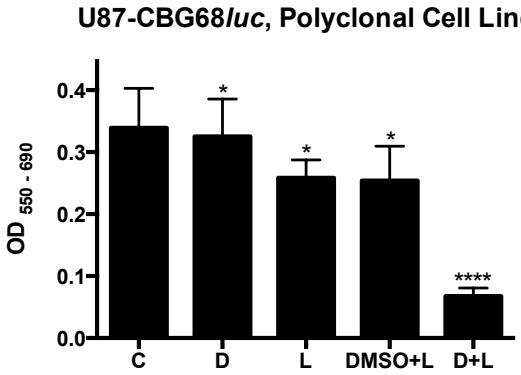

Figure 57 The effect of incubating U87-CBG68*luc* cells with hypericin for 4 hrs followed by d-luciferin, as demonstrated by the MTT assay

C = control, D = drug only, L = d-luciferin only, DMSO+L = cells exposed to DMSO and d-luciferin, D+L = cells exposed to drug and d-luciferin. Asterisks indicate the degree of significance of the difference in OD between each condition and control, where * $p > 0.05$, ** $p \leq 0.05$, *** $p < 0.01$, **** $p < 0.001$, ***** $p < 0.0001$. Incubation with hypericin for 4 hrs, then d-luciferin, led to a fall in the cell population to 20.0 ± 2.22% of control ($p < 0.001$) in a U87-CBG68*luc* polyclonal cell line.

8.3.2 Hypericin, Long Incubation

Incubation with hypericin for 24 hrs, then subsequent incubation with d-luciferin (see Figure 58), led to a fall in the cell population to 25.4 ± 12.0% of control ($p < 0.01$). Having already shown that DMSO is an inactive solvent, experiments were only performed with a 'DMSO+L' control: there was again no significant difference between this and other controls, confirming that DMSO was indeed an inactive solvent, supporting the contention that it was an interaction between hypericin and d-luciferin that led to cell death.

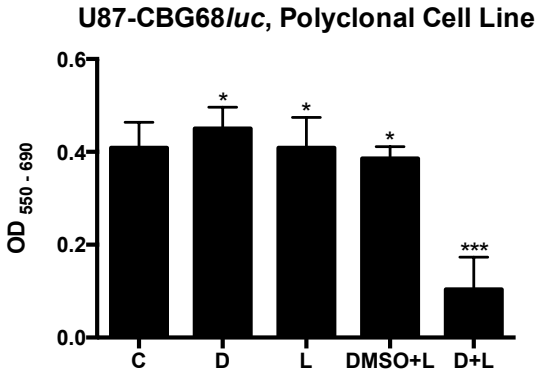

Figure 58 The effect of incubating U87-CBG68*luc* cells with hypericin for 24 hrs followed by d-luciferin, as demonstrated by the MTT assay

C = control, D = drug only, L = d-luciferin only, DMSO+L = cells exposed to DMSO and d-luciferin, D+L = cells exposed to drug and d-luciferin. Asterisks indicate the degree of significance of the difference in OD between each condition and control, where * $p > 0.05$, ** $p \leq 0.05$, *** $p < 0.01$, **** $p < 0.001$, ***** $p < 0.0001$. Incubation with hypericin for 24 hrs, then d-luciferin, led to a fall in the cell population to 25.4 ± 12.0% of control ($p < 0.01$) in a U87-CBG68*luc* polyclonal cell line.

8.3.3 *m*THPC Short Incubation

Incubation with *m*THPC for 3 hrs, then subsequent incubation with d-luciferin (see Figure 59), did not lead to cell death when using the MTT assay as an assessment of cell viability. When assessing cell viability using haemocytometry, the test cell population was seen to fall to 57.1 ± 5.83% of control, which trended towards significance (95% CI -0.301 to 6.30, $p > 0.05$).

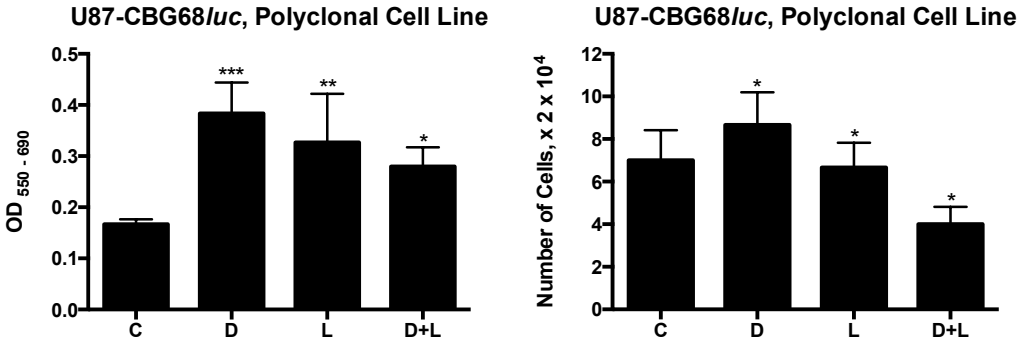

Figure 59 The effect of incubating a U87-CBG68*luc* polyclonal cell line with *m*THPC for 3 hrs followed by d-luciferin, as demonstrated by the MTT assay, haemocytometry and growth assay

C = control, D = drug only, L = d-luciferin only, D+L = cells exposed to drug and d-luciferin. Asterisks indicate the degree of significance of the difference in OD or cell number between each condition and control, where * $p > 0.05$, ** $p \leq 0.05$, *** $p < 0.01$, **** $p < 0.001$, ***** $p < 0.0001$. Incubation with *m*THPC for 3 hrs, then subsequent incubation with d-luciferin, did not lead to significant cell death when using the MTT assay as an assessment of cell viability. When assessing cell viability using haemocytometry, the test cell population was seen to fall to 57.1 ± 5.83%, which trended towards significance ($p > 0.05$, 95% CI -0.301 to 6.30).

8.3.4 *m*THPC Long Incubation

Incubation with *m*THPC for 24 hrs, then subsequent incubation with d-luciferin (see Figure 60), did not lead to significant cell death when assessed by MTT assay or haemocytometry. Although there was a significant fall in cell survival to 59.5 ± 3.80% of control ($p < 0.01$) when using the MTT assay, this was not significantly different from the 'drug only' or 'light only' controls, 82.4 ± 9.17% and 73.9 ± 4.06% of control, respectively. Similarly, although there was a significant fall in cell survival to 38.7 ± 4.44% of control ($p < 0.0001$) when using haemocytometry, this was not significantly different from the 'light only' control, 55.0 ± 3.53%.

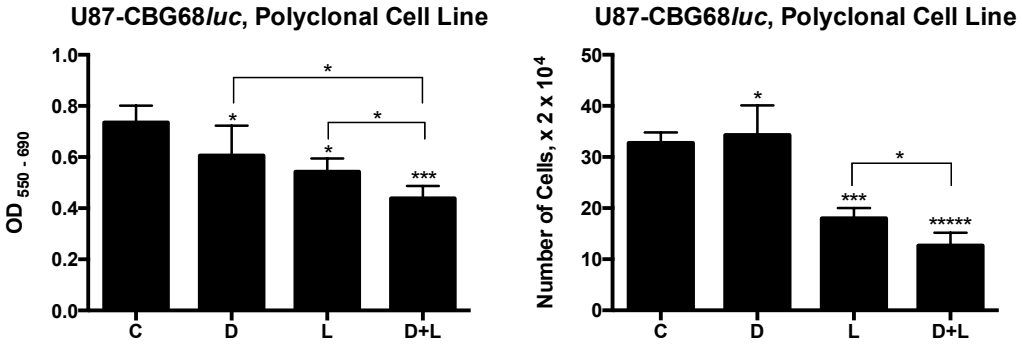

Figure 60 The effect of incubating a U87-CBG68*luc* polyclonal cell line with *m*THPC for 24 hrs followed by d-luciferin, as demonstrated by the MTT assay, haemocytometry and growth assay

C = control, D = drug only, L = d-luciferin only, D+L = cells exposed to drug and d-luciferin. Asterisks indicate the degree of significance of the difference in OD or cell number between each condition and control, where * $p > 0.05$, ** $p \leq 0.05$, *** $p < 0.01$, **** $p < 0.001$, ***** $p < 0.0001$. Incubation with *m*THPC for 24 hrs, then subsequent incubation with d-luciferin, did not lead to significant cell death when assessed by MTT assay or haemocytometry: although there was a significant fall in cell survival to 59.5 ± 3.80% ($p < 0.01$) and 38.7 ± 4.44% ($p < 0.0001$) of control respectively, this was not significantly different to the 'drug only' and 'light only' controls of the MTT assay, and the 'light only' control from haemocytometry.

These experiments show that the bioluminescence generated by the oxidation of d-luciferin by click beetle luciferase, can activate the photosentiser, hypericin, and mediate a photodynamic effect causing significant cell death; another demonstration of bPDT. However, such bioluminescence is not able activate the photosensitiser, *m*THPC, to mediate a photodynamic effect to cause cell death. Further testing with different monoclonal and polyclonal lines, and cell viability assessments with haemocytometry and growth assay were not pursued due to time contraints.

8.4 U87-*hRluc*

So far, it has been established that the bioluminescence produced by U87-*luc* and U87-CBG68*luc* cells using d-luciferin as a substrate can activate a photosensitiser to mediate a photodynamic effect and cause significant cell death, bPDT. Here, the concept of bPDT is tested in a completely different model, using U87-*hRluc* cells and the substrate EnduRen™. The U87-*hRluc* monoclonal line E was chosen for testing, as it was the cell line that produced maximum bioluminescence. The substrate used was 30 μM of EnduRen™. Cell viability was assessed by haemocytometry and growth assay.

8.4.1 Hypericin, Short Incubation

Incubation with hypericin for 4 hrs, then subsequent incubation with EnduRen™ (see Figure 61), did not lead to a fall in the test cell population. Furthermore, no cell kill was evident on delayed testing with the growth assay.

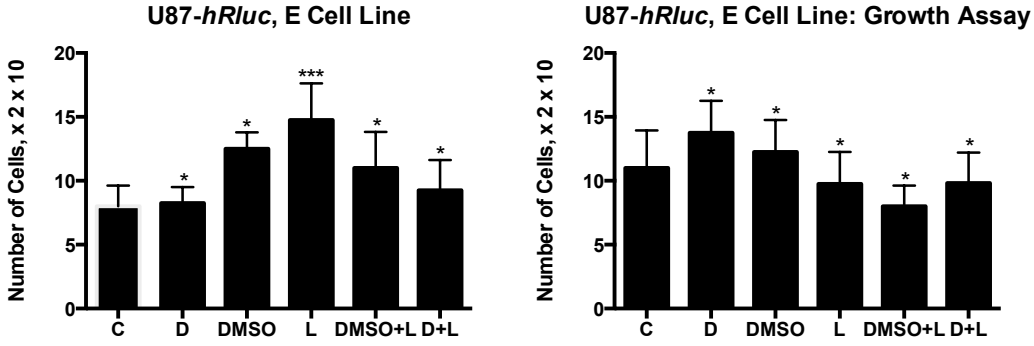

Figure 61 The effect of incubating U87-*hRluc* cells with hypericin for 4 hrs followed by EnduRen™, as demonstrated by haemocytometry and growth assay

C = control, D = drug only, L = EnduRen™ only, DMSO+L = cells exposed to DMSO and EnduRen™, D+L = cells exposed to drug and EnduRen™. Asterisks indicate the degree of significance of the difference in cell number between each condition and control, where * $p > 0.05$, ** $p \leq 0.05$, *** $p < 0.01$, **** $p < 0.001$, ***** $p < 0.0001$. Incubation with hypericin for 4 hrs, then EnduRen™, did not lead to a fall in cell population on initial testing by haemocytometry or delayed testing by growth assay.

8.4.2 Hypericin, Long Incubation

Incubation with hypericin for 24 hrs, then subsequent incubation with EnduRen™ (see Figure 62), did not lead to a fall in the test cell population. Furthermore, no cell kill was evident on delayed testing with the growth assay.

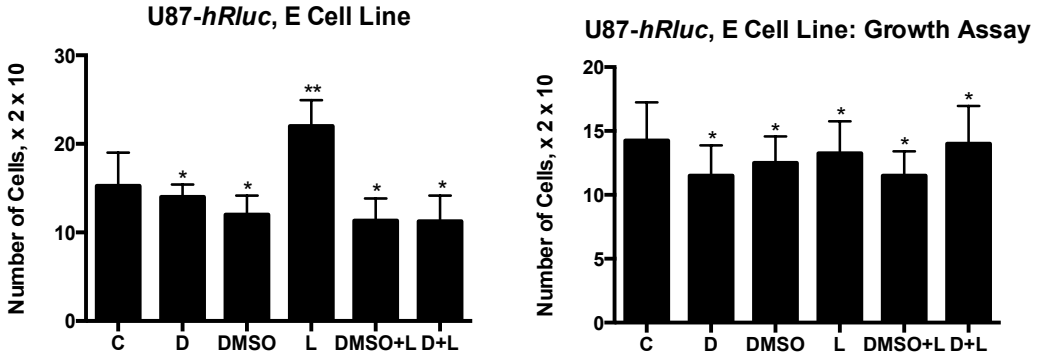

Figure 62 The effect of incubating U87-*hRluc* cells with hypericin for 24 hrs followed by EnduRen™, as demonstrated by haemocytometry and growth assay

C = control, D = drug only, L = EnduRen™ only, DMSO+L = cells exposed to DMSO and EnduRen™, D+L = cells exposed to drug and EnduRen™. Asterisks indicate the degree of significance of the difference in cell number between each condition and control, where * $p > 0.05$, ** $p \leq 0.05$, *** $p < 0.01$, **** $p < 0.001$, ***** $p < 0.0001$. Incubation with hypericin for 24 hrs, then EnduRen™, did not lead to a fall in cell population on initial testing by haemocytometry or delayed testing by growth assay.

8.4.3 *m*THPC, Short Incubation

Incubation with *m*THPC for 3 hrs, then subsequent incubation with EnduRen™ (see Figure 63), did not lead to a fall in the test cell population. Furthermore, no cell kill was evident on delayed testing with the growth assay.

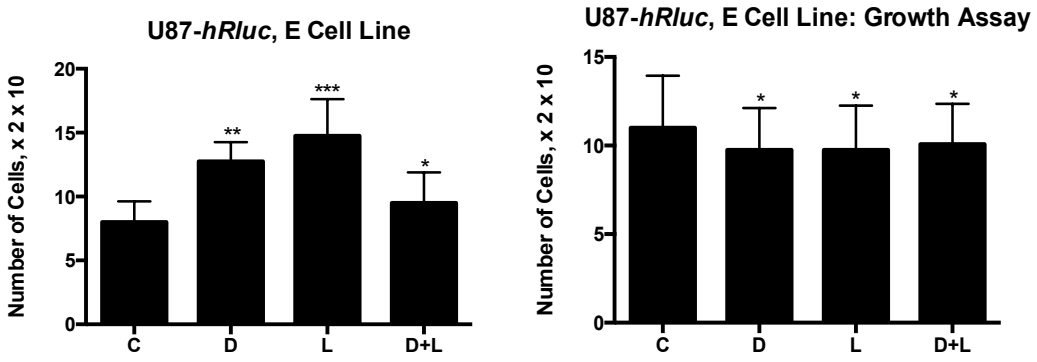

Figure 63 The effect of incubating U87-*hRluc* cells with *m*THPC for 3 hrs followed by EnduRen™, as demonstrated by haemocytometry and growth assay

C = control, D = drug only, L = EnduRen™ only, D+L = cells exposed to drug and EnduRen™. Asterisks indicate the degree of significance of the difference in cell number between each condition and control, where * $p > 0.05$, ** $p \leq 0.05$, *** $p < 0.01$, **** $p < 0.001$, ***** $p < 0.0001$. Incubation with *m*THPC for 3 hrs, then EnduRen™, did not lead to a fall in cell population on initial testing by haemocytometry or delayed testing by growth assay.

8.4.4 *m*THPC, Long Incubation

Incubation with *m*THPC for 24 hrs, then subsequent incubation with EnduRen™ (see Figure 64), led to a fall in the cell population to 57.1 ± 3.11% of control ($p < 0.001$). This fall was more pronounced in the growth assay, where these 'test' cells were found to be 25.5 ± 5.79% of control ($p < 0.0001$).

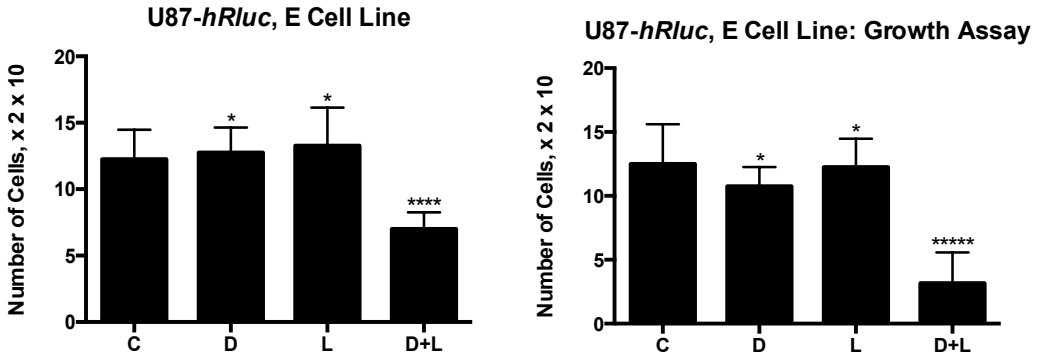

Figure 64 The effect of incubating U87-*hRluc* cells with *m*THPC for 24 hrs followed by EnduRen™, as demonstrated by haemocytometry and growth assay

C = control, D = drug only, L = EnduRen™ only, D+L = cells exposed to drug and EnduRen™. Asterisks indicate the degree of significance of the difference in cell number between each condition and control, where * $p > 0.05$, ** $p \leq 0.05$, *** $p < 0.01$, **** $p < 0.001$, ***** $p < 0.0001$. Incubation with *m*THPC for 24 hrs, then EnduRen™, led to a fall in the test cell population to 57.1 ± 3.11% ($p < 0.001$) and 25.5 ± 5.79% ($p < 0.0001$) on initial haemocytometry and growth assay, respectively.

Furthermore, in some experiments, incubation with *m*THPC for 24 hrs, then subsequent exposure to EnduRen™, would initially lead to a fall in the cell population. However, this fall was not sustained on growth assay. For example, in Figure 65, the test cell population initially fell to 60.9 ± 3.40% of control ($p < 0.0001$). However, on growth assay, the test cell population recovered and there was no difference between this and the control.

In contrast, in other experiments, incubation with *m*THPC for 24 hrs, then subsequent exposure to EnduRen™, would not lead to an initial fall in the test cell population. However, a fall in the test cell population would become apparent on growth assay. For example, in Figure 66, although the test cell population fell to 76.5 ± 3.83% of control, which appeared to be significant ($p \leq 0.05$), this was not significantly different to the 'drug only' control, 77.9 ± 5.57%. However, on growth assay, the test cell population fell to 58.5 ± 3.03 of control ($p < 0.0001$).

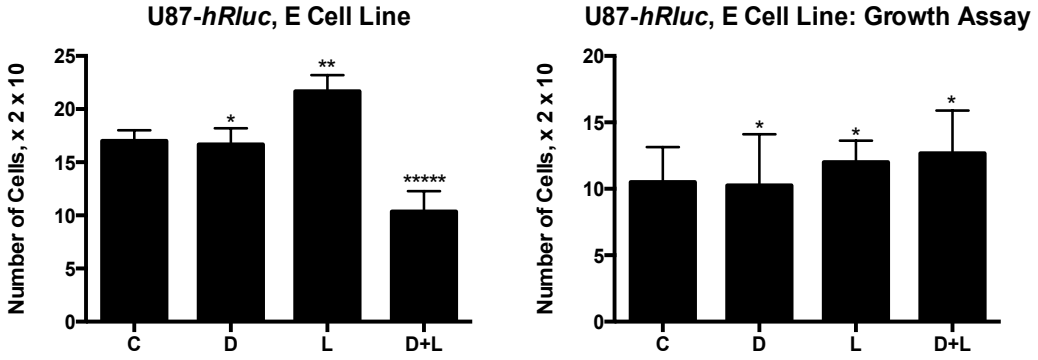

Figure 65 The effect of incubating U87-*hRluc* cells with *m*THPC for 24 hrs followed by EnduRen™, as demonstrated by haemocytometry and growth assay: a second pattern for outcome

C = control, D = drug only, L = EnduRen™ only, D+L = cells exposed to drug and EnduRen™. Asterisks indicate the degree of significance of the difference in cell number between each condition and control, where * $p > 0.05$, ** $p \leq 0.05$, *** $p < 0.01$, **** $p < 0.001$, ***** $p < 0.0001$. Incubation with *m*THPC for 24 hrs, then EnduRen™, led to a fall in the test cell population to 60.9 ± 3.40 % ($p < 0.0001$), which was not sustained on growth assay where the test cell population was not significantly different to control.

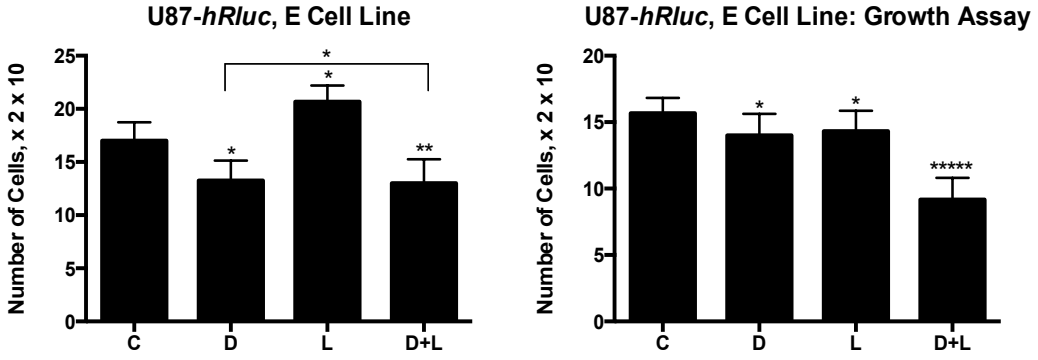

Figure 66 The effect of incubating U87-*hRluc* cells with *m*THPC for 24 hrs followed by EnduRen™, as demonstrated by haemocytometry and growth assay: a third pattern for outcome

C = control, D = drug only, L = EnduRen™ only, D+L = cells exposed to drug and EnduRen™. Asterisks indicate the degree of significance of the difference in cell number between each condition and control, where * $p > 0.05$, ** $p \leq 0.05$, *** $p < 0.01$, **** $p < 0.001$, ***** $p < 0.0001$. Incubation with *m*THPC for 24 hrs, then EnduRen™, led to a fall in the test cell population to 76.5 ± 3.83 % ($p \leq 0.05$), which was not significantly different to the 'drug only' control. However, on growth assay, the test cell population fell to 58.5 ± 3.03 of control ($p < 0.0001$).

The bioluminescence generated by the addition of EnduRen™ to U87-*hRluc* cells, did not seem to activate the photosensitisers, hypericin and *m*THPC, to mediate a photodynamic effect leading to significant cell death, except in the condition where cells were incubated with *m*THPC for 24 hrs. In this latter condition, cell death was either evident on initial haemocytometry and became more profound on growth assay or was not evident on initial haemocytometry, but became apparent on growth assay; or cell death was evident on initial haemocytometry, but cells had recovered on the growth assay such that there was no difference to control. Of note, although the U87-*hRluc* cells grew well in culture and passaged well, once they were plated into 96 well plates, and particularly when they were transitioned to the 12 well plates for the growth assay, they did not grow well, such that the growth assay was performed 8 days after initial haemocytometry compared to the typical 5 days to allow control cells to reach subconfluence. In view of concerns for the robustness of this model, experiments were not repeated with ViviRen™.

8.5 Inhibiting the Effect

To provide further proof that it is indeed bioluminescence activating photosensitiser to cause a photodynamic effect that is mediating cell kill, experiments were repeated but with the additional condition of lycopene. Lycopene is an antioxidant. As the photodynamic effect is mediated by the generation of singlet oxygen, the effect can be inhibited by an antioxidant. If the cell death in our model is truly secondary to bPDT, cell death should be inhibited by the presence of lycopene.

Experiments were repeated as described in sections 8.1 and 8.2 using a U87-*luc* polyclonal cell line and d-luciferin as substrate; this model chosen for the robustness of results, but with the following variations. Control wells were divided into pure 'control' wells, which were exposed to neither photosensitiser, lycopene, acetone, nor d-luciferin; 'drug only' wells, which were exposed only to photosensitiser; 'lycopene only' wells, which were exposed only to lycopene; 'acetone only' wells, which were exposed only to acetone; 'light only' wells, which were exposed only to d-lucferin; 'drug and acetone' wells, which were exposed only to photosensitiser and acetone; 'drug and lycopene' wells, which were exposed only to photosensitiser and lycopene; 'acetone and light' wells, which were exposed only to acetone and d-luciferin; 'lycopene and light' wells, which were exposed only to lycopene and d-luciferin. The

acetone controls were included to account for the acetone that lycopene was reconstituted in.

After incubating with the photosensitisers, hypericin or *m*THPC, for the appropriate times, all wells were washed twice with 0.1 ml of PBS and 0.1 ml of fresh complete media was replaced. 0.1 ml of d-luciferin was then added to 'light only,' 'acetone and light,' and 'lycopene and light,' 'drug and light,' and 'drug, lycopene and light' wells to give a final concentration of 2.5 mM of d-luciferin. Remaining wells had 0.1 ml of PBS added. At this time, 5 μM of lycopene (Sigma) was added to 'lycopene only,' 'drug and lycopene,' 'lycopene and light,' and 'drug, light and lycopene' wells. Additionally, at this time, acetone, equal to the volume used to reconstitute the lycopene, was added to 'acetone only,' 'drug and acetone,' and 'acetone and light' wells. Cells were allowed to incubate for a further 20-24 hrs, following which cell viability was assessed by haemocytometry and growth assay. Each condition was tested in triplicate. Experiments repeated a minimum of three times. The most representative results are shown.

8.5.1 Hypericin, Short Incubation

Incubation with hypericin for 4 hrs, then subsequent incubation with d-luciferin (see Figure 67), led to a fall in the cell population to 38.0 ± 4.00% of control ($p < 0.001$) and this fall persisted in the growth assay where the test cell population was 38.0 ± 1.78% of control ($p < 0.0001$). In contrast, when cells were incubated with photosensitiser, then exposed to d-luciferin and lycopene simultaneously, there was no significant fall in the cell population (87.8 ± 6.12% and 98.0 ± 5.57% with initial haemocytometry then growth assay, respectively): the lycopene was able to prevent the interaction between the photosensitiser and the bioluminescence generated by the addition of d-luciferin.

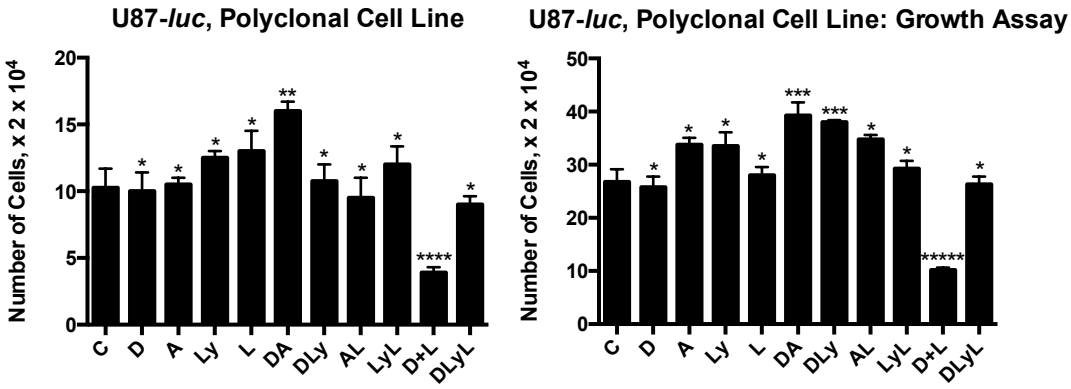

Figure 67 The effect of adding lycopene, an antioxidant, to U87-*luc* cells that have been incubating with hypericin for 4 hrs, then exposed to d-luciferin, as demonstrated by haemocytometry and growth assay

C = control, D = drug only, A = acetone only, Ly = lycopene only, L = d-luciferin only, DA = cells exposed to drug and acetone, DLy = cells exposed to drug and lycopene, AL = cells exposed to acetone and d-luciferin, LyL = cells exposed to lycopene and d-luciferin, D+L = cells exposed to drug and d-luciferin, DLyL = cells exposed to drug, lycopene and d-luciferin. Asterisks indicate the degree of significance of the difference in cell number between each condition and control, where * $p > 0.05$, ** $p \leq 0.05$, *** $p < 0.01$, **** $p < 0.001$, ***** $p < 0.0001$. Incubation with hypericin for 4 hrs, then subsequent incubation with d-luciferin, led to a fall in the cell population to 38.0 ± 4.00% ($p < 0.001$) and 38.0 ± 1.78% ($p < 0.0001$) of control ($p < 0.001$) with initial haemocytometry then subsequent growth assay, respectively. When cells were incubated with photosensitiser, then exposed to d-luciferin and lycopene simultaneously, there was no significant fall in the cell population (87.8 ± 6.12% and 98.0 ± 5.57% with initial haemocytometry then growth assay, respectively).

8.5.2 Hypericin, Long Incubation

Incubation with hypericin for 24 hrs, then subsequent incubation with d-luciferin (see Figure 68), led to a fall in the cell population to 32.3 ± 4.82% of control ($p < 0.0001$). When cells were incubated with photosensitiser, then exposed to d-luciferin and lycopene simultaneously, although there was a significant fall in the cell population to 57.1 ± 2.46% of control ($p < 0.0001$), this degree of cell death was significantly less profound than that of the test cell population ($p \leq 0.05$), indicating partial inhibition of the bPDT effect. Furthermore, on growth assay, there was partial recovery of the cells exposed to photosensitier and d-lucifeirn to 61.7 ± 2.08% of control, which was still significantly less than control ($p < 0.001$), but there was complete recovery of the cell population exposed to drug, lycopene and light to 107 ± 4.16 % of control ($p > 0.05$), again indicating that lycopene was able to prevent the interaction between photosensitiser and the bioluminescence generated by the addition of d-luciferin.

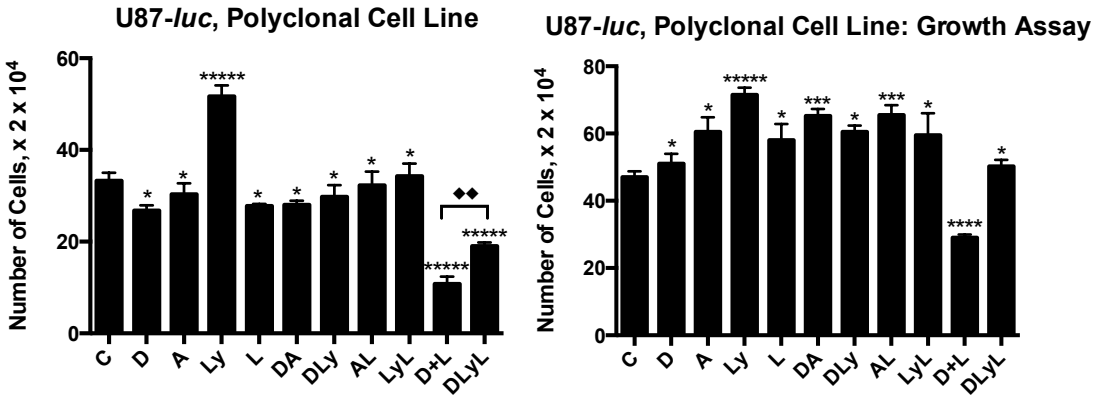

Figure 68 The effect of adding lycopene, an antioxidant, to U87-*luc* cells that have been incubating with hypericin for 24 hrs, then exposed to d-luciferin, as demonstrated by haemocytometry and growth assay

C = control, D = drug only, A = acetone only, Ly = lycopene only, L = d-luciferin only, DA = cells exposed to drug and acetone, DLy = cells exposed to drug and lycopene, AL = cells exposed to acetone and d-luciferin, LyL = cells exposed to lycopene and d-luciferin, D+L = cells exposed to drug and d-luciferin, DLyL = cells exposed to drug, lycopene and d-luciferin. Asterisks indicate the degree of significance of the difference in cell number between each condition and control, where * $p > 0.05$, ** $p \leq 0.05$, *** $p < 0.01$, **** $p < 0.001$, ***** $p < 0.0001$. Diamonds indicate the degree of significance in the difference in cell number between the D+L and DLyL conditions on initial haemocytometry, where ♦♦$p \leq 0.05$. Incubation with hypericin for 24 hrs, then subsequent incubation with d-luciferin, led to a fall in the cell population to 32.3 ± 4.82% of control ($p < 0.0001$), with some recovery on growth assay to 61.7 ± 2.08% of control, which was still significantly less than control ($p < 0.001$). When cells were incubated with photosensitiser, then exposed to d-luciferin and lycopene simultaneously, although there was a significant fall in the cell population to 57.1 ± 2.46% of control ($p < 0.0001$), this degree of cell death was significantly less profound than that of the test cell population ($p \leq 0.05$), and completely recovered to 107 ± 4.16 % of control ($p > 0.05$) on growth assay, indicating that lycopene was able to prevent the interaction between photosensitiser and the bioluminescence generated by the addition of d-luciferin.

8.5.3 *m*THPC, Short Incubation

Incubation with *m*THPC for 3 hrs, then subsequent incubation with d-luciferin (see Figure 69), led to a fall in the cell population to 22.3 ± 3.02% of control ($p < 0.0001$) and this fall persisted in the growth assay where the test cell population was 30.5 ± 2.80% of control ($p < 0.0001$). In contrast, when cells were incubated with photosensitiser, then exposed to d-luciferin and lycopene simultaneously, there was no significant fall in the cell population (103 ± 6.81% and 105 ± 5.73% with initial haemocytometry then growth assay, respectively): the lycopene was able to prevent the interaction between the photosensitiser and the bioluminescence generated by the addition of d-luciferin.

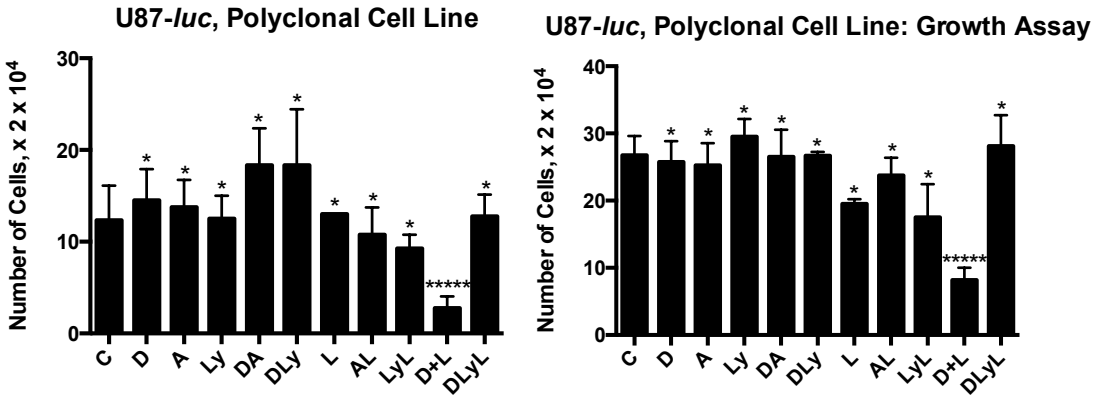

Figure 69 The effect of adding lycopene, an antioxidant, to U87-*luc* cells that have been incubating with *m*THPC for 3 hrs, then exposed to d-luciferin, as demonstrated by haemocytometry and growth assay

C = control, D = drug only, A = acetone only, Ly = lycopene only, L = d-luciferin only, DA = cells exposed to drug and acetone, DLy = cells exposed to drug and lycopene, AL = cells exposed to acetone and d-luciferin, LyL = cells exposed to lycopene and d-luciferin, D+L = cells exposed to drug and d-luciferin, DLyL = cells exposed to drug, lycopene and d-luciferin. Asterisks indicate the degree of significance of the difference in cell number between each condition and control, where * $p > 0.05$, ** $p \leq 0.05$, *** $p < 0.01$, **** $p < 0.001$, ***** $p < 0.0001$. Incubation with *m*THPC for 3 hrs, then subsequent incubation with d-luciferin, led to a fall in the cell population to 22.3 ± 3.02% ($p < 0.0001$) and 30.5 ± 2.80% of control ($p < 0.0001$) with initial haemocytometry then subsequent growth assay, respectively. When cells were incubated with photosensitiser, then exposed to d-luciferin and lycopene simultaneously, there was no significant fall in the cell population (103 ± 6.81% and 105 ± 5.73% with initial haemocytometry then growth assay, respectively).

8.5.4 *m*THPC, Long Incubation

Incubation with *m*THPC for 24 hrs, then subsequent incubation with d-luciferin (see Figure 70), led to a fall in the cell population to 28.2 ± 3.01% of control ($p < 0.0001$). When cells were incubated with photosensitiser, then exposed to d-luciferin and lycopene simultaneously, there was a only a mild fall in the cell population to 68.6 ± 3.04% of control ($p < 0.01$); this cell population still being significantly greater than the cells that had been exposed to photosensitiser and d-luciferin only. The mild fall in the cell population exposed to photosensitiser, then d-luciferin and lycopene, was likely accounted for by a slight fall in cell population associated with the addition of d-luciferin only (70.1 ± 3.95% of control, $p \leq 0.05$), which was also seen in the 'acetone and light' (73.7 ± 3.43% of control, $p \leq 0.05$), and 'lycopene and light' (73.7 ± 3.65% of control, $p \leq 0.05$) controls. On growth assay, there was no lasting evidence of toxicity attributable to d-luciferin, and the cell population exposed to photosensitiser then d-luciferin remained significantly decreased at 42.2 ± 3.46% of control ($p < 0.0001$). Moreover, there was no significant fall in the cell population that had been exposed to photosensitiser, then lycopene and d-luciferin (78.5 ± 5.61% of control).

Overall, results indicate that lycopene was able to prevent the interaction between photosensitiser and the bioluminescence generated by the addition of d-luciferin.

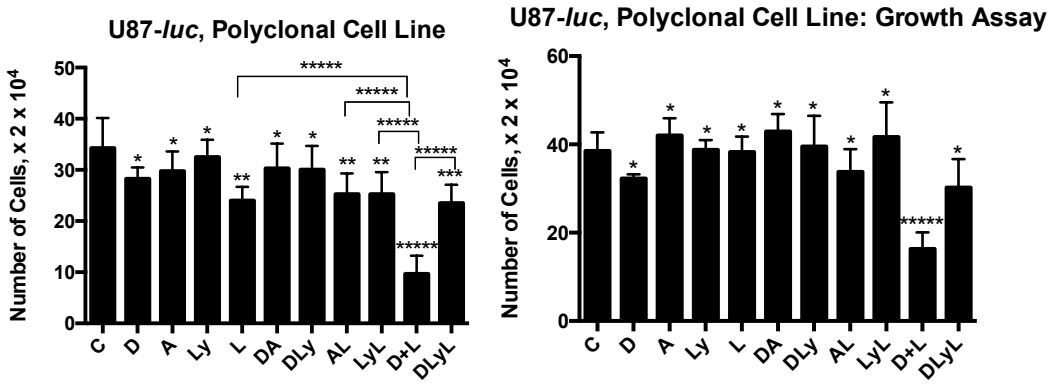

Figure 70 The effect of adding lycopene, an antioxidant, to U87-*luc* cells that have been incubating with *m*THPC for 24 hrs, then exposed to d-luciferin, as demonstrated by haemocytometry and growth assay

C = control, D = drug only, A = acetone only, Ly = lycopene only, L = d-luciferin only, DA = cells exposed to drug and acetone, DLy = cells exposed to drug and lycopene, AL = cells exposed to acetone and d-luciferin, LyL = cells exposed to lycopene and d-luciferin, D+L = cells exposed to drug and d-luciferin, DLyL = cells exposed to drug, lycopene and d-luciferin. Asterisks indicate the degree of significance of the difference in cell number between each condition and control, where * $p > 0.05$, ** $p \leq 0.05$, *** $p < 0.01$, **** $p < 0.001$, ***** $p < 0.0001$. Incubation with *m*THPC for 24 hrs, then subsequent incubation with d-luciferin, led to a fall in the cell population to 28.2 ± 3.01% of control ($p < 0.0001$). When cells were incubated with photosensitiser, then exposed to d-luciferin and lycopene simultaneously, there was a only a mild fall in the cell population to 68.6 ± 3.04% of control ($p < 0.01$); this cell population still being significantly greater than the cells that had been exposed to photosensitiser and d-luciferin only. The mild fall in the cell population exposed to photosensitiser, then d-luciferin and lycopene, was likely accounted for by a slight fall in cell population associated with the addition of d-luciferin only (70.1 ± 3.95% of control, $p \leq 0.05$), which was also seen in the 'acetone and light' (73.7 ± 3.43% of control, $p \leq 0.05$), and 'lycopene and light' (73.7 ± 3.65% of control, $p \leq 0.05$) controls. On growth assay, there was no lasting evidence of toxicity attributable to d-luciferin, and the cell population exposed to photosensitiser then d-luciferin remained significantly decreased at 42.2 ± 3.46% of control ($p < 0.0001$). Moreover, there was no significant fall in the cell population that had been exposed to photosensitiser, then lycopene and d-luciferin (78.5 ± 5.61% of control).

Lycopene was able to prevent the cell death that occurred when luciferase-producing cells were incubated with photosensitiser then d-luciferin. This further supports that it is the bioluminescence, generated by adding d-luciferin to luciferase-producing cells, that activates the photosensitiser to cause a photodynamic effect, which is an effect mediated by singlet oxygen, and subsequent cell death.

8.6 Establishing Subcellular Localisation

To gain further understanding of bPDT, investigations were undertaken to establish the subcellular localisation of the luciferase substrate d-luciferin, compared to that of the photosensitisers, hypericin and *m*THPC.

U87-*luc* cells were harvested after trypsinisation, plated on 5.5 cm diameter plates, which had been coated with 0.42 ml of poly-l-lysine (Sigma-Aldrich), at a density of $0.7x10^6$ cells per plate, and returned to the incubator. After 24 hrs of incubation the plates were examined under the microscope to confirm that the cells had adhered adequately. Media was then aspirated from each plate, the cells washed twice with 2.5 ml of PBS. The following conditions were tested: 'control' plates, which were not exposed to photosensitiser or d-luciferin; 'hypericin only' plates, which were exposed to hypericin alone for 24 hrs; '*m*THPC only' plates, which were exposed to *m*THPC alone for 24 hrs; 'light only' plates, which were exposed to d-luciferin alone for 24 hrs; and 'test plates,' which were either exposed to hypericin for 4 or 24 hrs followed by d-luciferin for 20-24 hrs or *m*THPC for 3 or 24 hrs followed by d-luciferin for 20-24 hrs.

'Control' plates had 5 ml of serum free media without phenol red replaced. 2.5 ml of photosensitiser, made up in serum free media without phenol red, was added to the appropriate plates to give final concentrations of either 12.5 μM or 10.0 μM of hypericin for 4 hrs and 24 hrs incubation respectively, or 12.5 μg/ml or 2.5 μg/ml of *m*THPC for 3 hrs and 24 hrs incubation respectively. The 'light only' plate had 2.5 ml of serum free media without phenol red replaced, then 2.5 ml of d-luciferin added to give a final concentration of 2.5 mM.

After 24 hrs, the 'control,' 'hypericin only,' '*m*THPC only,' and 'light only' plates were removed from the incubator. The media was aspirated, the plates were washed twice with 2.5 ml of PBS, and 5 ml of serum free media without phenol red was replaced. Cells were then examined using a Leica TCS microscope with a confocal SPE head and a x40 water immersion, quartz objective (NA 0.8). 'Hypericin only' and 'light only' plates were excited with 405, 488 and 532 nm of light, and '*m*THPC only' plates were excited with 488 and 532 nm of light, from the HeNe laser (45-50% total laser power). Data was analysed using LAS AF software. Lambda scans were generated for each control condition, detecting fluorescence up to 695-705 nm. From these, the excitation wavelengths that would allow the separate fluorescence signals to be

detected from exciting hypericin and d-luciferin simultaneously and from exciting *m*THPC and d-luciferin simultaneously within specific emission parameters were determined. Once these parameters were determined, the 'control' plates were subject to each excitation wavelength as a negative control (see section 8.6.2.1).

Regarding the test plates, after the appropriate time of incubation with the photosensitisers, media was aspirated and the plates washed twice with 2.5 ml of PBS. 2.5 ml of serum free media without phenol red was replaced and 2.5 ml of d-luciferin was added to give a final concentration of 2.5 mM. The plates were incubated for a further 20-24 hrs, then examined under the confocal microscope. The plates were then subject to excitation with the appropriate wavelengths of light and the resulting fluorescence captured within the appropriate ranges, as determined by analysis of the control plates described above.

8.6.1 Lambda scans

Exciting cells that had been incubating with hypericin (see Figure 71) with light at a wavelength of 405 nm led to fluorescence characterised by moderate intensity peaks at 595 and 645 nms. Exciting such cells with light at a wavelength of 488 nm led to fluorescence characterised by a high intensity peak at 600 nm and a moderate intensity peak at 660 nm. Exciting such cells with light at a wavelength of 532 nm led to fluorescence characterised by a high intensity peak at 600 nm and a moderate intensity peak at 650 nm.

Exciting cells that had been incubating with *m*THPC (see Figure 72) with light at a wavelength of 405 nm led to fluorescence characterised by a low intensity peak at 650 nm. Exciting such cells with light at a wavelength at 532 nm led to fluorescence characterised by a high intensity peak at approximately 648 nm.

Exciting cells that had been incubating with d-luciferin (see Figure 73) with light at a wavelength of 450 nm led to fluorescence characterised by moderate intensity peaks at 502 and 554 nm. Exciting such cells with light at a wavelength of 488 nm led to fluorescence characterised by extremely low intensity and poorly defined peaks at 532 and 660 nm. Similarly, exciting such cells with light at a wavelength of 532 nm led to an extremely low and poorly defined peak between 624 and 644 nm.

In examining the lambda scans, the excitation wavelengths that generated fluorescence signals in markedly different parts of the electromagnetic spectrum when comparing hypericin and d-luciferin, and *m*THPC and d-luciferin, were identified, allowing co-localisation (see Table 9). It was decided that cells that had been incubating with hypericin and d-luciferin be excited with 488 and 405 nm, capturing fluorescence from hypericin between 640-720 nm and that from d-luciferin between 410-530 nm. The smaller fluorescence peak from hypericin was chosen for detection, as the larger peak would have required capture between 580-620 nm, which would have also captured the second fluorescence peak generated by exciting d-luciferin with 405 nm (see Figure 71 and Figure 73). Furthermore, it was decided that cells that had been incubating with *m*THPC and d-luciferin be excited with 532 and 405 nm, capturing fluorescence from *m*THPC between 620-690 nm and that from d-luciferin between 410-530 nm (see Figure 72 and Figure 73).

To detect:	Excitation Wavelength, nm	Emission, nm, collected between:
Hypericin	488	640-720
*m*THPC	532	620-690
d-Luciferin	405	410-530

Table 9 Excitation and Emission Parameters Used to Study the Subcellular Localisation of hypericin, *m*THPC, and d-luciferin

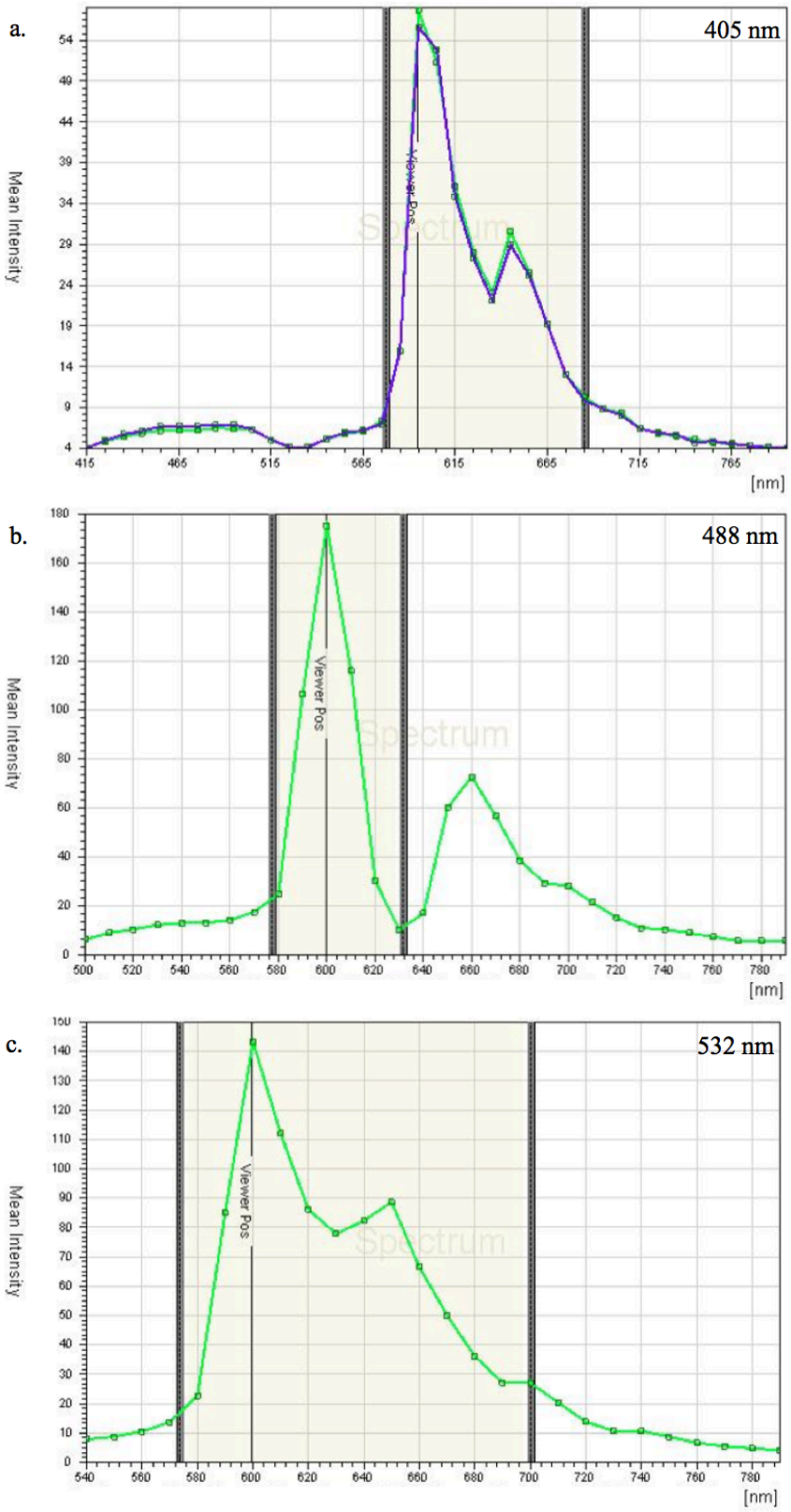

Figure 71 Lambda scans obtained from cells incubated with hypericin then excited with light with wavelengths at a. 405 nm, b. 488 nm, and c. 532 nm

Exciting cells incubated with hypericin with light at 405, 488, and 532 nm led to fluorescence with moderate intensity peaks at 595 and 645 nm; a high intensity peak at 600 nm and a moderate intensity peak at 660 nm; and a high intensity peak at 600 nm and a moderate intensity peak at 650 nm, respectively.

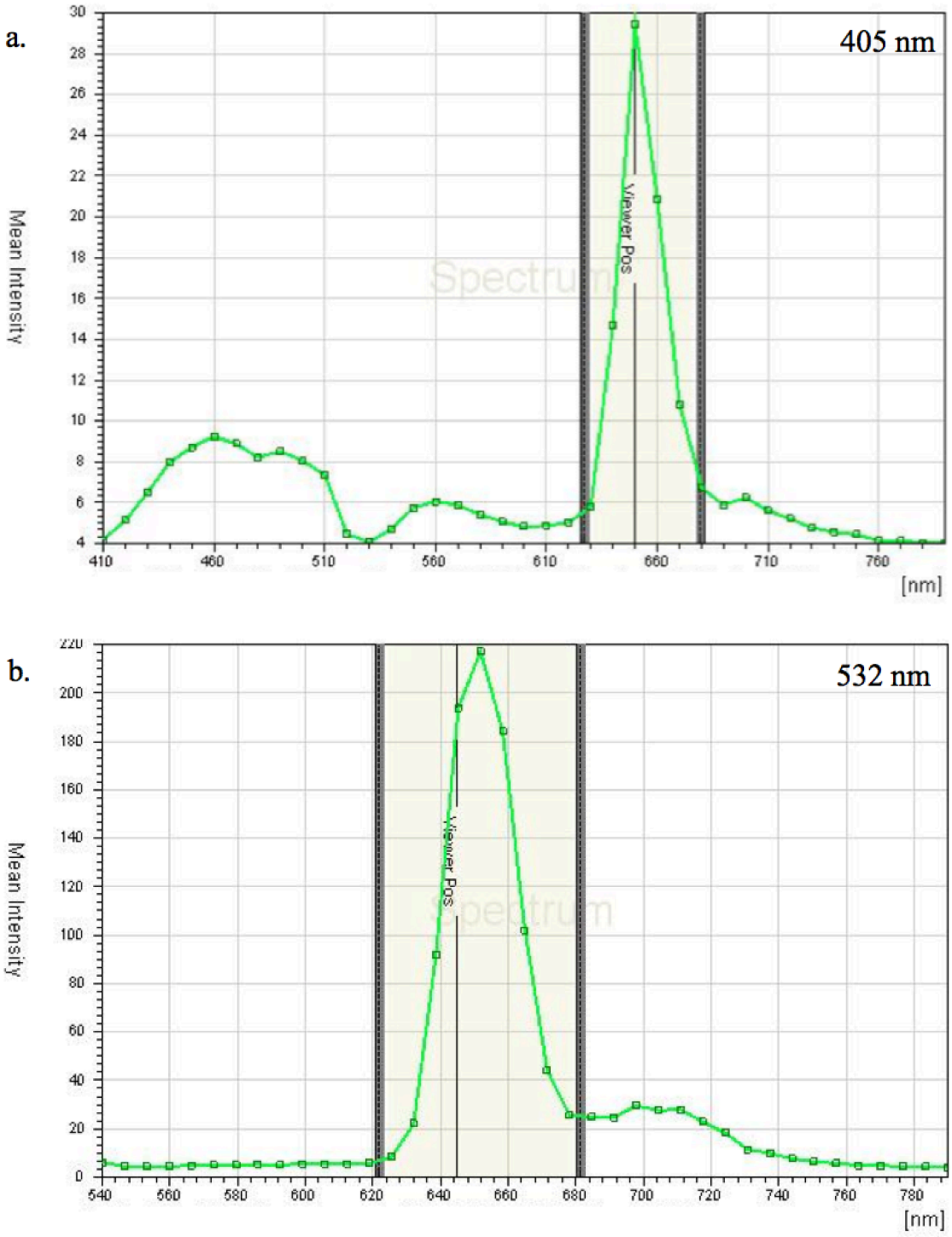

Figure 72 Lambda scans obtained from cells incubated with *m*THPC then excited with light with wavelengths at a. 405 nm, and b. 532 nm

Exciting cells incubated with *m*THPC with light at 405, and 532 nm led to fluorescence with a low intensity peak at 650 nm and a high intensity peak at 648 nm, respectively.

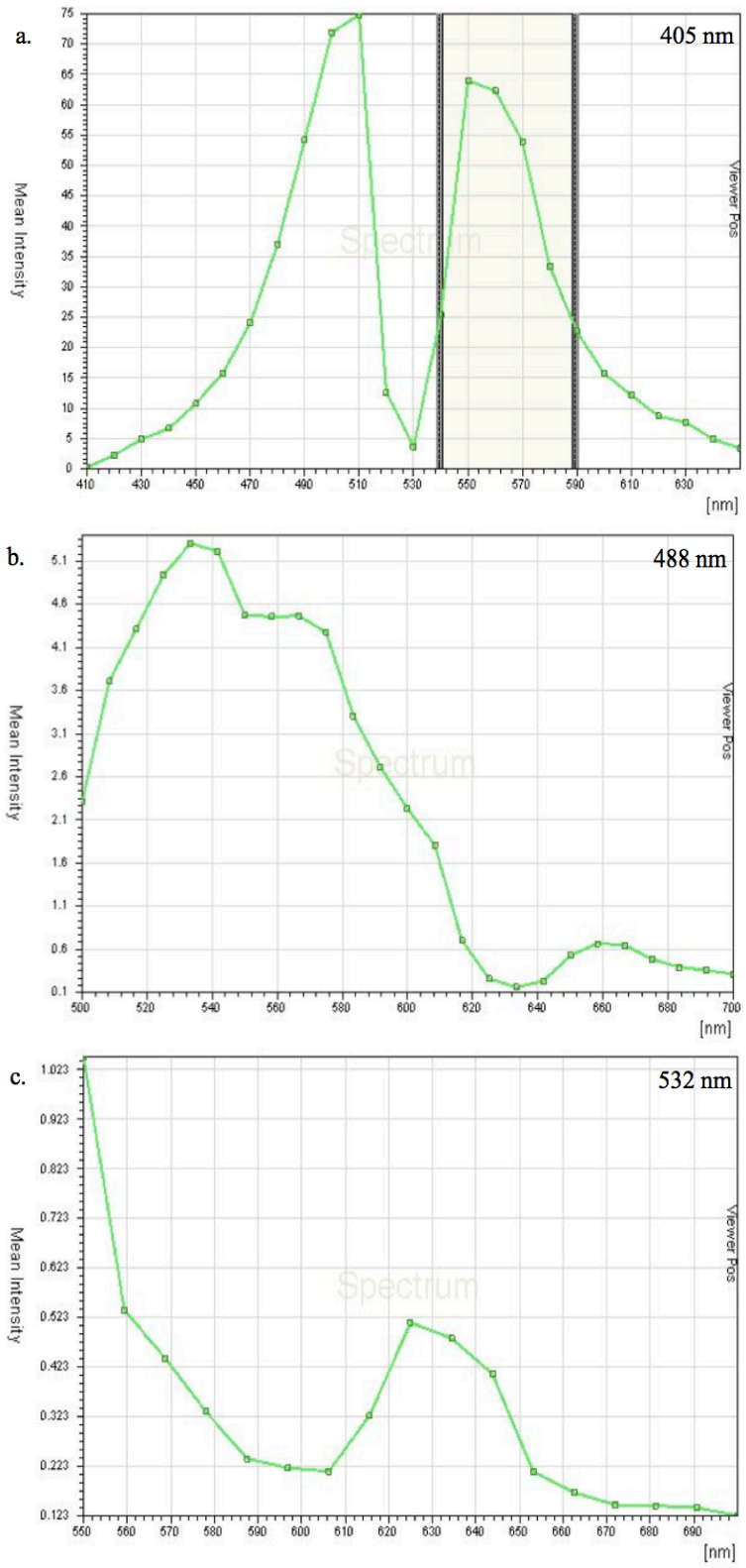

Figure 73 Lambda scans obtained from cell incubated with d-luciferin then excited with light with wavelengths at a. 405 nm, b. 488 nm, and c. 532 nm

Exciting cells that had been incubating with d-luciferin with light at wavelengths of 450, 488, and 532 nm led to fluorescence characterised by moderate intensity peaks at 502 and 554 nm; extremely low intensity and poorly defined peaks at 532 and 660 nm; and an extremely low and poorly defined peak between 624 and 644 nm, respectively.

8.6.2 Subcellular Localisation of Photosensitiser and d-Luciferin

8.6.2.1 Negative Control

Having established the excitation wavelengths and the parameters for capturing emission (see Table 9), negative controls were first established. The 'control' plate was exposed to all three wavelengths, 405, 488, and 532 nm. For each excitation wavelength, fluorescence was captured within the pre-determined parameters. It was clear, as expected, that no fluorescence was detected (see Figure 74).

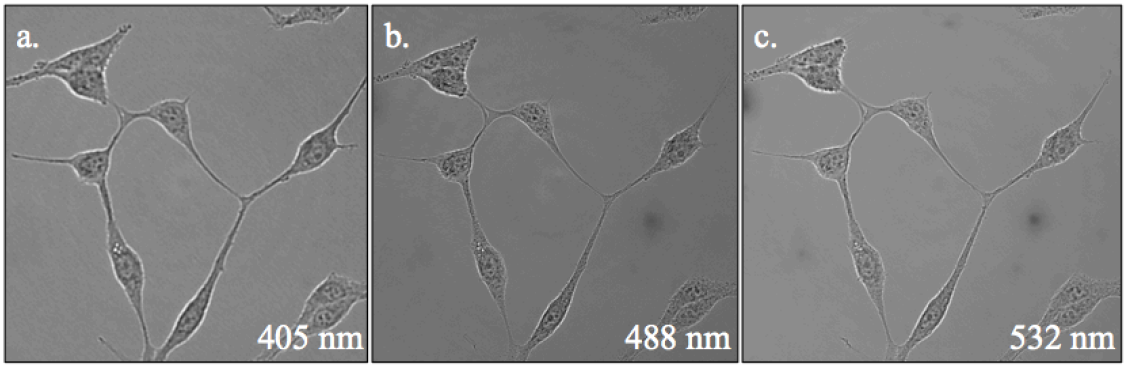

Figure 74 Subcellular localisation of photosensitiers and d-luciferin: negative control

When pure 'control' cells are excited with a. 405, b. 488, and c. 532 nm wavelengths, no fluorescence is detected within pre-determined parameters.

8.6.2.2 Hypericin and d-Luciferin

Cells that had been incubating with hypericin followed by d-luciferin, were excited with 405 nm, capturing fluorescence between 410-530 nm, and 488 nm, capturing fluorescence between 640-720 nm, revealing the cellular localisation of d-luciferin and hypericin, respectively (see Figure 75). d-Luciferin was evenly distributed throughout the cytoplasm of the cell. Hypericin was also localised throughout the cytoplasm of the cell after both 4 hr and 24 hr incubation, with some moderately prominent fluorescence in the perinuclear region, and in some cells, some brighter fluorescence within the cytoplasm to one side of the nucleus.

These findings are consistent with the literature. d-Luciferin has been shown to have a diffuse cytosolic distribution[140]. The distribution of hypericin described above has also been reported[165]. Hypericin fluorescence is limited to the cytoplasm[148] and has been observed in all subcellular organelles[146], but particularly within lysosomes, consistent with the endocytic uptake of the drug, which has corresponded with the perinuclear enhancement observed[166]. There is suggestion that the brighter fluorescence to one side of the nucleus represents uptake in the endoplasmic reticulum[165].

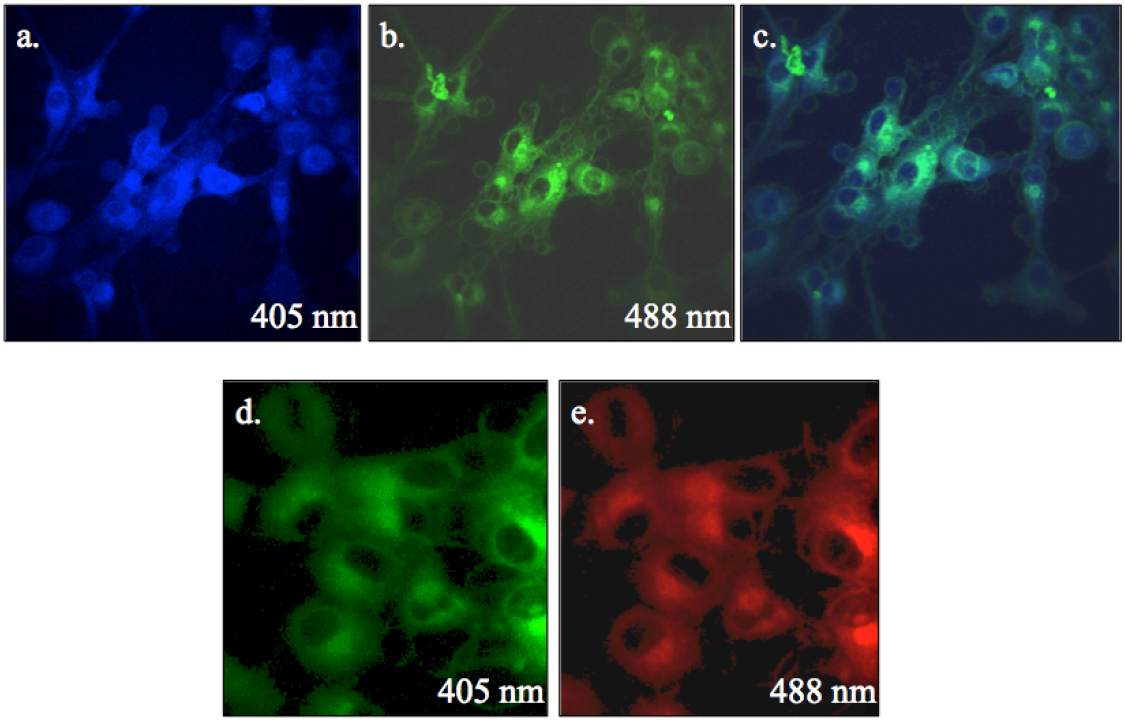

Figure 75 Subcellular localisation of a. d-luciferin b. hypericin after 4hr incubation and c. overlap of their fluorescence, as well as d. d-luciferin and e. hypericin after 24 hr incubation

d-Luciferin was evenly distributed throughout the cytoplasm of the cell. Hypericin was also localised throughout the cytoplasm of the cell after both 4 hr and 24 hr incubation, with some moderately prominent fluorescence in the perinuclear region, and in some cells, some brighter fluorescence within the cytoplasm to one side of the nucleus.

8.6.2.3 d-Luciferin and mTHPC

Cells that had been incubating with *m*THPC followed by d-luciferin, were excited with 532 nm, capturing fluorescence between 620 -690 nm, then 405 nm, capturing fluorescence between 410-530 nm, revealing the cellular localisation of *m*THPC and d-luciferin and *m*THPC, respectively (see Figure 76). When exciting with 405 nm followed by 532 nm, the 405 nm wavelength caused the fluorescence from *m*THPC to bleach, hence excitation with 532 nm was undertaken first. d-Luciferin was evenly distributed throughout the cytoplasm of the cell, consistent with findings above (see section 9.6.2.2). *m*THPC was also evenly distributed throughout the cytoplasm of the cell after 3 hr incubation. However, after 24 hr incubation, although *m*THPC was still localised to the cytoplasm, the pattern was that of a more punctate fluorescence.

This pattern of *m*THPC fluorescence has been described, with a punctate, perinucelar, fluorescence characteristic of 24 hr incubation, representing the accumulation of aggregated species[155]. The primary sites of *m*THPC localisation are the Golgi apparatus

and endoplasmic reticulum. Extending incubation to 24 hrs results in leakage of *m*THPC from the Golgi apparatus with an enhanced accumulation in the endoplasmic reticulum[159].

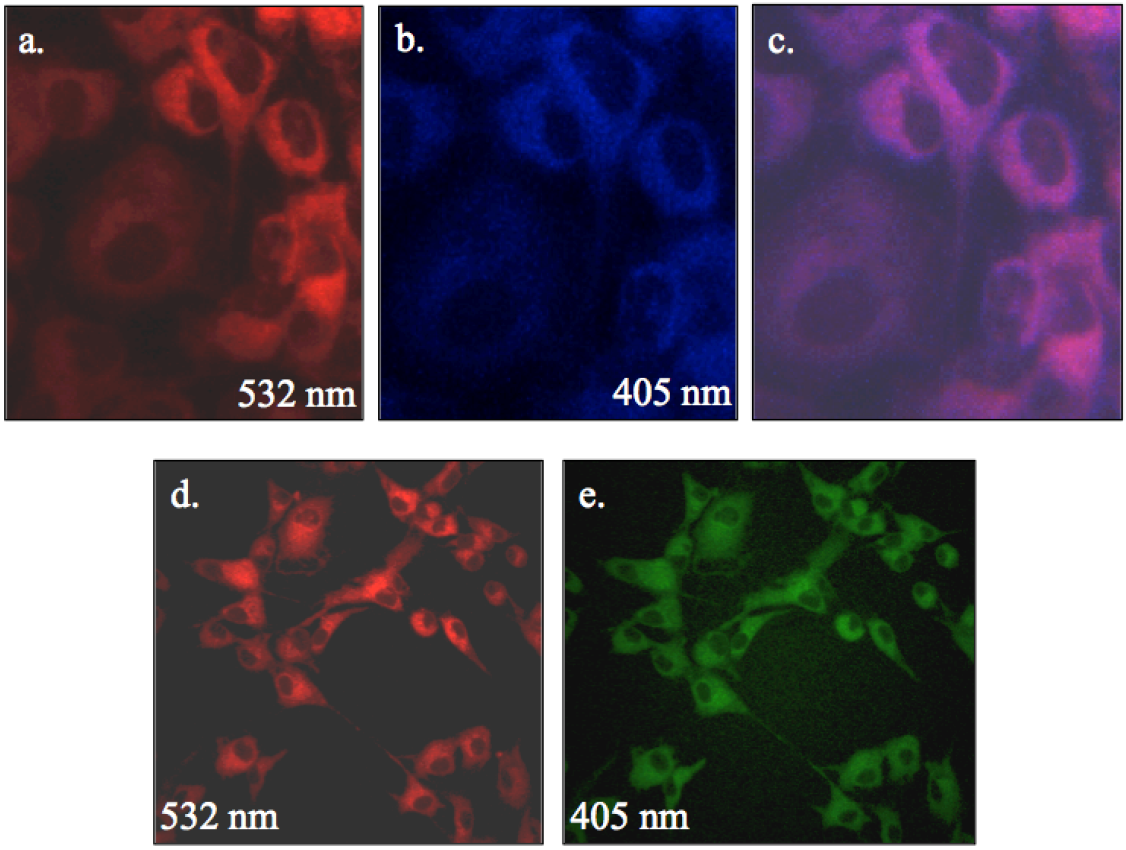

Figure 76 Subcellular localisation of a. *m*THPC after 3 hr incubation b. d-luciferin and c. overlap of their fluorescence, as well as d. *m*THPC after 24 hr incubation and e. d-luciferin

Excitation with 532 nm was undertaken first, as excitation with 405 nm caused bleaching of the fluorescence from *m*THPC. d-Luciferin and *m*THPC after 3 hr incubation was evenly distributed throughout the cytoplasm of the cell. After 24 hr incubation, although *m*THPC was still localised to the cytoplasm, the pattern was that of a more punctate fluorescence.

Overall, d-luciferin co-localises with hypericin and *m*THPC within the cytoplasm of cells. This study was challenging, as cells within the test plates containing both d-luciferin and photosensitiser were undergoing cell death, as evident by the lytic changes particularly noticeable on the hypericin plates above (see Figure 75) and it was difficult to find patches of adherent cells to examine. With more time and resources, this study could have been repeated with fluorescent probes for various subcellular organelles, particularly as this has not been described in the literature for d-luciferin.

8.7 Summary and Discussion

Experiments have shown that bioluminescence, generated by the addition of d-luciferin to luciferase-producing cells, is able to activate a photosensitiser, and mediate a photodynamic effect resulting in significant cell death: bPDT. This has been most thoroughly studied in U87-*luc* cells (see Table 10). Incubation of these cells with the photosensitisers, hypericin or *m*THPC, led to significant cell death with the addition of d-luciferin. When these experiments were repeated in non-luciferase producing U87 cells, there was no change in cell survival, demonstrating that it is not the chemical interaction between photosensitiser and d-luciferin, but the interaction between photosensitiser and the bioluminescence generated by the addition of d-luciferin that leads to cell death. Moreover, lycopene was able to inhibit the cell death that occurred when luciferase-producing cells were incubated with photosensitiser followed by d-luciferin. This further supports that cell death is occurring by a photodynamic effect, which is mediated by singlet oxygen, and hence, is inhibited by the presence of an anti-oxidant such as lycopene.

As there was good overlap between the emission profile of the bioluminescence generated by the oxidation of d-luciferin by firefly luciferase and the absorption spectra of hypericin and *m*THPC, this result is not unexpected. Furthermore, our studies are consistent with current literature showing that d-luciferin and both photosensitisers co-localise to the cytoplasm. Where U87-*luc* cells were incubated with hypericin, there was a suggestion, particularly from the MTT assay data, that longer incubation with the photosensitiser led to more profound cell death. It has been reported that higher doses of hypericin can lead to the formation of aggregates, which contribute negligible phototoxicity[166]. However, initial haemocytometry and growth assay data support a more comparable effect between short and long incubation with hypericin. This is more consistent with the confocal microscopy, which did not demonstrate aggregate formation. Moreover, there is little difference between the doses for short and long incubation, 12.5 vs 10.0 μM, respectively: the dose associated with aggregate formation was 50 μM. In contrast, when U87-*luc* cells were incubated with *m*THPC, the short incubation time more consistently led to more profound cell death compared with the longer incubation time, evident on initial haemocytometry and on growth assay. This is consistent with reports of aggregate formation, again associated with a reduction in extinction coefficient and less phototoxicity than the monomeric form,

with longer incubation times[155]. This is further supported by confocal images that are suggestive of aggregate formation with the longer incubation with *m*THPC.

When repeating the experiments in U87-CBG68*luc* cells, the bioluminescence generated by the oxidation of d-luciferin by click beetle luciferase was able to activate hypericin to mediate a photodynamic effect that led to significant cell death. Although an emission profile of the bioluminescence in this model was not generated, from the literature and knowing that the peak bioluminescence is expected to be at 537 nm, this is an expected result. However, this bioluminescence was not able to activate *m*THPC. This was surprising as there should be enough overlap of the emission profile of this bioluminescence with the absorption spectra of *m*THPC. An emission profile of this bioluminescence was not generated, the experiment was only conducted in one polyclonal line, and conditions were not optimised in this cell line due to time constraints: this would be a further avenue to explore.

The bioluminescence generated by the oxidation of EnduRen™ by Renilla luciferase in U87-*hRluc* cells did not activate hypericin to cause cell death. This was not unexpected as the emission profile of this bioluminescence was shown to have poor overlap with the absorption spectra of hypericin. Interestingly, this bioluminescence was able to activate *m*THPC to cause a photodynamic effect and cell death, but only when the cells had been incubated with *m*THPC for 24 hrs and not 3 hrs. There is some overlap of the emission profile of bioluminescence generated by Renilla luciferase with the absorption spectrum of *m*THPC, although there is no overlap of peak emission with peak absorption. A bPDT effect was not necessarily expected with these conditions either. However, it is unexpected that an effect should occur with 24 hr incubation of *m*THPC but not 3 hr incubation. As mentioned above, the longer incubation leads to the formation of aggregates, which are less phototoxic, hence a bPDT effect, if any, would be expected with the shorter incubation. This experiment was only performed in one monoclonal cell line, and there were concerns with the health of this cell line as mentioned above. Further study would be warranted.

These studies have also served to demonstrate the value of the growth assay. bPDT seems to be most effective when there is an initial fall in cell survival as seen by haemocytometry, and this fall continues and is evident on growth assay, representing an ongoing effect despite the removal of substrates, such as is seen most commonly in

U87-*luc* cells that have been incubated with *m*THPC for 3 hrs then exposed to d-luciferin. However, the following circumstances are also seen: where a fall in cell survival is seen on initial haemocytometry and persists on the growth assay, showing definitive cell kill by bPDT without recovery; a fall in cell survival is seen on initial haemocytometry with partial recovery on growth assay, indicating that cells, although damaged, can recover; and rarely, there is no evidence of cell kill on initial haemocytometry, but cell kill becomes apparent on growth assay, again demonstrating a delayed effect.

Overall, there is good evidence to support that bPDT can cause cell death. It was most effectively demonstrated with U87-*luc* cells that had been incubated with *m*THPC for 3 hrs then exposed to d-luciferin. Animal studies therefore proceeded, with the plan of generating an animal model of glioma using U87-*luc* cell, then exposing the animal to *m*THPC followed by d-luciferin.

U87-*luc*	Hypericin 4 hr Incubation Cell Survival, % Control ± SEM			Hypericin 24 hr Incubation Cell Survival, % Control ± SEM		
Cell Line	MTT	IH	GA	MTT	IH	GA
Monoclonal D1	48.8 ± 7.42*****	61.5 ± 4.68***	55.3 ± 4.16*****	26.1 ± 2.29*****	31.4 ± 3.34*****	34.6 ± 3.64*****
Monoclonal A1	45.2 ± 2.76*****			32.1 ± 5.22*****		
Monoclonal B1	40.5 ± 1.33*****			26.1 ± 2.49*****		
Polyclonal	40.5 ± 2.44*****	34.3 ± 2.48*****	13.0 ± 2.48*****	27.3 ± 0.46****	34.0 ± 3.72*****	17.8 ± 3.32*****
Polyclonal		38.0 ± 4.00****	38.0 ± 1.78*****		32.3 ± 4.82*****	61.7 ± 2.08****

U87-*luc*	*m*THPC 3 hr Incubation Cell Survival, % Control ± SEM		*m*THPC 24 hr Incubation Cell Survival, % Control ± SEM	
Cell Line	IH	GA	IH	GA
Monoclonal D1	22.1 ± 3.32*****	49.8 ± 3.03*****	43.8 ± 4.41*****	59.7 ± 7.48***
Monoclonal D1, HIS	47.2 ± 8.17***	21.8 ± 4.00*****		
Polyclonal	25.8 ± 4.00*****	4.26 ± 1.57*****		
Polyclonal, HIS	9.55 ± 2.26*****	5.59 ± 1.62*****	31.9 ± 3.65*****	31.1 ± 6.56*****
Polyclonal	22.3 ± 3.02*****	30.5 ± 2.80*****	28.2 ± 3.01*****	42.2 ± 3.46*****

Table 10 Summary of the results of investigating bPDT in U87-*luc* cells

Cell survival of the 'test' plates are tabulated as % of control ± SEM, where IH = initial haemocytometry, GA = growth assay. Asterisks indicate the degree of significance of the difference in OD or cell number between each test and control, where * $p > 0.05$, ** $p \leq 0.05$, *** $p < 0.01$, **** $p < 0.001$, ***** $p < 0.0001$. Regarding cell lines, HIS = heat inactivated serum.

Chapter 9 Using Bioluminescence to Mediate Photodynamic Therapy *in vivo*

Before being able to study the concept of bPDT *in vivo*, an animal model bearing a luciferase-expressing tumour had to be created. The generation of a subcutaneous model was embarked upon first. Then, as this treatment was originally envisioned for astrocytoma, attempts to develop an intracranial model were also made. As the luciferase-expressing cell line, U87-*luc*, originated from a human tumour, to limit the potential for rejection, an athymic mouse breed, which has previously been used to propagate human glioma subcutaneously and intracranially[172-176], was used as the host. Although athymic rats[177] have been successfully used to propagate human glioma, producing larger tumours more easily localised with imaging modalities, mice were chosen for logistical reasons. Tumour development was followed with bioluminescence imaging (BLI), which has been validated as a reliable measure of tumour progression both in subcutaneous[132] and intracranial[175] tumour models. If a successful animal model was achieved, bPDT could then be tested.

9.1 Developing an animal model

9.1.1 Methodology

9.1.1.1 Animals

4-6 week old CD1 nu/nu mice (athymic) were purchased from Charles River Laboratories (France). The animals were maintained under pathogen-free conditions, using sterilised plastic cages, covered with polyester bacterial filter tops, and were fed sterilised fat enriched food and sterilised water. All animal work was conducted at the Queen Mary University of London Cancer Institute in accordance with institutional guidelines. The animals were experimented on when they were 6-8 weeks old.

9.1.1.2 Source of Cells Injected

9.1.1.2.1 Cell Lines

Both the U87-*luc* polyclonal and monoclonal cell lines that were shown to produce the strongest bioluminescence with the addition of d-luciferin were used to provide cells to develop the animal models. All cells were maintained using standard cell culture techniques and in complete media containing 1 mg/ml neomycin, which will continue to be referred to as 'media' for ease of discussion. For injection into animals, cells were harvested using standard techniques, resuspended in complete media, counted, then

resuspended in PBS, and kept on ice for injection. Variations in the standard techniques are mentioned within context below.

9.1.1.2.2 Subcutaneous tumour

In order to improve the survival of the xenografts and also to shorten the time taken for the tumours to reach their exponential growth phase, the subcutaneous tumours were passaged subcutaneously from one animal into another[172]. Here, an animal with a subcutaneous tumour, originating from the cells described above, identified to have reached its exponential growth phase with BLI (see below), was culled, and the tumour dissected out. The tumour was carefully minced with a one-sided razor blade and resuspended in PBS. The tumour suspension was aspirated into a syringe and reinjected into the dorsal flank of another animal.

9.1.1.2.3 Intracranial tumour

In order to optimise tumour survival and shorten the time taken to reach the exponential growth phase, the effect of repeat xenografting an intracranial U87-*luc* tumour was tested. Here, an animal with an intracranial tumour, originating from the cells described above, identified to have reached its exponential growth phase on BLI (see below), was culled and the tumour dissected out. The tumour was carefully minced with a one-sided razor blade. 1 ml of trpysin was added and the tumour, incubated for 4 mins, after which the tumour was transferred to a 15 ml tube and resuspended in 5 ml of complete media. The tumour suspension was centrifuged at 1000 rpm for 5 mins and the supernatant aspirated. The pellet was resuspended in 12 ml of complete media and the cells replated in all 6 wells of a 6 well plate. These cells were then expanded, passaged and maintained using standard cell culture techniques. This cell line was denoted U87bp-*luc* and were used for intracranial injection to produce a 'repeat-xenograft tumour' in certain experiments.

Additionally, to select out the cells with putatively improved tumour initiating ability, cells from the U87bp-*luc* line were cultured to form neurospheres[178], which were then injected intracranially. U87bp-*luc* cells were harvested and resuspended in the pro-mitogenic Dulbecco's modified Eagle's medium/Ham F12 medium (DMEM/Ham F12, Sigma) supplemented with 1x1 B27 (Gibco), 1.000 U/ml Penicillin/Streptomycin (P/S, Lonza), 20 ηg/ml recombinant murine EGF (Peprotech), and 20 ηg/ml recombinant human bFGF (Peprotech). The cells were plated out and left in the incubator for five days before replacing the medium. Following this, media changes were performed

every two to three days. The cells grew as free-floating aggregates (neurospheres). Once the spheres were deemed big enough, they were harvested for intracranial injection. The neurospheres in their media were transferred to a 50 ml tube and centrifuged at 700 rpm for 3 mins. The supernatant was aspirated and 2.5 ml of trypsin added. After incubation for 2 mins, the cells were dissociated by gentle resuspension using a glass pipette, following which 5 ml of pro-mitogenic media was added to inactivate the trypsin, and the cells were counted. After counting, the cells were centrifuged again at 700 rpm and resuspended in an appropriate volume of PBS for intracranial injection, and placed on ice.

9.1.1.3 Anaesthesia

For subcutaneous tumour implantation, the inhalational anaesthetic, isofluorane, was used. For intracranial tumour implantation, the animals were anaesthetised with a 2:1:3 volume ratio of ketamine (100 mg/ml), xylazine (20 mg/ml), and 0.9% saline, given intraperitoneally (ip). At the beginning of experimentation, the mice weighed 20-22g on average and required 80-100 μl of anaesthesia.

9.1.1.4 Tumour Implantation: Subcutaneous Model

Having ensured that the animals were adequately anaesthetised, the harvested cells were injected subcutaneously into the dorsal flank.

9.1.1.5 Tumour Implantation: Intracranial Model

The stereotaxic method for injecting tumour cells intracranially was used[179,180]. Having ensured that the animals were adequately anaesthetised, the head was secured in a stereotaxic frame (see Figure 77). A linear incision was made in the midline from the level of the orbits to the occiput and the bregma identified. A Hamilton needle was loaded with 10 μl of cell suspension and the co-ordinates were set to allow an injection 0.5 mm posterior and 2.5 mm lateral to the bregma, to a depth of 3.5 mm into the brain parenchyma. The cells were injected slowly over 5 minutes before the needle was pulled out.

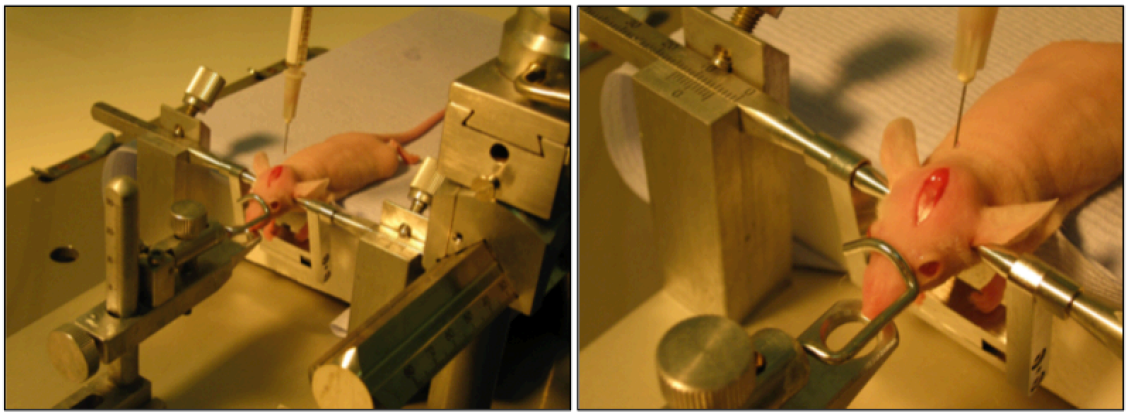

Figure 77 Stereotaxic intracranial injection

For intracranial injections, animals were anaesthetised and their head secured in a stereotaxic frame. A linear incision was made in the midline from the level of the eyes to the occiput and the bregma identified. A Hamilton needle was loaded with 10 µl of cell suspension and the co-ordinates were set to allow an injection 0.5 mm posterior and 2.5 mm lateral to the bregma, to a depth of 3.5 mm into the brain parenchyma. The cells were injected slowly over 5 minutes before the needle was pulled out.

9.1.1.6 Bioluminescence Imaging (BLI)

The day after tumour implantation, then weekly thereafter, mice were imaged with the Xenogen IVIS system (Xenogen Corporation, Alameda, CA) to record the bioluminescent signal emitted from the engrafted tumours. The animals were anaesthetised with isofluorane, given an ip injection of 1.5 mg/g of d-luciferin (Caliper Life Sciences), and placed in the imaging chamber, which was set at a temperature of 27^0C and allowed maintenance of inhalational anaesthesia. The IVIS 100 cooled CCD camera system was used for emitted light acquisition and Living Image software (Xenogen Corp.) was used for data analysis. Imaging started approximately 2-3 mins after injection. Acquisitions were then obtained at 30 secs, 1 min, then every minute thereafter for a total of 5 mins to ensure that peak photon emission was captured. Exposure times of 0.5 secs-5 mins were used, depending on the strength of the signal. Photon emission was recorded as total flux (photons/sec) and average radiance (photons/sec/cm^2/sr). From the displayed images, regions of interest (ROI) were designated around the tumour sites. Data was analysed based on the average radiance, which is normalised for exposure time and size of ROI, over the ROI.

9.1.1.7 Computed Tomography Imaging

In an attempt to validate the use of BLI as an accurate assessment of change in intracranial tumour volume, a second imaging modality was employed, computed tomography (CT): magnetic resonance imaging (MRI) was not available. Imaging was performed with 1000 msec exposure and 180 projections were taken. 125 µl of contrast

(Binitio eXIA160XL 160 mg/ml) was then injected into the tail vein, and a repeat CT was taken at 0 and 20 mins following contrast injection.

9.1.2 The Subcutaneous Model

In the first trial, $5x10^6$ cells from the U87-*luc* polyclonal cell line were injected subcutaneously in a volume of 200 μl into 5 mice. Figure 78 is an image of the bioluminescent signal captured by the Xenogen IVIS 100 cooled CCD camera system (Xenogen Corp.) after the animals were injected with 1.5 mg/g of d-luciferin ip. The animals were positioned in the imaging chamber with their heads set in a nasal piece that delivered inhalational anaesthesia. 1 week after cell transplantation, the cells seemed to be growing well. From Figure 78a, it seemed that the cells injected into mouse 5 were not producing bioluminescence. However, this was likely due to misinjection of d-luciferin, as repeat injection generated a signal, as illustrated in Figure 78b. By week 7, it became clear qualitatively (Figure 78c) and quantitatively (Figure 78d) that there was a 60% success rate in establishing tumour implantation with 3 out of the 5 tumours beginning their exponential growth phase at week 7.

In order to improve the survival of the xenografts and establish a tumour line that would consistently reach its exponential growth phase within 1-2 weeks of tumour implantation, subcutaneous passaging of tumour was attempted. The animal displaying the strongest bioluminescent signal from the trial above, Mouse 5, was culled, the subcutaneous tumour isolated, prepared, and injected into two other mice: subcutaneous passage 1 (see Figure 79). From observation, it was clear that these tumours started their exponential growth phase at week 3 following tumour implantation and this was confirmed with BLI and expressed quantitatively in Figure 79a. Again, the animal displaying the strongest bioluminescent signal at week 3, Mouse 2, was culled, the subcutaneous tumour isolated, prepared, and injected into two other mice: subcutaneous passage 2. There was a marked difference between the degree of bioluminescence generated by these animals, hence the results are plotted on two different graphs (see Figure 79b and c). Despite this, the onset of the exponential growth phase was unclear. Again, the animal displaying the strongest bioluminescent signal at week 5, Mouse 2, was culled, the subcutaneous tumour isolated, prepared, and injected into three other mice: subcutaneous passage 3. Here (see Figure 79d), the implanted tumours reached their exponential growth phase by week 2 and the bioluminescent signal being generated between the tumours was uniform. Based on this, the fourth subcutaneous passage of tumour was planned for a treatment group. Of

note, from the first subcutaneous passage, the rate of successful tumour establishment was 100%.

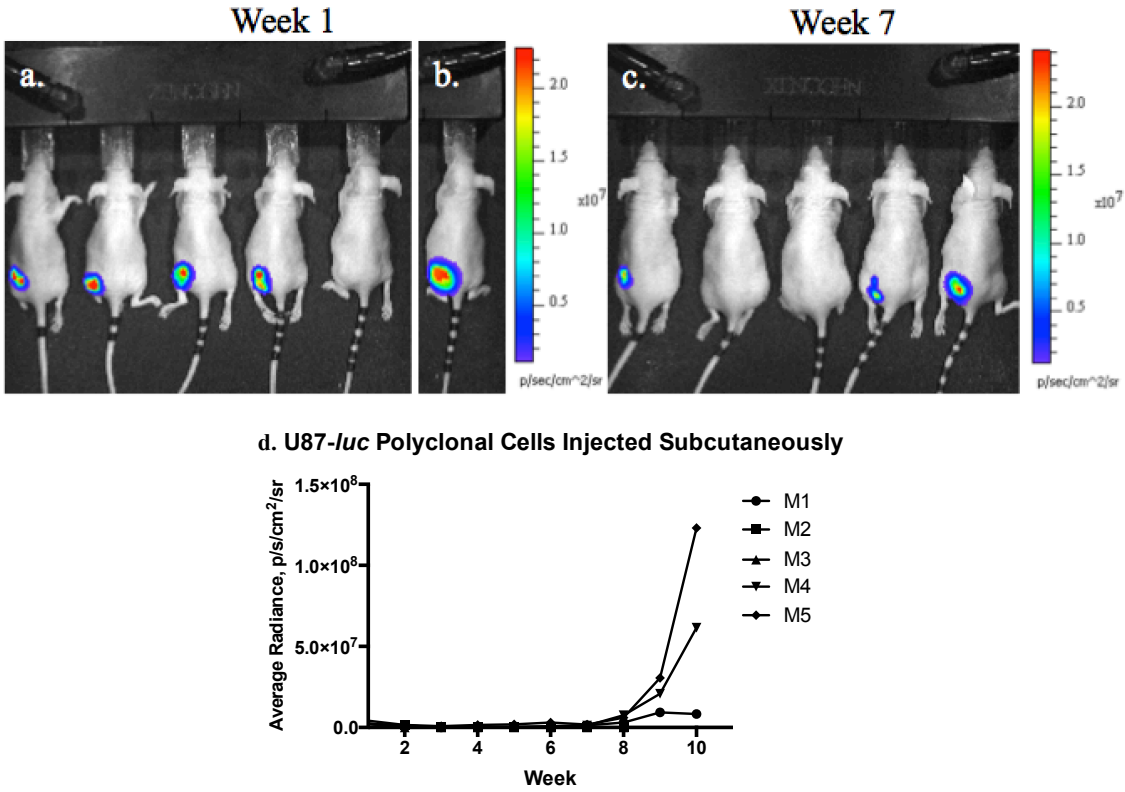

Figure 78 Qualitative and quantitative assessment of injecting U87-*luc* polyclonal cells subcutaneously

'a' and 'b' are qualitative illustrations of the effect of injecting U87-*luc* cell subcutaneously at 1 week post tumour implantation. The signal is the bioluminescence captured by the Xenogen IVIS 100 cooled CCD camera system after the animals were injected with 1.5 mg/g of d-luciferin ip. Due to misinjection of d-luciferin, the cells injected into Mouse 5 did not seem to produce bioluminescence (a), but with reinjection, a bioluminescent signal was detected (b). At 7 weeks post injection, the bioluminescent signals detected are illustrated qualitatively (c) and quantitatively (d). In 'd,' the bioluminescent signal within a designated ROI is expressed as average radiance. There was a 60% success rate in establishing tumour implantation with 3 out of the 5 tumours beginning their exponential growth phase at week 7.

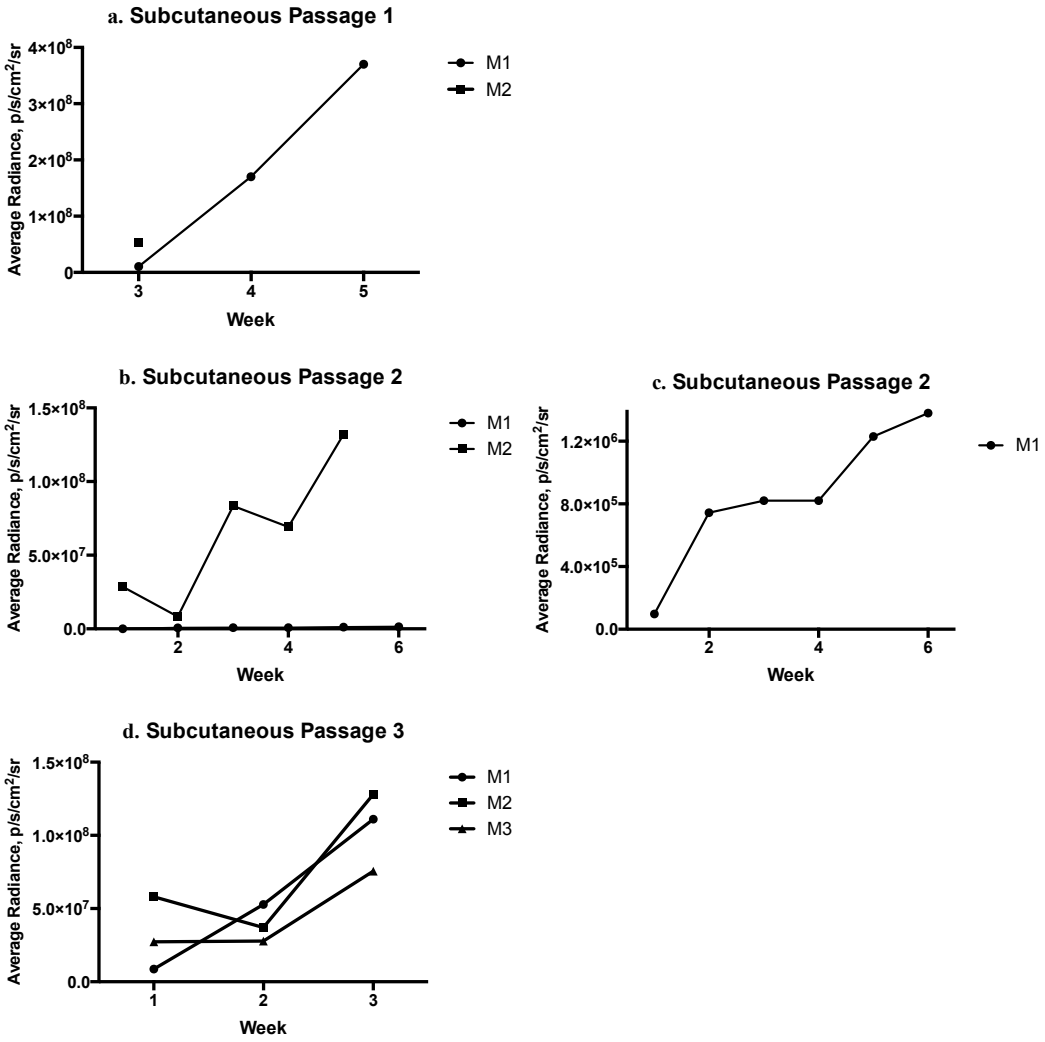

Figure 79 Subcutaneous passaging of tumour

In developing a robust subcutaneous model, the tumour from Mouse 5 in the first trial above was harvested, prepared and reinjected into 3 mice (subcutaneous passage 1, 'a'). This U87-*luc* polyclonal derived tumour was passaged 2 further times (subcutaneous passages 2, 'b' 'c' and 3, 'd') in this way. The bioluminescence from the tumour was captured by the Xenogen IVIS 100 cooled CCD camera system after the animals were injected with 1.5 mg/g of d-luciferin ip. The bioluminescent signal within a designated ROI was expressed as average radiance and expressed quantitatively. With each passage, the start of the exponential growth phase became earlier, thus, by the third subcutaneous passage, the exponential growth phase started within 2 weeks of tumour implantation. Furthermore, by this third passage, the tumours were generating a more uniform bioluminescence.

9.1.3 The Intracranial Model

8 attempts were made to produce a robust intracranial model, and each will be described as follows.

9.1.3.1 Intracranial Model: Trial 1

In the first trial, $1x10^5$ cells from the U87-*luc* polyclonal cell line were injected intracranially in a volume of 10 μl, as per standard protocol, into 6 mice (as exemplified in Figure 77). Mouse 3 died from anaesthetic complications. Figure 80a-e are images of the bioluminescent signal captured by the Xenogen IVIS 100 cooled CCD camera system (Xenogen Corp.) after the animals were injected with 1.5 mg/g of d-luciferin ip. The animals were positioned in the imaging chamber with their heads set in a nasal piece that delivered inhalational anaesthesia. 1 day after injection, BLI confirmed that cells had been successfully delivered intracranially (see Figure 80a): although the fourth mouse from the left, Mouse 5, did not seem to emit a bioluminescent signal initially, reinjection and a longer exposure time revealed a bioluminescent signal, albeit weak (see Figure 80b).

One week after injection, BLI revealed that there had been a drop in the bioluminescent signal in all mice (see Figure 80c and d): mouse 1 was imaged separately with a longer exposure time to detect the relatively weaker bioluminescent signal (see Figure 80c), and note Mouse 5, in position 4 in Figure 80d, had no qualitatively detectable signal, which may have been due to poor health and the mouse was culled after imaging. Furthermore, at this time point, CT imaging was undertaken in an attempt to provide validation for BLI. The CT was performed without and with contrast; the 'with' contrast images being taken immediately after contrast was delivered and also 20 min later. The mouse with the highest BLI signal was selected for CT imaging (see Figure 80f). CT was not able to detect the tumour. Moreover, an artifact in the left lower quadrant of the image, corresponding with the intracranial injection site, produced a distortion of the image that compromised the resolution. In view of logistics and resources, further CT imaging was not pursued.

The remaining mice were followed with weekly BLI and the progression of bioluminescent signal over time is represented quantitatively in Figure 80g and h. The results for Mouse 2 and 4 were plotted separately in order to ascertain more clearly the change over time (see Figure 80h). The exponential growth phase for Mouse 2 started at week 8. However, by week 10, the mouse developed exophthalmos and displayed

signs of neurological deficit. BLI revealed not only increasing intracranial bioluminescent signal reflecting tumour growth, but also the development of a spinal metastasis (see Figure 80e): the mouse was culled at this time. In Mouse 4, the tumour seemed to start its exponential growth phase at week 5. However, after a peak in bioluminescent signal at week 10, there was a dramatic fall in signal that did not recover, and hence the mouse was culled at week 24. The tumour implanted into Mouse 6 began its exponential growth phase at week 14: the mouse was electively culled at week 17, the tumour dissected out, and regrown in culture, thereby generating the U87bp-*luc* cell line, which was subsequently used for further intracranial injections. The tumour implanted in the remaining mouse, Mouse 1, started its exponential growth phase at week 20, and developed neurological deficit by week 29, which coincided with a dramatic increase in bioluminescent signal: the mouse was culled at this time. Overall, of the 6 mice that were injected, two mice were lost for reasons unrelated to tumour implantation. Of the remaining 4 mice, there was a 75% success rate in the implanted tumour establishing growth. However, the time taken for the tumours to reach exponential growth was long, 8, 14 and 20 weeks, which is not optimal for a tumour model in which to test treatment.

Day 1 Post Injection of U87-*luc* Polyclonal Cells

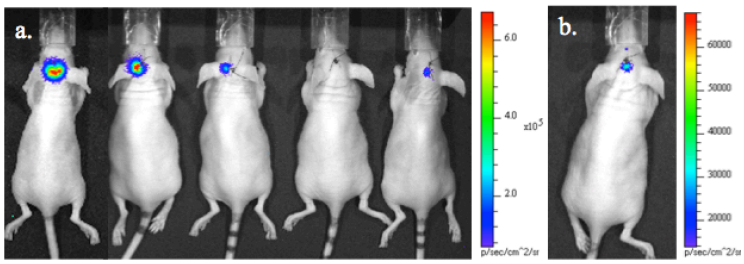

Week 1 Post Injection of U87-*luc* Polyclonal Cells

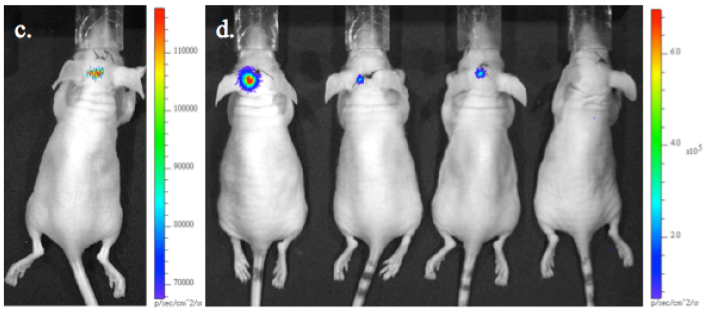

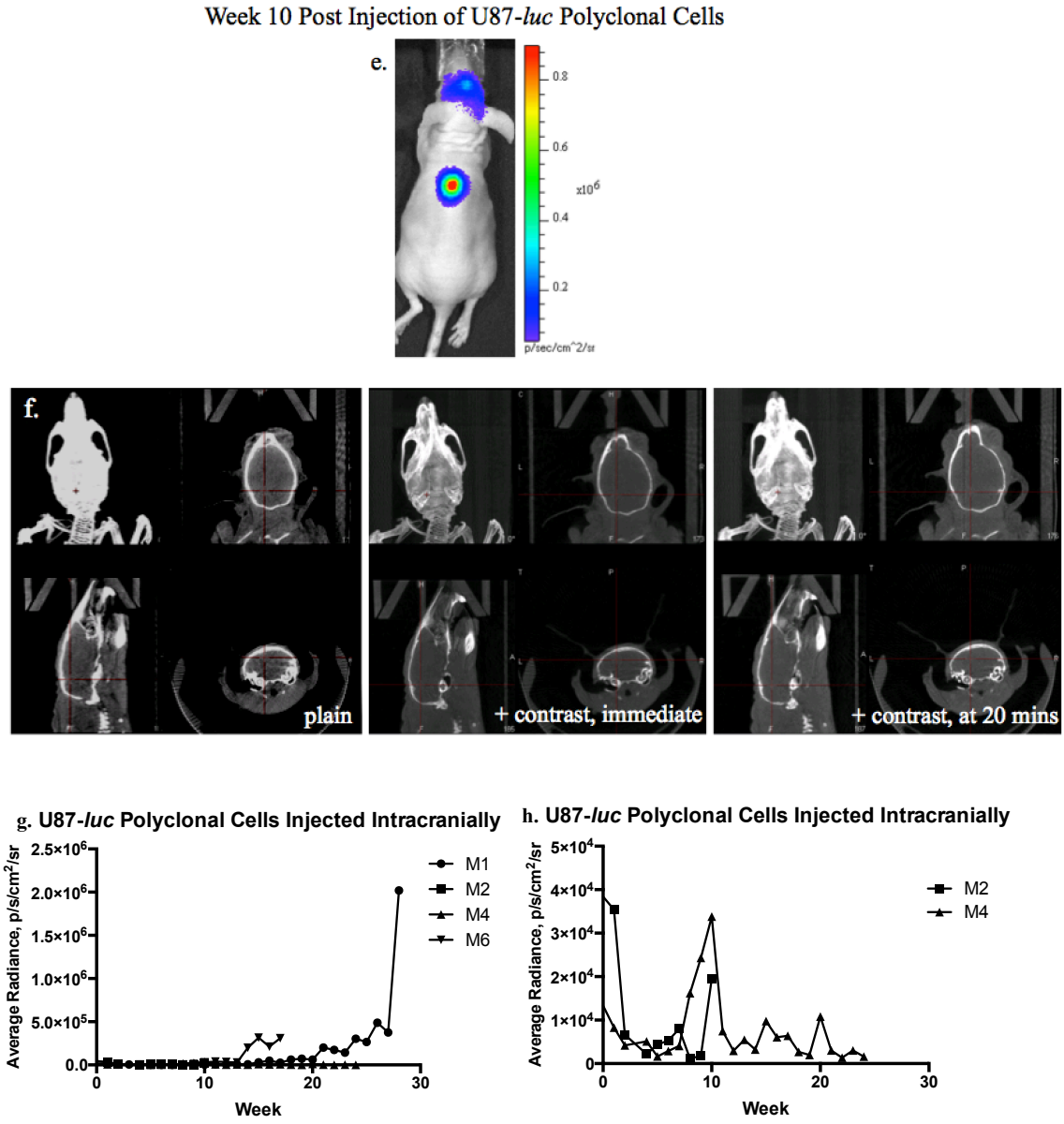

Figure 80 Quantitative and qualitative assessment of injecting U87-*luc* polyclonal cells intracranially

'a-e' are qualitative illustrations of the bioluminescent signal generated after injecting U87-*luc* cells intracranially. The bioluminescent signal generated by the implanted cells was captured by the Xenogen IVIS 100 cooled CCD camera system after the animals were injected with 1.5 mg/g of d-luciferin ip. BLI on day 1 following intracranial injection (a) indicated that the cells had been delivered successfully: one mouse required reinjection and a longer exposure time to demonstrate successful implantation of cells (b). BLI 1 week following injection (c, d) revealed a dramatic fall in bioluminescent signal, one mouse requiring a longer exposure time to demonstrate ongoing survival of the cells (c). CT of the mouse generating the highest bioluminescent signal at this time failed to reveal the tumour and was complicated by artifact in the lower left quadrant in the region of tumour injection (f), and was therefore abandoned as an imaging modality. BLI was used to follow tumour development weekly thereafter and 'g' and 'h' quantitatively illustrate the change in bioluminescent signal over time: the bioluminescent signal within a designated ROI was expressed as average radiance and expressed quantitatively. Overall, of the 6 mice that were injected, two mice were lost to reasons unrelated to tumour implantation. Of the remaining 4 mice, there was a 75% success rate in the implanted tumour establishing growth. However, the time taken for the tumours to reach exponential growth was long, 8, 14 and 20 weeks, which is not optimal for a tumour model in which to test treatment. 'e' is a BLI image that illustrates the development of a spinal metastasis in one of the mice (Mouse 2) at week 10.

9.1.3.2 Intracranial Model: Trial 2

With the aim of improving the survival of the xenografts and to establish a tumour line that would consistently reach its exponential growth phase within weeks of injection, the effect of increasing the inoculate was investigated. Using U87-*luc* polyclonal cells, 1.25 x10^5 cells (n=1), 2.5 x 10^5 cells (n=2), and 5 x 10^5 (n=2) cells were injected in 10 µl into the brain parenchyma of 5 mice. Figure 81a demonstrates that over 14 weeks, none of the implanted tumours in the animals had reached their exponential growth phase, hence the experiment was terminated.

9.1.3.3 Intracranial Model: Trial 3

Another strategy employed was to inject a monoclonal line instead of the polyclonal line. Using U87-*luc* monoclonal cells, 5x10^5 cells were injected into the brain parenchyma of 3 mice in 10 µl. Figure 81b indicates that the tumour in Mouse 2 entered exponential growth at week 4. However, when the mouse was culled, this tumour was found to be extra-axial. None of the tumours implanted intraparenchymally reached their exponential growth phase within a reasonable time, and hence the animals were culled.

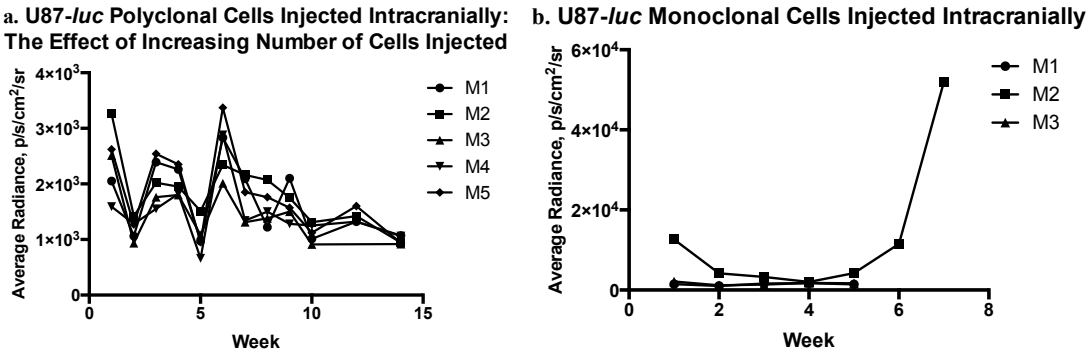

Figure 81 Effect of increasing the concentration of U87-*luc* polyclonal cells injected and the effect of injecting U87-*luc* monoclonal cells intracranially on tumour establishment and growth

Using U87-*luc* polyclonal cells, 1.25 x10^5 cells (M1), 2.5 x 10^5 cells (M2 and 3), and 5 x 10^5 (M4 and 5) cells were injected in 10 µl into the brain parenchyma of 5 mice (a). Using U87-*luc* monoclonal cells, 5x10^5 cells were injected into the brain parenchyma of 3 mice in 10 µl (b). The bioluminescent signal generated by the implanted cells was captured by the Xenogen IVIS 100 cooled CCD camera system after the animals were injected with 1.5 mg/g of d-luciferin ip. The bioluminescent signal within a designated ROI was expressed as average radiance and expressed quantitatively. Neither increasing the concentration of U87-*luc* polyclonal cells or injecting U87-*luc* monoclonal cells led to tumours that reached an exponential growth phase within an acceptable time: although results from Mouse 1 of the group injected with U87-*luc* monoclonal cells seemed promising, autopsy revealed that the tumour was extra-axial.

9.1.3.4 Intracranial Model: Trial 4

In an ongoing effort to establish a more robust intracranial tumour model, the effect of repeat xenografting was attempted. The tumour implanted into Mouse 6 from the first trial of intracranial injections (see Figure 80g) started its exponential growth phase at week 14 post injection. At week 17, the mouse was electively culled, the tumour harvested, and the cells regrown in culture, thereby establishing the U87bp-*luc* cell line. These cells grew well in culture (see Figure 82a). After two passages, $1x10^5$ cells in 10 μl were injected into the brain parenchyma of 3 mice. It was clear after 2 weeks that the implanted tumour had not reached an exponential growth phase, indicating that the exponential growth phase of the original tumour was not maintained, and the experiment was terminated (see Figure 82b).

9.1.3.5 Intracranial Model: Trial 5

The effect of increasing the concentration of the cells injected for serial xenografting was also investigated. Using U87bp-*luc* cells, 5×10^5 cells were injected in 10 μl into the brain parenchyma of 5 mice. The tumour in one animal, Mouse 3, displayed a bioluminescent signal consistently superior to the others and entered into its exponential growth phase at week 6 (see Figure 82c). However, on autopsy, this tumour was found to be extra-axial. Of the remaining tumours, this method achieved tumours with a more uniform bioluminescent signal (see Figure 82d). However, after 5 weeks, the tumours had not entered into their exponential growth phase, and for the same reason as above, the animals were culled and the experiment terminated.

9.1.3.6 Intracranial Model: Trial 6

In all the above xenograft experiments, cells had been resuspended in PBS for injection. Hypothesizing that the cell survival may be improved by resuspending cells in serum free media for injection, using U87bp-*luc* cells, $1x10^5$ cells in 10 μl of serum free media were injected into the brain parenchyma of 2 mice. Figure 82e demonstrates that although the bioluminescent signal immediately following injection was an order of magnitude greater than when cells were resuspended in PBS (see Figure 82b), this did not translate into improved establishment of tumour growth, hence, after 7 weeks, the animals were culled electively and the experiment aborted.

9.1.3.7 Intracranial Model: Trial 7

Lastly, the effect of resuspending cells in serum free media as well as increasing the concentration was investigated. Using U87bp-*luc* cells, $1x10^5$ cells (M0) and $2x10^5$ (M1 and M2) were injected in 10 μl of serum free media into the brain parenchyma of

3 mice. The tumour implanted into Mouse 1 was seen to enter its exponential growth phase at week 1 (see Figure 82f). By week 4, the mouse became unwell, which coincided with a dramatic increase in bioluminescent signal consistent with marked tumour growth, and hence the mouse was culled. At autopsy the tumour was found to be extra-axial. Of the remaining mice, although resuspending cells in serum free media increased the bioluminescent signal immediately following injection, this did not translate into faster establishment of tumour growth and there was no advantage to injecting an increased concentration of cells (see Figure 82g). These mice were culled electively after 5 weeks.

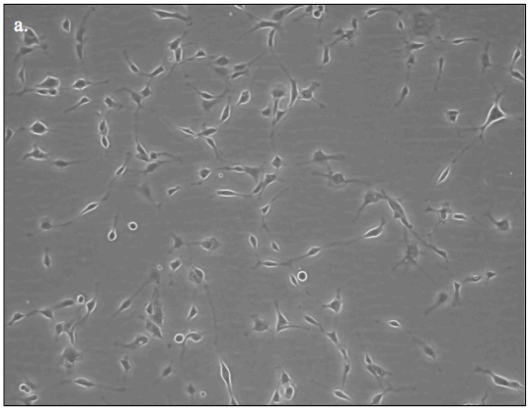

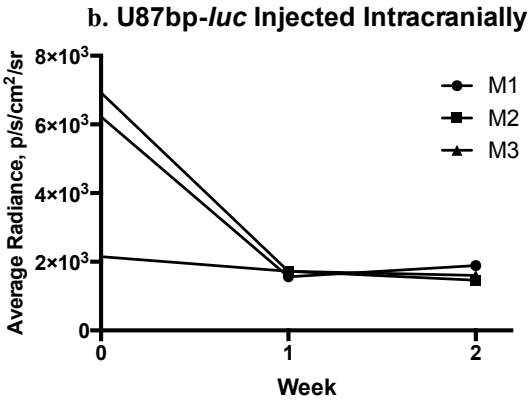

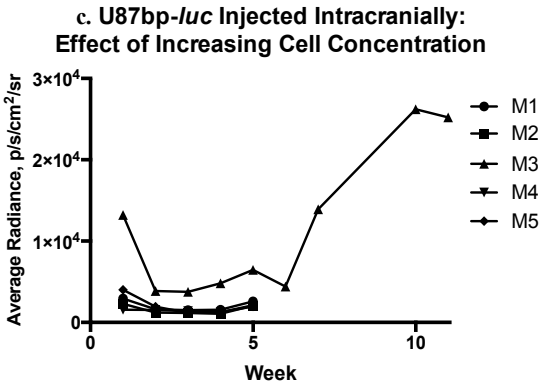

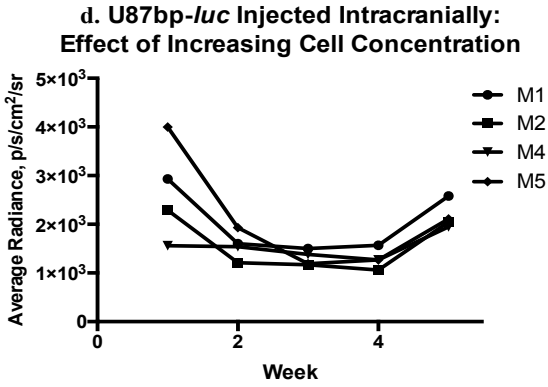

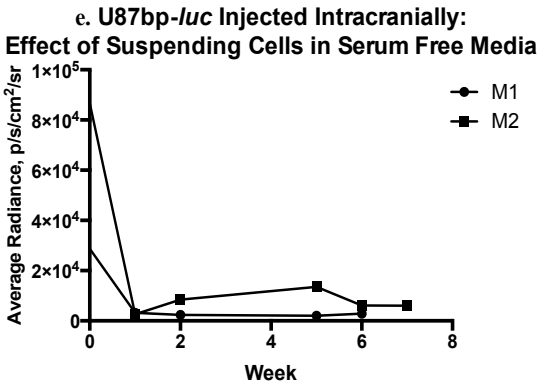

.3

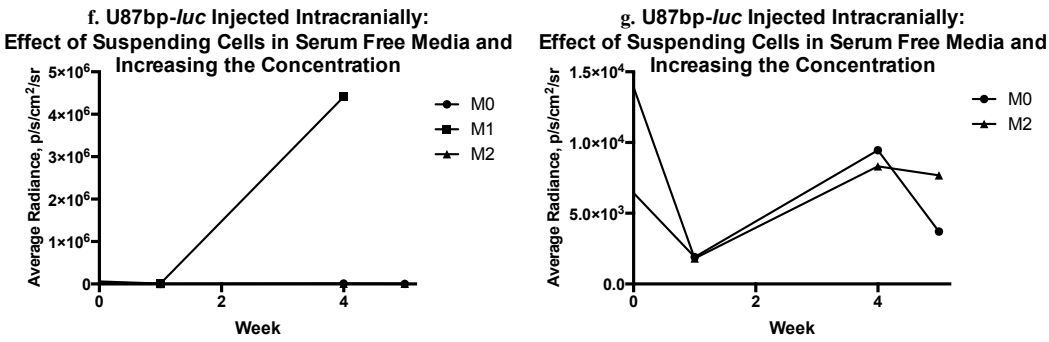

Figure 82 The effect of repeat xenografting cells derived from U87-*luc* polyclonal cells grown intracranially

The cells from a successfully implanted intracranial tumour derived from U87-*luc* polyclonal cells were harvested and regrown in culture, developing the U87bp-*luc* cell line. These cells grew well in culture (a). $1x10^5$ (b) and $5x10^5$ cells (c and d) in 10 µl of PBS were injected intracranially. $1x10^5$ (e) and $1x10^5$ (Mouse 0) and $2x10^5$ cells (Mouse 1 and 2) (f and g) in 10 µl of serum free media were also injected. The animals underwent BLI weekly. The bioluminescent signal generated by the implanted cells was captured by the Xenogen IVIS 100 cooled CCD camera system after the animals were injected with 1.5 mg/g of d-luciferin ip. The bioluminescent signal within a designated ROI was expressed as average radiance and expressed quantitatively. Injection of serial xenograft did not increase the time to reach exponential growth phase. Increasing cell concentration was not advantageous. Although resuspending the tumour cells in serum free media led to a higher bioluminescent signal the day after injection, this did not translate into a faster time to exponential growth. The tumours that did begin exponential growth within weeks of injection (c, Mouse 3; f, Mouse 1) were extra-axial.

9.1.3.8 Intracranial Model: Trial 8

In a separate set of experiments to achieve a robust intracranial tumour model, U87bp-*luc* cells were cultured in pro-mitogenic media to form neurospheres[178], in an attempt to select out the cells with tumour initiating capacity. Neurospheres were successfully grown (see Figure 83a and b) and once deemed of sufficient size were harvested and $1x10^5$ cells were injected in 10 µl of serum free media into the brain parenchyma of 2 mice. The bioluminescent signal of the implanted cells the day after implantation were on average an order of magnitude greater than that of the cells previously injected intracranially, as described above (see Figure 83c). Furthermore, exponential growth seemed to be established 1 week after injection.

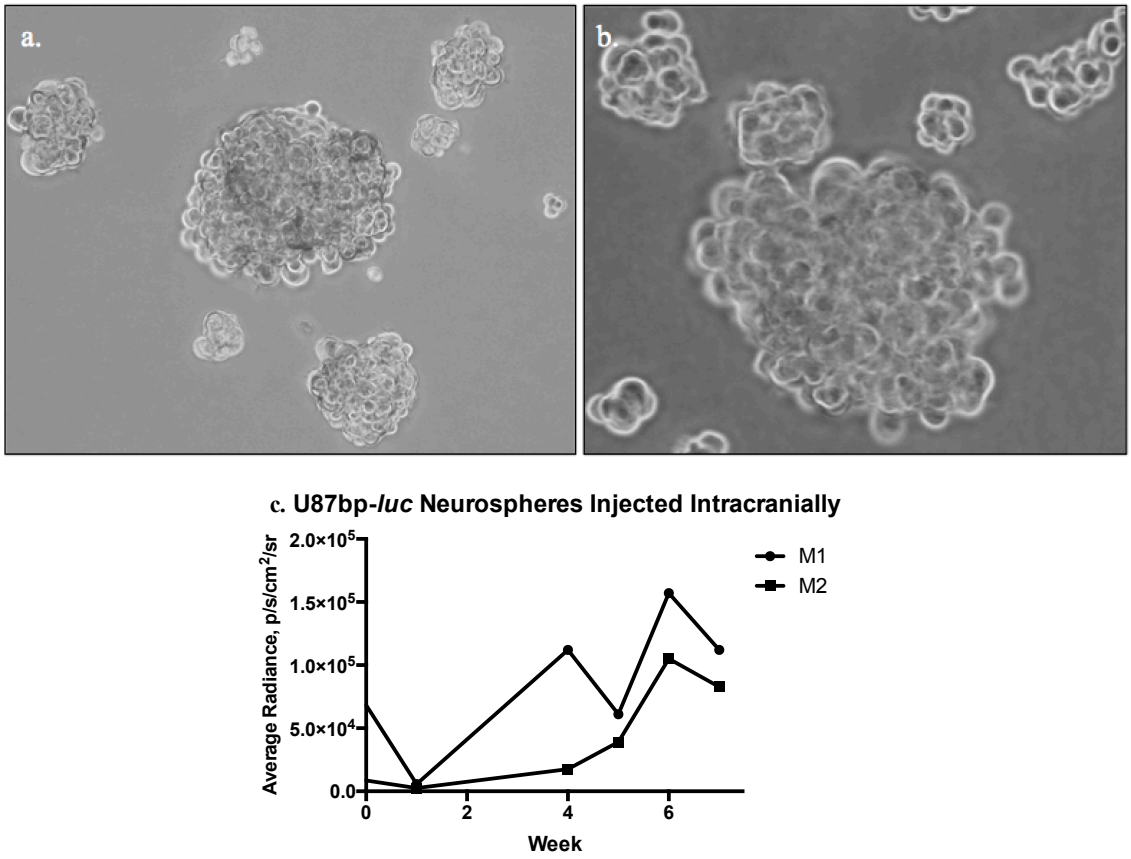

Figure 83 The effect of injecting neurospheres derived from U87bp-*luc* cells intracranially

Neurospheres were successfully generated by culturing U87bp-*luc* cells in pro-mitogenic media (a and b). Once large enough the neurospheres were harvested and 1x10^5 cells were injected in 10 µl of serum free media into the brain parenchyma of 2 mice. The animals underwent BLI weekly. The bioluminescent signal generated by the implanted cells was captured by the Xenogen IVIS 100 cooled CCD camera system after the animals were injected with 1.5 mg/g of d-luciferin ip. The bioluminescent signal within a designated ROI was expressed as average radiance and expressed quantitatively. The bioluminescent signal of the implanted cells the day after implantation were on average an order of magnitude greater than that of any of the cell lines previously injected intracranially and exponential growth seemed to be established 1 week after injection.

9.1.4 Summary and Discussion

Using an athymic mouse as the host for a human-derived glioma transplanted subcutaneously[172-174,181] and intracranially[175,176,181,182] has been well described. Regarding the subcutaneous model, it has been demonstrated here that by passaging the tumours subcutaneously, a higher success rate of tumour establishment and a shorter time for the tumour to reach its exponential growth phase is achieved, and indeed, this is supported by the literature[172,181]. In fact, not all human-derived glioma lines will survive upon initial injection[181]. Although the athymic mouse is immunocompromised in that it does not produce T cells, it still has natural killer cells and is able to mount an antibody response. As human neoplastic tissue retains a human karyotype and human enzymatic phenotypes even after serial passage in athymic mice[183-185], a host immune response is

likely to underlie this observed phenomenon. As the tumour is serially passaged subcutaneously, it most likely gains a degree of immune compatibility and/or the host develops a degree of immunologic tolerance, and hence improved tumour establishment and growth.

Despite there being reports of luciferase-expressing U87 cells having been successfully transplanted and grown intracranially in nude mice[175], attempts at establishing an intracranial tumour in this study proved more challenging. 8 trials, summarised in Table 11, were required before finding a suitable model. The variables included the cell line injected, the cell number injected, and the solute in which the cells were injected. Overall, the complication rate of the actual procedure was low, with only 2 deaths out of the 8 trials, which were associated with anaesthetic complications. Regarding technique, there were only 3 extra-axial tumours out of a total of 29 subjects.

	Intracranial Trials							
	1	2	3	4	5	6	7	8
Cell Line	U87-*luc* polyclonal	U87-*luc* polyclonal	U87-*luc* monoclonal	U87bp-*luc*	U87bp-*luc*	U87bp-*luc*	U87bp-*luc*	U87bp-*luc* NS
Cell Number	$1x10^5$	$1.25x10^5$ $2.5x10^5$ $5x10^5$	$5x10^5$	$1x10^5$	$5x10^5$	$1x10^5$	$1x10^5$ $2x10^5$	$1x10^5$
Solute	PBS	PBS	PBS	PBS	PBS	SFM	SFM	SFM
Subject number	6	5	3	3	5	2	3	2
T, weeks	8-20	>14	>8	>2	>5	>7	>5	1
Complication	2 deaths		1 extra-axial		1 extra-axial		1 extra-axial	

Table 11 Summary of the 8 trials conducted to develop an intracranial model of high-grade astrocytoma

The variables in each trial were the cell line, the number of cells injected, and the solute in which the cells were suspended. A model was deemed successful once the exponential rate of tumour growth reached within 1-2 weeks of xenografting. Overall, the complication rate was low, with only 2 deaths related to anaesthesia, and the generation of only 3 extracranial tumours, which reflects the competence of technique. SFM = serum free media, t = time to exponential growth of tumour.

Several contributing factors may be attributable to our challenge of generating a robust intracranial model. One may be the athymic mouse mounting an immune response to

the transplanted human-derived tumour line. Certainly, patients with a high-grade astrocytoma have been shown to mount a humoral response to the tumour[186,187], albeit the clinical significance remains questionable. However, as the tumours that had been inadvertently xenografted extra-axially tended to establish growth with more success, the local environment within the brain itself may have also been inhibitory. In order to overcome either local or systemic humoral responses, an intraparenchymal tumour that had successfully established growth was harvested and the cells regrown in culture U87bp-*luc)* before reinjection. However, all attempts with this cell line did not show improved growth rates. This may have partly been due to the cells being exposed to trypsin upon reculturing: it has been observed that exposing cells to trypsin prior to reinjection has been inhibitory to cell growth[172], leading to the attempts at establishing an intracranial tumour by direct implantation of a subcutaneous tumour[188].

Aside from host immune responses, it has also been demonstrated that not all brain tumour cells have the ability to form a new tumour[189,190]. There is increasing evidence to support that the tumour-initiating ability resides in a specific subpopulation of cells, termed 'brain tumour stem cells,' with characteristics similar to normal neural stem cells[190,191] i.e. the ability for self-renewal, multipotential properties, and the ability to initiate tumour growth. Neurosphere assays that utilise a selective serum-free culture system that allows neural stem cells and brain tumour stem cells to proliferate and generate multipotent floating cell clusters are used to identify these unique stem cell populations[178,192-194]. In our final attempt to generate an intracranial tumour model, trial 8, neurospheres were cultured from the intraparenchymal tumour that had successfully grown from the implanted U87-*luc* polyclonal cells. Using this method, an intracranial model with improved implant survival and established growth was achieved.

In summary, subcutaneous and intracranial animal models with established and growing tumours derived from a human high-grade glioma cell line with the ability to bioluminesce were generated. The subcutaneous model was achieved by subcutaneous passaging. The most robust intracranial model was achieved by implanting neurospheres derived from an intraparenchymal tumour that had successfully grown from implanted U87-*luc* polyclonal cells. In preparation for testing bPDT, the character of the bioluminescence that could be generated from these tumours was investigated further.

9.2 Characterising Bioluminescence Generated *in vivo*

Using the successfully established subcutaneous and intracranial models developed above, a more detailed investigation into the bioluminescence that could be generated was performed. First, the change in bioluminescence over time following an ip bolus of d-luciferin was assessed. Then a method of generating a more sustained bioluminescence was tested.

9.2.1 Change in bioluminescence over time

The first group of mice xenografted with U87-*luc* polyclonal cells intracranially were given an ip injection of 1.5 mg/g of d-luciferin 1 week later. The bioluminescent signal was recorded immediately following injection, then at 1, 2, 3, 4, and 5 mins, then every 5 mins thereafter for a total of 60 mins.

The bioluminescent signal quickly peaked within 2-3 mins, before gradually declining over 60 mins to near negligible levels at 55-60 mins (see Figure 84).

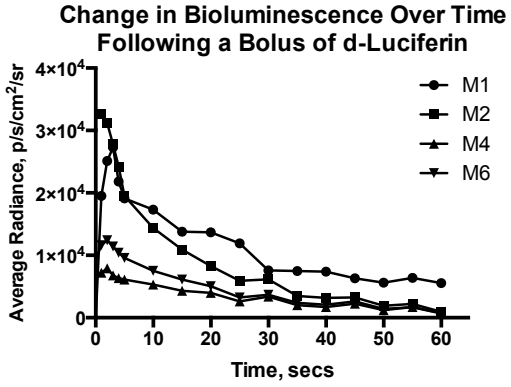

Figure 84 Change in bioluminescence over time following a bolus of d-luciferin

1 week after intracranial injection of U87-*luc* polyclonal cells, the bioluminescent signal generated by the tumours implanted into the first trial group of mice following an ip bolus of 1.5 mg/g of d-luciferin was followed over 60 mins with BLI. The bioluminescent signal generated by the implanted cells was captured by the Xenogen IVIS 100 cooled CCD camera system. The bioluminescent signal within a designated ROI was expressed as average radiance and expressed quantitatively. The bioluminescent signal quickly peaked within 2-3 mins, before gradually declining over 60 mins to near negligible levels at 55-60 mins.

It seemed unlikely that such a short exposure to bioluminescence would be able to activate a photosensitiser, and therefore a method of generating a more sustained bioluminescence over time was needed.

9.2.2 Generating Sustained Bioluminescence: Use of an Osmotic Pump

With the aim of generating a more sustained bioluminescence over time, the use of a subcutaneous osmotic pump (model 2001, ALZET, Durect Corporation, Cupertino,

USA) was tested. The model selected was the largest that could be tolerated by the size of animal being used (3.0 x 0.7 cm, 1.1g wt). Under sterile conditions, the osmotic pump was filled to its maximum volume of 200 μl with 50 mg/ml of d-luciferin. One mouse with a xenografted subcutaneous tumour and one with a xenografted intracranial tumour derived from U87-*luc* polyconal and U87bp-*luc* cells cultured to derive neurospheres, respectively, were anaesthesised with inhalational anaesthesia and an incision made in their dorsal cervical skin. A subcutaneous pocket was bluntly created and the pump implanted. The skin was closed with interrupted, 3'0 prolene, vertical mattress sutures. This pump delivered drug at a rate of 1.0 μl/hr for 1 week. Using BLI, the mice were imaged after pump implantation, thereby providing a measurement of the bioluminescent signal generated by the pump alone. The mice were then given a 1.5 mg/g ip bolus of d-luciferin and reimaged, thereby providing the comparison signal achieved with a standard bolus of d-luciferin. The bioluminescent signal generated by the d-luciferin delivered by the pump was also followed with BLI over the course of 1 week in the subcutaneous model with images being taken at days 1, 4, and 7 after the pump was inserted.

Figure 85a and Figure 85b show the subcutaneously placed osmotic pump and the bioluminescent signal generated by the d-luciferin that it was delivering in a subcutaneous and intracranial model. It is clear that the bioluminescent signal generated by the d-luciferin being delivered via the pump was orders of magnitude lower than the signal generated by giving d-luciferin as an ip bolus (see Figure 85c and d), which is consistent with the dose of d-luciferin being given at any one time (0.05 mg/hr via the pump vs a 1.5 mg/g bolus). However, the pump was able to produce a more sustained bioluminescent signal over the course of one week (see Figure 85e).

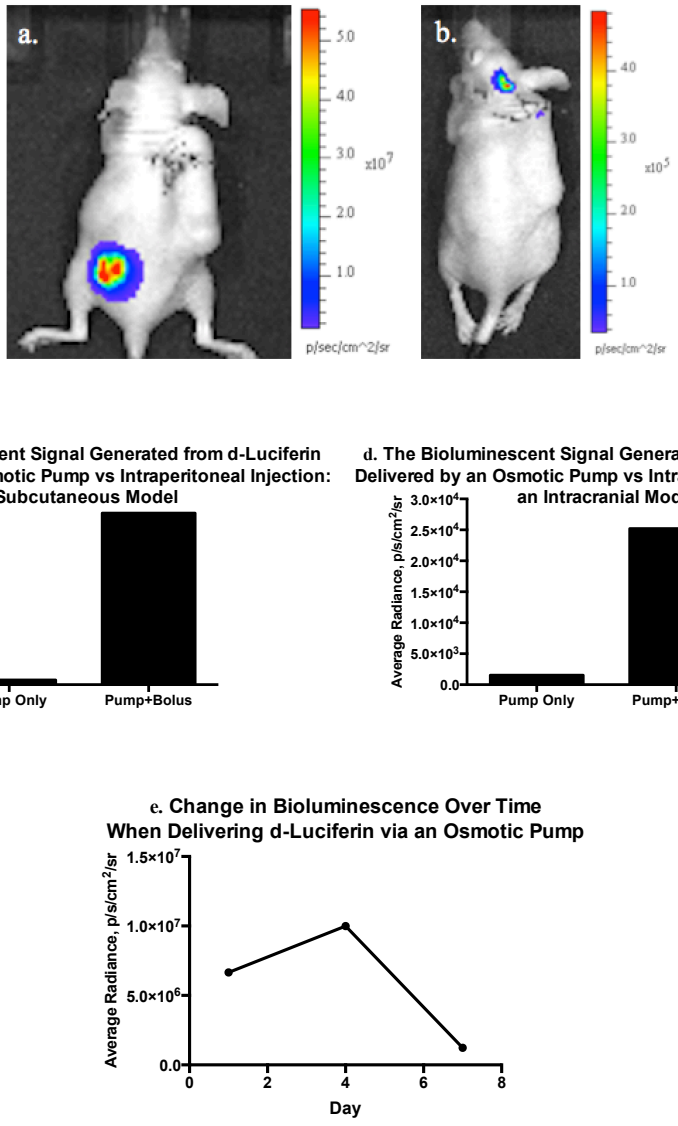

Figure 85 Delivering d-luciferin via an osmotic pump.

One mouse with a transplanted subcutaneous tumour and one with a transplanted intracranial tumour were implanted with a subcutaneous osmotic pump containing 200 µl of 50 mg/ml d-luciferin, which delivered d-luciferin at 1.0 µl/hr for 1 week. The mice were imaged with BLI after pump implantation (a, b), then were given a 1.5 mg/g ip bolus of d-luciferin and reimaged. The mouse with the subcutaneous tumour was also imaged over 1 week with BLI without a d-luciferin bolus. The bioluminescent signal generated by the implanted cells was captured by the Xenogen IVIS 100 cooled CCD camera system. The bioluminescent signal within a designated ROI was expressed as average radiance and expressed quantitatively. The bioluminescent signal generated by d-luciferin delivered by the pump alone was orders of magnitude less than that generated by the standard bolus dose of d-luciferin (c, d), although it was sustained over the course of 1 week (e).

9.2.3 Summary and Discussion

The literature demonstrates that with a single-dose ip injection of d-luciferin, there is a slow rise in bioluminescent signal, reaching a peak at approximately 15 mins, followed by a more gradual drop[195]. The change in bioluminescence over time in this study was more akin to that achieved with an intravenous injection[195]. Nevertheless, as the

photosensitiser selected for testing bPDT, *m*THPC, remains at a significant concentration in tumour tissue over days (see below), a method of delivering d-luciferin in a sustained manner, thereby maximising the time over which *m*THPC would be exposed to bioluminescence, might be more efficacious. The subcutaneous osmotic pump was shown to be able to do this, enabling the generation of a stable amount of bioluminescence over a week, albeit sacrificing the peak-value of bioluminescence.

9.3 Bioluminescence-Mediated Photodynamic Therapy: a Pilot Study

By transplanting U87bp-*luc* cells that had been cultured to form neurospheres (see Figure 83), a reliable intracranial tumour model with established exponential growth within a week of implantation had been achieved. As the model was being followed, then used to test the subcutaneous osmotic pump (see Figure 85), the opportunity to carry out a small pilot study was taken.

7 weeks following cell implantation, both mice in this group had osmotic pumps filled with d-luciferin implanted subcutaneously, as described in section 9.2.2. The mice underwent BLI to confirm d-luciferin delivery. The following day, Mouse 2, was injected with 0.3 mg/kg ip of *m*THPC (see section 9.4.1.3). 1 week later, both mice underwent BLI.

After implantation of the osmotic pump, BLI revealed that the pump was effectively delivering d-luciferin (see Figure 86a). BLI 1 week after the start of treatment, 8 weeks after cell implantation, Mouse 1, the mouse that only had an osmotic pump inserted but no exposure to *m*THPC, was found unwell, thin, and with an ataxic gait, which was consistent with the dramatic increase in bioluminescent signal from the intracerebral tumour, signifying significant tumour growth (see Figure 86b). In contrast, the tumour of the mouse that had been exposed to both d-luciferin and *m*THPC, Mouse 2, showed markedly less growth, indicating relative inhibition in growth compared to the tumour in Mouse 1. Both mice were culled at this point.

From Figure 83c, the tumours of both Mouse 1 and Mouse 2 were following a similar growth curve before institution of treatment. These results suggest that the treatment at least suppressed the natural growth of the tumour in the treated mouse. For demonstration of true cell kill, Mouse 2 would have had to have been followed for

longer, particularly as *in vitro* studies have shown that bPDT can have a delayed effect. Although a limited study, based on these results, further investigation was warranted.

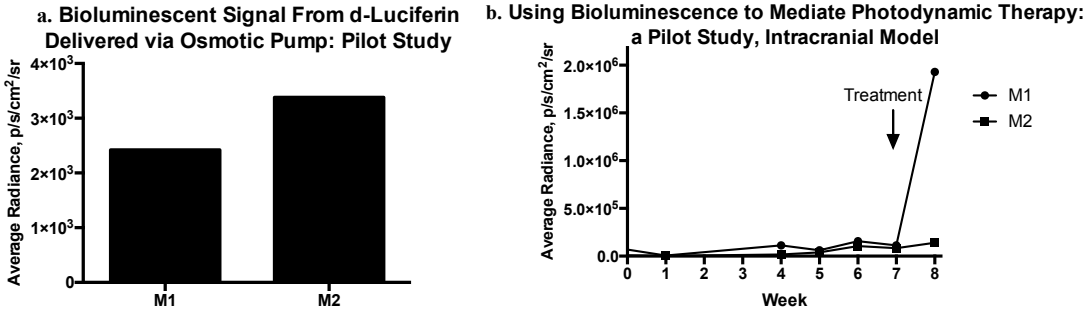

Figure 86 Using bioluminescence to mediate photodynamic therapy: a pilot study in an intracranial model

7 weeks after intracranial injection of neurospheres derived fromU87bp-l*uc* cells into two mice, the mice were implanted with a subcutaneous osmotic pump loaded with d-luciferin. The day after implantation, mouse 2 was injected with 0.03 mg/kg *m*THPC. The bioluminescent signal generated by the implanted cells was captured by the Xenogen IVIS 100 cooled CCD camera system after the animals were injected with 1.5 mg/g of d-luciferin ip. The bioluminescent signal within a designated ROI was expressed as average radiance and expressed quantitatively. BLI, without a bolus of d-luciferin, after the implantation of the osmotic pumps confirmed that they were delivering d-luciferin effectively (a). 1 week after treatment, the tumour in Mouse 1, exposed to d-luciferin only, had a dramatic increase in bioluminescent signal, indicating marked tumour growth, consistent with the development of neurological signs. However, the tumour in Mouse 2, exposed to sustained d-luciferin and *m*THPC, did not seem to follow the same growth curve as Mouse 1 as indicated by BLI, and seemed to have undergone suppression of growth.

9.4 Testing Bioluminescence Mediated Photodynamic Therapy

As results from the pilot study were encouraging, a more extensive test of bPDT seemed justified. A summary of the animal models used, the derivation of the tumours, and the outcomes measured is given in Table 12. 3 subcutaneous models and 1 intracranial model were used. Outcomes measured included survival, tumour volume, and bioluminescent signal. Once all animals were culled, all tumours were subjected to histolopathological and immunohistochemical analysis.

The bPDT treatment required two elements, the delivery of photosensitiser and the generation of bioluminescence. *m*THPC was delivered ip at a dose of 0.3 mg/kg, which is a standard *in vivo* dose[114,196]. In rodents, *m*THPC reaches its maximum concentration within the tumour between 36 and 48 hrs after administration, then gradually decreases, with just under half of its maximum concentration remaining between 6 and 7 days after administration[114,115]. Bioluminescence was generated by supplying the implanted U87-*luc* cells with a constant dose of d-luciferin over 7 days via a subcutaneous

osmotic pump. Use of the osmotic pump allowed the prolonged exposure of the photosensitiser to bioluminescence, thereby maximising upon the duration that the photosensitiser remains in significant levels within the tumour.

	bPDT Trial			
	1	**2**	**3**	**4**
Outcomes	Subcutaneous, Passage 4	Subcutaneous, U87-*luc* cells	Subcutaneous, Passage 3	Intracranial, Neurospheres
Survival	✓	✓	-	-
Tumour Volume	✓	-	✓	-
Bioluminescent Signal	✓	✓	✓	✓
Histopathology and Immunohistochemistry	✓	✓	✓	✓

Table 12 Summary of the animal models used and the outcomes measured in each trial

bPDT was tested in 4 trials: 3 subcutaneous models and 1 intracranial model. This table summarises the origin of the tumours in each of the trials and the outcomes measured.

9.4.1 Detailed Methodology

9.4.1.1 The Animal Models

Using the methods described in section 9.1 animal models were generated for testing bPDT: bPDT trials 1-3 were conducted in subcutaneous models and bPDT trial 4 was conducted in an intracranial model (see Table 12).

In bPDT trial 1, the subcutaneous tumours were derived from 4 subcutaneous passages of a tumour that had originated from U87-*luc* polyclonal cells. The tumours for bPDT trial 3 were derived in a similar manner, but resulted from 3 subcutaneous passages of tumour. In bPDT trial 2, the subcutaneous tumours were derived from injection of U87-*luc* polyclonal cells into the dorsal flank of the animals. In bPDT trial 4, the cells injected intracranially were the neurospheres that had been derived from U87bp-*luc* cells. The details of each model are described within the context of each experiment discussed below.

9.4.1.2 The Substrate: d-Luciferin

d-Luciferin was delivered via an osmotic pump (model 2001, ALZET, Durect Corporation, Cupertino, USA). The pump was filled to its maximum volume of 200 µl with 50 mg/ml of d-luciferin and implanted subcutaneously under inhalational anaesthesia, as described above (section 9.2.2).

9.4.1.3 The Photosensitiser, mTHPC

A stock solution of *m*THPC (4mg/ml) was diluted in 3 mls PEG 400, 2 mls ethanol, and 5 mls distilled water to achieve a final concentration of 0.03 mg/ml. The drug was sterile filtered and injected ip into the animals at a dose of 0.3 mg/kg. Once the photosensitiser had been injected into the mice, they were kept in the dark, with black plastic used to shield their cages and their daily care was undertaken with the room lights switched off to minimise inadvertent photoactivation of the photosensitiser by ambient light.

9.4.1.4 The Treatment

At a designated time point following tumour implantation, which is detailed within the context of each experiment below, the mice were divided into 'control' only, 'drug only,' 'light only,' and 'treatment' (i.e. drug + light) groups following either random allocation or randomisation according to bioluminescent signal. The mice in the 'light only' and 'treatment' groups were implanted with the d-luciferin filled osmotic pumps. Then the mice in the 'drug only' and 'treatment' groups were injected with 0.3 mg/kg of *m*THPC ip. After 1 week, the osmotic pumps were removed. BLI was not undertaken during the first week of treatment to avoid the confounding effect of the d-luciferin bolus necessary for BLI.

9.4.1.5 Outcome Measures

9.4.1.5.1 Survival

Animals were culled at the designated end point of the experiment, or if they became unwell and displayed any signs of distress. Animals with subcutaneous tumours were also culled if the tumours reached > 12 mm in any direction, as per institutional protocol. Survival was recorded in bPDT trials 1 and 2.

9.4.1.5.2 Tumour Volume

The subcutaneous tumours generated in bPDT trials 1 and 3 became large enough for caliper measurements to be made. From these measurements, tumour volume was estimated: the depth of the tumour was difficult to determine and was assumed to equal the width, and thus, assuming the tumour to be a rectangle, the volume was estimated as 'width^2 x length.' In bPDT trial 1, tumour volumes were trended throughout the course of the experiment.

9.4.1.5.3 Bioluminescent Signal

After the end of treatment, in all bPDT trials, bioluminescent signal was trended throughout the course of the experiment. BLI was conducted as detailed in section 9.1.1.6.

9.4.1.5.4 Validation of BLI

In bPDT trials 1 and 3, where both tumour volume and bioluminescent signal were measured at a specific time point, an attempt at validating BLI as a measure of tumour progression was made.

9.4.1.6 Histopathology and Immunohistochemistry

2 hrs before culling, the mice were injected with 5 mg/ml ip of 5-bromo-2'-deoxyuridine (BrdU) to allow identification of cells that were actively replicating their DNA at the time of injection via anti-BrdU antibody detection. The mice were culled with CO_2 then cervical fracture, in accordance with institutional guidelines. In the subcutaneous model, the tumours were dissected out and placed in formalin. In the intracranial model, the brains were dissected out and placed in formalin. The tissues were then sectioned. Slides were stained with haematoxylin and eosin (H and E) and labelled with antibody to BrdU. A piece of small intestine was also harvested to act as the positive control for the immunohistochemistry.

A representative section of each tumour was selected. The H and E stained slides were examined, the characteristics of the tumours noted, and a subjective assessment of the degree of necrosis made. Regarding immunohistochemistry, the BrdU positive and negative cells were counted in 4 randomly picked locations at x 40 magnification using Image-Pro Plus 50 software. The number of BrdU positive cells was expressed as the percentage of the total count and averaged for each group.

9.4.1.7 Statistical Analysis

Statistical analysis was conduced using GraphPad Prism software. For survival analysis, Kaplan-Meier curves were generated for each of the experimental groups and log-rank analysis using a Bonferroni correction threshold for multiple comparisons was used to determine if there was a significant difference between the groups.

For tumour volume, bioluminescent signal, and proportion of BrdU positive cells, results were averaged for each experimental group and expressed as the average ±SEM.

1-way ANOVA analysis was then conducted to determine if a significant difference existed between each group.

In validating BLI as a measure of tumour progression, linear regression was undertaken to examine the relationship between tumour volume and bioluminescent signal at a particular time point. An r^2 value was calculated to assess the goodness-of-fit of this relationship.

9.4.2 bPDT Trial 1: Subcutaneous Model – subcutaneous passage of tumour, passage 4

The mice implanted with tumours that had undergone 3 passages of subcutaneous transfer (see Figure 79d) were culled and the tumours harvested, prepared, and 100 µl of cell suspension was injected subcutaneously into the dorsal flank of 15 mice; subcutaneous passage 4. 4 days after injection, the mice underwent BLI. Based on their bioluminescent signal, the mice were randomised into 'control' only (n=3), 'drug only' (n=3), 'light only' (n=4), and 'treatment' (n=5) groups, such that each group generated similar amounts of bioluminescence. The following day, 5 days after tumour implantation, treatment began. After its completion, the animals underwent BLI every other day. Once the tumours were large enough, caliper measurements of the implanted tumours were also made in conjunction with BLI, and tumour volumes estimated.

9.4.2.1 Randomisation

Randomisation 4 days after tumour implantation allowed the animals to be divided into 4 groups whose collective bioluminescent signal within each group following a bolus of d-luciferin was not significantly different between each group (see Figure 87). Groups A, B, C, and D became the 'control' (n=3), 'drug only' (n=3), 'light only' (n=4), and 'treatment' (n=5) groups, respectively.

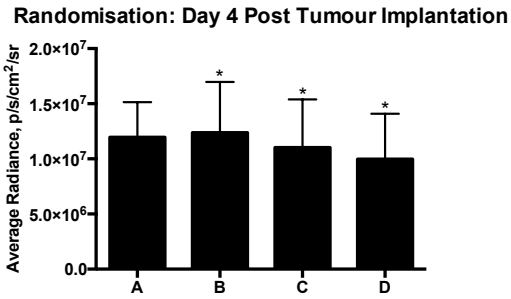

Figure 87 Randomisation of animals according to bioluminescent signal 4 days after tumour implantation

A, B, C, and D denote the 4 groups that the animals were randomised into. Asterisks indicate the degree of significance of the difference in bioluminescent signal generated between each group and group A, where *p > 0.05. The bioluminescent signal generated by the implanted cells was captured by the Xenogen IVIS 100 cooled CCD camera system after the animals were injected with 1.5 mg/g of d-luciferin ip. The bioluminescent signal within a designated ROI was expressed as average radiance and expressed quantitatively. Randomisation allowed the animals to be divided into 4 groups whose collective bioluminescent signal within each group was not significantly different between groups.

9.4.2.2 Validation of BLI

Caliper measurements of the subcutaneous tumours began the day after the end of treatment, 13 days following tumour implantation. The bioluminescent signal from each tumour was plotted against its estimated volume and linear regression analysis undertaken. Figure 88 shows that overall the greater the tumour volume, the greater the bioluminescent signal. However, this relationship becomes stronger over time: although the r^2 value 13 days after tumour implantation is close to and not significantly different from 0 (0.093, $p > 0.05$), indicating that bioluminescent signal is not predictable from tumour volume, this value increases to close to 0.5 (0.48, $p < 0.01$) over the next 4 days. Only 2 mice survived beyond day 17 and on days 19 and 21 this relationship continued. However, on day 24, there was a reversal in the correlation, with a lower bioluminescent signal being associated with the greater tumour volume. This likely reflected the point where the tumour outgrew its blood supply and necrosis became predominant. Overall, the bioluminescent signal detected by BLI can be used as a surrogate measure for tumour volume. However, care should be taken in interpreting the findings both early and late in tumour progression.

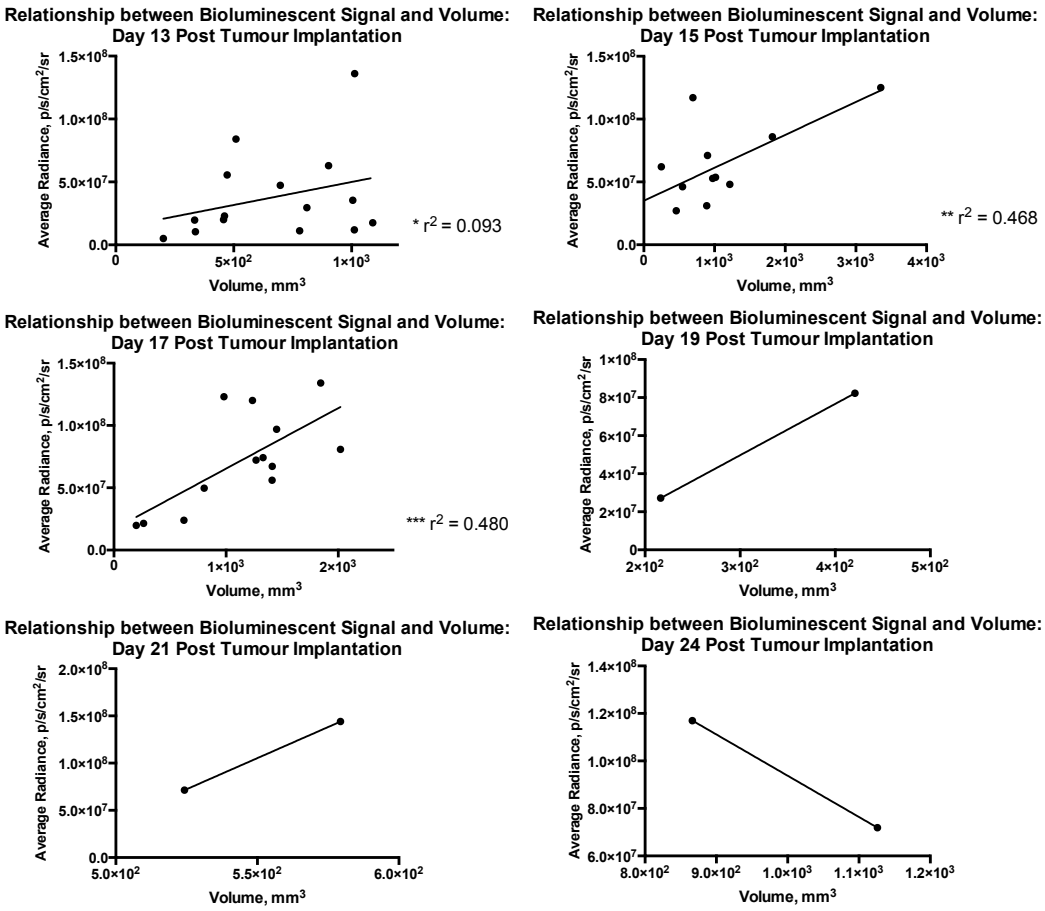

Figure 88 Validation of BLI: correlating bioluminescent signal with tumour volume

The bioluminescent signal from each tumour was plotted against its estimated volume and linear regression analysis undertaken. The bioluminescent signal generated by the implanted cells was captured by the Xenogen IVIS 100 cooled CCD camera system after the animals were injected with 1.5 mg/g of d-luciferin ip. The bioluminescent signal within a designated ROI was expressed as average radiance and expressed quantitatively. Asterisks indicate the degree of significance of the difference in the slope generated from linear regression analysis and 0 where *p > 0.05, **p ≤ 0.05, ***p < 0.01. Tumours became large enough for caliper measurements on day 13 post tumour implantation. The greater the tumour volume, the greater the bioluminescent signal, and as the tumours became larger from days 13 to 17, this relationship became stronger, as reflected by the r^2 value. In the 2 mice surviving beyond day 17, this relationship continued until day 24, when there was a reversal in the correlation, likely reflecting the point where the tumour outgrew its blood supply and necrosis became predominant. Overall, the bioluminescent signal detected by BLI can be used as a surrogate measure for tumour volume. However, care should be taken in interpreting the findings both early and late in tumour progression.

9.4.2.3 Outcome: Survival

14 days after tumour implantation, one control mouse, Mouse 2, was culled due to ulceration of the subcutaneous tumour. One mouse from the treatment group, Mouse 0, was chosen at random and culled at the same time point to enable histopathological comparison (see Figure 93a and b): this mouse was censored from the survival analysis. 17 days after tumour implantation, all remaining mice, except for two treatment mice, Mouse 3 and Mouse 4, fulfilled the criteria for culling. Mouse 3 and Mouse 4 from the

treatment group finally succumbed 24 and 26 days following tumour implantation, respectively.

A Kaplan-Meier curve was generated for each of the groups (see Figure 89). Although the median survival of the 'treatment' group was greater than that of the 'control,' 'drug only,' and 'light only' groups, 20.5 vs 17 days respectively, log-rank analysis using a Bonferroni correction threshold for multiple comparisons did not find any significant difference between the curves: the p value of 0.0926 resulted from comparing the survival curves of the 'control' and 'treatment' groups as an example.

There seems to be a trend towards improved survival in the 'treatment' group. However, the data is limited by the size of the population tested.

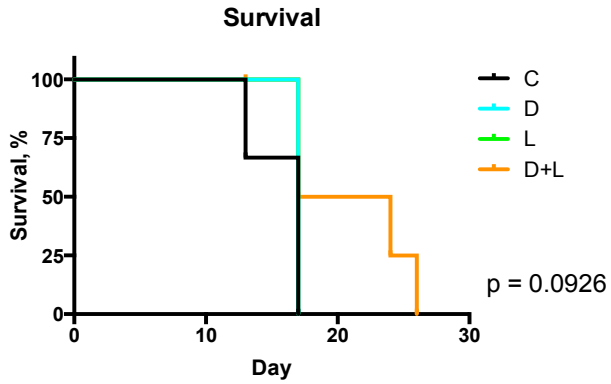

Figure 89 Kaplan-Meier curves demonstrating survival: bPDT Trial 1

A Kaplan-Meier curve was generated for each of the groups in the study, where C = control, D = drug only, L = d-lucifeirn only, and D+L = animals exposed to drug and d-luciferin. The x axis represents the number of days following tumour implantations. Although the median survival of the 'treatment' group was greater than that of the 'control,' 'drug only,' and 'light only' groups, 20.5 vs 17 days respectively, log-rank analysis using a Bonferroni correction threshold for multiple comparisons did not find any significant difference between the curves: the p value of 0.0926 resulted from comparing the survival curves of the 'control' and 'treatment' groups as an example.

9.4.2.4 Outcome: Tumour Volume

Caliper measurements of the subcutaneous tumours began 13 days following tumour implantation, allowing an estimation of tumour volume. From this point, the change in tumour volume over time was trended. The data for the individual animals (see Figure 90a) and the average tumour volumes in each group (see Figure 90b) are presented.

The data for the individual animals revealed an aberrant measurement for Mouse 5 in the 'treatment' group on day 15: this data point was excluded from the average

calculations. There was no significant difference between the groups at any time point. However, from the grouped data, the 'treatment' group did seem to have lower tumour volumes. Furthermore, there seemed to be a delay in the onset of the exponential growth phase of the tumours in the 'treatment' group: tumours in the animals in the control groups had reached their exponential growth by day 13, whereas this started at day 19 in the 'treatment' group. Moreover, there seemed to be a halt in tumour growth in the 'treatment' group from day 13-17, with a fall in tumour volume from day 17-19, before the onset of exponential growth. From the individual data, this trend in the 'treatment' group was mainly due to the effect of treatment on two mice, Mouse 3 and Mouse 4, and was reflected by their increased survival.

Overall, there is a suggestion that the treatment had at least some effect in suppressing tumour growth. However, the data is limited by the size of the population tested.

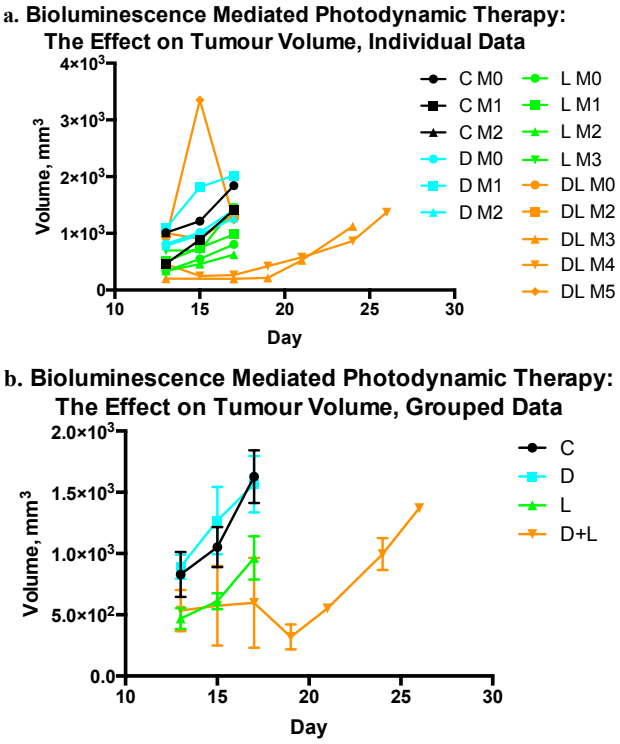

Figure 90 Bioluminescence-mediated photodynamic therapy: the effect on tumour volume – bPDT Trial 1

C = control, D = drug only, L = d-luciferin only, DL/D+L = animals exposed to drug and d-luciferin, M = mouse. The x axis represents the number of days following tumour implantation. Caliper measurements of the subcutaneous tumours began 13 days after tumour implantation. The data for individual animals (a) and the average tumour volumes in each group (b) are presented: what seemed to be an aberrant measurement from mouse 5 in the 'treatment' group on day 15 was excluded from the 'averaged' data. Although there was no significant difference in tumour volume between the groups at any time point, the 'treatment' group seemed to have a lower average tumour volume and a delay in the tumour starting exponential growth, This trend was mainly due to the effect of treatment on two mice in the treatment group, Mouse 3 and Mouse 4, and was also reflected in their increased survival.

9.4.2.5 Outcome: Bioluminescent Signal

The day after the end of treatment, 13 days after tumour implantation, the animals underwent BLI, and every other day thereafter. The data for the individual animals (see Figure 91a) and the average bioluminescent signal in each group (see Figure 91b) are presented.

There was no significant difference in the bioluminescent signal between the groups at any time point. From the 'grouped' data, the exponential growth phase of the tumours in the control groups seemed to start 13 days following tumour implantation. In the 'treatment' group, the start of exponential growth was less clear, with a subtle fall in bioluminescent signal from days 15-19, before a brief increase from days 19-21, then another gradual fall in signal from days 21-26.

The trends in tumour progression are less clear when measuring bioluminescent signal compared to tumour volume. The balance between ongoing tumour growth and the degree of necrosis that occurs as the tumour outgrows its blood supply likely confounds the bioluminescent signal, as discussed above. This was demonstrated by Mouse 2 in the 'light only' group and Mouse 4 in the 'treatment' group, where a rapid increase in bioluminescent signal was followed by a steep decline, even though progressively increasing tumour volumes were seen (see Figure 90). A trend towards a treatment effect was less clear when analysing bioluminescent signal, which is consistent with the limitations of BLI revealed by the validation study.

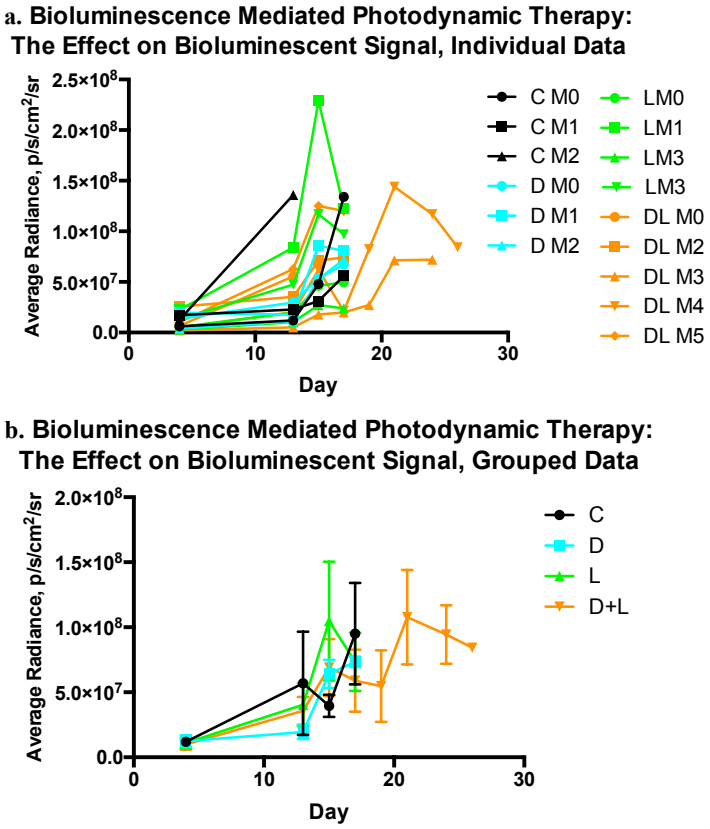

Figure 91 Bioluminescence-mediated photodynamic therapy: the effect on bioluminescent signal – bPDT Trial 1

C = control, D = drug only, L = d-luciferin only, DL/D+L = animals exposed to drug and d-luciferin, M = mouse. The x axis represents the number of days following tumour implantation. The bioluminescent signal generated by the implanted cells was captured by the Xenogen IVIS 100 cooled CCD camera system after the animals were injected with 1.5 mg/g of d-luciferin ip. The bioluminescent signal within a designated ROI was expressed as average radiance and expressed quantitatively. The data for the individual animals (a) and the average bioluminescent signal in each group (b) are presented. There was no significant difference in the bioluminescent signal between the groups at any time point. From the 'grouped' data there seemed to be a delay in the exponential growth phase in the 'treatment' group compared with the control groups. Overall, the trends in tumour progression were less clear when following bioluminescent signal compared to tumour volume.

9.4.2.6 Outcome: Histopathology and Immunohistochemistry

As the mice were culled, their tumours were harvested, fixed in formalin, embedded in paraffin, and sectioned. H and E stain revealed the tumours to be hypercellular and consist of a monomorphic population of cells on a fibrillary background, consistent with astrocytoma. Areas of necrosis were evident, as were several mitoses, (see Figure 92), consistent with a grade 4, tumour.

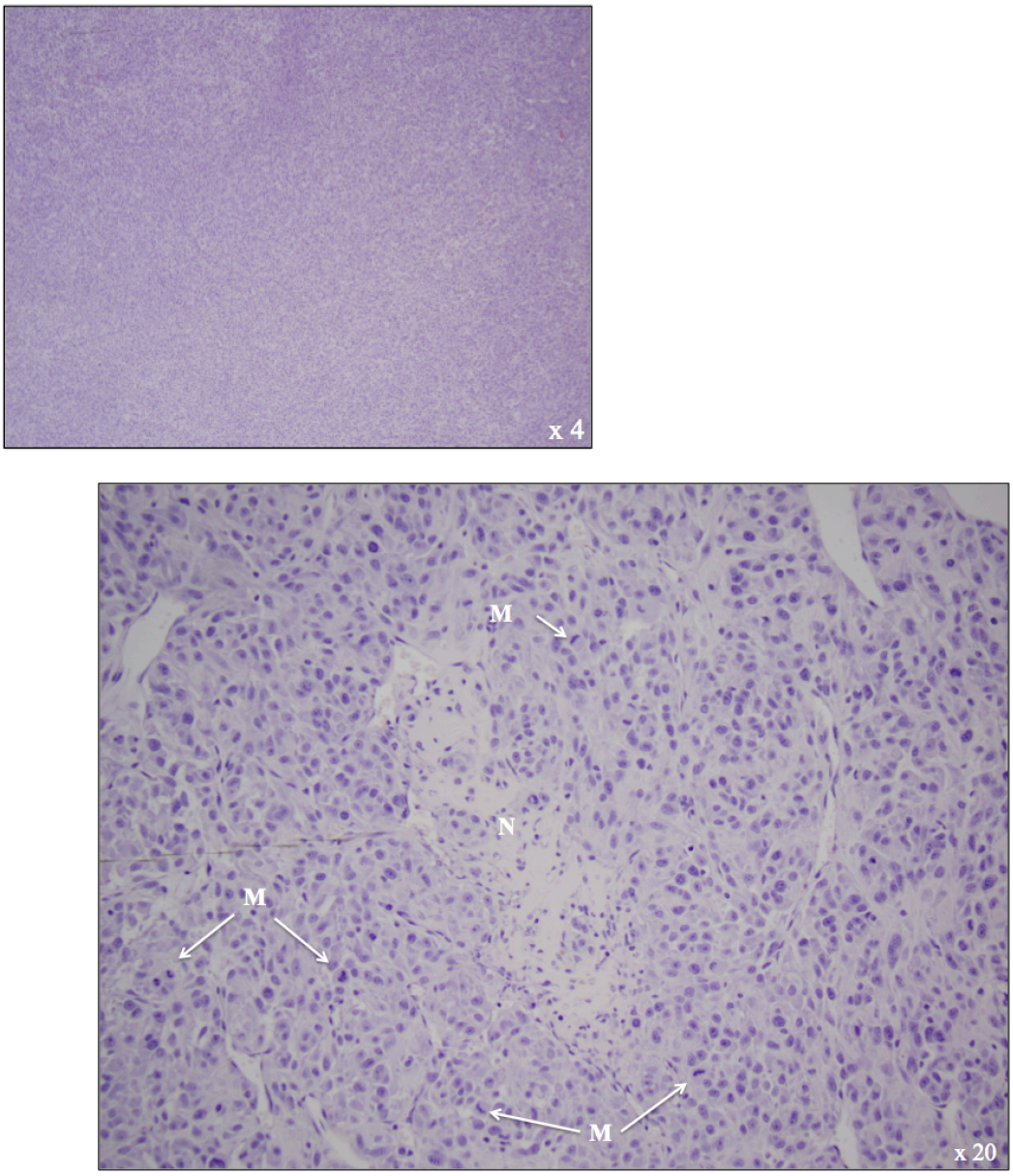

Figure 92 H and E stained section of an implanted subcutaneous tumour derived from U87-*luc* polyclonal cells

This is an H and E stained section from the tumour of a mouse in the 'control' group seen at low (x4) and high (x20) magnifications, and is representative of the tumours derived from U87-*luc* polyclonal cells subjected to 4 passages of subcutaneous transfer. The tumour is seen to be hypercellular and to consist of a monomorphic population of cells on a fibrillary background, consistent with astrocytoma. There is evidence of both multiple mitoses (M) and necrosis (N), consistent with a grade 4 astrocytoma tumour.

Furthermore, subjectively, there was more necrosis seen in the 'treatment' group compared with the control groups. This was first evident when comparing the tumour of the control mouse that was culled 13 days following tumour implantation due to tumour ulceration and the tumour of the 'treatment' group mouse that was electively

culled at the same time for comparison (see Figure 93a and b). This observation was also made during the final analysis (see Figure 93c, d, and e).

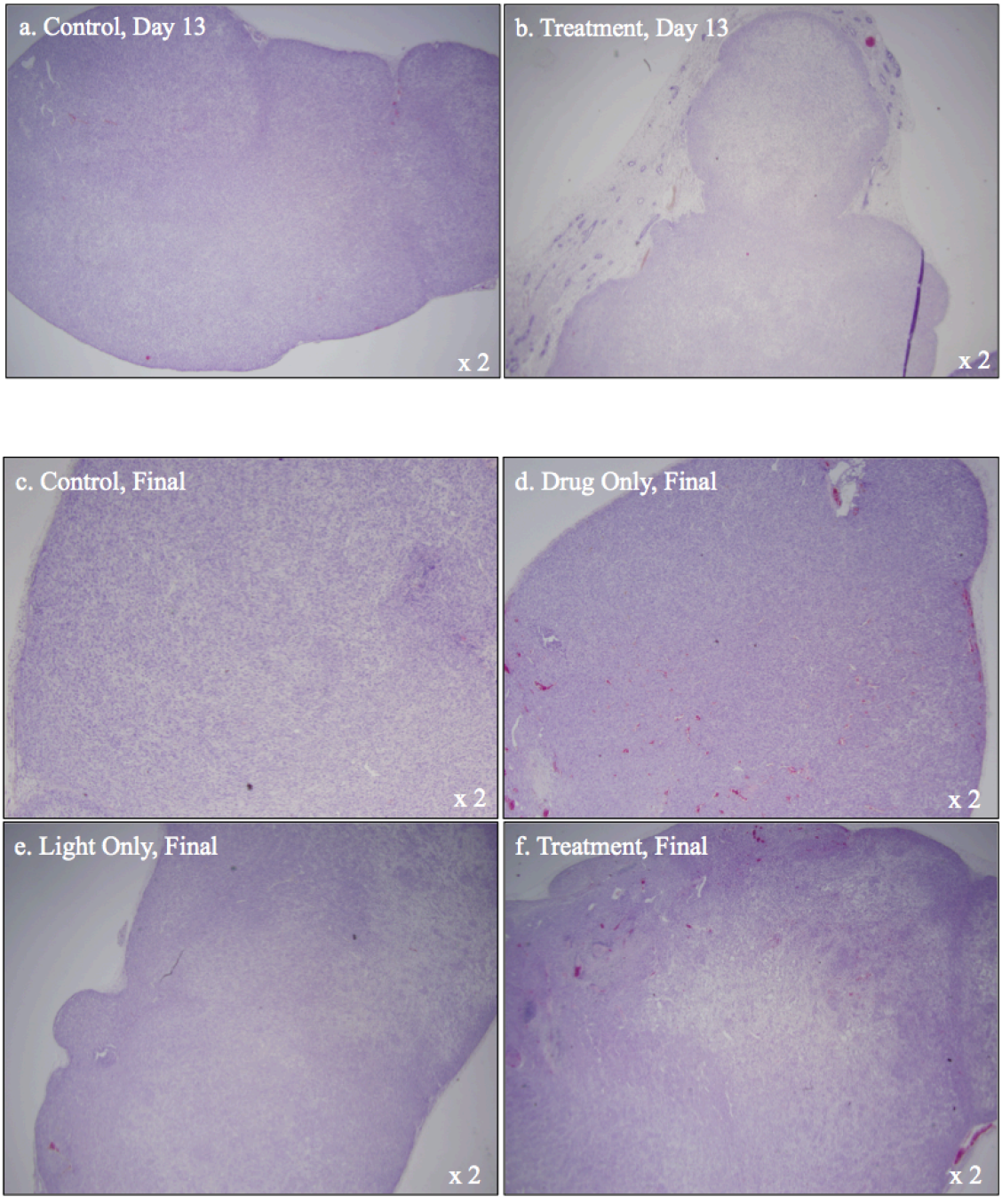

Figure 93 Comparing H and E stained sections of subcutaneous tumours derived from U87-*luc* polyclonal cells from the different study groups.

Subjectively, more necrosis was seen in the 'treatment' group compared with the control groups. This was first evident when comparing the tumours from the 'control' (a) and 'treatment' group (b) mice that were culled on day 13. This observation was also made during the final analysis: representative sections of tumour from the 'control' (c), 'drug only' (d), 'light only' (e), 'treatment' groups (f) are presented.

2 hours prior to being culled, the mice were injected with BrdU. Sections were subsequently labelled with antibody to BrdU, which labelled cells that were actively replicating their DNA at the time of injection. A typical section labelled with antibody to BrdU is seen (see Figure 94a) along with its positive control, a piece of small intestine (see Figure 94b) with the constantly dividing stem cells in the crypts being labelled: the BrdU positive cells are coloured brown, compared to the blue of the BrdU negative cells. For each tumour, the BrdU positive and negative cells were counted in 4 randomly picked locations at x 40 magnification. The number of BrdU positive cells was expressed as the percentage of the total count and averaged for each group (see Figure 94c). 3 tumours were excluded from analysis due to poor immunolabelling: Mouse 1 from the 'drug only' group, Mouse 2 from the 'light only' group, and Mouse 4 from the 'treatment' group. There were significantly less BrdU positive cells in the 'treatment' group compared to the 'control,' 'drug only,' and 'light only' groups (16.0 ± 0.546 vs 29.4 ± 0.996, 29.2 ± 0.738, 29.8 ± 1.02, respectively, $p < 0.0001$). This suggests that the treatment caused partial inhibition of DNA replication.

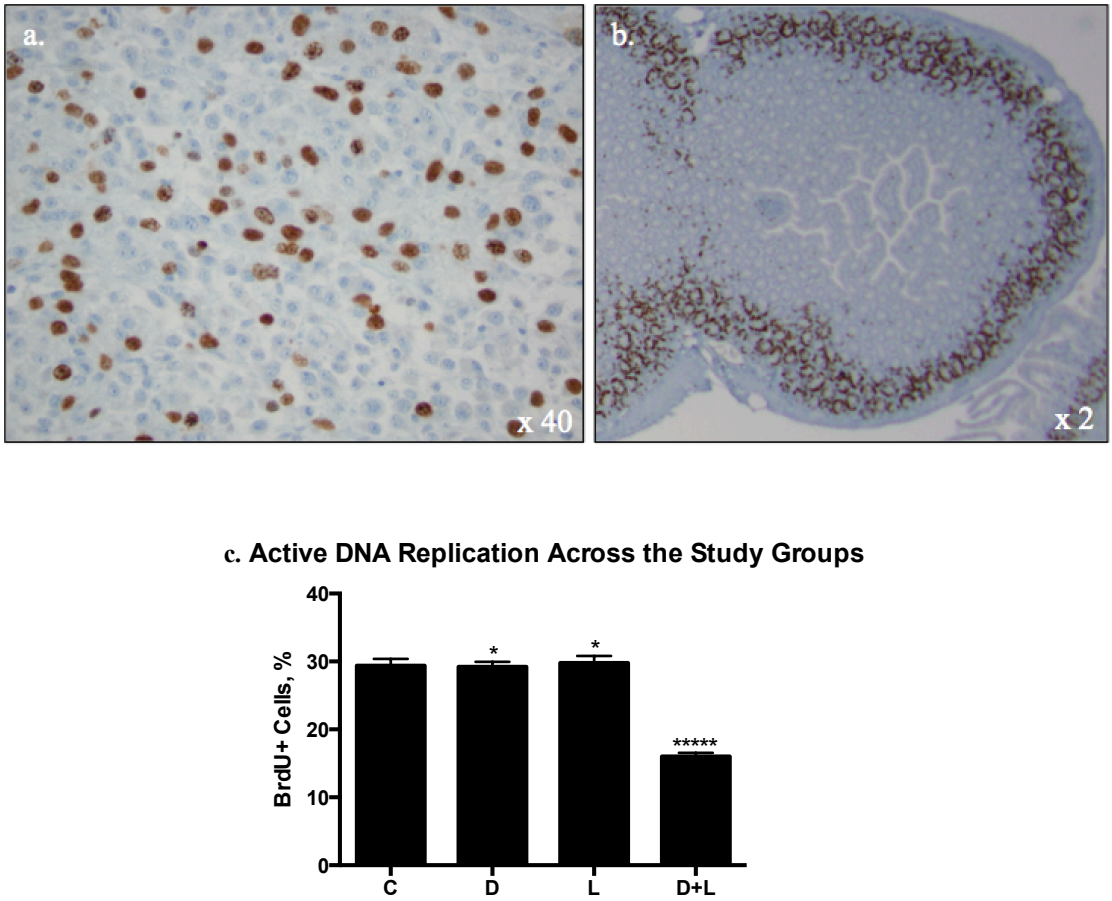

Figure 94 BrdU immunolabelling of subcutaneous tumours derived from U87-*luc* polyclonal cells

2 hours prior to being culled, the mice were injected with BrdU. Sections were subsequently labelled with antibody to BrdU. A typical section labelled with antibody to BrdU is seen (a) along with a positive control, a piece of small intestine (b): the BrdU positive cells are coloured brown, compared to the blue of the BrdU negative cells. For each tumour, the BrdU positive and negative cells were counted in 4 randomly picked locations at x 40 magnification. The number of BrdU positive cells was expressed as the percentage of the total count and averaged for each group, where C = control, D = drug only, L = d-luciferin only, D+L = animals exposed to drug and d-luciferin. There were significantly less BrdU positive cells in the 'treatment' group compared to the control groups (c), indicating that the treatment, at the very least, caused some inhibition of DNA replication.

9.4.2.7 Summary: bPDT Trial Group 1, Subcutaneous Model

There was a trend to prolonged survival in the 'treatment' group. This is consistent with the suggestion of a delay in onset of exponential growth in the 'treatment' group, as revealed by trending tumour volumes, and certainly correlates with significantly reduced DNA replication in the 'treatment' group.

The change in tumour progression was not so clearly reflected by following bioluminescent signal as with tumour volume. As shown by the validation study, interpretation of the trend in bioluminescent signal requires some caution.

9.4.3 bPDT Trial 2: Subcutaneous Model – U87-*luc* polyclonal cells

40 mice were injected with 5 x10^6 U87-*luc* polyclonal cells in 200 µl of PBS. The following day, the mice were randomly designated into 'control' only (n=22), 'drug only' (n=6), 'light only' (n=6), and 'treatment' (n=6) groups and treatment was started. At the end of treatment, the animals underwent BLI, and weekly thereafter.

9.4.3.1 Survival

2 mice, one from the 'light only' group and one from the 'treatment' group were culled during the first week after tumour implantation as the site of the osmotic pumps appeared inflammed and infected. These mice were censored from ongoing analysis. 1 mouse from the 'control' group was culled 6 weeks following tumour implantation as the mouse had developed a large tumour affecting the movement of its leg. This tumour was harvested for subcutaneous passaging (see Trial 3). 5 mice from the control group were removed from the study at 7 weeks, as no subcutaneous tumours were developing, as indicated by persistent negligible bioluminescent signal: these mice were censored from ongoing analysis and were used as hosts for subcutaneous passaging (see Trial 3). 2 mice, one from the 'control' group and one from the 'drug only' group were culled 8 weeks following tumour implantation, as the tumour was affecting movement of the leg and the mouse was losing weight, respectively. Overall, there was no significant difference in survival between the groups (see Figure 95): the p value of 0.361 resulted from comparing the survival curves of the 'control' and 'treatment' groups as an example.

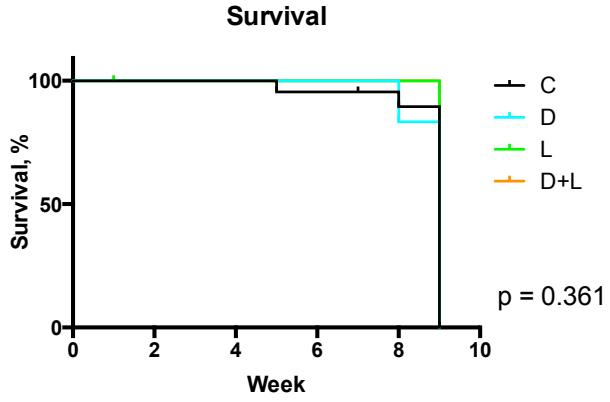

Figure 95 Kaplan-Meier curves demonstrating survival: bPDT Trial 2

A Kaplan-Meier curve was generated for each of the groups in the study, where C = control, D = drug only, L = d-lucifeirn only, and D+L = animals exposed to drug and d-luciferin. The x axis represents the number of weeks following tumour implantations. The plot for D+L follows that of L. There was no significant difference in survival between the groups: the p value of 0.361 resulted from comparing the survival curves of the 'control' and 'treatment' groups as an example.

9.4.3.2 Outcome: Bioluminescent Signal

Animals underwent BLI at the end of treatment, then weekly thereafter. The average bioluminescent signal in each group (see Figure 96) is presented. There was no significant difference in the bioluminescent signal between the groups at any time point. Consistent with findings from development of the model (see Figure 78d), the tumours started their exponential growth phase 7 weeks after tumour implantation.

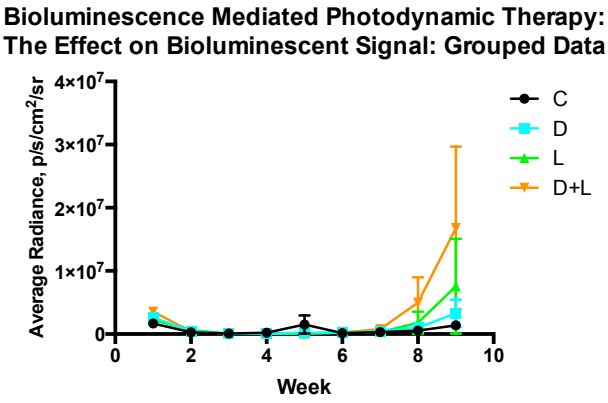

Figure 96 Bioluminescence-mediated photodynamic therapy: the effect on bioluminescent signal – bPDT Trial 2

C = control, D = drug only, L = d-luciferin only, DL/D+L = animals exposed to drug and d-luciferin. The x axis represents the number of weeks following tumour implantation. The bioluminescent signal generated by the implanted cells was captured by the Xenogen IVIS 100 cooled CCD camera system after the animals were injected with 1.5 mg/g of d-luciferin ip. The bioluminescent signal within a designated ROI was expressed as average radiance and expressed quantitatively. The average bioluminescent signal in each group is presented. There was no significant difference in the bioluminescent signal between the groups at any time point.

9.4.3.2 Outcome: Histopathology and Immunohistochemistry

When the mice were culled, their tumours were harvested, fixed in formalin, embedded in paraffin, and sectioned. H and E stain revealed little difference between these tumours obtained from U87-*luc* polyclonal cells harvested from culture then directly implanted compared with the tumours that had undergone several subcutaneous passages. Again, the tumours were hypercellular and consisted of a monomorphic population of cells on a fibrillary background, consistent with astrocytoma, with areas of necrosis and several mitoses, consistent with a grade 4 tumour (see Figure 97a and b).

Mice were again injected with BrdU ip 2 hours prior to culling. There was no clear difference between the proportions of BrdU positive cells, expressed as a percentage of the total cell count, between the study groups (see Figure 97c): there was only slight

toxicity demonstrated in the 'light only' group compared to 'control' (33.6 vs 25.3%, p ≤ 0.05, 95% CI 0.675 to 15.9).

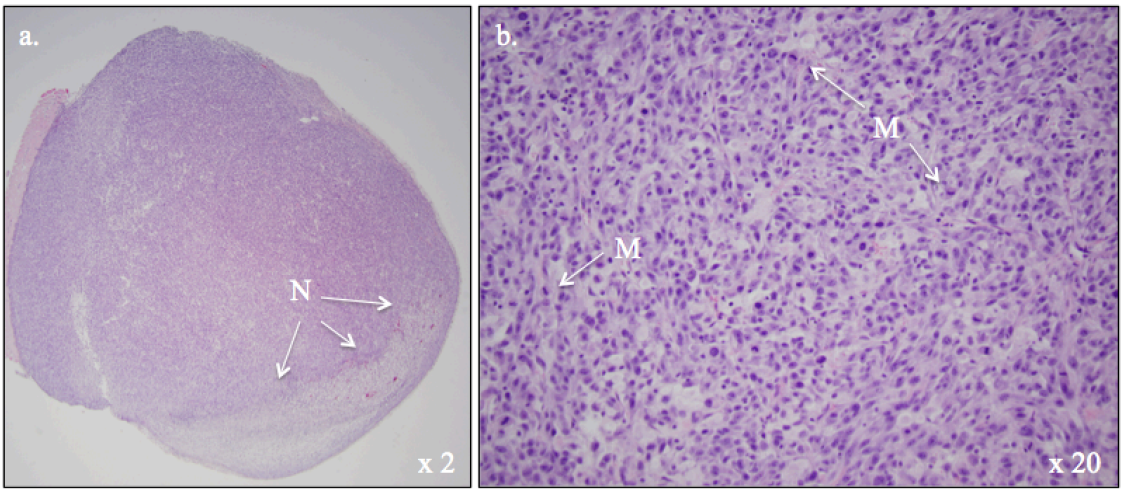

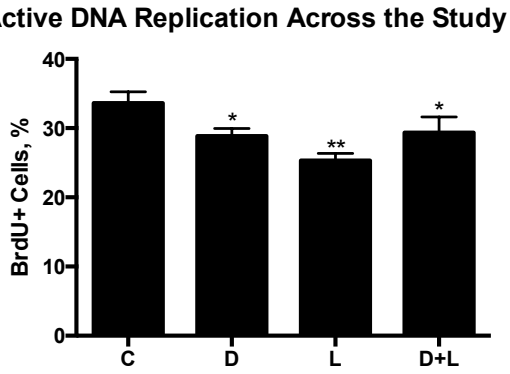

Figure 97 Histopathology and Immunohistochemistry: bPDT Trial 2

H and E stain revealed little difference between these tumours obtained from U87-*luc* polyclonal cells harvested from culture then directly implanted compared with the tumours that had undergone several subcutaneous passages: again, the tumours were hypercellular and consisted of a monomorphic population of cells (a) with areas of necrosis and several mitoses (b), consistent with a grade 4 astroyctoma. Mice were injected with BrdU ip 2 hours prior to culling. There was no clear difference between the proportions of BrdU positive cells between the study groups (c), where C = control, D = drug only, L = d-luciferin only, D+L = animals exposed to drug and d-luciferin: only slight toxicity was demonstrated in the 'light only' group compared to 'control' (33.6 vs 25.3%, p ≤ 0.05, 95% CI 0.675 to 15.9).

9.4.3.3 Summary: bPDT Trial Group 2, Subcutaneous Model

From tumour model development, it was known that this model has a 60% success rate in generating subcutaneous tumours, and hence a large number of mice were injected to account for this. Furthermore, it was known that the rate of tumour growth was slow, with tumours predicted to start their exponential growth 7 weeks after tumour implantation. Upon final analysis, there was no evidence of a treatment effect, or even a trend towards an effect. Results from Trial 1 suggest that any treatment effect would

have been a short-lived suppression in tumour growth. It would be consistent that if there had been such an effect, it would have likely been lost over the long follow up of 9 weeks.

9.4.4 bPDT Trial 3: Subcutaneous Model – subcutaneous passage of tumour, passage 3

The subcutaneous tumour from the mouse of the 'control' group of Trial 2 culled at week 6 was harvested, prepared, and 100 μl of cell suspension injected into the dorsal flank of 6 mice, passage 1. After 10 days of growth, these 6 tumours were harvested, pooled, prepared, and 100 μl of cell suspension injected into the dorsal flank of the 5 'control' group mice from Trial 2 removed from the study at week 7, on the contralateral side to the first cell implantation, passage 2. After another 10 days, these tumours were harvested, pooled, prepared, and 100 μl of cell suspension injected into the dorsal flank of the 12 mice, passage 3.

2 days after tumour implantation, the mice underwent BLI. Based on their bioluminescent signal, the mice were randomised into 'control' only (n=3), 'drug only' (n=3), 'light only' (n=3), and 'treatment' (n=3) groups, such that each group generated similar amounts of bioluminescence. The following day, 3 days after tumour implantation, treatment began. After 1 week of treatment, 10 days after tumour implantation, caliper measurements were made of all the implanted tumours and tumour volumes estimated. The animals also underwent BLI allowing tumour volumes to be correlated with bioluminescent signal. The animals were then culled due to time constraints.

9.4.4.1 Randomisation

Randomisation 2 days after tumour implantation allowed the animals to be divided into 4 groups whose collective bioluminescent signal within each group following a bolus of d-luciferin was not significantly different between the groups (see Figure 98). Groups A, B, C, and D became the 'control' (n=3), 'drug only' (n=3), 'light only' (n=3), and 'treatment' (n=3) groups, respectively.

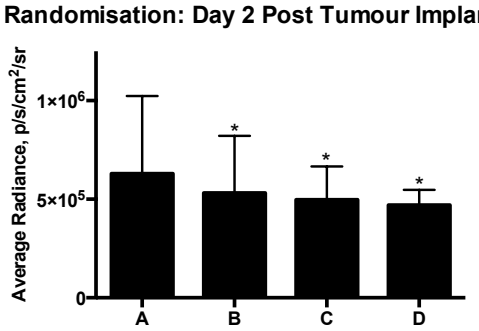

Figure 98 Randomisation of animals according to bioluminescent signal 4 days after tumour implantation

A, B, C, and D denote the 4 groups that the animals were randomised into. Asterisks indicate the degree of significance of the difference in bioluminescent signal generated between each group and group A, where *p > 0.05. The bioluminescent signal generated by the implanted cells was captured by the Xenogen IVIS 100 cooled CCD camera system after the animals were injected with 1.5 mg/g of d-luciferin ip. The bioluminescent signal within a designated ROI was expressed as average radiance and expressed quantitatively. Randomisation allowed the animals to be divided into 4 groups whose collective bioluminescent signal within each group was not significantly different between groups.

9.4.4.2 Validation of BLI

Before the mice were culled at the end of treatment, 10 days after tumour implantation, caliper measurements of the subcutaneous tumours were made before BLI. It was noted that determining tumour volume at this early time point was challenging, as the tumours were not yet well formed with distinct margins. Nevertheless, an attempt at correlating the estimated tumour volume with bioluminescent signal was made. At this time point, there was a weak correlation between bioluminescent signal and tumour volume (see Figure 99): no significant difference was found between the slope generated by linear regression analysis and 0. Supported by findings from Trial 1, this confirms that using bioluminescent signal as a measure of early tumour growth must be interpreted with caution.

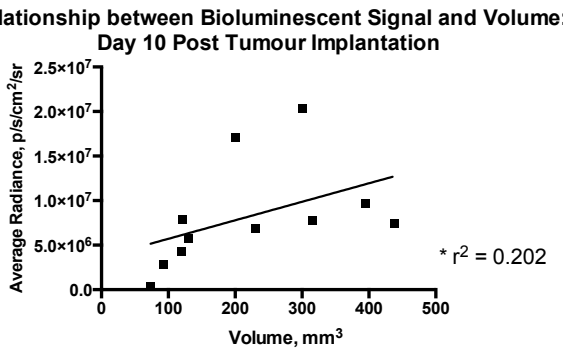

Figure 99 Validation of BLI: correlating bioluminescent signal with tumour volume

At the end of treatment, 10 days after tumour implantation, the bioluminescent signal from each tumour was plotted against its estimated volume and linear regression analysis undertaken. The bioluminescent signal generated by the implanted cells was captured by the Xenogen IVIS 100 cooled CCD camera system after the animals were injected with 1.5 mg/g of d-luciferin ip. The bioluminescent signal within a designated ROI was expressed as average radiance and expressed quantitatively. Asterisks indicate the degree of significance of the difference in the slope generated from linear regression analysis and 0 where *p > 0.05. At this time point, there was a poor correlation between volume and bioluminescent signal, where there was no significant difference found between the slope generated by linear regression analysis and 0.

9.4.4.3 Outcome: Tumour Volume

Caliper measurements of the subcutaneous tumours 10 days following tumour implantation were made to attempt an estimation of tumour volume. As mentioned above, at this early time point, determining tumour volume was challenging as the tumours were not yet well formed with distinct margins. No significant difference was found in tumour volume between the study groups (see Figure 100).

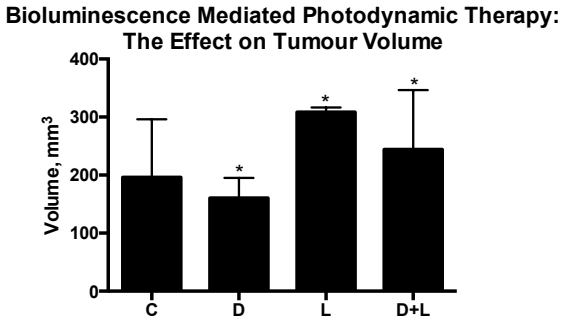

Figure 100 Bioluminescence-mediated photodynamic therapy: the effect on tumour volume – bPDT Trial 3

C = control, D = drug only, L = d-luciferin only, D+L = animals exposed to drug and d-luciferin. Asterisks indicate the degree of significance of the difference in the average tumour volume of each group compared to control, where *p > 0.05. Tumour volumes were estimated at the end of treatment. There was no significant difference in tumour volume between groups.

9.4.4.4 Outcome: Bioluminescent Signal

Animals underwent BLI the day before and the day after the end of treatment. The average bioluminescent signal in each group (see Figure 101) is presented. There was no significant difference in the bioluminescent signal between the groups at any time point.

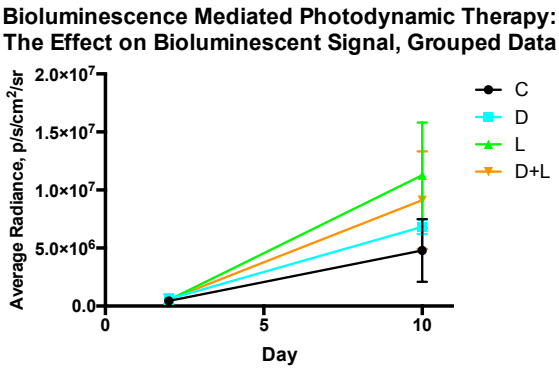

Figure 101 Bioluminescence-mediated photodynamic therapy: the effect on bioluminescent signal – bPDT Trial 3

C = control, D = drug only, L = d-luciferin only, D+L = animals exposed to drug and d-luciferin. The x axis represents the number of days following tumour implantation. The bioluminescent signal generated by the implanted cells was captured by the Xenogen IVIS 100 cooled CCD camera system after the animals were injected with 1.5 mg/g of d-luciferin ip. The bioluminescent signal within a designated ROI was expressed as average radiance and expressed quantitatively. There was no significant difference in the bioluminescent signal between the groups at any time point.

9.4.4.5 Outcome: Histopathology and Immunohistochemistry

When the mice were culled, their tumours were harvested, fixed in formalin, embedded in paraffin, and sectioned. It was noted that these tumours were not as well defined as the tumours in the previous studies, likely associated with the early end point, and the tumours were commonly harvested in several pieces. Furthermore, upon harvesting, tumours of 2 mice in the 'treatment' group were noted to be haemorrhagic and necrotic, unlike the tumours harvested from the other animals. Microscopically, although tumours in all study groups had some degree of necrosis, that of the 'treatment'group seemed more profound (see Figure 102a, b, c, and d).

Mice were injected with BrdU ip 2 hours prior to culling. The number of BrdU positive cells were expressed as the percentage of the total count and averaged for each group (see Figure 102e). There were significantly less BrdU positive cells in the 'treatment' group compared to the 'control,' 'drug only,' and 'light only' groups (23.4 ± 0.850 vs 34.6 ± 1.01, 33.9 ± 0.757, 36.8 ± 1.77, respectively, $p < 0.0001$). This suggests that the treatment caused partial inhibition of DNA replication.

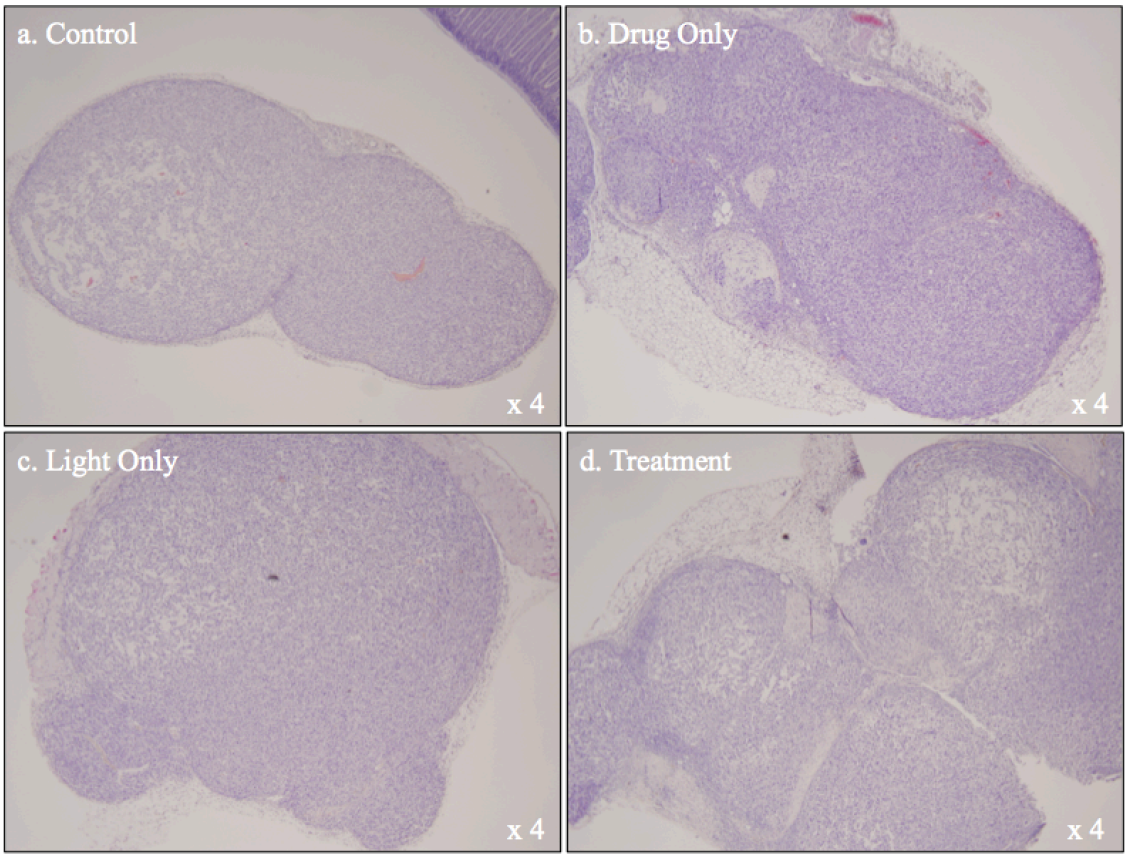

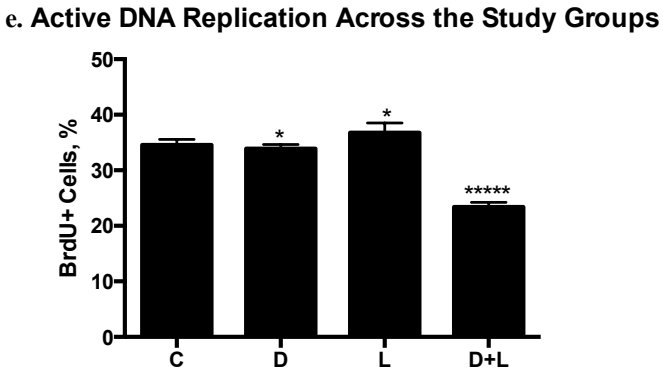

Figure 102 Histopathology and Immunohistochemistry: bPDT Trial 3

Representative H and E stained sections from the 'control' (a), 'drug only' (b), 'light only' (c), and 'treatment' (d) groups are presented. Examination of the sections suggested that although there was some degree of necrosis in all the tumours in each study group, that of the 'treatment' group was most profound. Mice were injected with BrdU ip 2 hours prior to culling. The difference in proportion of BrdU positive cells as a percentage of the total cell count is presented (e), where C = control, D = drug only, L = d-luciferin only, D+L = animals exposed to drug and d-luciferin. Asterisks indicate the degree of significance of the difference in the proportion of BrdU positive cells in each group compared to control, where *p > 0.05, ** p ≤ 0.05, ***p < 0.01, ****p < 0.001, *****p < 0.0001. There were significantly less BrdU positive cells in the 'treatment' group.

9.4.4.6 Summary: bPDT Trial 3, Subcutaneous Model

This experiment was markedly limited by time. Despite using a robust tumour model derived from U87-*luc* polyclonal cells that had undergone 3 subcutaneous passages, the tumours were not well defined either at the beginning or by the end of the treatment. For this reason, estimated tumour volumes were challenging to obtain. Nevertheless, results from attempting to validate BLI as measure of tumour progression supported findings from Trial 1, where there was poor correlation between BLI and tumour volume at such an early time point. Neither tumour volumes nor bioluminescent signal revealed a treatment effect. However, both macroscopically and microscopically, the tumours from the 'treatment' group seemed to be more necrotic, which was consistent with significantly less BrdU positive cells in the 'treatment' group, suggesting that treatment had a suppressive effect on tumour progression. If time had allowed the tumour to establish growth before the onset of treatment and the animals to have been followed for longer, trending tumour volumes and bioluminescent signal might have revealed a significant treatment effect.

9.4.5 bPDT Trial 4: Intracranial Model – U87bp-*luc* cells grown as neurospheres

Following the appropriate anaesthesia, $1x10^5$ cells of U87bp-l*uc* cells that had been grown to form neurospheres were injected in 10 µl of PBS into 18 mice. The mice were randomly designated into 'control' (n=4), 'drug only' (n=4), 'light only' (n=4), and 'treatment'groups (n=6). The day after tumour implantation treatment started. At the end of treatment, the animals underwent BLI, and weekly thereafter for 8 weeks.

9.4.5.1 Outcome: Bioluminescent Signal

Animals underwent BLI 1 week after tumour implantation, at the end of treatment, and weekly thereafter for 8 weeks. The data for the individual animals (see Figure 103a) and the average bioluminescent signal in each group (see Figure 103b) are presented.

There was no significant difference in the bioluminescent signal between the groups at any time point. The tumour from Mouse 0 from the 'treatment' group seemed to generate an aberrantly high bioluminescent signal compared to the other tumours in its group and this was consistent with the tumour having a significant extraparenchymal component (see Figure 104), discovered upon autopsy. Even when this mouse was excluded from analysis, there was no significant difference between the 'treatment' group and the controls (see Figure 103c). Lastly, closer analysis of tumour progression in the first 4 weeks following tumour implantation (see Figure 103d) revealed that only

the tumours in 3 mice entered into their exponential growth phase during this time: Mouse 2 and Mouse 3 from the 'control' group and Mouse 0 from the 'treatment' group. This was consistent with the finding that not only did the tumour from Mouse 0 of the 'treatment' group have a significant extraparenchymal component, so did Mouse 2 and Mouse 3 from the 'control' group (see Figure 104).

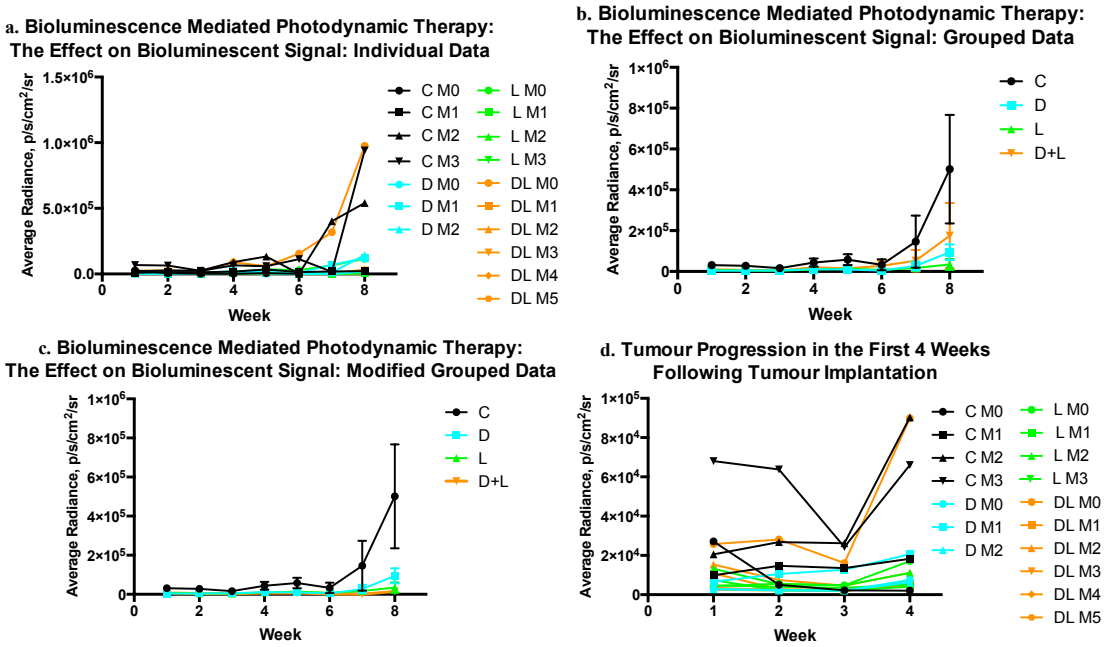

Figure 103 Bioluminescence-mediated photodynamic therapy: the effect on bioluminescent signal – bPDT Trial 4

C = control, D = drug only, L = d-luciferin only, DL/D+L = animals exposed to drug and d-luciferin, M = mouse. The x axis represents the number of weeks following tumour implantation. The bioluminescent signal generated by the implanted cells was captured by the Xenogen IVIS 100 cooled CCD camera system after the animals were injected with 1.5 mg/g of d-luciferin ip. The bioluminescent signal within a designated ROI was expressed as average radiance and expressed quantitatively. The data for the individual animals (a) and the average bioluminescent signal in each group (b) are presented. The tumour from Mouse 0 from the 'treatment' group generated a bioluminescent signal aberrantly high compared to others in its group. The average bioluminescent signal was represented having excluded this mouse from analysis (c). Overall, there was no significant difference in the bioluminescent signal between the groups at any time point. Further analysis of the first 4 weeks of tumour progression indicated that only tumours in 3 mice (Mouse 2 and Mouse 3 in the 'control' group and Mouse 0 in the 'treatment' group) entered into their exponential growth during this time, which was subsequently found to be consistent with a significant extraparenchymal component.

9.4.5.2 Outcome: Histopathology and Immunohistochemistry

When the mice were culled, their brains were harvested, fixed in formalin, embedded in paraffin, and sectioned. H and E stain revealed the tumours to be hypercellular and to consist of a monomorphic population of cells on a fibrillary background, consistent with astrocytoma. Several mitoses, as well as areas of necrosis and vascular endothelial

proliferation were evident, all of which are characteristic of a grade 4 tumour (see Figure 104).

Mice were injected with BrdU ip 2 hours prior to culling. The number of BrdU positive cells were expressed as the percentage of the total count and averaged for each group (see Figure 104f). There were significantly less BrdU positive cells in the 'treatment' group compared to the 'control,' 'drug only,' and 'light only' groups (8.38 ± 1.15 vs 21.1 ± 1.44, 24.5 ± 4.23, 25.9 ± 3.17, respectively, $p < 0.01$). This suggests that the treatment caused partial inhibition of DNA replication.

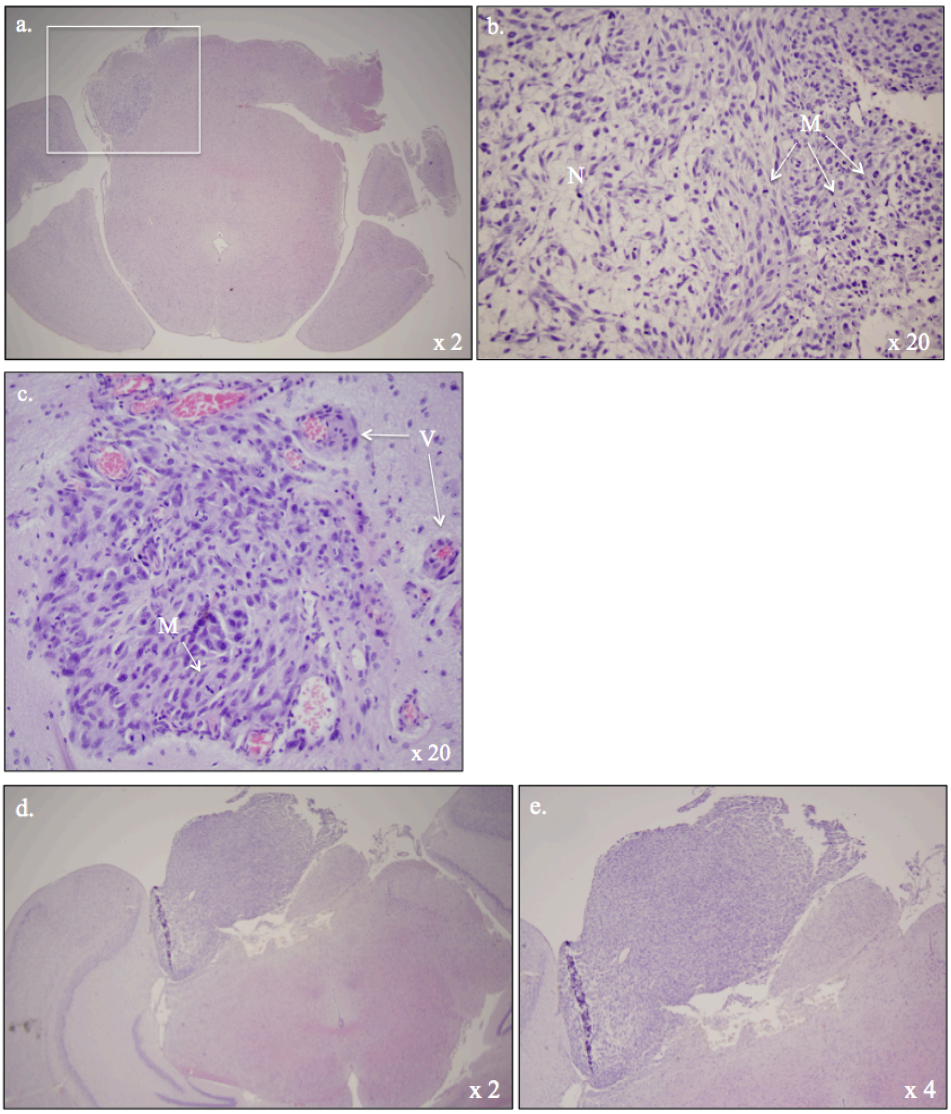

f. Active DNA Replication Across the Study Groups

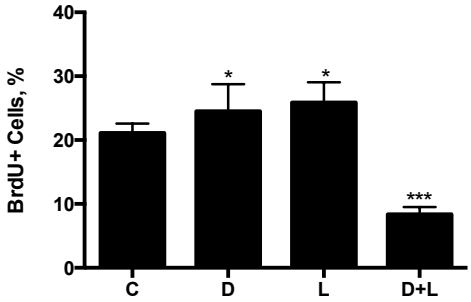

Figure 104 Histopathology and Immunohistochemistry: bPDT Trial 4

Representative H and E stained sections of the intracranial tumours from the control group of Trial 4 are shown. Most tumours were intra-axial (a). The area within the square in (a) is shown at higher magnification in (b) and (c): several mitoses (M) and necrosis (N) were seen (b), and also vascular endothelial proliferation (V) (c). Some extra-axial tumours (d and e) resulted from cell injection. Mice were injected with BrdU ip 2 hours prior to culling. The difference in proportion of BrdU positive cells as a percentage of the total cell count is presented (f), where C = control, D = drug only, L = d-luciferin only, D+L = animals exposed to drug and d-luciferin. Asterisks indicate the degree of significance of the difference in the proportion of BrdU positive cells in each group compared to control, where *p > 0.05, ** p ≤ 0.05, ***p < 0.01, ****p < 0.001, *****p < 0.0001. There were significantly less BrdU positive cells in the 'treatment' group.

9.4.5.3 Summary: bPDT Trial 4, Intracranial Model

Consistent tumour growth was not achieved despite injecting neurospheres that had been derived from U87bp-l*uc* cells (compare to Figure 83c). Due to time constraints, treatment had to start the day after injection, rather than after giving the tumours time to become well established as in the pilot (see section 9.3). Furthermore, some cell injections led to extraparenchymal tumours, indicating that our technique required refining. However, the tumours that did develop displayed characteristics consistent with grade 4 astrocytoma.

BLI data did not reveal a treatment effect. This was not unexpected as validation studies in the subcutaneous tumour models advise that these results should be interpreted with caution. Validating BLI as a reliable measure of tumour progression was not possible in the intracranial model as CT was found not to be sensitive enough to detect the tumours and MRI was not available. 2D or even 3D capture of bioluminescence might have been more accurate.

Immunohistochemistry demonstrated significantly fewer BrdU positive cells in the 'treatment' group compared with the control groups. As in the other trials, this represents a treatment effect where treatment has been shown to suppress tumour growth.

9.5 Summary and Discussion

A summary of the results from the 4 trials of bPDT is given in Table 13.

	bPDT Trial			
	1	**2**	**3**	**4**
Model	Subcutaneous, Passage 4	Subcutaneous	Subcutaneous, Passage 3	Intracranial
Cell line of origin	U87-*luc* polyclonal cells	U87-*luc* polyclonal cells	U87-*luc* polyclonal cells	Neurospheres from U87bp-*luc* cells
Duration of study	26 days	9 weeks	10 days	8 weeks
Outcomes				
Survival	Trend towards improved survival	No difference in survival	-	-
Tumour Volume	Trend towards a decrease in tumour volume	-	No difference in tumour volume	-
Bioluminescent Signal	Trend towards a reduction in bioluminescence signal	No difference in bioluminescence signal	No difference in bioluminescence signal	No difference in bioluminescence signal
Histopathology	Increased necrosis	-	Increased necrosis	-
Immunohistochemistry	Reduced proportion of BrdU positive cells, $p < 0.0001$	No difference in proportion of BrdU positive cells	Reduced proportion of BrdU positive cells, $p < 0.0001$	Reduced proportion of BrdU positive cells, $p < 0.0001$

Table 13 Summary of findings from the 4 trials of bPDT

The results for the treatment group are described for each outcome compared to the control groups.

bPDT Trial 1 was the most comprehensive study. It revealed a trend towards reduced tumour growth and delay in the start of the exponential growth phase with treatment, particularly evident when following tumour volumes. This was consistent with the

trend towards improved survival and the significantly reduced proportion of BrdU positive cells in the 'treatment' group.

A trend towards a treatment effect when measuring survival, tumour volume, or bioluminescent signal was not seen in the other trials. However, bPDT Trials 3 and 4 did reveal a significantly reduced proportion of BrdU positive cells in their 'treatment' groups. Endpoints for bPDT Trial 3 were taken at the cessation of treatment and provide the most accurate insight into the immediate effects of bPDT. Interestingly, after a long follow up of 8 weeks in bPDT Trial 4, a treatment effect still persisted, with a significantly reduced proportion of BrdU positive cells.

In contrast, in bPDT Trial 2, which had a long follow up of 9 weeks, there was no significant difference in the proportion of BrdU positive cells in the 'treatment' group compared to the control groups. This was most likely secondary to the length of follow up (9 weeks) and any initial treatment effect, as indicated by bPDT Trial 3, would likely have been masked.

Overall, in 3 out of 4 trials, 2 in subcutaneous models and 1 in an intracranial model, a treatment effect was demonstrated by there being significantly fewer BrdU positive cells in the 'treatment' group compared to controls, indicating suppression of tumour cell replication and growth. Although numbers are small, these results are encouraging, and further investigation is certainly warranted.

In order to develop this study further, a number of adjustments should be made. Firstly, the development of a more reliable and robust intracranial model is required. A reliable subcutaneous model has been achieved by serial subcutaneous passaging. Consistent with the literature, the morphology of the subcutaneous tumours displayed the characteristics of a high-grade astrocytoma and there was little change from one passage to the next[172]. Although successful xenografting of luciferase-expressing U87 cells into mouse brain has been described[175], development of a model for this study was challenging. The transplantation of neurospheres was associated with the best survival rate, and those tumours displayed features consistent with a grade 4 astrocytoma. However, bPDT Trial 4 demonstrates that the neurospheres should be given time to establish growth before treatment is commenced. Furthermore, mirroring the serial passaging technique of the subcutaneous model, perhaps the neurospheres should be

passaged several more times by harvesting established intracranial tumours and growing neurospheres in culture, then re-injecting them intracranially, to develop a more reliable subculture. Failing these methods, a different host, such as a Swiss Webster nude mouse, which was used in the study cited above, could be tried.

Although BLI has been validated and used as a method of following tumour progression in subcutaneous[132] and intracranial[175,176,197] models used for testing various treatments, results of this study indicate that BLI may not be wholly reliable, particularly when tumours are either small or large. Ideally, for proof-of-principle studies, BLI would have to be validated within the studies. For the subcutaneous tumours, growth can also be followed by caliper measurements, as performed here. Following growth of intracranial tumours would be more challenging: CT is not sensitive enough to detect these small tumours and MRI is time consuming, and the length of anaesthetic required demanding on the wellbeing of the mouse. Part of the intracranial study may need to involve mice being culled at specified time points, the tumours dissected out and sectioned, and a volume measured. This would then be correlated with a BLI signal obtained just before the mouse was culled.

Lastly, in order to provide proof-of-principle, some variations within the treatment protocol could be made. One option would be to increase the concentration of d-luciferin loaded into the osmotic pumps thereby increasing the amount of sustained bioluminescence that could be generated. A study to find the optimal concentration of d-luciferin would need to be undertaken, such that there would be no toxicity to the host or the tumour and such that the enzyme, luciferase, would not be saturated. Another option would be to supplement the d-luciferin delivered by the pump with ip boluses of d-luciferin. The boluses could be given 3 times a day either over the 7 days of treatment or only over 2 days to cover the 36-48 hrs of peak tissue *m*THPC concentration.

Although limited by time and resources, results from this study are definitely encouraging with 3 of the 4 trials consistently showing a suppressive effect on DNA replication. A more robust intracranial model, more reliable methods of following real-time tumour progression, and changes to treatment protocol may all provide definitive proof-of-principle.

Part 3 Conclusion and The Future

Chapter 10 Future Directions

10.1 Summary of Results

Experiments in cell culture have shown that bioluminescence, generated by the addition of d-luciferin to luciferase-producing cells, is able to activate a photosensitiser, and mediate a photodynamic effect resulting in significant cell death: bPDT. This has been most thoroughly studied in U87-*luc* cells: a cell line derived from a human grade 4 astrocytoma cloned to express luciferase. Incubation of these cells with the photosensitisers, hypericin or *m*THPC, led to significant cell death with the addition of d-luciferin. When these experiments were repeated in non-luciferase producing U87 cells, there was no change in cell survival, demonstrating that it is not the chemical interaction between photosensitiser and d-luciferin, but the interaction between photosensitiser and the bioluminescence generated by the addition of d-luciferin that leads to cell death. Moreover, lycopene was able to inhibit the cell death that occurred when the luciferase-producing cells were incubated with photosensitiser followed by d-luciferin. This further supports that cell death is occurring by a photodynamic effect, which is mediated by singlet oxygen, and hence, is inhibited by the presence of an anti-oxidant such as lycopene.

In animals xenografted with luciferase-expressing U87 cells subcutaneously or intracranially, then treated with a systemic photosensitiser and continuous d-luciferin, DNA replication within the tumour is consistently suppressed. This was demonstrated by finding significantly fewer BrdU positive cells in harvested tumours of the 'treatment' group compared to controls. In the most comprehensive study where tumours were xenografted subcutaneously, treatment was also associated with a trend towards suppression of tumour growth, as shown by trending tumour volumes, and improved survival. Although limited, these early *in vivo* studies suggest a bPDT effect.

As discussed above, in the first instance efforts should be made to provide definitive proof-of-principle in animals transplanted with luciferase-expressing U87 cells. This will involve developing a more robust and reliable intracranial animal model and optimising the treatment protocol, mainly by improving light dosimetry. If bPDT mediated cell kill can be demonstrated effectively, then the ability of bPDT to kill the infiltrating cells of high-grade astrocytomas that underlie the poor prognosis of disease can be tested. For these experiments, an animal model that can replicate the true

invasive nature of high-grade astrocytoma will be needed, and methods of targeting the tumour to confer an ability to bioluminescence will need to be developed.

10.2 Transgenic Animal Models

Xenograft models, as used in this study, lack the stepwise genetic changes that are thought to underlie tumour development. Furthermore, implanted cells have often undergone several passages leading to alterations in genetic profile due to different selective pressures[198]. As a result, xenograft tumours rarely recapitulate the phenotype of the desired tumour: intracranial injection of human high-grade glioma cells into mice tend to form well circumscribed, compact tumours with little infiltration into the surrounding brain parenchyma[199,200]. In contrast, by replicating mutations in genes characteristic of a particular human malignancy, strains of mice have been genetically engineered to spontaneously and predictably develop tumours with similar characteristics to the human malignancy: the phenotype of the desired tumour is therefore more accurately represented. In the case of grade 4 astrocytoma, a transgenic model should replicate the true invasive nature of the disease.

Inactivation of several tumour suppressor genes has been implicated in the development of gliomas, such as *Nf1*, *PTEN*, and *Rb*. However, global knockout of these genes, which are widely expressed, would likely result in early lethality[201]. More recently, the Cre/lox system has been used to limit gene modifications or deletions to specific cells of interest. This strategy requires two stages. The first stage is to generate transgenic mice that express the Cre enzyme under the control of a cell-specific promoter. The second stage requires the breeding of the Cre transgenics with mice carrying an allele containing the critical region flanked by loxP sites. This results in excision of the floxed sequence specifically in the cells expressing the Cre transgene[202-204]. With respect to astrocytomas, a transgenic mouse line expressing Cre under the control of the promoter of glial fibrillary acidic protein (GFAP), a protein relatively specific to astrocytes, has been developed[205]. Recombination of floxed *Rb*, *p53*, and *PTEN* alleles in various combinations by tamoxifen-inducible GFAP-cre activation in parenchymal astrocytes and subventricular zone progenitor cells has yielded high-grade astrocytomas[206-208]. Furthermore, recombination of floxed *p53* and *PTEN* in combination by an *h*GFAP-Cre transgene has been shown to generate a tumour with striking clinical, pathological and molecular resemblance to grade 4 astrocytoma in humans[209].

An additional advantage of such transgenic models compared to tumour xenografts is that they can remain immunocompetent. As the cell kill caused by PDT is partly mediated by stimulation of the host immune system, the use of a transgenic model of grade 4 astrocytoma will allow a more true reflection of the cell kill that can be achieved with bPDT.

10.3 Targeting Astrocytomas *in situ*

With a transgenic animal model that will spontaneously develop an intracranial tumour with clinical, histopathological, and molecular characteristics similar to that of a grade 4 astrocytoma, in order to test bPDT, a method of conferring the ability to bioluminesce to the tumour cells has to be found. Firstly, the cells of the astrocytoma have to be targeted. Then, once targeted, either the luciferase enzyme or the gene encoding for the enzyme, *luc*, can be delivered to the cell.

10.3.1 Potential Targets

The recognition that epigenetic silencing of the *MGMT* (O^6-methylguanine-DNA methyltransferase) gene by promoter methylation is associated with a survival advantage and an increased responsiveness to temozolomide chemotherapy in those with grade 4 astrocytoma[24] spurred the interest in the molecular characterisation of gliomas. Extensive genetic analyses across a range of diffuse gliomas have been carried out[210,211] and amongst many genetic alterations, mutations in two particular genes have been associated with grade 4 astrocytoma; epidermal growth factor receptor (*EGFR*) and isocitrate dehydrogenase 1 (*IDH1*).

Clinically, two types of grade 4 astrocytoma have been identified; primary and secondary. Primary tumours are those that develop *de novo*. They are typically associated with an older age of presentation and a relatively rapid clinical progression. Secondary tumours arise from lower grade tumours and typically arise in younger patients. Although primary and secondary tumours have similar histopathological features, they differ markedly on a molecular level.

Primary grade 4 astrocytomas are classically characterized by the amplification and mutation of *EGFR*. Amplification of *EGFR* leads to overexpression of the EGFR protein, and is the most common genetic alteration, occurring at frequencies of 34-63%[212-218]. Of these cases, 63-75% also carry mutations of the gene, resulting in

tumours carrying both the wild type (wt) and mutated receptor[213,219-222]. The most common mutation is an inframe deletion of exons 2-7, leading to translation of the mutated protein termed EGFRvIII, which is found at a frequency of 25-64%. Epidermal growth factor receptor is a transmembrane, tyrosine kinase, cell surface receptor. Activation of the receptor by its growth factor ligands leads to a transition from an inactive monomeric form to an active homodimer, and this dimerisation stimulates its intrinsic intracellular protein-tyrosine kinase activity, ultimately resulting in DNA synthesis and proliferation. EGFRvIII, the mutated receptor, is tumour specific and devoid in normal tissues. It is not able to bind any known ligands. Despite this, EGFRvIII displays constitutive signalling that is augmented by reduced internalization and downregulation. It has been found to be the driving force in tumour progression, being clinically correlated with increased glioma cell growth, proliferation, invasion, and angiogenesis[222-224]. Some studies suggest that EGFRvIII is associated with poor prognosis[216,225]. One study has shown that EGFRvIII expression in combination with EGFR gene amplification is an independent and significant negative prognostic factor for survival[216]. Although, not all studies have been able to link EGFRvIII with patient outcome[226,227], EGFR and EGFRvIII are potential targets for primary grade 4 astrocytomas.

In contrast to *EGFR*, mutations in *IDH1* have been shown to be expressed at high frequency in approximately 75% of all glioma subtypes except for primary grade 4 astrocytoma. As mutations in *IDH1* are homogenously expressed in all tumour cells, even single infiltrating cells, it has been hypothesised that mutations in *IDH1* represent some of the earliest genetic events that drive the malignant transformation of lower grade tumours. In fact, mutations in *IDH1* are so fundamental to gliomas that two large studies of glioma genetics[211,228] base their classification of gliomas on the presence or absence of the mutation in combination with the presence of other key alterations e.g. 1p 19q co-deletion. IDH1 is an enzyme located in the cytoplasm and in peroxisomes where it participates in lipid metabolism and glucose detection. It catalyses the oxidative decarboxylation of isocitrate to 2-alpha ketoglutarate (αKG). The most widely cited tumour-specific mutation of *IDH1* consists of a missense mutation at amino acid 132 that replaces an active site arginine residue with histidine. The mutant enzyme consists of a dimer between the wild-type and mutant proteins. Among many proposals of how mutant IDH1 leads to tumourogensis, one suggests that whereas normal IDH1 converts isocitrate to αKG, mutant IDH1 converts αKG to 2-

hydroxyglutarate (2HG)[229]. It has been suggested that 2HG inhibits a variety of dioxygenases, including prolyl hydroxylase, *TET2,* and histone demethylases[230], which could trigger aberrant angiogenesis and aberrant gene expression. Interestingly, the presence of the *IDH1* mutation has been shown to be a prognostic indicator, but not predictive of response to therapy[231-236]: patients with the mutation have a better prognosis that those without. Due to its high frequency in gliomas except for primary grade 4 astrocytomas, the IDH1 mutant enzyme could potentially be a good target for secondary grade 4 astrocytomas.

Notably, as well as providing information on potential targets, the molecular classification of gliomas has been found to capture the biologic features of glioma variants better than histopathological evaluation. Indeed, it is beginning to redefine the range of gliomas and their treatment.

10.3.2 Method of Delivery: Conjugation to a Monoclonal Antibody

Monoclonal antibodies to EGFR have been developed and have been trialed as anti-tumour agents in themselves. Cetuximab is a recombinant human-murine chimeric monoclonal antibody specifically targeting EGFR. It is has been approved for use in the treatment of metastatic colorectal cancer, metastatic non-small cell lung cancer, and squamous cell carcinoma of the head and neck. *in vitro* and *in vivo* studies of grade 4 astrocytoma have shown that cetuximab is able to bind to both EGFR[237,238] and EGFRvIII[239,240] with high specificity and affinity, and has effective anti-tumour activity. Phase 1 studies with nonhumanised anti-EGFR monoclonal antibody demonstrated the presence of the monoclonal antibody within resected glioma tissue[241,242]. Unfortunately, phase II studies have been disappointing in not revealing a robust effect of cetuximab against grade 4 astrocytoma[243].

Nevertheless, the targeting capabilities of monoclonal antibodies raised against EGFR and EGFRvIII, like cetuximab, have been exploited. These antibodies have been successfully used to selectively deliver boron for neutron capture therapy[244] and chemotherapeutic agents such as methotrexate[245] *in vivo*, as well as radiolabelled iodine in humans[246,247], to treat grade 4 astrocytomas by direct conjugation. A systemically administered cetuximab-fluorescent probe conjugate was sensitive and specific enough to human grade 4 astrocytoma cells transplanted subcutaneously and intracranially in mice to allow optimisation of resection by fluorescence guidance[248].

Furthermore, a monoclonal antibody has been raised against the protein resulting from the most common *IDH1* mutation[249]. Although there has been some recent interest in developing vaccinations against IDH1 and its mutant proteins[250,251], overall there is little in the literature regarding their targeting.

With monoclonal antibodies being raised against two potential targets for grade 4 astrocytoma, EGFR and IDH1, and their mutants, and evidence that chemicals with therapeutic potential can be conjugated to these antibodies, suggests that perhaps the enzyme luciferase can also be conjugated to these monoclonal antibodies. Certainly, luciferase has been successfully conjugated to a monoclonal antibody. An anti-carcinoembryonic antigen (CEA) antibody fragment, anti-CEA diabody, has been fused to luciferase from Renilla reniformis to generate a novel optical imaging probe that when injected intravenously successfully localizes to subcutaneously transplanted CEA expressing cells and causes those cells to bioluminesce[252] with the addition of coelenterazine as the substrate.

10.3.3 Method of Delivery: Nanoparticles

Nanoparticles are objects generally less than 100 nm in dimension. There are several general advantages to using nanoparticles as a drug delivery platform. Firstly, the loading and releasing of active agents can be controlled: the loaded amount is controlled by changing the size of the nanoparticle or the number of linkers inside and on the surface of the nanoparticles, and release can be controlled by the type of nanoparticle polymer matrix. Secondly, specific molecular targeting factors can be attached for localized binding to and/or uptake by the tumour cells. Thirdly, a hydrophilic coating can be given to the nanoparticle to reduce uptake by the reticular endothelial system, thereby increasing drug delivery to the tumour and reducing systemic side effects. Fourthly, the nanoparticle matrix provides protection for the drug from enzymatic or environmental degradation. Lastly, the nanoparticle can overcome multidrug resistance by masking the drugs trapped inside it.

Specific to brain cancer, the biggest challenge in delivering drugs is overcoming the BBB, and some nanoparticles have been found to successfully cross the BBB. They are often nanoparticles covalently linked to peptides or coated with surfactant (for example polysorbate). The exact mechanism of nanoparticle transport into the brain is not fully understood, but most likely relies on receptor-mediated endocytosis, phagocytosis, and/or passive leakage of nanoparticles across defects in the BBB[253,254]. For example,

nanoparticles conjugated with synthetic peptides similar in structure to opioid peptides can be successfully transported across the BBB, presumably via the mechanism used by endogenous opioid peptides[255]; the opioid peptides binding to specific receptors on the capillary walls, which help carry them into the brain[256]. Additionally, polysorbate coated nanoparticles are thought to mimic low-density lipoproteins (LDLs), allowing them to be transported into the brain by the same endocytotic process LDLs undergo at the BBB[257,258]. Polysorbate 80-coated poly(butyl cyanoacrylate) nanoparticles have enabled an improved distribution of doxorubicin into the brain. Rats xenografted intracranially with grade 4 astrocytoma were given different intravenous formulations of doxorubicin, including one formulation where doxorubicin was bound to polysorbate-coated nanoparticles. High intracerebral doxorubicin concentrations were achieved with this formulation, whereas all control preparations did not achieve any detectable levels in the brain[259]. Furthermore, animals treated with this formulation had significantly longer survival times compared with all other groups with over 20% of the animals showing long term remission. Histology also confirmed smaller tumour sizes and lower values for proliferation and apoptosis in the group[260].

10.3.3.1 Targeting Nanoparticles

Not only can nanoparticles cross the BBB, but they can also be designed to target brain tumours. Two different monoclonal antibodies, an anti-mouse transferrin receptor antibody and a mouse autoimmune anti-nucleosome antibody 2C5, have been simultaneously covalently conjugated onto a poly(beta-L-malic acid) drug delivery nanoplatform. The active anti-tumour drug, antisense oligonucleotides to vascular protein laminin-8, were attached to the same carrier molecule. The resulting drug was administered intravenously into mice bearing xenografted intracranial gliomas. The anti-mouse transferrin receptor antibody targeted the mouse endothelial system, allowing uptake of the drug across the BBB, and the anti-nucleosome antibody 2C5 targeted the tumour cell surface. The targeting efficacy with two antibodies was found to be greater than with one antibody alone[261].

Human grade 4 astrocytomas have been found to selectively express receptors for IL13[262] and when liposomes are conjugated with IL13, they will deliver chemotherapeutics to subcutaneously xenografted gliomas in mice more effectively than unconjugated liposomes. Furthermore, when mice bearing intracranial U87 xenografts were given ip doxorubicin encapsulated by IL13-conjugated liposomes, they had a 5-fold reduction in intracranial tumour volume over 6 weeks and 4 of the 7

animals survived beyond 200 days after tumour implantation. In contrast, the animals that received doxorubicin encapsulated by unconjugated liposomes displayed no evidence of reduction in tumour size and did not survive beyond 35 days.

Another glioma targeting molecule that has been conjugated with nanoparticles is Chlorotoxin (Cltx). Unlike other targeting ligands that are specific to only certain types of glioma cells e.g. the EGFR receptor, Cltx targets the vast majority of glial-derived tumours[263]. It is a small 36 amino acid peptide purified from the venom of the giant Israeli scorpion and binds with high affinity to the membrane-bound matrix metalloproteinase-2 (MMP-2) endopeptidase, which is preferentially upregulated in gliomas[264-266]. A nanoprobe synthesized by coating iron oxide nanoparticles with covalently bound bifunctional polyethylene glycol polymer and functionalized with Cltx and a near infrared fluoresceing molecule is preferentially taken up by glioma cells *in vitro*, as demonstrated by MRI and fluorescence microscopy[267]. Conjugating small peptides such as Cltx on nanoparticles is attractive, as they overcome the restrictions of the widely used antibodies, which are bulky, exhibit a short half-life in blood[268], have limited tissue penetration[269] and retention[268], and have reduced cellular uptake[269].

10.3.3.2 Nanoparticles and PDT

Nanoparticles have been engineered to deliver photosensitisers for PDT to brain tumours. F3 is a vascular homing peptide specific to the angiogenic endothelial cells within tumour vasculature. An F3 targeted polymeric nanoparticle was engineered to encapsulate iron oxide and the photosensitiser, Photofrin®[270]. The nanoparticle was delivered intravenously to rats bearing 9L gliomas xenografted intracranially. The animals underwent PDT with the light source being introduced via the same burr hole used for xenografting the tumours. Tumour uptake of the nanoparticle was confirmed with MRI, which could detect the iron oxide. Increased survival was associated with use of the F3 targeted Photofrin® encapsulated nanoparticle, compared to use of a non-targeted Photofrin® encapsulated nanoparticle or Photofrin® alone.

10.3.3.3. Nanoparticles and Bioluminescence

Nanoparticles that confer bioluminescence have also been designed. Renilla luciferase has been successfully conjugated to gold nanoparticles, which were then used for protease detection[271]. Moreover, a gold nanoparticle (AuNP)-capped mesoporous silica nanoparticle (Au-MSN) platform has been used to co-deliver luciferase and luciferin to

cells. Luciferin is released from the interior pores of MSN upon AuNP uncapping in response to disulfide-reducing antioxidants. Simultaneously, luciferase is co-delivered from the PEGylated exterior surface of Au-MSN. When such nanoparticles are incubated with HeLa cells, the cells are subsequently seen to bioluminesce[272]. There are several advantage to such a co-delivery system. Mesoporous silica nanoparticles are excellent candidates for co-delivery as they have an interior pore and exterior particle surface for loading various guest molecules. Additionally, luciferin has a short half-life and encapsulation by a nanoparticle allows a greater concentration of luciferin to be delivered directly to the cell, thereby potentially increasing the degree of bioluminescence that can be generated.

Not only are nanoparticles able to deliver luciferin and luciferase, but they can also deliver the gene that encodes luciferase (*luc*). Gelatin nanoparticles loaded with plasmids containing luciferase DNA (pCMV-*luc*) have been used to successfully transfect B16 and F10 cells in culture with *luc*, conferring to them an ability to bioluminesce with the addition of luciferin[273]. A deferoxamine-coated superparamagnetic iron oxide nanoparticles containing circular plasmid DNA of Renilla luciferase has been shown to be internalised by U87 cells[274].

Luciferase gene delivery via nanoparticles has also been successful *in vivo*. Compacting *luc* into discrete nanoparticles using polyethylene glycol-substituted poly-l-lysine, the formulation was then delivered into mice via intratracheal and intranasal instillation[275]. Luciferase activity was then measured in lung tissue post mortem. Mice that were given the compacted *luc* plasmid were not only found to display luciferase activity in their lungs, as measured by the degree of bioluminescence generated with the addition of substrate, but this activity was 200 fold more than that seen in animals treated with naked DNA.

10.3.4 Method of Delivery: Viral Vectors

A more classic method of gene delivery is via viral vectors. Indeed, the luciferase gene has already been incorporated into several different viral vectors, mainly to act as a reporter gene.

One of the most favoured vectors is that of the adenovirus. Adenoviruses have evolved into being highly efficient at delivering, transcribing, and translating their genome in eukaryotic cells. They are known to infect a wide variety of human cells. The two

particular serotypes that are most extensively used in clinical applications, Ad5 and Ad2, are associated with self-limiting and usually mild human diseases, most commonly respiratory tract infections, gastroenteritis, and conjunctivitis. Adenoviruses have long been engineered to function as vectors for delivering therapeutic genes by replacing part of their genome with a therapeutic anticancer gene[276]. The region that is typically replaced is the part that would prepare the host cell for viral DNA replication by driving the host cell into S phase and suppressing the host cell's apoptotic machinery, otherwise known as the E1 region. By replacing another region, termed the E3 region, which modifies the host's immunological environment, larger inserts can be introduced. As these regions are of vital importance in viral replication, removing them typically renders the adenovirus replication deficient and converts it from being a lytic pathogen to a vector for gene delivery. Specific to brain tumours, adenoviruses have been used to deliver the herpes simplex-thymidine kinase (HSV-TK) gene, the interferon-β gene, the interferon-α gene, and the p53 gene. These have been tested in phase 1 clinical trials.

With regards to the luciferase gene, an adenovirus recombinant containing the firefly luciferase gene (Ad5-Luc 3) has been shown to infect HeLa cells *in vitro* with relative efficiency[277]. When inoculated into mice via ip injection, luciferase activity was subsequently detected in the liver, spleen, kidney, and lung. Although a single ip inoculation was sufficient to raise anti-luciferase antibodies, luciferase activity could still be detected in these organs following a second inoculation. Adenoviral vectors have also been engineered where the luciferase gene replaces either the E1 or E3 region whilst maintaining their oncolytic and replication properties. In this way, the luciferase gene acted as reporter enabling BLI to assess the effect of the virus on a panel of glioma cells in culture, and also on a subcutaneously xenografted U87 tumour in a mouse model when injected intratumourally. The effectiveness of BLI was independent of the position of luciferase gene insertion[278].

An alternative to an adenovirus vector is a lentivirus vector, which enables stable integration of a transgene into the host genome irrespective of their state of division[279,280]. A bimodal viral vector has been engineered by fusing a lentivirus vector with the dual bioluminescent and fluorescent markers, Renilla luciferase-DsRed2 and GFP-Renilla luciferase[281]. Human neural stem cells were transfected with these vectors

in vitro, then implanted intracranially into mice. The migration of the stem cells could then be followed by BLI.

The luciferase gene has also been successfully incorporated into herpes simplex virus vectors. For example, the luciferase gene has been integrated into a herpes virus vector under the control of a tetracycline-responsive promoter system allowing BLI to reveal the effect of using tetracycline to control inducible gene expression *in vitro* in cultures of hippocampal neurons and *in vivo* when directly injected intracerebrally into Ammon's horn of the hippocampus[282].

Lastly, the luciferase gene has been integrated into the vaccina virus, which is attractive as a vector because due to its large size there are many non-essential genes that can be exchanged for therapeutic genes. A gene encoding a bioluminescent-fluorescent fusion protein (Renilla-luciferase-Aequorea green fluorescent protein) has been inserted into a vaccina virus vector[283] and when given intravenously to human breast tumour bearing nude mice, BLI clearly demonstrated localisation of the vector to the tumour and allowed the response of the tumour to the oncolytic properties of the vector to be followed over time[284].

10.4 Concluding Remarks

The concept of bioluminescence-mediated PDT was conceived to overcome the diffuse infiltrative nature of grade 4 astrocytoma. The *in vitro* studies carried out here have provided proof-of-principle that bPDT can lead to tumour cell kill in human grade 4 astrocytoma derived cell lines. Results from the *in vivo* studies carried out in subcutaneous and intracranial mouse models with xenografted tumours derived from human grade 4 astrocytoma derived cell lines provide encouraging results. However, to provide definitive proof-of-principle in an *in vivo model*, a more robust and reliable intracranial animal model is needed and the treatment protocol requires optimisation. With such improvements, we contend that proof-of-principle *in vivo* is hopeful.

Once achieved, to advance the field, bPDT will need to be proven in a transgenic animal model, where the diffuse and infiltrative nature of grade 4 astrocytoma is recapitulated. With the Cre/loxP system, there are several options. However, before doing this, a means of targeting the tumour cells to confer to them the ability to bioluminesce must be found. Understanding the molecular biology of grade 4

astrocytoma has provided several targeting options, and several delivery platforms have been explored. Of these, nanoparticles do seem the most versatile. With nanoparticles, either the luciferase protein or the gene encoding luciferase can be delivered to the tumour cell, with or without luciferin, and targeting options can include a more traditional antibody or a smaller peptide.

Such an endeavour draws from so many scientific disciplines that include photobiology and photochemistry, molecular biology, and nanotechnology; and the specific interest in grade 4 astryoctoma requires expertise in neurobiology, neuroscience and neuropathology. It is vital that time be spent in developing an infrastructure that can support success in this intriguing field of study.

Appendix

1 Conventional Photodynamic Therapy, 'Light Only' Wells

The effect of exposing U87, U251, MCF-7 and NIH 3T3 cells to varying light intensities compared to a 'control' not exposed any light, as part of the conventional PDT experiments described in Chapter 6.2, is presented here. Where more than one graph is used to illustrate the effect of varying light intensities on a particular cell line, this represents separate experiments where those particular light intensities were tested at separate times.

1.1 Short Incubation Experiments

See Figure 105. For U87 cells, there is no significant difference in survival between 'control' and the cells exposed to light, regardless of light intensity. For U251 cells, strict p-value interpretation would indicate the exposure to 1 sec of light caused significant toxicity. However, the OD of cells exposed to this intensity of light was 82.8% of control and the 95% CI (0.0191 – 0.187) extremely close to 0, hence, the result was not considered significantly different from control. Exposure to 180 secs of light caused significant cell growth in MCF-7 cells. Similarly, exposure to 10 and 180 secs of light caused significant cell growth in NIH 3T3 cells.

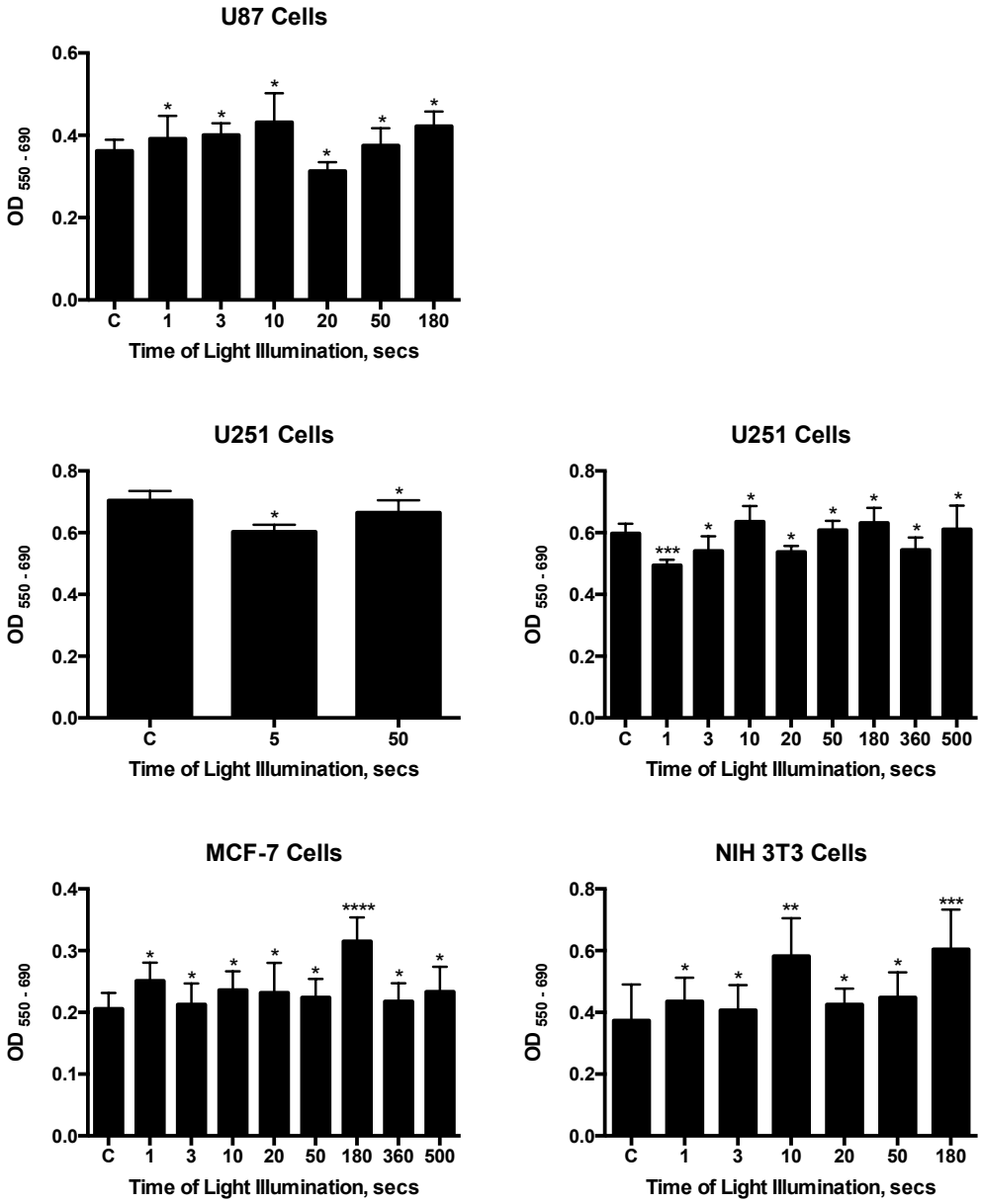

Figure 105 The Effect of Exposing Cell Lines to Varying Intensities of Light in 'Short Incubation' Experiments

For U87 and U251 cells, exposure to varying intensities of light has no significant effect on cell growth. Although p-value interpretation would indicate exposure of U251 cells to 1 sec of light is toxic, the actual OD of these cells is 82.8% of control and the 95% CI (0.0191-0.187) close to 0, hence, this intensity of light was not considered toxic. For MCF-7 cells, exposure to 180 secs of light stimulated growth, as did exposure of NIH 3T3 cells to 10 and 180 secs of light.

1.2 Long Incubation Experiments

See Figure 106. For U87 cells, exposure to 3 secs of light caused significant cell growth. Likewise, exposure of U251 cells to 5 and 500 secs of light caused significant cell growth. For MCF-7 and NIH 3T3 cells, exposure of cells of light to various light intensities caused no significant change in cell growth compared to control.

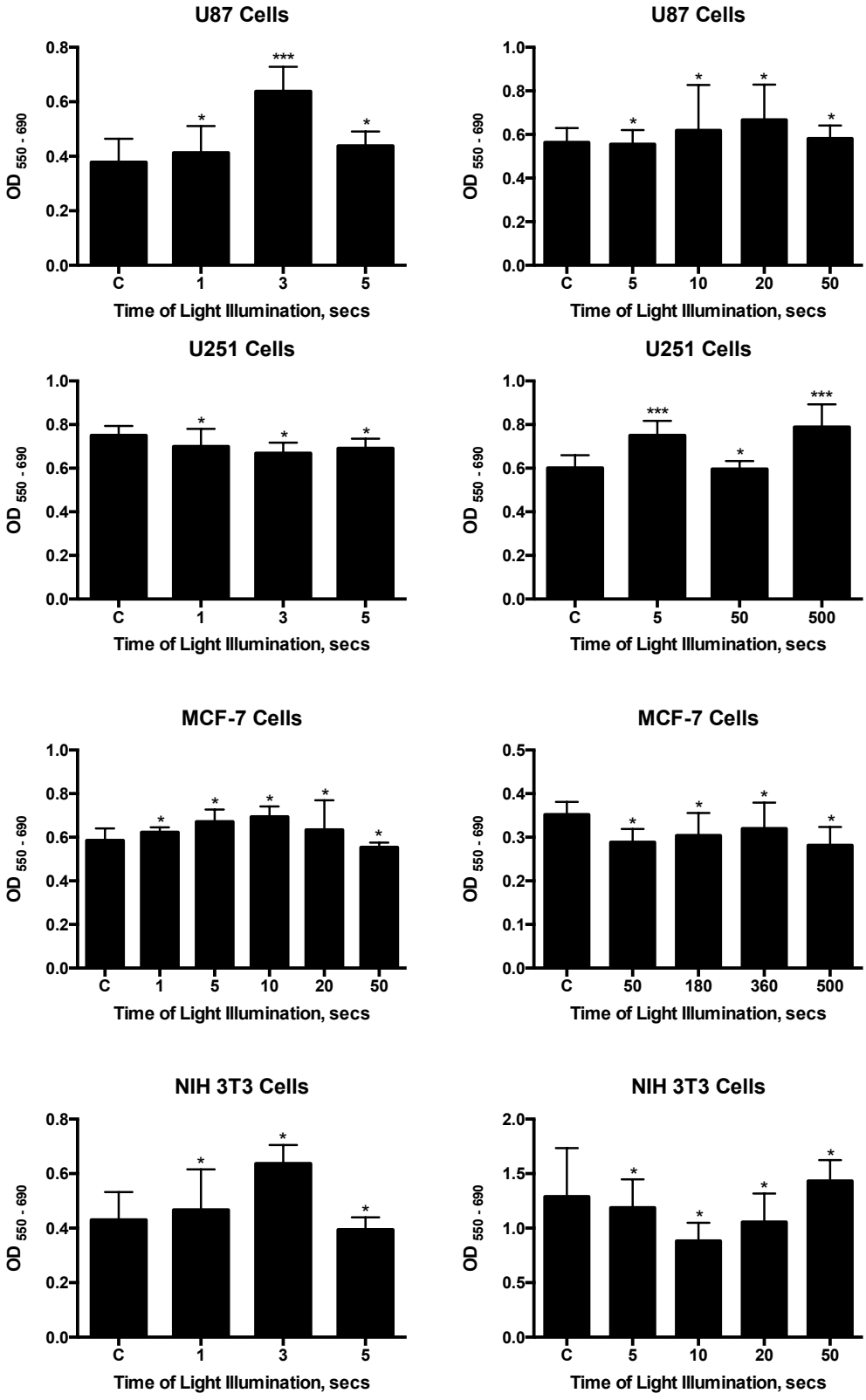

Figure 106 The Effect of Exposing Cell Lines to Varying Intensities of Light in 'Long Incubation' Experiments.

Exposure of U87 cells to 3 secs of light caused significant cell growth. Likewise, exposure of U251 cells to 5 and 500 secs of light caused significant cell growth. Exposure of MCF-7 and NIH 3T3 cells to light to various intensities caused no significant change in cell growth compared to control.

Exposure to light alone has been show to be non-toxic to cells, and this is well-established in the literature[153]. Moreover, in some circumstances, light has been shown to cause cell proliferation: MCF-7 cells with a light fluence of 1260 $mJcm^{-2}$ (equivalent to180 secs of illumination) and NIH 3T3 cells with light fluences of 70 and 1260 $mJcm^{-2}$ (equivalent to 10 and 180 secs of illumination) in the short incubation experiments, and U87 cells with a light fluence of 21$mJcm^{-2}$ (equivalent to 3 secs of illumination) and U251 cells with light fluences of 35 and 3500 $mJcm^{-2}$ (equivalent to 5 and 500 secs of illumination) in the long incubation experiments. This phenomenon of low light fluences stimulating cell growth has been described in the literature in both non-tumour[285] and tumour cell lines[152]. Suggested underlying mechanisms include an increase in the transmembrane electrochemical proton-gradient in mitochondria stimulating calcium release into the cytoplasm thereby triggering mitosis[286], and also the stimulation of growth factors[285].

2 Vector circle maps of pcDNA3.1(+), pGL3[*luc*], pCBG68, and pGL4.70 [*hRluc*]

See Figure 107. The pcDNA3.1(+) map is reproduced from Invitrogen, and the pGL3[*luc*], pCBG68, and pGL4.70 [*hRluc*] maps are reproduced from Promega. Note the origin of replication for *E.Coli*, a CMV promoter, and sequences for ampicillin and neomycin resistance in the pcDNA3.1(+) vector, and the HindIII and XbaI cleavage sequences in the multiple cloning region of the pcDNA3.1(+) vector, and either side of the luciferase gene in the pGL3[*luc*] and pCBG68 vectors. The HindIII cleavage site is shown on the 5' end of the hRluc gene. Although not clear, Xba I is on the other end and is evident in the actual map.

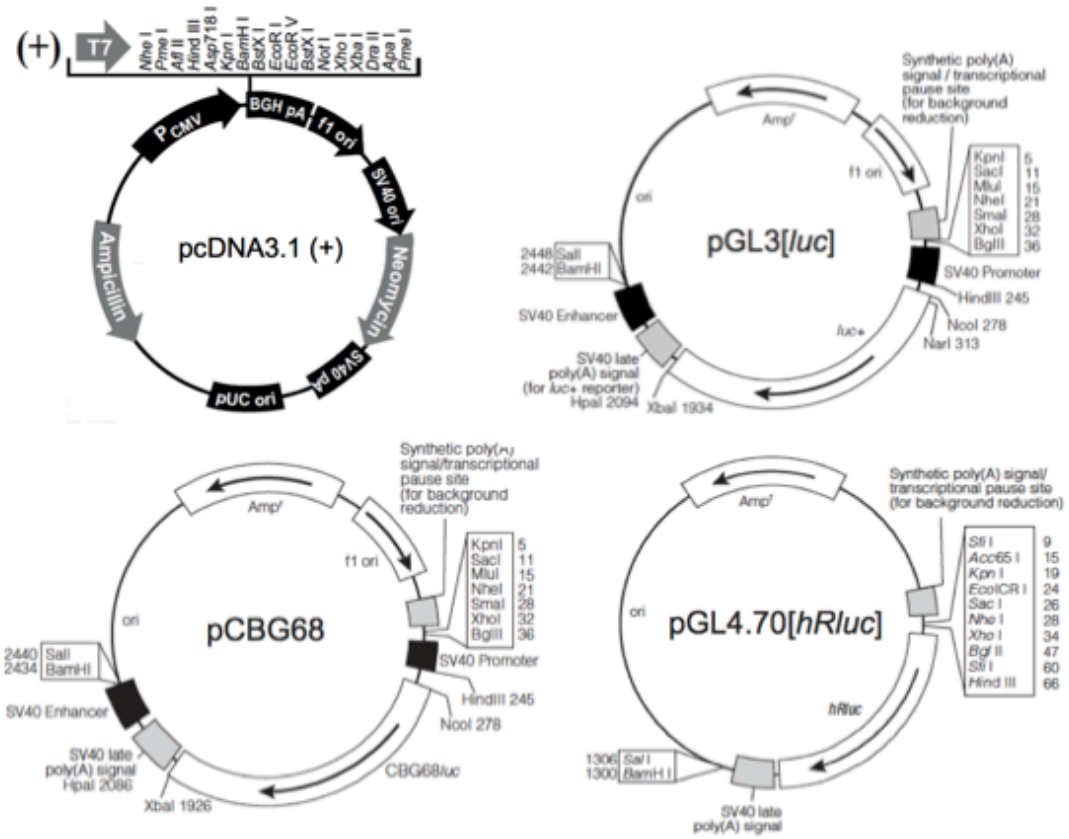

Figure 107 Vector circle maps of pcDNA3.1(+), pGL3[*luc*], pCBG68, and pGL4.70 [*hRluc*]

References

1. Ostrom QT, Gittleman H, Liao P, et al. CBTRUS statistical report: primary brain and central nervous system tumors diagnosed in the United States in 2007-2011. Neuro Oncol 2014;16 Suppl 4:iv1-63.
2. WHO Classification of Tumours of the Central Nervous System. 4th ed. Lyon: International Agency for Research on Cancer; 2007.
3. SEER Stat Fact Sheets: Female Breast Cancer. National Cancer Institute, 2016. (Accessed 1 May 2016, 2016, at www.seer.cancer.gov/statfacts/html/breast.html.)
4. SEER Stat Fact Sheets: Lung and Bronchus Cancer. National Cancer Institute, 2016. (Accessed 1 May 2016, 2016, at www.seer.cancer.gov/statfacts/html/lungb.html.)
5. Frankel SA, German WJ. Glioblastoma multiforme; review of 219 cases with regard to natural history, pathology, diagnostic methods, and treatment. J Neurosurg 1958;15:489-503.
6. Walker MD, Alexander E, Jr., Hunt WE, et al. Evaluation of BCNU and/or radiotherapy in the treatment of anaplastic gliomas. A cooperative clinical trial. J Neurosurg 1978;49:333-43.
7. Andersen AP. Postoperative irradiation of glioblastomas. Results in a randomized series. Acta radiologica: oncology, radiation, physics, biology 1978;17:475-84.
8. Kristiansen K, Hagen S, Kollevold T, et al. Combined modality therapy of operated astrocytomas grade III and IV. Confirmation of the value of postoperative irradiation and lack of potentiation of bleomycin on survival time: a prospective multicenter trial of the Scandinavian Glioblastoma Study Group. Cancer 1981;47:649-52.
9. Stewart LA. Chemotherapy in adult high-grade glioma: a systematic review and meta-analysis of individual patient data from 12 randomised trials. Lancet 2002;359:1011-8.
10. Randomized trial of procarbazine, lomustine, and vincristine in the adjuvant treatment of high-grade astrocytoma: a Medical Research Council trial. J Clin Oncol 2001;19:509-18.
11. Stupp R, Mason WP, van den Bent MJ, et al. Radiotherapy plus concomitant and adjuvant temozolomide for glioblastoma. N Engl J Med 2005;352:987-96.
12. Chi AS, Sorensen AG, Jain RK, Batchelor TT. Angiogenesis as a therapeutic target in malignant gliomas. The oncologist 2009;14:621-36.
13. Plate KH, Breier G, Weich HA, Risau W. Vascular endothelial growth factor is a potential tumour angiogenesis factor in human gliomas in vivo. Nature 1992;359:845-8.
14. Berkman RA, Merrill MJ, Reinhold WC, et al. Expression of the vascular permeability factor/vascular endothelial growth factor gene in central nervous system neoplasms. The Journal of clinical investigation 1993;91:153-9.
15. Hicklin DJ, Ellis LM. Role of the vascular endothelial growth factor pathway in tumor growth and angiogenesis. Journal of clinical oncology : official journal of the American Society of Clinical Oncology 2005;23:1011-27.
16. Friedman HS, Prados MD, Wen PY, et al. Bevacizumab alone and in combination with irinotecan in recurrent glioblastoma. J Clin Oncol 2009;27:4733-40.

17. Kreisl TN, Kim L, Moore K, et al. Phase II trial of single-agent bevacizumab followed by bevacizumab plus irinotecan at tumor progression in recurrent glioblastoma. J Clin Oncol 2009;27:740-5.
18. Gilbert MR, Dignam JJ, Armstrong TS, et al. A randomized trial of bevacizumab for newly diagnosed glioblastoma. N Engl J Med 2014;370:699-708.
19. Neagu MR, Huang RY, Reardon DA, Wen PY. How treatment monitoring is influencing treatment decisions in glioblastomas. Current treatment options in neurology 2015;17:343.
20. Robins HI, Lassman AB, Khuntia D. Therapeutic advances in malignant glioma: current status and future prospects. Neuroimaging clinics of North America 2009;19:647-56.
21. Magnuson W, Ian Robins H, Mohindra P, Howard S. Large volume reirradiation as salvage therapy for glioblastoma after progression on bevacizumab. Journal of neuro-oncology 2014;117:133-9.
22. Pegg AE, Byers TL. Repair of DNA containing O6-alkylguanine. FASEB journal : official publication of the Federation of American Societies for Experimental Biology 1992;6:2302-10.
23. Gerson SL. MGMT: its role in cancer aetiology and cancer therapeutics. Nature reviews Cancer 2004;4:296-307.
24. Hegi ME, Diserens AC, Gorlia T, et al. MGMT gene silencing and benefit from temozolomide in glioblastoma. N Engl J Med 2005;352:997-1003.
25. Maxwell HP. The incidence of interhemispheric extension of glioblastoma multiforme through the corpus callosum. J Neurosurg 1946;3:54-7.
26. Watanabe M, Tanaka R, Takeda N. Magnetic resonance imaging and histopathology of cerebral gliomas. Neuroradiology 1992;34:463-9.
27. Kelly PJ, Daumas-Duport C, Scheithauer BW, Kall BA, Kispert DB. Stereotactic histologic correlations of computed tomography- and magnetic resonance imaging-defined abnormalities in patients with glial neoplasms. Mayo Clin Proc 1987;62:450-9.
28. Choucair AK, Levin VA, Gutin PH, et al. Development of multiple lesions during radiation therapy and chemotherapy in patients with gliomas. J Neurosurg 1986;65:654-8.
29. Laws ER, Parney IF, Huang W, et al. Survival following surgery and prognostic factors for recently diagnosed malignant glioma: data from the Glioma Outcomes Project. J Neurosurg 2003;99:467-73.
30. Quigley MR, Maroon JC. The relationship between survival and the extent of the resection in patients with supratentorial malignant gliomas. Neurosurgery 1991;29:385-8; discussion 8-9.
31. Hess KR. Extent of resection as a prognostic variable in the treatment of gliomas. J Neurooncol 1999;42:227-31.

32. Lacroix M, Abi-Said D, Fourney DR, et al. A multivariate analysis of 416 patients with glioblastoma multiforme: prognosis, extent of resection, and survival. J Neurosurg 2001;95:190-8.
33. Sanai N, Polley MY, McDermott MW, Parsa AT, Berger MS. An extent of resection threshold for newly diagnosed glioblastomas. Journal of neurosurgery 2011;115:3-8.
34. Stummer W, Pichlmeier U, Meinel T, Wiestler OD, Zanella F, Reulen HJ. Fluorescence-guided surgery with 5-aminolevulinic acid for resection of malignant glioma: a randomised controlled multicentre phase III trial. Lancet Oncol 2006;7:392-401.
35. Schag CC, Heinrich RL, Ganz PA. Karnofsky performance status revisited: reliability, validity, and guidelines. Journal of clinical oncology : official journal of the American Society of Clinical Oncology 1984;2:187-93.
36. Laperriere N, Zuraw L, Cairncross G. Radiotherapy for newly diagnosed malignant glioma in adults: a systematic review. Radiotherapy and oncology : journal of the European Society for Therapeutic Radiology and Oncology 2002;64:259-73.
37. Shapiro WR, Green SB, Burger PC, et al. Randomized trial of three chemotherapy regimens and two radiotherapy regimens and two radiotherapy regimens in postoperative treatment of malignant glioma. Brain Tumor Cooperative Group Trial 8001. J Neurosurg 1989;71:1-9.
38. Souhami L, Seiferheld W, Brachman D, et al. Randomized comparison of stereotactic radiosurgery followed by conventional radiotherapy with carmustine to conventional radiotherapy with carmustine for patients with glioblastoma multiforme: report of Radiation Therapy Oncology Group 93-05 protocol. Int J Radiat Oncol Biol Phys 2004;60:853-60.
39. Armstrong CL, Hunter JV, Ledakis GE, et al. Late cognitive and radiographic changes related to radiotherapy: initial prospective findings. Neurology 2002;59:40-8.
40. Levin VA, Prados MR, Wara WM, et al. Radiation therapy and bromodeoxyuridine chemotherapy followed by procarbazine, lomustine, and vincristine for the treatment of anaplastic gliomas. Int J Radiat Oncol Biol Phys 1995;32:75-83.
41. Phillips TL, Levin VA, Ahn DK, et al. Evaluation of bromodeoxyuridine in glioblastoma multiforme: a Northern California Cancer Center Phase II study. Int J Radiat Oncol Biol Phys 1991;21:709-14.
42. Prados MD, Seiferheld W, Sandler HM, et al. Phase III randomized study of radiotherapy plus procarbazine, lomustine, and vincristine with or without BUdR for treatment of anaplastic astrocytoma: final report of RTOG 9404. Int J Radiat Oncol Biol Phys 2004;58:1147-52.
43. Agarwala SS, Kirkwood JM. Temozolomide, a novel alkylating agent with activity in the central nervous system, may improve the treatment of advanced metastatic melanoma. The oncologist 2000;5:144-51.

44. Johnston TP, McCaleb GS, Montgomery JA. THE SYNTHESIS OF ANTINEOPLASTIC AGENTS. XXXII. N-NITROSOUREAS. I. Journal of medicinal chemistry 1963;6:669-81.
45. Chang CH, Horton J, Schoenfeld D, et al. Comparison of postoperative radiotherapy and combined postoperative radiotherapy and chemotherapy in the multidisciplinary management of malignant gliomas. A joint Radiation Therapy Oncology Group and Eastern Cooperative Oncology Group study. Cancer 1983;52:997-1007.
46. Green SB, Byar DP, Walker MD, et al. Comparisons of carmustine, procarbazine, and high-dose methylprednisolone as additions to surgery and radiotherapy for the treatment of malignant glioma. Cancer treatment reports 1983;67:121-32.
47. Selker RG, Shapiro WR, Burger P, et al. The Brain Tumor Cooperative Group NIH Trial 87-01: a randomized comparison of surgery, external radiotherapy, and carmustine versus surgery, interstitial radiotherapy boost, external radiation therapy, and carmustine. Neurosurgery 2002;51:343-55; discussion 55-7.
48. De Vita VT, Carbone PP, Owens AH, Jr., Gold GL, Krant MJ, Edmonson J. Clinical trials with 1,3-bis(2-chloroethyl)-1-nitrosourea, NSC-409962. Cancer Res 1965;25:1876-81.
49. Crittenden D, Tranum BL, Haut A. Pulmonary fibrosis after prolonged therapy with 1,3-bis (2-chloroethyl)-1-nitrosourea. Chest 1977;72:372-3.
50. Litam JP, Dail DH, Spitzer G, et al. Early pulmonary toxicity after administration of high-dose BCNU. Cancer treatment reports 1981;65:39-44.
51. Cohen RJ, Wiernik PH, Walker MD. Acute nonlymphocytic leukemia associated with nitrosourea chemotherapy: report of two cases. Cancer treatment reports 1976;60:1257-61.
52. Michels SD, McKenna RW, Arthur DC, Brunning RD. Therapy-related acute myeloid leukemia and myelodysplastic syndrome: a clinical and morphologic study of 65 cases. Blood 1985;65:1364-72.
53. Schabel FM, Jr. Nitrosoureas: a review of experimental antitumor activity. Cancer treatment reports 1976;60:665-98.
54. Garfield J, Dayan AD, Weller RO. Postoperative intracavitary chemotherapy of malignant supratentorial astrocytomas using BCNU. Clinical oncology 1975;1:213-22.
55. Yang MB, Tamargo RJ, Brem H. Controlled delivery of 1,3-bis(2-chloroethyl)-1-nitrosourea from ethylene-vinyl acetate copolymer. Cancer Res 1989;49:5103-7.
56. Tamargo RJ, Myseros JS, Epstein JI, Yang MB, Chasin M, Brem H. Interstitial chemotherapy of the 9L gliosarcoma: controlled release polymers for drug delivery in the brain. Cancer Res 1993;53:329-33.
57. Grossman SA, Reinhard C, Colvin OM, et al. The intracerebral distribution of BCNU delivered by surgically implanted biodegradable polymers. J Neurosurg 1992;76:640-7.

58. Domb AJ, Rock M, Perkin C, Yipchuck G, Broxup B, Villemure JG. Excretion of a radiolabelled anticancer biodegradable polymeric implant from the rabbit brain. Biomaterials 1995;16:1069-72.
59. Wu MP, Tamada JA, Brem H, Langer R. In vivo versus in vitro degradation of controlled release polymers for intracranial surgical therapy. Journal of biomedical materials research 1994;28:387-95.
60. Dang W, Daviau T, Brem H. Morphological characterization of polyanhydride biodegradable implant gliadel during in vitro and in vivo erosion using scanning electron microscopy. Pharmaceutical research 1996;13:683-91.
61. Brem H, Piantadosi S, Burger PC, et al. Placebo-controlled trial of safety and efficacy of intraoperative controlled delivery by biodegradable polymers of chemotherapy for recurrent gliomas. The Polymer-brain Tumor Treatment Group. Lancet 1995;345:1008-12.
62. Valtonen S, Timonen U, Toivanen P, et al. Interstitial chemotherapy with carmustine-loaded polymers for high-grade gliomas: a randomized double-blind study. Neurosurgery 1997;41:44-8; discussion 8-9.
63. Westphal M, Hilt DC, Bortey E, et al. A phase 3 trial of local chemotherapy with biodegradable carmustine (BCNU) wafers (Gliadel wafers) in patients with primary malignant glioma. Neuro-oncol 2003;5:79-88.
64. Fleming AB, Saltzman WM. Pharmacokinetics of the carmustine implant. Clinical pharmacokinetics 2002;41:403-19.
65. McGovern PC, Lautenbach E, Brennan PJ, Lustig RA, Fishman NO. Risk factors for postcraniotomy surgical site infection after 1,3-bis (2-chloroethyl)-1-nitrosourea (Gliadel) wafer placement. Clinical infectious diseases : an official publication of the Infectious Diseases Society of America 2003;36:759-65.
66. Weber EL, Goebel EA. Cerebral edema associated with Gliadel wafers: two case studies. Neuro Oncol 2005;7:84-9.
67. Gallego JM, Barcia JA, Barcia-Marino C. Fatal outcome related to carmustine implants in glioblastoma multiforme. Acta neurochirurgica 2007;149:261-5; discussion 5.
68. Bobo RH, Laske DW, Akbasak A, Morrison PF, Dedrick RL, Oldfield EH. Convection-enhanced delivery of macromolecules in the brain. Proceedings of the National Academy of Sciences of the United States of America 1994;91:2076-80.
69. Bruce JN, Fine RL, Canoll P, et al. Regression of recurrent malignant gliomas with convection-enhanced delivery of topotecan. Neurosurgery 2011;69:1272-9; discussion 9-80.
70. Patel SJ, Shapiro WR, Laske DW, et al. Safety and feasibility of convection-enhanced delivery of Cotara for the treatment of malignant glioma: initial experience in 51 patients. Neurosurgery 2005;56:1243-52; discussion 52-3.

71. Wersall P, Ohlsson I, Biberfeld P, et al. Intratumoral infusion of the monoclonal antibody, mAb 425, against the epidermal-growth-factor receptor in patients with advanced malignant glioma. Cancer immunology, immunotherapy : CII 1997;44:157-64.
72. Bogdahn U, Hau P, Stockhammer G, et al. Targeted therapy for high-grade glioma with the TGF-beta2 inhibitor trabedersen: results of a randomized and controlled phase IIb study. Neuro-oncology 2011;13:132-42.
73. Voges J, Reszka R, Gossmann A, et al. Imaging-guided convection-enhanced delivery and gene therapy of glioblastoma. Annals of neurology 2003;54:479-87.
74. Kunwar S, Chang S, Westphal M, et al. Phase III randomized trial of CED of IL13-PE38QQR vs Gliadel wafers for recurrent glioblastoma. Neuro-oncology 2010;12:871-81.
75. Joshi BH, Plautz GE, Puri RK. Interleukin-13 receptor alpha chain: a novel tumor-associated transmembrane protein in primary explants of human malignant gliomas. Cancer Res 2000;60:1168-72.
76. Vogelbaum MA, Aghi MK. Convection-enhanced delivery for the treatment of glioblastoma. Neuro-oncology 2015;17 Suppl 2:ii3-ii8.
77. Sugiyama S, Saito R, Nakamura T, et al. Safety and feasibility of convection-enhanced delivery of nimustine hydrochloride co-infused with free gadolinium for real-time monitoring in the primate brain. Neurological research 2012;34:581-7.
78. Yang X, Saito R, Nakamura T, et al. Peri-tumoral leakage during intra-tumoral convection-enhanced delivery has implications for efficacy of peri-tumoral infusion before removal of tumor. Drug delivery 2015:1-6.
79. Felsberg J, Thon N, Eigenbrod S, et al. Promoter methylation and expression of MGMT and the DNA mismatch repair genes MLH1, MSH2, MSH6 and PMS2 in paired primary and recurrent glioblastomas. Int J Cancer 2011;129:659-70.
80. Tentori L, Orlando L, Lacal PM, et al. Inhibition of O6-alkylguanine DNA-alkyltransferase or poly(ADP-ribose) polymerase increases susceptibility of leukemic cells to apoptosis induced by temozolomide. Molecular pharmacology 1997;52:249-58.
81. Tentori L, Graziani G. Chemopotentiation by PARP inhibitors in cancer therapy. Pharmacological research 2005;52:25-33.
82. Wedge SR, Porteous JK, Newlands ES. 3-aminobenzamide and/or O6-benzylguanine evaluated as an adjuvant to temozolomide or BCNU treatment in cell lines of variable mismatch repair status and O6-alkylguanine-DNA alkyltransferase activity. British journal of cancer 1996;74:1030-6.
83. Robins HI, Zhang P, Gilbert MR, et al. A randomized phase I/II study of ABT-888 in combination with temozolomide in recurrent temozolomide resistant glioblastoma: an NRG oncology RTOG group study. J Neurooncol 2015.

84. Bobola MS, Kolstoe DD, Blank A, Chamberlain MC, Silber JR. Repair of 3-methyladenine and abasic sites by base excision repair mediates glioblastoma resistance to temozolomide. Frontiers in oncology 2012;2:176.
85. Jiricny J. The multifaceted mismatch-repair system. Nature reviews Molecular cell biology 2006;7:335-46.
86. Parker NR, Hudson AL, Khong P, et al. Intratumoral heterogeneity identified at the epigenetic, genetic and transcriptional level in glioblastoma. Scientific reports 2016;6:22477.
87. Luo H, Chen Z, Wang S, et al. c-Myc-miR-29c-REV3L signalling pathway drives the acquisition of temozolomide resistance in glioblastoma. Brain : a journal of neurology 2015;138:3654-72.
88. Dougherty TJ, Gomer CJ, Henderson BW, et al. Photodynamic therapy. J Natl Cancer Inst 1998;90:889-905.
89. Daniell MD, Hill JS. A history of photodynamic therapy. The Australian and New Zealand journal of surgery 1991;61:340-8.
90. Ackroyd R, Kelty C, Brown N, Reed M. The history of photodetection and photodynamic therapy. Photochem Photobiol 2001;74:656-69.
91. Spikes JD. Primary Photoprocesses in Biology and Medicine. New York: Plenum Press; 1985.
92. Finsen NR. Phototherapy. London: Edward Arnold; 1901.
93. Dolmans DE, Fukumura D, Jain RK. Photodynamic therapy for cancer. Nat Rev Cancer 2003;3:380-7.
94. Schwartz SK, Abolon, K., and Vermund, H. Some relationships of porphyrins, X-rays and tumours. University of Minnesota Medical Bulletin 1955;27:7-8.
95. Dougherty TJ, Grindey GB, Fiel R, Weishaupt KR, Boyle DG. Photoradiation therapy. II. Cure of animal tumors with hematoporphyrin and light. J Natl Cancer Inst 1975;55:115-21.
96. Kelly JF, Snell ME, Berenbaum MC. Photodynamic destruction of human bladder carcinoma. Br J Cancer 1975;31:237-44.
97. Henderson BW, Dougherty TJ. How does photodynamic therapy work? Photochem Photobiol 1992;55:145-57.
98. Moan J, Berg K. The photodegradation of porphyrins in cells can be used to estimate the lifetime of singlet oxygen. Photochem Photobiol 1991;53:549-53.
99. Redmond RW, Gamlin JN. A compilation of singlet oxygen yields from biologically relevant molecules. Photochem Photobiol 1999;70:391-475.
100. Grant WE, Speight PM, MacRobert AJ, Hopper C, Bown SG. Photodynamic therapy of normal rat arteries after photosensitisation using disulphonated aluminium phthalocyanine and 5-aminolaevulinic acid. Br J Cancer 1994;70:72-8.
101. Hopper C. Photodynamic therapy: a clinical reality in the treatment of cancer. Lancet Oncol 2000;1:212-9.

102. Josefsen LB, Boyle RW. Photodynamic therapy and the development of metal-based photosensitisers. Metal-based drugs 2008;2008:276109.
103. Hudson R, Carcenac M, Smith K, et al. The development and characterisation of porphyrin isothiocyanate-monoclonal antibody conjugates for photoimmunotherapy. Br J Cancer 2005;92:1442-9.
104. Dummin H, Cernay T, Zimmermann HW. Selective photosensitization of mitochondria in HeLa cells by cationic Zn (II) phthalocyanines with lipophilic side-chains. J Photochem Photobiol B 1997;37:219-29.
105. Morton CA, McKenna KE, Rhodes LE. Guidelines for topical photodynamic therapy: update. The British journal of dermatology 2008;159:1245-66.
106. Kennedy TC, McWilliams A, Edell E, et al. Bronchial intraepithelial neoplasia/early central airways lung cancer: ACCP evidence-based clinical practice guidelines (2nd edition). Chest 2007;132:221s-33s.
107. Jenkins MP, Buonaccorsi GA, Raphael M, et al. Clinical study of adjuvant photodynamic therapy to reduce restenosis following femoral angioplasty. The British journal of surgery 1999;86:1258-63.
108. Diamond I, Granelli SG, McDonagh AF, Nielsen S, Wilson CB, Jaenicke R. Photodynamic therapy of malignant tumours. Lancet (London, England) 1972;2:1175-7.
109. Sandeman DR, Bradford R, Buxton P, Bown SG, Thomas DG. Selective necrosis of malignant gliomas in mice using photodynamic therapy. Br J Cancer 1987;55:647-9.
110. Boggan JE, Walter R, Edwards MS, et al. Distribution of hematoporphyrin derivative in the rat 9l gliosarcoma brain tumor analyzed by digital video fluorescence microscopy. J Neurosurg 1984;61:1113-9.
111. Wharen RE, Jr., Anderson RE, Laws ER, Jr. Quantitation of hematoporphyrin derivative in human gliomas, experimental central nervous system tumors, and normal tissues. Neurosurgery 1983;12:446-50.
112. Kostron H. Photodynamic diagnosis and therapy and the brain. In: Gomer CJ, ed. Photodynamic Therapy, Methods in Molecular Biology: Springer Science and Business Media; 1980:261-80.
113. Kostron H, Bellnier DA, Lin CW, Swartz MR, Martuza RL. Distribution, retention, and phototoxicity of hematoporphyrin derivative in a rat glioma. Intraneoplastic versus intraperitoneal injection. Journal of neurosurgery 1986;64:768-74.
114. Obwegeser A, Jakober R, Kostron H. Uptake and kinetics of 14C-labelled meta-tetrahydroxyphenylchlorin and 5-aminolaevulinic acid in the C6 rat glioma model. Br J Cancer 1998;78:733-8.
115. Peng Q, Moan J, Ma LW, Nesland JM. Uptake, localization, and photodynamic effect of meso-tetra(hydroxyphenyl)porphine and its corresponding chlorin in normal and tumor tissues of mice bearing mammary carcinoma. Cancer Res 1995;55:2620-6.

116. Kostron H, Obwegeser A, Jakober R. Photodynamic therapy in neurosurgery: a review. J Photochem Photobiol B 1996;36:157-68.
117. Jiang F, Chopp M, Katakowski M, et al. Photodynamic therapy with photofrin reduces invasiveness of malignant human glioma cells. Lasers Med Sci 2002;17:280-8.
118. Madsen SJ, Sun CH, Tromberg BJ, Hirschberg H. Repetitive 5-aminolevulinic acid-mediated photodynamic therapy on human glioma spheroids. Journal of neuro-oncology 2003;62:243-50.
119. Chopp M, Madigan L, Dereski M, Jiang F, Li Y. Photodynamic therapy of human glioma (U87) in the nude rat. Photochem Photobiol 1996;64:707-11.
120. Perria C, Capuzzo T, Cavagnaro G, et al. Fast attempts at the photodynamic treatment of human gliomas. Journal of neurosurgical sciences 1980;24:119-29.
121. Laws ER, Jr., Cortese DA, Kinsey JH, Eagan RT, Anderson RE. Photoradiation therapy in the treatment of malignant brain tumors: a phase I (feasibility) study. Neurosurgery 1981;9:672-8.
122. Kostron H, Hochleitner BW, Obwegeser A, Seiwald M. Clinical and experimental results of photodynamic therapy in neurosurgery. SPIE 5th International Photodynamic Association Biennal Meeting; 1995.
123. Muller PJ, Wilson BC. Photodynamic therapy of brain tumors--a work in progress. Lasers in surgery and medicine 2006;38:384-9.
124. Stylli SS, Kaye AH, MacGregor L, Howes M, Rajendra P. Photodynamic therapy of high grade glioma - long term survival. Journal of clinical neuroscience : official journal of the Neurosurgical Society of Australasia 2005;12:389-98.
125. Stylli SS, Howes M, MacGregor L, Rajendra P, Kaye AH. Photodynamic therapy of brain tumours: evaluation of porphyrin uptake versus clinical outcome. Journal of clinical neuroscience : official journal of the Neurosurgical Society of Australasia 2004;11:584-96.
126. Zimmermann A, Ritsch-Marte M, Kostron H. mTHPC-mediated photodynamic diagnosis of malignant brain tumors. Photochem Photobiol 2001;74:611-6.
127. Eljamel MS, Goodman C, Moseley H. ALA and Photofrin fluorescence-guided resection and repetitive PDT in glioblastoma multiforme: a single centre Phase III randomised controlled trial. Lasers in medical science 2008;23:361-7.
128. Harvey EN. Studies on Bioluminescence. XIII. Luminescence in the Coelenterates Biological Bulletin 1921;41:280-7.
129. Rhodes WC, Mc EW. The synthesis and function of luciferyl-adenylate and oxyluciferyl-adenylate. The Journal of biological chemistry 1958;233:1528-37.
130. McElroy WD, Seliger HH, White EH. Mechanism of bioluminescence, chemiluminescence and enzyme function in the oxidation of firefly luciferin. Photochem Photobiol 1969;10:153-70.

131. Seliger HH, Mc EW. Spectral emission and quantum yield of firefly bioluminescence. Archives of biochemistry and biophysics 1960;88:136-41.
132. Jenkins DE, Oei Y, Hornig YS, et al. Bioluminescent imaging (BLI) to improve and refine traditional murine models of tumor growth and metastasis. Clin Exp Metastasis 2003;20:733-44.
133. Zhao H, Doyle TC, Coquoz O, Kalish F, Rice BW, Contag CH. Emission spectra of bioluminescent reporters and interaction with mammalian tissue determine the sensitivity of detection in vivo. J Biomed Opt 2005;10:41210.
134. Drake JM, Gabriel CL, Henry MD. Assessing Tumor Growth and Distribution in a Model of Prostate Cancer Metastasis using Bioluminescence Imaging. Clin Exp Metastasis 2005;22:674-84.
135. Adams JY, Johnson M, Sato M, et al. Visualization of advanced human prostate cancer lesions in living mice by a targeted gene transfer vector and optical imaging. Nat Med 2002;8:891-7.
136. Iyer M, Salazar FB, Wu L, Carey M, Gambhir SS. Bioluminescence imaging of systemic tumor targeting using a prostate-specific lentiviral vector. Hum Gene Ther 2006;17:125-32.
137. Lyons SK, Lim E, Clermont AO, et al. Noninvasive bioluminescence imaging of normal and spontaneously transformed prostate tissue in mice. Cancer Res 2006;66:4701-7.
138. Carpenter S, Fehr MJ, Kraus GA, Petrich JW. Chemiluminescent activation of the antiviral activity of hypericin: a molecular flashlight. Proc Natl Acad Sci U S A 1994;91:12273-7.
139. Wen J, Chowdhury P, Wills NJ, et al. Toward the molecular flashlight: preparation, properties, and photophysics of a hypericin-luciferin tethered molecule. Photochem Photobiol 2002;76:153-7.
140. Theodossiou T, Hothersall JS, Woods EA, Okkenhaug K, Jacobson J, MacRobert AJ. Firefly luciferin-activated rose bengal: in vitro photodynamic therapy by intracellular chemiluminescence in transgenic NIH 3T3 cells. Cancer Res 2003;63:1818-21.
141. Schipper ML, Patel MR, Gambhir SS. Evaluation of firefly luciferase bioluminescence mediated photodynamic toxicity in cancer cells. Mol Imaging Biol 2006;8:218-25.
142. Pfleger KD, Eidne KA. Illuminating insights into protein-protein interactions using bioluminescence resonance energy transfer (BRET). Nature methods 2006;3:165-74.
143. Wu P, Brand L. Resonance energy transfer: methods and applications. Analytical biochemistry 1994;218:1-13.
144. Couldwell WT, Gopalakrishna R, Hinton DR, et al. Hypericin: a potential antiglioma therapy. Neurosurgery 1994;35:705-9; discussion 9-10.

145. Ritz R, Wein HT, Dietz K, et al. Photodynamic therapy of malignant glioma with hypericin: comprehensive in vitro study in human glioblastoma cell lines. Int J Oncol 2007;30:659-67.
146. Huntosova V, Nadova Z, Dzurova L, Jakusova V, Sureau F, Miskovsky P. Cell death response of U87 glioma cells on hypericin photoactivation is mediated by dynamics of hypericin subcellular distribution and its aggregation in cellular organelles. Photochem Photobiol Sci 2014;11:1428-36.
147. Agostinis P, Vantieghem A, Merlevede W, de Witte PA. Hypericin in cancer treatment: more light on the way. Int J Biochem Cell Biol 2002;34:221-41.
148. Adigbli DK, Wilson DG, Farooqui N, et al. Photochemical internalisation of chemotherapy potentiates killing of multidrug-resistant breast and bladder cancer cells. Br J Cancer 2007;97:502-12.
149. Ma L, Moan J, Berg K. Evaluation of a new photosensitizer, meso-tetra-hydroxyphenyl-chlorin, for use in photodynamic therapy: a comparison of its photobiological properties with those of two other photosensitizers. Int J Cancer 1994;57:883-8.
150. Fiedler DM, Wierrani F, Schnitzhofer G, et al. Does the in-vitro efficiency of meso-tetrahydroxy-phenyl-chlorin depend on pre-treatment of sensitizer? J Photochem Photobiol B 1997;38:241-4.
151. Melnikova VO, Bezdetnaya LN, Bour C, et al. Subcellular localization of meta-tetra (hydroxyphenyl) chlorin in human tumor cells subjected to photodynamic treatment. J Photochem Photobiol B 1999;49:96-103.
152. Hornung R, Jentsch B, Crompton NE, Haller U, Walt H. In vitro effects and localisation of the photosensitizers m-THPC and m-THPC MD on carcinoma cells of the human breast (MCF-7) and Chinese hamster fibroblasts (V-79). Lasers Surg Med 1997;20:443-50.
153. Rezzoug H BL, A'amar O, Merlin JL, Guillemin. Parameters affecting photodynamic activity of foscan or meta-tetatra(hydroxyphenyl) chlorin (mTHPC) in vitro and in vivo. Lasers Med Sci 1998;13:119-25.
154. Teiten MH, Bezdetnaya L, Merlin JL, et al. Effect of meta-tetra(hydroxyphenyl)chlorin (mTHPC)-mediated photodynamic therapy on sensitive and multidrug-resistant human breast cancer cells. J Photochem Photobiol B 2001;62:146-52.
155. Sasnouski S, Pic E, Dumas D, et al. Influence of incubation time and sensitizer localization on meta-tetra(hydroxyphenyl)chlorin (mTHPC)-induced photoinactivation of cells. Radiat Res 2007;168:209-17.
156. Rousset N, Keminon E, Eleouet S, et al. Use of alkaline Comet assay to assess DNA repair after m-THPC-PDT. J Photochem Photobiol B 2000;56:118-31.
157. Ris HB, Altermatt HJ, Stewart CM, et al. Photodynamic therapy with m-tetrahydroxyphenylchlorin in vivo: optimization of the therapeutic index. Int J Cancer 1993;55:245-9.

158. Mannino S, Molinari A, Sabatino G, et al. Intratumoral vs systemic administration of meta-tetrahydroxyphenylchlorin for photodynamic therapy of malignant gliomas: assessment of uptake and spatial distribution in C6 rat glioma model. Int J Immunopathol Pharmacol 2008;21:227-31.
159. Teiten MH, Bezdetnaya L, Morliere P, Santus R, Guillemin F. Endoplasmic reticulum and Golgi apparatus are the preferential sites of Foscan localisation in cultured tumour cells. Br J Cancer 2003;88:146-52.
160. EnduRen Live Cell Substrate Technical Manual. 2016. (Accessed 1 May 2016, 2016, at www.promega.com/resources/protocols/technical-manuals/0/enduren-live-cell-substrate-protocol.)
161. ViviRen Live Cell Subtrate Technical Manual. 2016. (Accessed 1 May 2016, at www.promega.com/resources/protocols/technical-manuals/0/viviren-live-cell-substrate-protocol/.)
162. Du HY, Bay BH, Olivo M. Biodistribution and photodynamic therapy with hypericin in a human NPC murine tumor model. Int J Oncol 2003;22:1019-24.
163. Zimmermann A, Ritsch-Marte M, Kostron H. In vitro investigation on the pH dependence of the absorption and fluorescence properties of the photosensitizer mTHPC. Photochem Photobiol 2002;75:335-8.
164. Wills NJ, Park J, Wen J, et al. Tumor cell toxicity of hypericin and related analogs. Photochem Photobiol 2001;74:216-20.
165. Uzdensky AB, Ma LW, Iani V, Hjortland GO, Steen HB, Moan J. Intracellular localisation of hypericin in human glioblastoma and carcinoma cell lines. Lasers Med Sci 2001;16:276-83.
166. Theodossiou T, Spiro MD, Jacobson J, Hothersall JS, Macrobert AJ. Evidence for intracellular aggregation of hypericin and the impact on its photocytotoxicity in PAM 212 murine keratinocytes. Photochem Photobiol 2004;80:438-43.
167. Kocanova S, Hornakova T, Hritz J, et al. Characterization of the interaction of hypericin with protein kinase C in U-87 MG human glioma cells. Photochem Photobiol 2006;82:720-8.
168. Mosmann T. Rapid colorimetric assay for cellular growth and survival: application to proliferation and cytotoxicity assays. J Immunol Methods 1983;65:55-63.
169. Ball DJ, Wood SR, Vernon DI, Griffiths J, Dubbelman TM, Brown SB. The characterisation of three substituted zinc phthalocyanines of differing charge for use in photodynamic therapy. A comparative study of their aggregation and photosensitising ability in relation to mTHPC and polyhaematoporphyrin. J Photochem Photobiol B 1998;45:28-35.
170. Gillet JP, Efferth T, Remacle J. Chemotherapy-induced resistance by ATP-binding cassette transporter genes. Biochim Biophys Acta 2007;1775:237-62.

171. Inouye S, Shimomura O. The use of Renilla luciferase, Oplophorus luciferase, and apoaequorin as bioluminescent reporter protein in the presence of coelenterazine analogues as substrate. Biochem Biophys Res Commun 1997;233:349-53.
172. Schold SC, Jr., Bullard DE, Bigner SH, Jones TR, Bigner DD. Growth, morphology, and serial transplantation of anaplastic human gliomas in athymic mice. J Neurooncol 1983;1:5-14.
173. Rana MW, Pinkerton H, Thornton H, Nagy D. Heterotransplantation of human glioblastoma multiforme and meningioma to nude mice. Proc Soc Exp Biol Med 1977;155:85-8.
174. Shapiro WR, Basler GA, Chernik NL, Posner JB. Human brain tumor transplantation into nude mice. J Natl Cancer Inst 1979;62:447-53.
175. Szentirmai O, Baker CH, Lin N, et al. Noninvasive bioluminescence imaging of luciferase expressing intracranial U87 xenografts: correlation with magnetic resonance imaging determined tumor volume and longitudinal use in assessing tumor growth and antiangiogenic treatment effect. Neurosurgery 2006;58:365-72; discussion -72.
176. Rubin JB, Kung AL, Klein RS, et al. A small-molecule antagonist of CXCR4 inhibits intracranial growth of primary brain tumors. Proc Natl Acad Sci U S A 2003;100:13513-8.
177. Saris SC, Bigner SH, Bigner DD. Intracerebral transplantation of a human glioma line in immunosuppressed rats. J Neurosurg 1984;60:582-8.
178. Guerrero-Cazares H, Chaichana KL, Quinones-Hinojosa A. Neurosphere culture and human organotypic model to evaluate brain tumor stem cells. Methods Mol Biol 2009;568:73-83.
179. Barker M, Hoshino T, Gurcay O, et al. Development of an animal brain tumor model and its response to therapy with 1,3-bis(2-chloroethyl)-1-nitrosourea. Cancer Res 1973;33:976-86.
180. Barker M, Hoshino T, Wheeler KT, Wilson CB. Chemotherapeutic implications of early tumor cell growth in an animal brain-tumor model. J Natl Cancer Inst 1975;54:851-3.
181. Bullard DE, Schold SC, Jr., Bigner SH, Bigner DD. Growth and chemotherapeutic response in athymic mice of tumors arising from human glioma-derived cell lines. J Neuropathol Exp Neurol 1981;40:410-27.
182. Levin VA, Giglio P, Puduvalli VK, et al. Combination chemotherapy with 13-cis-retinoic acid and celecoxib in the treatment of glioblastoma multiforme. J Neurooncol 2006;78:85-90.
183. Fogh J, Tiso J, Orfeo T, Sharkey FE, Daniels WP, Fogh JM. Thirty-four lines of six human tumor categories established in nude mice. J Natl Cancer Inst 1980;64:745-51.
184. Giovanella BC, Stehlin JS, Jr., Williams LJ, Jr., Lee SS, Shepard RC. Heterotransplantation of human cancers into nude mice: a model system for human cancer chemotherapy. Cancer 1978;42:2269-81.

185. Povlsen CO, Visfeldt J, Rygaard J, Jensen G. Growth patterns and chromosome constitutions of human malignant tumours after long-term serial transplantation in nude mice. Acta Pathol Microbiol Scand A 1975;83:709-16.
186. Kornblith PL, Dohan FC, Jr., Wood WC, Whitman BO. Human astrocytoma: serum-mediated immunologic response. Cancer 1974;33:1512-9.
187. Wood WC, Kornblith PL, Quindlen EA, Pollock LA. Detection of humoral immune response to human brain tumors: specificity and reliability of microcytotoxicity assay. Cancer 1979;43:86-90.
188. Schold SC, Jr., Rawlings CE, 3rd, Bigner SH, Bigner DD. Intracerebral growth of a human glioma tumor line in athymic mice and treatment with procarbazine, 1,3-bis(2-chloroethyl)-1-nitrosourea, aziridinylbenzoquinone, and cis-platinum. Neurosurgery 1983;12:672-7.
189. Singh SK, Hawkins C, Clarke ID, et al. Identification of human brain tumour initiating cells. Nature 2004;432:396-401.
190. Singh SK, Clarke ID, Terasaki M, et al. Identification of a cancer stem cell in human brain tumors. Cancer Res 2003;63:5821-8.
191. Ignatova TN, Kukekov VG, Laywell ED, Suslov ON, Vrionis FD, Steindler DA. Human cortical glial tumors contain neural stem-like cells expressing astroglial and neuronal markers in vitro. Glia 2002;39:193-206.
192. Singec I, Knoth R, Meyer RP, et al. Defining the actual sensitivity and specificity of the neurosphere assay in stem cell biology. Nat Methods 2006;3:801-6.
193. Vescovi AL, Galli R, Gritti A. Clonal analyses and cryopreservation of neural stem cell cultures. Methods Mol Biol 2002;198:115-23.
194. Chaichana K, Zamora-Berridi G, Camara-Quintana J, Quinones-Hinojosa A. Neurosphere assays: growth factors and hormone differences in tumor and nontumor studies. Stem Cells 2006;24:2851-7.
195. Keyaerts M, Verschueren J, Bos TJ, et al. Dynamic bioluminescence imaging for quantitative tumour burden assessment using IV or IP administration of D: -luciferin: effect on intensity, time kinetics and repeatability of photon emission. Eur J Nucl Med Mol Imaging 2008;35:999-1007.
196. Lilge L, Portnoy M, Wilson BC. Apoptosis induced in vivo by photodynamic therapy in normal brain and intracranial tumour tissue. Br J Cancer 2000;83:1110-7.
197. Rehemtulla A, Stegman LD, Cardozo SJ, et al. Rapid and quantitative assessment of cancer treatment response using in vivo bioluminescence imaging. Neoplasia (New York, NY) 2000;2:491-5.
198. Li A, Walling J, Kotliarov Y, et al. Genomic changes and gene expression profiles reveal that established glioma cell lines are poorly representative of primary human gliomas. Molecular cancer research : MCR 2008;6:21-30.

199. Finkelstein SD, Black P, Nowak TP, Hand CM, Christensen S, Finch PW. Histological characteristics and expression of acidic and basic fibroblast growth factor genes in intracerebral xenogeneic transplants of human glioma cells. Neurosurgery 1994;34:136-43.
200. Radaelli E, Ceruti R, Patton V, et al. Immunohistopathological and neuroimaging characterization of murine orthotopic xenograft models of glioblastoma multiforme recapitulating the most salient features of human disease. Histology and histopathology 2009;24:879-91.
201. Brannan CI, Perkins AS, Vogel KS, et al. Targeted disruption of the neurofibromatosis type-1 gene leads to developmental abnormalities in heart and various neural crest-derived tissues. Genes & development 1994;8:1019-29.
202. Gu H, Zou YR, Rajewsky K. Independent control of immunoglobulin switch recombination at individual switch regions evidenced through Cre-loxP-mediated gene targeting. Cell 1993;73:1155-64.
203. Kuhn R, Schwenk F, Aguet M, Rajewsky K. Inducible gene targeting in mice. Science (New York, NY) 1995;269:1427-9.
204. Tsien JZ, Huerta PT, Tonegawa S. The essential role of hippocampal CA1 NMDA receptor-dependent synaptic plasticity in spatial memory. Cell 1996;87:1327-38.
205. Zhuo L, Theis M, Alvarez-Maya I, Brenner M, Willecke K, Messing A. hGFAP-cre transgenic mice for manipulation of glial and neuronal function in vivo. Genesis (New York, NY : 2000) 2001;31:85-94.
206. Jacques TS, Swales A, Brzozowski MJ, et al. Combinations of genetic mutations in the adult neural stem cell compartment determine brain tumour phenotypes. The EMBO journal 2010;29:222-35.
207. Chow LM, Endersby R, Zhu X, et al. Cooperativity within and among Pten, p53, and Rb pathways induces high-grade astrocytoma in adult brain. Cancer cell 2011;19:305-16.
208. Henriquez NV, Forshew T, Tatevossian R, et al. Comparative expression analysis reveals lineage relationships between human and murine gliomas and a dominance of glial signatures during tumor propagation in vitro. Cancer Res 2013;73:5834-44.
209. Zheng H, Ying H, Yan H, et al. p53 and Pten control neural and glioma stem/progenitor cell renewal and differentiation. Nature 2008;455:1129-33.
210. Brat DJ, Verhaak RG, Aldape KD, et al. Comprehensive, Integrative Genomic Analysis of Diffuse Lower-Grade Gliomas. N Engl J Med 2015;372:2481-98.
211. Eckel-Passow JE, Lachance DH, Molinaro AM, et al. Glioma Groups Based on 1p/19q, IDH, and TERT Promoter Mutations in Tumors. N Engl J Med 2015;372:2499-508.
212. Libermann TA, Nusbaum HR, Razon N, et al. Amplification, enhanced expression and possible rearrangement of EGF receptor gene in primary human brain tumours of glial origin. Nature 1985;313:144-7.

213. Ekstrand AJ, James CD, Cavenee WK, Seliger B, Pettersson RF, Collins VP. Genes for epidermal growth factor receptor, transforming growth factor alpha, and epidermal growth factor and their expression in human gliomas in vivo. Cancer research 1991;51:2164-72.
214. Wong AJ, Ruppert JM, Bigner SH, et al. Structural alterations of the epidermal growth factor receptor gene in human gliomas. Proceedings of the National Academy of Sciences of the United States of America 1992;89:2965-9.
215. Smith JS, Tachibana I, Passe SM, et al. PTEN mutation, EGFR amplification, and outcome in patients with anaplastic astrocytoma and glioblastoma multiforme. Journal of the National Cancer Institute 2001;93:1246-56.
216. Shinojima N, Tada K, Shiraishi S, et al. Prognostic value of epidermal growth factor receptor in patients with glioblastoma multiforme. Cancer research 2003;63:6962-70.
217. Heimberger AB, Hlatky R, Suki D, et al. Prognostic effect of epidermal growth factor receptor and EGFRvIII in glioblastoma multiforme patients. Clinical cancer research : an official journal of the American Association for Cancer Research 2005;11:1462-6.
218. Mellinghoff IK, Wang MY, Vivanco I, et al. Molecular determinants of the response of glioblastomas to EGFR kinase inhibitors. The New England journal of medicine 2005;353:2012-24.
219. Malden LT, Novak U, Kaye AH, Burgess AW. Selective amplification of the cytoplasmic domain of the epidermal growth factor receptor gene in glioblastoma multiforme. Cancer research 1988;48:2711-4.
220. Yamazaki H, Fukui Y, Ueyama Y, et al. Amplification of the structurally and functionally altered epidermal growth factor receptor gene (c-erbB) in human brain tumors. Molecular and cellular biology 1988;8:1816-20.
221. Sugawa N, Ekstrand AJ, James CD, Collins VP. Identical splicing of aberrant epidermal growth factor receptor transcripts from amplified rearranged genes in human glioblastomas. Proceedings of the National Academy of Sciences of the United States of America 1990;87:8602-6.
222. Frederick L, Wang XY, Eley G, James CD. Diversity and frequency of epidermal growth factor receptor mutations in human glioblastomas. Cancer Res 2000;60:1383-7.
223. Nagane M, Coufal F, Lin H, Bogler O, Cavenee WK, Huang HJ. A common mutant epidermal growth factor receptor confers enhanced tumorigenicity on human glioblastoma cells by increasing proliferation and reducing apoptosis. Cancer Res 1996;56:5079-86.
224. Learn CA, Hartzell TL, Wikstrand CJ, et al. Resistance to tyrosine kinase inhibition by mutant epidermal growth factor receptor variant III contributes to the neoplastic phenotype of glioblastoma multiforme. Clin Cancer Res 2004;10:3216-24.
225. Feldkamp MM, Lala P, Lau N, Roncari L, Guha A. Expression of activated epidermal growth factor receptors, Ras-guanosine triphosphate, and mitogen-activated protein kinase in human glioblastoma multiforme specimens. Neurosurgery 1999;45:1442-53.

226. Aldape KD, Ballman K, Furth A, et al. Immunohistochemical detection of EGFRvIII in high malignancy grade astrocytomas and evaluation of prognostic significance. Journal of neuropathology and experimental neurology 2004;63:700-7.
227. Viana-Pereira M, Lopes JM, Little S, et al. Analysis of EGFR overexpression, EGFR gene amplification and the EGFRvIII mutation in Portuguese high-grade gliomas. Anticancer research 2008;28:913-20.
228. Ellison DW. Multiple Molecular Data Sets and the Classification of Adult Diffuse Gliomas. N Engl J Med 2015;372:2555-7.
229. Dang L, White DW, Gross S, et al. Cancer-associated IDH1 mutations produce 2-hydroxyglutarate. Nature 2010;465:966.
230. Lee SM, Koh HJ, Park DC, Song BJ, Huh TL, Park JW. Cytosolic NADP(+)-dependent isocitrate dehydrogenase status modulates oxidative damage to cells. Free radical biology & medicine 2002;32:1185-96.
231. Dubbink HJ, Taal W, van Marion R, et al. IDH1 mutations in low-grade astrocytomas predict survival but not response to temozolomide. Neurology 2009;73:1792-5.
232. Sanson M, Marie Y, Paris S, et al. Isocitrate dehydrogenase 1 codon 132 mutation is an important prognostic biomarker in gliomas. Journal of clinical oncology : official journal of the American Society of Clinical Oncology 2009;27:4150-4.
233. Yan H, Parsons DW, Jin G, et al. IDH1 and IDH2 mutations in gliomas. N Engl J Med 2009;360:765-73.
234. Gravendeel LA, Kloosterhof NK, Bralten LB, et al. Segregation of non-p.R132H mutations in IDH1 in distinct molecular subtypes of glioma. Human mutation 2010;31:E1186-99.
235. SongTao Q, Lei Y, Si G, et al. IDH mutations predict longer survival and response to temozolomide in secondary glioblastoma. Cancer Sci 2012;103:269-73.
236. van den Bent MJ, Dubbink HJ, Marie Y, et al. IDH1 and IDH2 mutations are prognostic but not predictive for outcome in anaplastic oligodendroglial tumors: a report of the European Organization for Research and Treatment of Cancer Brain Tumor Group. Clin Cancer Res 2010;16:1597-604.
237. Eller JL, Longo SL, Hicklin DJ, Canute GW. Activity of anti-epidermal growth factor receptor monoclonal antibody C225 against glioblastoma multiforme. Neurosurgery 2002;51:1005-13; discussion 13-4.
238. Eller JL, Longo SL, Kyle MM, Bassano D, Hicklin DJ, Canute GW. Anti-epidermal growth factor receptor monoclonal antibody cetuximab augments radiation effects in glioblastoma multiforme in vitro and in vivo. Neurosurgery 2005;56:155-62; discussion 62.
239. Patel D, Lahiji A, Patel S, et al. Monoclonal antibody cetuximab binds to and down-regulates constitutively activated epidermal growth factor receptor vIII on the cell surface. Anticancer Res 2007;27:3355-66.

240. Fukai J, Nishio K, Itakura T, Koizumi F. Antitumor activity of cetuximab against malignant glioma cells overexpressing EGFR deletion mutant variant III. Cancer Sci 2008;99:2062-9.
241. Faillot T, Magdelenat H, Mady E, et al. A phase I study of an anti-epidermal growth factor receptor monoclonal antibody for the treatment of malignant gliomas. Neurosurgery 1996;39:478-83.
242. Stragliotto G, Vega F, Stasiecki P, Gropp P, Poisson M, Delattre JY. Multiple infusions of anti-epidermal growth factor receptor (EGFR) monoclonal antibody (EMD 55,900) in patients with recurrent malignant gliomas. Eur J Cancer 1996;32A:636-40.
243. Neyns B, Sadones J, Joosens E, et al. Stratified phase II trial of cetuximab in patients with recurrent high-grade glioma. Ann Oncol 2009;20:1596-603.
244. Barth RF, Wu G, Yang W, et al. Neutron capture therapy of epidermal growth factor (+) gliomas using boronated cetuximab (IMC-C225) as a delivery agent. Appl Radiat Isot 2004;61:899-903.
245. Wu G, Barth RF, Yang W, Kawabata S, Zhang L, Green-Church K. Targeted delivery of methotrexate to epidermal growth factor receptor-positive brain tumors by means of cetuximab (IMC-C225) dendrimer bioconjugates. Molecular cancer therapeutics 2006;5:52-9.
246. Epenetos AA, Courtenay-Luck N, Pickering D, et al. Antibody guided irradiation of brain glioma by arterial infusion of radioactive monoclonal antibody against epidermal growth factor receptor and blood group A antigen. Br Med J (Clin Res Ed) 1985;290:1463-6.
247. Kalofonos HP, Pawlikowska TR, Hemingway A, et al. Antibody guided diagnosis and therapy of brain gliomas using radiolabeled monoclonal antibodies against epidermal growth factor receptor and placental alkaline phosphatase. J Nucl Med 1989;30:1636-45.
248. Warram JM, de Boer E, Korb M, et al. Fluorescence-guided resection of experimental malignant glioma using cetuximab-IRDye 800CW. Br J Neurosurg 2015:1-9.
249. Kato Y, Jin G, Kuan CT, McLendon RE, Yan H, Bigner DD. A monoclonal antibody IMab-1 specifically recognizes IDH1R132H, the most common glioma-derived mutation. Biochemical and biophysical research communications 2009;390:547-51.
250. Schumacher T, Bunse L, Pusch S, et al. A vaccine targeting mutant IDH1 induces antitumour immunity. Nature 2014;512:324-7.
251. Pellegatta S, Valletta L, Corbetta C, et al. Effective immuno-targeting of the IDH1 mutation R132H in a murine model of intracranial glioma. Acta Neuropathol Commun 2015;3:4.
252. Venisnik KM, Olafsen T, Loening AM, Iyer M, Gambhir SS, Wu AM. Bifunctional antibody-Renilla luciferase fusion protein for in vivo optical detection of tumors. Protein Eng Des Sel 2006.
253. Begley DJ. Delivery of therapeutic agents to the central nervous system: the problems and the possibilities. Pharmacol Ther 2004;104:29-45.

254. Muldoon LL, Sandor M, Pinkston KE, Neuwelt EA. Imaging, distribution, and toxicity of superparamagnetic iron oxide magnetic resonance nanoparticles in the rat brain and intracerebral tumor. Neurosurgery 2005;57:785-96; discussion -96.
255. Costantino L, Gandolfi F, Tosi G, Rivasi F, Vandelli MA, Forni F. Peptide-derivatized biodegradable nanoparticles able to cross the blood-brain barrier. J Control Release 2005;108:84-96.
256. Witt KA, Davis TP. CNS drug delivery: opioid peptides and the blood-brain barrier. AAPS J 2006;8:E76-88.
257. Kreuter J, Shamenkov D, Petrov V, et al. Apolipoprotein-mediated transport of nanoparticle-bound drugs across the blood-brain barrier. J Drug Target 2002;10:317-25.
258. Kreuter J, Ramge P, Petrov V, et al. Direct evidence that polysorbate-80-coated poly(butylcyanoacrylate) nanoparticles deliver drugs to the CNS via specific mechanisms requiring prior binding of drug to the nanoparticles. Pharm Res 2003;20:409-16.
259. Gulyaev AE, Gelperina SE, Skidan IN, Antropov AS, Kivman GY, Kreuter J. Significant transport of doxorubicin into the brain with polysorbate 80-coated nanoparticles. Pharm Res 1999;16:1564-9.
260. Steiniger SC, Kreuter J, Khalansky AS, et al. Chemotherapy of glioblastoma in rats using doxorubicin-loaded nanoparticles. Int J Cancer 2004;109:759-67.
261. Fujita M, Lee BS, Khazenzon NM, et al. Brain tumor tandem targeting using a combination of monoclonal antibodies attached to biopoly(beta-L-malic acid). J Control Release 2007;122:356-63.
262. Madhankumar AB, Slagle-Webb B, Wang X, et al. Efficacy of interleukin-13 receptor-targeted liposomal doxorubicin in the intracranial brain tumor model. Molecular cancer therapeutics 2009;8:648-54.
263. Kircher MF, Mahmood U, King RS, Weissleder R, Josephson L. A multimodal nanoparticle for preoperative magnetic resonance imaging and intraoperative optical brain tumor delineation. Cancer Res 2003;63:8122-5.
264. Deshane J, Garner CC, Sontheimer H. Chlorotoxin inhibits glioma cell invasion via matrix metalloproteinase-2. J Biol Chem 2003;278:4135-44.
265. Kachra Z, Beaulieu E, Delbecchi L, et al. Expression of matrix metalloproteinases and their inhibitors in human brain tumors. Clin Exp Metastasis 1999;17:555-66.
266. Lyons SA, O'Neal J, Sontheimer H. Chlorotoxin, a scorpion-derived peptide, specifically binds to gliomas and tumors of neuroectodermal origin. Glia 2002;39:162-73.
267. Veiseh O, Sun C, Gunn J, et al. Optical and MRI multifunctional nanoprobe for targeting gliomas. Nano Lett 2005;5:1003-8.
268. Yamamoto Y, Tsutsumi Y, Mayumi T. Molecular design of bioconjugated cell adhesion peptide with a water-soluble polymeric modifier for enhancement of antimetastatic effect. Curr Drug Targets 2002;3:123-30.

269. Aina OH, Sroka TC, Chen ML, Lam KS. Therapeutic cancer targeting peptides. Biopolymers 2002;66:184-99.
270. Reddy GR, Bhojani MS, McConville P, et al. Vascular targeted nanoparticles for imaging and treatment of brain tumors. Clin Cancer Res 2006;12:6677-86.
271. Kim YP, Daniel WL, Xia Z, Xie H, Mirkin CA, Rao J. Bioluminescent nanosensors for protease detection based upon gold nanoparticle-luciferase conjugates. Chem Commun (Camb) 2010;46:76-8.
272. Sun X, Zhao Y, Lin VS, Slowing, II, Trewyn BG. Luciferase and luciferin co-immobilized mesoporous silica nanoparticle materials for intracellular biocatalysis. J Am Chem Soc 2011;133:18554-7.
273. Zwiorek K, Kloeckner J, Wagner E, Coester C. Gelatin nanoparticles as a new and simple gene delivery system. J Pharm Pharm Sci 2005;7:22-8.
274. Leung KC, Chak CP, Lee SF, et al. Enhanced cellular uptake and gene delivery of glioblastoma with deferoxamine-coated nanoparticle/plasmid DNA/branched polyethylenimine composites. Chem Commun (Camb) 2013;49:549-51.
275. Ziady AG, Gedeon CR, Miller T, et al. Transfection of airway epithelium by stable PEGylated poly-L-lysine DNA nanoparticles in vivo. Mol Ther 2003;8:936-47.
276. Vecil GG, Lang FF. Clinical trials of adenoviruses in brain tumors: a review of Ad-p53 and oncolytic adenoviruses. Journal of neuro-oncology 2003;65:237-46.
277. Mittal SK, McDermott MR, Johnson DC, Prevec L, Graham FL. Monitoring foreign gene expression by a human adenovirus-based vector using the firefly luciferase gene as a reporter. Virus Res 1993;28:67-90.
278. Nanda D, Vogels R, Havenga M, Avezaat CJ, Bout A, Smitt PS. Treatment of malignant gliomas with a replicating adenoviral vector expressing herpes simplex virus-thymidine kinase. Cancer Res 2001;61:8743-50.
279. Steffen D, Weinberg RA. The integrated genome of murine leukemia virus. Cell 1978;15:1003-10.
280. Naldini L, Blomer U, Gallay P, et al. In vivo gene delivery and stable transduction of nondividing cells by a lentiviral vector. Science 1996;272:263-7.
281. Shah K, Hingtgen S, Kasmieh R, et al. Bimodal viral vectors and in vivo imaging reveal the fate of human neural stem cells in experimental glioma model. J Neurosci 2008;28:4406-13.
282. Ho DY, McLaughlin JR, Sapolsky RM. Inducible gene expression from defective herpes simplex virus vectors using the tetracycline-responsive promoter system. Brain Res Mol Brain Res 1996;41:200-9.
283. Yu YA, Shabahang S, Timiryasova TM, et al. Visualization of tumors and metastases in live animals with bacteria and vaccinia virus encoding light-emitting proteins. Nature biotechnology 2004;22:313-20.

284. Zhang Q, Yu YA, Wang E, et al. Eradication of solid human breast tumors in nude mice with an intravenously injected light-emitting oncolytic vaccinia virus. Cancer Res 2007;67:10038-46.
285. Yu W, Naim JO, Lanzafame RJ. The effect of laser irradiation on the release of bFGF from 3T3 fibroblasts. Photochem Photobiol 1994;59:167-70.
286. Van Breugel HH, Bar PR. He-Ne laser irradiation affects proliferation of cultured rat Schwann cells in a dose-dependent manner. J Neurocytol 1993;22:185-90.